UiT The Arctic University of Norway

Faculty of Health Sciences

Institute of Medical Biology

Anticancer Activity of Amphipathic Barbiturates

Susannah von Hofsten

A dissertation for the degree of Philosophiae Doctor

March 2023

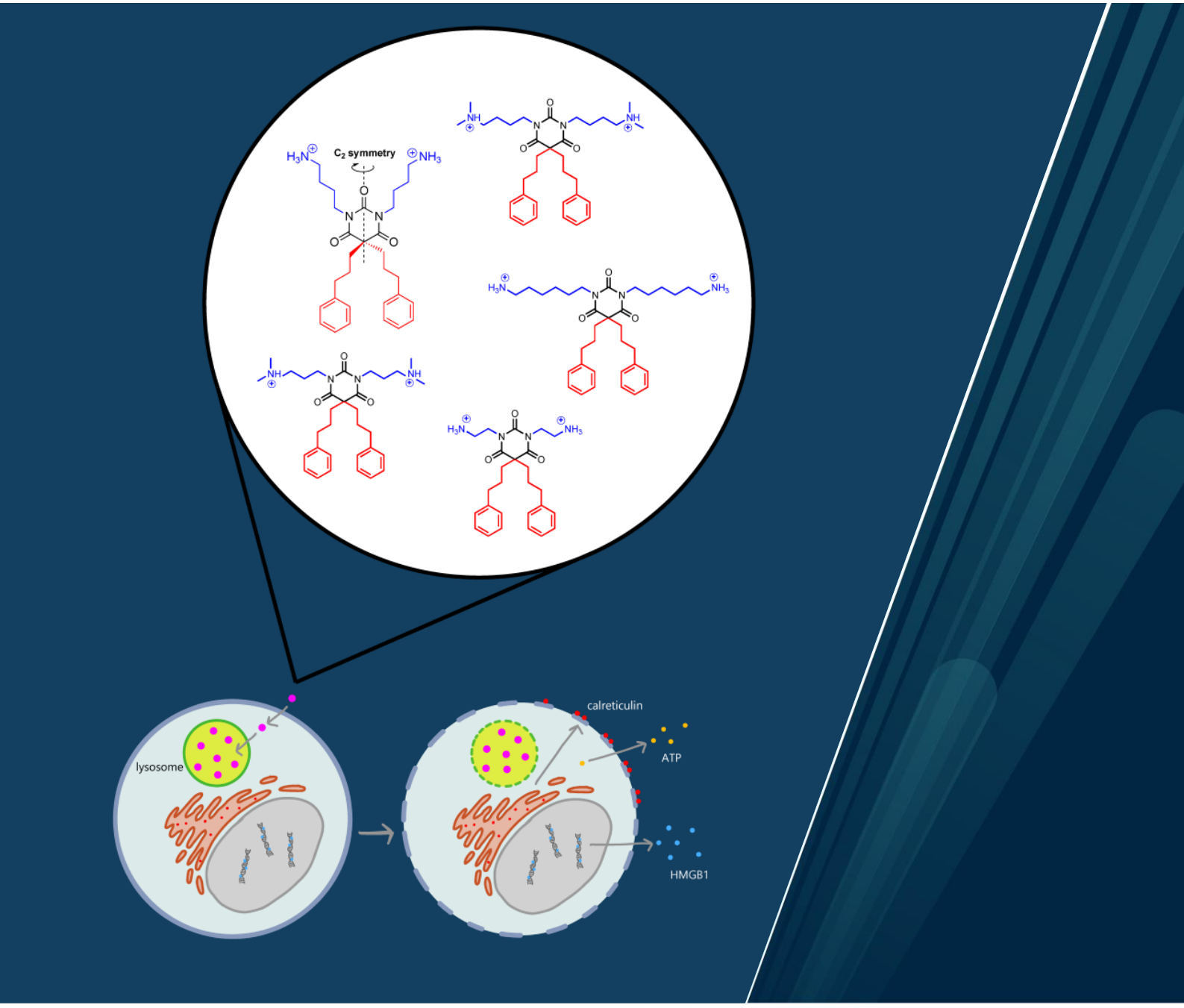

Anticancer Activity of Amphipathic Barbiturates

Susannah von Hofsten

A dissertation for the degree of Philosophiae Doctor

Tumor Biology Research Group
Department of Medical Biology
Faculty of Health Sciences
UiT – The Arctic University of Norway

March 2023

Table of Contents

Acknowledgements

The work presented in this thesis was carried out at the Tumor Biology Research Group (TBRG) at the Department of Medical Biology, Faculty of Health Sciences, University of Tromsø (UiT) – The Arctic University of Norway and was funded by UiT.

I have loved being a PhD student 98% of the time and I almost feel sad that this time of my life is coming to an end. At the same time, I feel proud of what I have accomplished and everything I have learned, and I feel excited about the future. I am also very grateful that I got the opportunity to do a PhD and for all the people who have supported me over the last 4-5 years.

First, I want to thank my main supervisor Gerd Berge. Thank you for seeing the potential in a shy master student in 2018 and giving me the opportunity to start working on the project that turned into my PhD. Thank you for always being supportive of my ideas and giving me the freedom to be independent. I could not have asked for a more encouraging supervisor.

I also want to thank my co-supervisors. Synnøve Magnussen, by participating in discussions and supervision meetings, you have contributed way more to my PhD project than what is probably expected from a co-supervisor, and I am forever grateful to you for that. Dominik Ausbacher, your knowledge in both cell biology and drug development has been of great help to me, and your input has been extremely valuable. Morten B. Strøm, my work in this thesis is largely based on your previous research and without you, my PhD project could not have existed. Thank you for initiating this project and letting me work on it.

To all the other past and present members of TBRG: Beate, Bente, Erik, Saikat, Anne, Ibrahim, Anna, Ruth, Gaute, Joffe, Oddveig, Elin, Sonja, Lars, you have all contributed to creating a fantastic work environment and I have loved spending my days in your company. A special thanks to Kjersti and May-Britt, I have loved having two colleagues my own age (even though you still think I am much younger than you) to chit chat with over coffee and hang with outside of the lab/office as well.

I also want to thank UiT for providing me with a travel grant and giving me the opportunity to spend four months in Helsinki as part of my PhD period. Thank you to the Helsinki group for welcoming me in your lab and teaching me your methods.

Thanks to Trond-Viggo Torgersen for writing the fantastic book *Kroppen*, which sparked my interest for human biology and disease at a young age.

To my best friends Amalie and Marte, thank you for always being supportive of my nerdy interests and for sticking with me all these years. Love you!

To Ingar, thank you for distracting me from work by cooking for me, traveling with me, climbing with me, and dragging me out into nature. I love you even though you don't know the difference between a molecule and a cell.

To my parents, thank you for always being supportive of my choices, encouraging me throughout school and my studies, and for showing that you are proud of me. Mamma, you are my first and greatest academic and personal role model.

Tromsø, March 2023

Susannah von Hofsten

Abstract

Cancer is one of the leading causes of death worldwide. Over the course of the last few decades, enormous efforts have been made to understand the mechanisms driving this diverse disease. This has led to the development of a large number of novel treatment options, including different forms of immunotherapy, which aim to stimulate the body's own immune system to fight the cancer, and have been very effective for some cancer patients. Nevertheless, challenges related to drug resistance, side effects, and poor response rates still persist. In this context, oncolytic therapies which can be administered directly intratumorally represent an alternative treatment mode, which has the potential to be used in several different types of solid tumors. The aim of oncolytic therapies is to kill cancer cells by inducing immunogenic cell death, which can activate a natural anti-tumor immune response.

The current PhD project focused on exploring the potential of amphipathic barbiturates as novel oncolytic compounds for cancer treatment. The amphipathic barbiturates were developed with inspiration from antimicrobial peptides and the *eusynstyelamides*, which are a group of natural compounds that have previously been isolated from marine animals. As such, the compounds studied in the current project have been dubbed marine product mimics (MPMs).

MPM-1 was the first compound studied in this project. It was demonstrated that MPM-1 could kill a range of different cell types and induced a necrosis like death in the head and neck squamous cell carcinoma (HNSCC) cell line HSC-3. Nine additional MPMs were later synthesized and included in further studies, also on HNSCC cell lines. In vitro experimentation indicated that the MPMs have an intracellular target and that they preferentially accumulate in lysosomes, which could be part of their mechanism of inducing cell death.

It was demonstrated that the MPMs could cause the release and exposure of damage-associated molecular patterns (DAMPs) which are associated with immunogenic cell death. This indicated that they could have the potential to be used in oncolytic cancer therapy. An in vivo study was performed where intratumoral injections of MPM-1 were administered to mice bearing B16F1 melanoma tumors. Complete tumor remission upon treatment was achieved. However, significant long-term protective effects against a rechallenge with the same cancer cells was not observed.

Taken together, the MPMs demonstrate potent anticancer activity but whether they have the potential to be used in treatment of human cancer remains to be seen.

List of Papers

The current thesis is based on the following papers, which are referred to in the text by their roman numerals:

Paper I

von Hofsten, S., Paulsen, M. H., Magnussen, S. N., Ausbacher, D., Kranz, M., Bayer, A., Strøm, M. B., Berge, G. (2022). **The marine natural product mimic MPM-1 is cytolytic and induces DAMP release from human cancer cell lines.** *Scientific Reports, 12*(1), 15586. doi:10.1038/s41598-022-19597-4

Paper II

von Hofsten, S., Langer, M. K., Korelin, K., Magnussen, S. N., Ausbacher, D., Anderssen, T., Salo, T., Strøm, M. B., Bayer, A., Al-Samadi, A., Berge, G. (2023). **Amphipathic barbiturates as marine product mimics with cytolytic and immunogenic effects on head and neck squamous cell carcinoma cell lines.** *Frontiers in Pharmacology*, 14:1141669.
doi: 10.3389/fphar.2023.1141669

Paper III

von Hofsten, S., Langer, M. K., Ausbacher, D., Strøm, M. B., Magnussen, S. N., Berge, G. (2023). **Intratumoral injection with the marine natural product mimic MPM-1 causes complete remission of B16F1 melanoma.** *Manuscript*

Abbreviations

AMP Antimicrobial peptide

ANXA1 Annexin A1

ATG Autophagy related gene

ATP Adenosine triphosphate

BafA1 Bafilomycin A1

CAF Cancer-associated fibroblast

CTLA4 T-lymphocyte-associated antigen 4

CXCL10 CXC-chemokine ligand 10

DAB 3,3'-diaminobenzidine tetra-hydrochloride

DAMP Damage-associated molecular pattern

DMEM Dulbecco's modification of Eagle's medium

eIF2α Eukaryotic initiation factor 2α

ER Endoplasmic reticulum

HMGB1 High mobility group box 1

HNSCC Head and neck squamous cell carcinoma

HSP70 Heat shock protein 70

HSP90 Heat shock protein 90

ICD Immunogenic cell death

LRP1 Lipoprotein receptor-related protein 1

MHC Major histocompatibility complex

MLKL Mixed lineage kinase domain like pseudokinase

MPM Marine product mimic

PD1 Programmed cell death protein 1

PDL1 Programmed death-ligand 1

PE Phosphatidylethanolamine

PI Propidium iodide

pKa Acid dissociation constant

PS Phosphatidylserine

RIPK3 Receptor-interacting serine/threonine-protein kinase 3

TLR4 Toll-like receptor 4

TME Tumor microenvironment

1 Introduction

1.1 Drug Discovery and Development

The discovery and development of novel drugs is a costly and time-consuming process (Figure 1)(1, 2). Depending on the chosen approach, several thousand drug candidates often have to be ruled out in the process of developing a single drug that ends up being approved for use in humans. After several steps of activity screening and structure optimization, a selection of lead molecules that hold promising features, is usually included in studies of their biological activity and mechanism of action in vitro. The next step is then to include the most promising candidates in preclinical studies, which involve testing them in animal models (in vivo studies). If satisfying results are obtained, the last stage is clinical testing in humans, which consists of three phases with increasing numbers of participants.

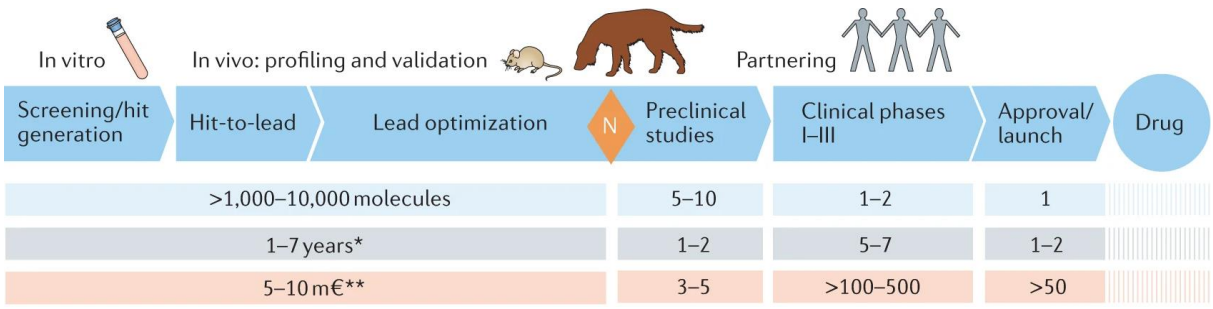

Figure 1 Schematic overview of the different stages involved in drug development, with approximate number of molecules included, years spent, and costs at each stage. The figure is based on numbers associated with the development of antimicrobial drugs, but similar numbers are applicable for other types of drugs as well. Adapted from Miethke et al. (2), reproduced with permission from Springer Nature.

The process outlined above often starts with the desire to develop a drug that can treat a specific disease. In modern times, the discovery of a specific protein or pathway that is connected with the disease can then lead to a very specific hunt for a drug which can alter the function of this protein or pathway (1). With the help from modern technology and methods, novel drugs can be designed and synthesized in a very deliberate manner. However, historically, the vast majority of drugs have been natural products from plants or animals that were discovered through a more accidental fashion. A classic example is penicillin, discovered by Alexander Fleming in 1928 as he was clearing out the mess in his laboratory and noticed reduced bacterial growth around a colony of mold in an old petri dish (3). While the discovery of new drugs is usually less coincidental today, many of them still originate from nature. Out of all new drugs approved between the beginning of 1981 and the end of 2019, a majority of

them are either natural products, natural product derivatives or synthetic molecules somehow inspired by natural products (4). Still, the interest in natural products for drug discovery has decreased during the last few decades, especially in the pharmaceutical industry (5). There are several reasons for this. For example, screening and identification of the bioactive molecules can be technically challenging, and it can be difficult to acquire sufficient material to perform the screenings and other analyses. Screening of unknown material can also often lead to the rediscovery of already known compounds. In addition, natural products often have complicated structures, making them difficult to synthesize for lead optimization and pharmaceutical manufacture. Nevertheless, the planet still contains much unexplored biological material. The ocean in particular remains largely unexplored, but has provided a number of effective drugs throughout history (6). The chemotherapeutic agent cytarabine and the analgesic agent ziconotide are examples of approved drugs of marine origin (6).

1.2 From Moss Animals to Amphipathic Barbiturates

With the aim of collecting biological material for the potential discovery of novel bioactive molecules, a research cruise traveled to the North Atlantic Ocean in 2007 and collected specimens of the moss animal (bryozoan) *Bidenkapia spitzbergensis* (previously referred to as *Tegella cf. spitzbergensis*)(Figure 2)(7).

Figure 2 A specimen of the moss animal *Bidenkapia spitzbergenis* kept at the marine biobank Marbank in Tromsø, Norway. The specimen is a colony consisting of many individual animals. Each square-like structure is one individual. Photo credit: Robert A. Johansen.

Extraction and analysis of the biological material from *B. spitzbergensis* led to the isolation of four compounds referred to as *eusynstyelamides*. The enantiomer of one, meaning the same molecule but with the opposite three-dimensional shape, had previously been isolated from an Australian ascidian (8). There are indications that the eusynstyelamides do not originate from the marine animals themselves, but from symbiotic bacteria (7). The eusynstyelamides isolated from *B. spitzbergensis* were all shown to have antimicrobial activity, and two of them were weakly cytotoxic to a human melanoma cell line.

The fact that the eusynstyelamides have antimicrobial properties is not surprising, as they share traits with antimicrobial peptides (AMPs). Virtually all living species produce AMPs, which form part of the innate immune system, to protect themselves from microbes (9). The common trait for AMPs is that they contain both cationic and hydrophobic amino acids which can fold in such a way that the hydrophobic residues face in one direction while the cationic groups face in the opposite direction, creating an amphipathic structure. The "Achille's heel" of bacteria, as put by Michael Zasloff (9), is that the outer leaflet of their plasma membrane contains a high number of negatively charged phospholipids. The cationic part of the AMPs therefore readily targets bacterial cell membranes, enabling the disruption of the membranes by the peptides. This can occur through different mechanisms, as demonstrated in Figure 3. In contrast, eukaryotic cell membranes generally have no net charge and are therefore not targeted by AMPs. In addition, eukaryotic cell membranes contain cholesterol, which is normally absent from bacterial membranes and helps to stabilize and protect eukaryotic membranes from disruption by AMPs (10).

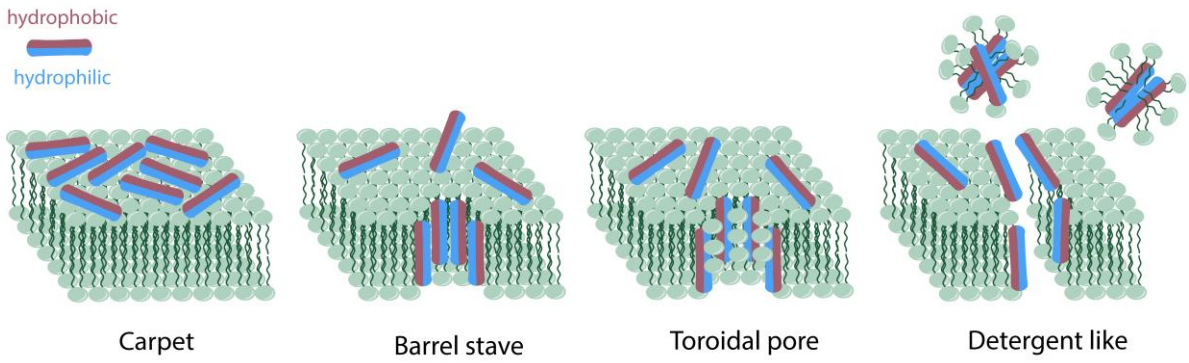

Figure 3 Antimicrobial peptides (AMPs) typically fold in such a way that one side is hydrophobic, and one side is hydrophilic, allowing them to interact with biological membranes through different mechanisms. In the carpet model, a high number of AMPs adsorb to the surface of the lipid bilayer, eventually causing unfavorable interactions and disintegration of the membrane. An intermediate step can be the formation of pores. Barrel stave pores consist of AMPs that interact with each other and are oriented with the hydrophobic part facing towards the lipid bilayer and the hydrophilic parts facing inwards. In the toroidal pore model, there is more space between the AMPs and the phospholipid head groups also form part of the pore. Any of these models may cause detergent like effects, where the membrane integrity is lost and micelles are formed. Figure produced with inspiration from (11).

Although it is possible to synthesize AMPs for the purpose of using them as antimicrobial drugs, they are not ideal drug candidates. AMPs are generally quite large, with some containing up to 50 amino acids (9). This decreases their oral bioavailability, makes them readily degradable by proteolytic enzymes, and it makes them recognizable for the immune system, suggesting that they may trigger unwanted immune responses. However, a study on the minimum requirements for charge and hydrophobicity (the pharmacophore) of antimicrobial peptides showed that a net charge of +2 and the presence of at least two hydrophobic moieties was enough to result in antimicrobial activity (12). This indicated that smaller amphipathic compounds could also function as antimicrobial drugs. Intriguingly, the eusynstyelamides fulfill this pharmacophore exactly and could therefore inspire the development of novel antimicrobial drugs. Nevertheless, as previously mentioned, natural products often have complicated structures which make them difficult to synthesize. This is the case for the eusynstyelamides, which contain a complex five-membered dihydroxybutyrolactam ring.

Inspired by the eusynstyelamides and the pharmacophore for small antimicrobial peptides, a library of synthetic mimics with simplified structures was created. The novel eusynstyelamide mimics were based on a barbiturate scaffold to which different cationic and lipophilic groups could be attached to create the desired amphipathic structure (13). The barbiturate scaffold has C_2 symmetry, which means that synthesis of the amphipathic barbiturates will not result in the production of different stereoisomers, as is the case for the eusynstyelamides (14). Numerous versions of the amphipathic barbiturates, containing different combinations of cationic and lipophilic groups, have been created and optimized for improved antimicrobial activity and reduced toxicity (15, 16). They represent promising lead molecules for the development of novel antibiotic drugs. However, during initial screening of a panel of amphipathic barbiturates, it was discovered that one of the compounds could kill cancer cells effectively but was not cytotoxic to red blood cells. This compound has later been named *marine product mimic 1*, or MPM-1, and is the focus of **Papers I** and **III** in this thesis. Attached to the barbiturate scaffold, MPM-1 has the same cationic groups, consisting of a hydrocarbon chain of four carbons and a primary amine, as are present in eusynstyelamide D (Figure 4). However, the hydrophobic groups are instead the same as those of the small anti-cancer peptidomimetic LTX-401, initially reported as BAA-1 (17). In **Paper II**, an extended panel of MPMs, further inspired by MPM-1, is presented and investigated for anti-cancer activity. They all contain the same barbiturate scaffold and hydrophobic groups as MPM-1, but the cationic groups differ.

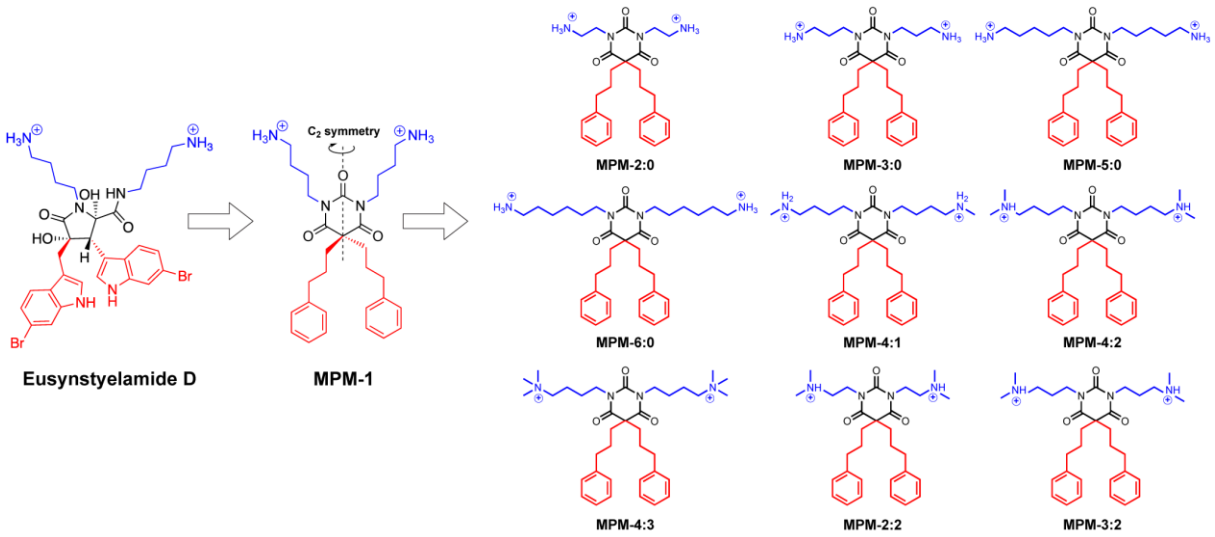

Figure 4 Chemical structure of the natural product Eusynstyelamide D, the synthetic mimic MPM-1, and the 9 other MPMs which were further developed from MPM-1. Cationic groups are colored blue and lipophilic groups red to highlight the amphipathic structure of all compounds.

1.3 The Hallmarks of Cancer

Cancer is a collective term for a number of diseases which are characterized by some common traits. In short, cancer can be described as the uncontrolled proliferation of cells which originally were part of the normal healthy body. Depending on the origin of the cells, this can cause the formation of tumors. If not detected and treated, the cancer cells may also begin to spread throughout the body and form secondary tumors in a process referred to as metastasis. In 2000, Hanahan and Weinberg published the famous paper *The Hallmarks of Cancer*, which described the capabilities that cells need to acquire to become cancer cells, and summarized them in six hallmarks (18). These hallmarks were self-sufficiency in growth signals, insensitivity to growth-inhibitory signals, evasion of programmed cell death, limitless replicative potential, sustained angiogenesis, and tissue invasion and metastasis. With time, the complexity of cancer biology has been further elucidated. Factors like genomic instability, altered metabolism, and control of the tumor immune response have also become recognized as important capabilities of cancer cells. As such, additional hallmarks have been included, both in 2011 and in 2022 (19, 20). There are now fourteen hallmarks of cancer, as proposed by Douglas Hanahan (Figure 5).

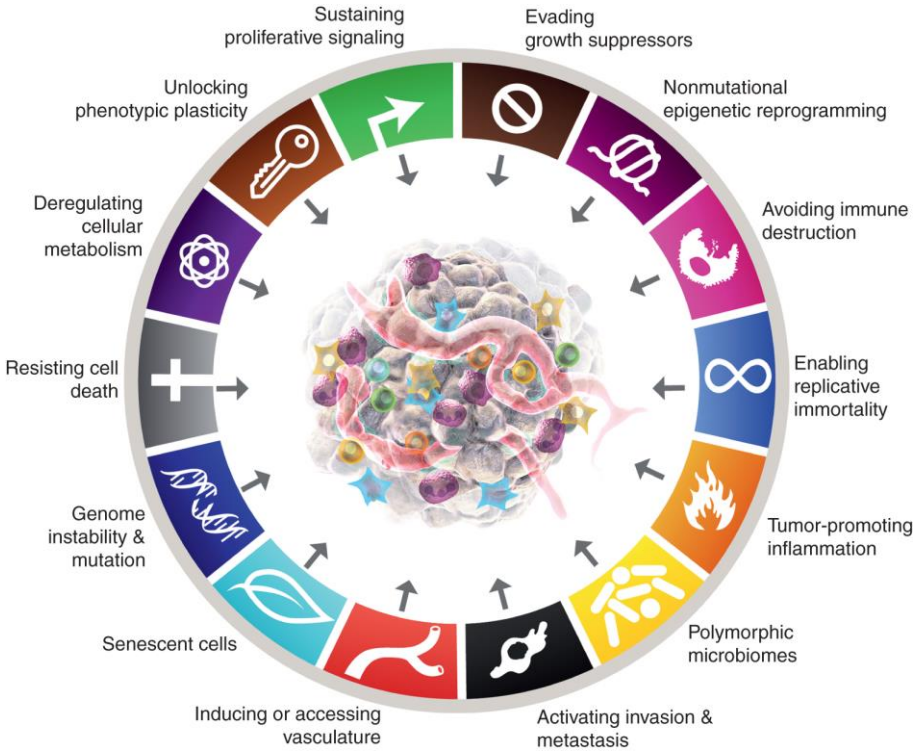

Figure 5 The fourteen hallmarks of cancer, as proposed by Douglas Hanahan in 2022. Figure reprinted from (20) with permission from AACR.

1.4 Tumor Microenvironment

Historically, tumors have been viewed as clumps of cancer cells that grow uncontrollably. As such, much of the early cancer research focused on trying to understand the mechanisms behind cancer development and progression largely by studying so-called oncogenes and tumor suppressor genes (21). However, more recent research has made it clear that tumors do not solely consist of cancer cells, nor are cancer cells the only contributors to cancer progression. During tumor development, cancer cells both recruit other cell types and manipulate resident cells to establish a microenvironment which favors tumor growth, the tumor microenvironment (TME). The tumor supporting cells include different types of immune cells, cancer-associated fibroblasts (CAFs), and endothelial cells. In addition, immune cells that are trying to inhibit tumor growth can be present inside tumors. Thus, the TME consists of many different cell types, which interact with each other in complex ways (Figure 6) (21).

Endothelial cells form blood vessels, which are necessary for providing oxygen, nutrients, and growth factors to cancer cells (21). Other cell types, including CAFs and myeloid derived suppressor cells, can stimulate angiogenesis, the creation of new blood vessels, by secreting vascular-endothelial growth factor (VEGF). Tumors generally have leaky vessels

which makes it easier for cancer cells to enter the blood stream and potentially form distant metastases (22). Metastasis is also supported by the release of proteolytic enzymes from immune cells and CAFs, which cleave extracellular matrix molecules to make it easier for cancer cells to migrate. CAFs also release growth signals and survival factors, as well as transforming growth factor beta (TGF-β), which stimulates the epithelial-to-mesenchymal transition in cancer cells, giving them a more migratory phenotype (23).

The majority of solid tumors contain some degree of infiltrating immune cells of different types, many of which have immunosuppressive functions. This includes regulatory T cells, myeloid derived suppressor cells, and type II macrophages. The tumor associated macrophages can block CD8 T cell proliferation and recruit regulatory T cells, which suppress immune responses (21, 24). Immune cells can also supply growth signals that stimulate tumor growth.

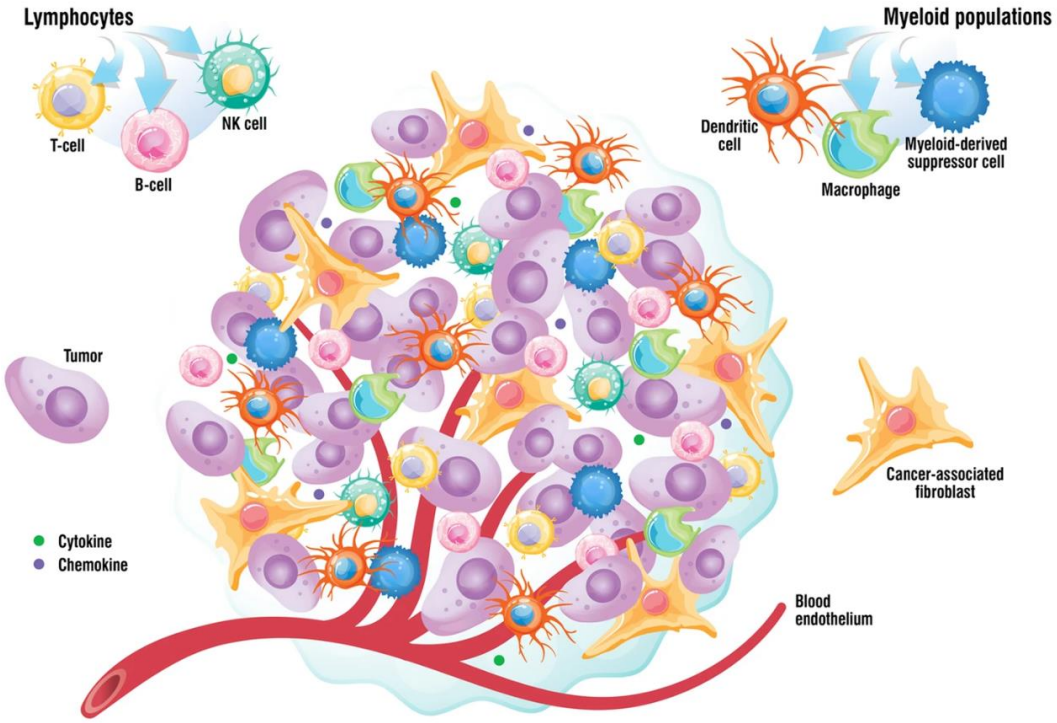

Figure 6 Overview of the main components of the tumor microenvironment. In addition to cancer cells, a tumor normally contains blood vessels, fibroblasts, T cells, B cells, NK cells, dendritic cells, macrophages, and myeloid-derived suppressor cells. The quantity of each cell type can vary greatly between tumors. Figure reprinted from (25) as permitted under the Creative Commons Attribution 4.0 (http://creativecommons.org/licenses/by/4.0/).

In addition to the different cell types found within the TME, there are additional factors that characterize the TME. For instance, tumors generally have low oxygen levels (hypoxia) and low extracellular pH (26). Low oxygen levels drive cells to produce lactate from pyruvate instead of letting the pyruvate enter the tricarboxylic acid cycle to produce more energy. Cancer

cells often employ this metabolic pathway, regardless of whether they suffer from hypoxia or not (27). This altered metabolism of cancer cells is referred to as the Warburg effect, after Otto Warburg who was the first to describe it (28). Lactate can be converted to lactic acid and exported to the extracellular environment, where it dissociates into lactate and hydrogen ions (H^+) which lower the extracellular pH (27). Lactic acid has also been shown to have suppressive effects on immune cells although the sensitivity differs between different types of immune cells. Interestingly, T regulatory cells have been shown to better maintain their suppressive functions in environments with high lactate concentrations as compared to environments with high concentrations of glucose (29). Low pH in the TME can also negatively affect the activity of some chemotherapeutic drugs (30).

1.4.1 Anti-Tumor Immune Responses

While several types of immune cells have immunosuppressive functions and thereby promote tumor growth, other types of immune cells actively try to inhibit tumor growth. When normal cells become transformed into cancer cells, they acquire genetic alterations that make them different from normal healthy cells (31). Mutations in genes cause the production of proteins that are different from the original version of the protein found in healthy cells. The altered proteins give rise to *neoantigens*, which can be recognized as foreign by the immune system. Neoantigens, also referred to as tumor antigens, are presented on major histocompatibility complex I (MHC I) molecules on the plasma membrane of cancer cells and can be recognized by CD8 T cells (32). Activated CD8 T cells (cytotoxic T cells) that have been primed by an antigen presenting cell which has engulfed and presented the same tumor antigen can kill those cancer cells that are expressing this antigen. A concept known as immunosurveillance describes how the immune system is constantly removing potential cancer cells from the body because they express neoantigens (33). However, sometimes cancer cells are not detected by the immune system, and they manage to proliferate, starting to create a tumor. At this stage, cancer cells generally acquire more mutations and alterations, resulting in their expression of more neoantigens. As such, the immune system is able to target many of these cells. However, at the same time, some cancer cells may acquire abilities that allow them to escape targeting by the immune system and thereby continue to proliferate. This results in a Darwinian selection of those cells that are best at avoiding immune attack. This concept is known as immunoediting (33). A variety of different immune escape mechanisms acquired by cancer cells have been described and include for example decreased expression of MHC

molecules, decreased expression of tumor antigens, increased expression of inhibitory cell surface proteins, and secretion of immunosuppressive cytokines (34-36).

Different tumors interact with the immune system in different ways. A common way to classify tumors is as “hot” and “cold” tumors. In this classification system, hot refers to tumors that are inflamed and have a high degree of T cell infiltration (37). Often, the infiltrating T cells are inhibited from killing cancer cells because the cancer cells express inhibitory proteins. In cold tumors, there is little or no infiltration of T-cells, for example due to a low expression of tumor antigens or because the T cells are physically blocked from entering the tumor by stromal cells (38, 39). The degree and type of immune cell infiltration affects prognosis and the success of different treatment forms. Since T cells can help to eradicate cancer cells, turning cold tumors hot is a goal for many new types of cancer treatment (40).

1.5 Treatment of Cancer

The ultimate goal of cancer treatment is to remove the entire primary tumor as well as any potential metastases and metastatic cells to inhibit disease recurrence. Throughout history, several different treatment modalities have been developed and implemented for cancer treatment. Surgery, radiation, and chemotherapy are the most commonly employed types of cancer treatment (41). They may be used alone or in combination. Surgery represents the oldest form of cancer treatment, dating back thousands of years. Nevertheless, surgery is still widely used today and the surgical techniques have seen major improvements over the last decades (42). Radiation therapy shrinks tumors by inhibiting cancer cell division and stimulating cancer cell death (43). Radiation therapy has been in use since the end of the 19th century and was developed after the discovery of X-rays, natural radioactivity, and radium by Röntgen, Becquerel, and Marie Curie, respectively (44). Radiotherapy has also seen great technical improvements during its use, with modern technology allowing for more precise and effective treatment regimens (44). Recently, the ability of radiation therapy to stimulate anti-tumor immune responses has also become increasingly recognized (45).

The term chemotherapy was introduced by the German chemist Paul Erlich at the beginning of the 20th century and refers to all chemicals that can be used to treat disease (46). Chemotherapy was not extensively employed until the 1950’s, when the discovery of novel chemotherapeutic agents really started to accelerate. Today, a large number of different chemotherapeutic drugs are in use for the treatment of different types of cancer. Most of these drugs cause cancer cells to die by activating programmed cell death (apoptosis, described further in section 1.7.1), for example by damaging the cells, which causes them to commit

cellular suicide (47). Cisplatin is a well-known chemotherapeutic agent which causes crosslinking of DNA, resulting in the inhibition of replication and transcription, as well as double stranded breaks (48). Etoposide and the anthracycline doxorubicin function by inhibiting topoisomerase II, which also causes double stranded DNA breaks (49). Fluorouracil and gemcitabine are examples of antimetabolites which get incorporated into DNA or RNA and thereby inhibit their synthesis (50). These mechanisms of action are not specific towards cancer cells, meaning that these drugs also cause harm to healthy cells, especially those that proliferate actively, such as hair follicles, digestive tract epithelium, and bone marrow stem cells (47). As such, these agents often cause serious side effects. Development of drug resistance is also a problem highly associated with chemotherapeutic drugs (51).

In addition to surgery, radiation, and chemotherapy, modern cancer treatment also involves the use of for instance targeted therapies, hormone therapy, gene therapy, bone marrow transplantation, and immunotherapy (41).

1.5.1 Triggering the Immune System to Improve Cancer Treatment

The knowledge that the immune system plays an important role in the biological reaction to tumors has existed for a very long time. Reports from as far back as ancient Egypt have described how tumor growth has spontaneously regressed after episodes of infection or high fever (52). However, at this time, knowledge around the composition and function of the immune system was of course limited. At the end of the 19th century, the first intentional infections of cancer patients with live bacteria were performed and successfully caused shrinkage of tumors (52). In the 1890's, William Coley developed *Coley's toxins*, which were heat-inactivated bacteria that were used to treat sarcomas (53). Coley has been referred to as one of the *fathers of immunotherapy*. However, for a long period, immunotherapy was not a widely used form of cancer treatment. Radiation and chemotherapy were developed and became more recognized treatments.

Today, our understanding of the immune system is much more comprehensive. Different types of immune cells, humoral factors and their interactions have been elucidated and described. This detailed knowledge has allowed for the development of novel, more specific immunotherapies, which have revolutionized cancer treatment during the last two decades. Some of the currently approved immunotherapies are adoptive T cell therapy, cancer vaccines, and immune checkpoint inhibitors (54). Especially immune checkpoint inhibitors have been very successful in the treatment of some cancers, particularly melanomas, which often have a hot phenotype. Cancer cells often overexpress specific ligands and receptors that

can bind to corresponding receptors and ligands on immune cells, stimulating inhibitory pathways in the immune cells (55). In this way, the cancer cells avoid being targeted by the immune cells. Immune checkpoint inhibitors are antibodies that bind to either the receptor or the ligand in this type of interaction, thereby inhibiting signaling. Thus, the immune cells are no longer inhibited. Immune checkpoint inhibitors that are currently in clinical use target T-lymphocyte-associated antigen 4 (CTLA4), programmed cell death protein 1 (PD1), and programmed death-ligand 1 (PD-L1) (54).

1.5.2 Oncolytic Immunotherapy

Despite the success of immune checkpoint inhibitors, many patients do not respond to this form of immunotherapy or are not eligible to receive it. Since the effect of immune checkpoint inhibitors relies on the existence of an ongoing anti-tumor immune response, this form of treatment is generally not suitable to treat tumors with little or no immune cell infiltration (56). In such cases, other forms of immunotherapy may be more effective, such as the direct intratumoral injection of oncolytic immunotherapies which can stimulate the activation of an anti-tumor immune response. Such therapies trigger the immune system because they induce a specific form of cell death referred to as immunogenic cell death (ICD) in cancer cells (described in detail in section 1.7.3) (57). This cell death causes recruitment and activation of immune cells, ultimately resulting in an adaptive immune response where naïve CD8 T cells mature into tumor-specific cytotoxic effector cells. The cytotoxic T cells are tumor-specific because they recognize tumor neoantigens or tumor associated antigens (58). Since oncolytic immunotherapy stimulates infiltration of immune cells into tumors it helps to turn cold tumors hot, thereby increasing the effect of immune checkpoint inhibitors (59).

Intratumoral injections can only be performed in accessible solid tumors, but local activation of an anti-tumor immune response may also benefit distant non-treated lesions because activated tumor-specific cytotoxic T cells can travel to other parts of the body where they may encounter metastases. This phenomenon is referred to as abscopal effects and has been demonstrated in both human patients and animal models (60, 61).

Talimogene laherparepvec (T-VEC), which is an oncolytic virus that kills cancer cells by inducing ICD, is currently in clinical use (59, 62). However, oncolytic compounds, including peptides and smaller molecules, are also being explored for their potential to be used in immunotherapy (57, 59). The oncolytic peptide LTX-315 is in clinical trials and has been demonstrated to cause tumor shrinkage and tumor infiltration of CD8 T cells in human patients (60, 63). Several other compounds have also been developed for use as oncolytic

immunotherapies, such as the peptides DTT-205, DTT-304, and RT53, as well as the smaller peptidomimetic LTX-401 (61, 64, 65). These compounds have all shown promising effects in animal models but have yet to reach clinical trials.

1.6 Head and Neck Squamous Cell Carcinoma

Much of the in vitro work presented in the current thesis, both in **Paper I** and **Paper II**, is performed on cell lines originating from head and neck squamous cell carcinoma (HNSCC). This is a collective term for cancers arising from the mucosal epithelium in the oral cavity, pharynx, and larynx (66). Common risk factors for developing HNSCC are regular use of tobacco and alcohol, which impose a synergistically higher risk when combined than when only one is consumed (67). Several countries in South Central Asia and Melanasia have a high incidence of HNSCC due to the popularity of betel nut chewing in these countries (68). The incidence of HNSCC is also higher in men, as compared to women, likely due to their higher consumption of tobacco and alcohol. Persistent viral infections with Epstein-Barr virus and Human Papilloma virus (HPV) are also risk factors for developing HNSCC (66). HPV infection is especially connected with oropharyngeal cancers, which have had an increasing incidence over the last few decades, particularly in younger men (69). However, increased vaccination against HPV is expected to reverse this trend over the coming decades (70).

Since HNSCC can arise from several different locations within the oral cavity, and as a consequence of different risk factors, the HNSCC tumors have varying phenotypes. Some have reported that HPV+ tumors are associated with a high tumor mutational burden, inflammation, T cell infiltration, and better prognosis than HPV– tumors (71). Others have not found the same clear distinction based on HPV status, but similarly report worse prognosis for those who have immunologically cold tumors (72).

Current treatment options for HNSCC include surgery, irradiation, chemotherapy with cisplatin and 5-fluorouracil, the targeted EGFR receptor cetuximab, and immune checkpoint inhibitors of PD1 for patients with recurrent or metastatic disease (66). Due to the location of HNSCC tumors, surgical resection and/or radiation of these tumors can cause severe side effects, such as facial deformities, mouth dryness, and difficulties with chewing, swallowing, and speaking (73). Chemotherapy is associated with nausea and fatigue, as well as drug resistance (74). Thus, the current treatment options for HNSCC patients often negatively affect the quality of life of these patients, and the development of novel therapies should be prioritized (75).

1.7 Cell Death

The death of cells is an essential part of human biology, which can occur in numerous different ways. The onset of cell death can be tightly regulated, completely accidental, or somewhere in between. In 2018, a review article written by the Nomenclature Committee on Cell Death defined and described twelve distinct forms of cell death, as well as some variants of these (76). However, increasing evidence is demonstrating that several different cell death pathways can be activated simultaneously and are often interconnected with each other. There are also different subtypes of the main forms of cell death, and different researchers sometimes use different terms and classifications when talking about cell death. Thus, the study of cell death is a complex research field.

1.7.1 Apoptosis

Programmed cell death is the controlled death of cells which become damaged or are no longer needed. Apoptosis is the most well-known form of programmed cell death. It plays a vital role in embryonic development, where cell death is essential for the formation of organs and tissues (77). In adult organisms, apoptosis also helps to maintain normal cellular homeostasis. In addition, apoptosis can also be initiated as a response to different types of stress, such as DNA damage, ER stress, or reactive oxygen species (48, 76).

DNA damage is dangerous because it can cause mutations that in time may lead to development of cancer cells. Cells that experience DNA damage must either repair the damage or undergo apoptosis. However, one of the hallmarks of cancer is the cancer cells' ability to resist death (20). This is something they can achieve because they often have mutations in genes that regulate apoptosis, for example TP53, which encodes p53 (48). Interestingly, many chemotherapeutic drugs work by inducing DNA damage to promote apoptosis (48). For example, cisplatin and doxorubicin both target DNA to promote damage and apoptosis. Resistance to both of them has also been linked with mutated p53 (78).

Apoptosis is characterized by a number of morphologic and biochemical traits. Cells dying of apoptosis shrink in size and form apoptotic bodies that bud off while their organelles and plasma membranes remain intact (76). Other hallmarks of apoptosis include chromatin condensation, depolarization of the mitochondrial membrane potential, and caspase activity. Caspases function as signal transducers in apoptotic signaling, but apoptosis can also be caspase-independent (79). Apoptotic cells expose phosphatidylserine (PS) on the outside of the plasma membrane. PS is a phospholipid which is normally found only in the inner leaflet of the plasma membrane (80). The exposure of PS functions as an "eat me" signal to immune cells,

mainly macrophages, stimulating them to clear away the apoptotic cells through phagocytosis, or *efferocytosis*, as it is often named in this context. PS is also immunosuppressive, causing apoptosis to be an immunologically silent event (81).

1.7.2 Necrosis

As opposed to the very controlled demise of cells undergoing apoptosis, necrosis has historically been considered a more accidental and uncontrolled form of cell death. Necrosis is characterized by cell swelling, plasma membrane rupture, and absence of chromatin condensation (82, 83). This is something that can occur due to overwhelming physical, chemical or mechanical stress or injury (76). In such cases, necrotic cell death is truly accidental. However, during recent times it has become increasingly recognized that necrosis can also occur as a regulated form of cell death. The most well-known form of regulated necrosis is necroptosis, which is dependent on the activity of the enzyme receptor-interacting serine/threonine-protein kinase 3 (RIPK3) and mixed lineage kinase domain like pseudokinase (MLKL)(76). Ferroptosis, pyroptosis and parthanatos are other examples of regulated necrosis that have received increasing interest as of late (76, 84). Since cancer cells often have dysfunctional apoptotic signaling, the activation of necrosis has been suggested as a potentially more beneficial approach to cancer treatment than stimulation of apoptosis (85). The plasma membrane rupture which occurs in cells dying of accidental and regulated forms of necrosis causes intracellular content to leak out. Some of the leaking molecules are so-called damage-associated-molecular-patterns (DAMPs) (76, 82, 86). These are molecules that operate as danger signals which recruit and activate immune cells, stimulating an inflammatory response.

1.7.3 Immunogenic Cell Death

Some drugs and other stimuli induce ICD, which is a type of cell death associated with DAMP-release and the subsequent activation of an adaptive immune response towards antigens originating from the dying cells (58, 76). ICD can occur as a response to viral infection and stimulate a virus-specific immune response, but this section will focus on ICD in relation to cancer. ICD in cancer cells can be induced by various cell stressors including conventional chemotherapeutic agents like doxorubicin and mitoxantrone, some targeted anti-cancer therapies, oncolytic compounds, oncolytic viruses, and ionizing radiation (45, 87-92). These treatments have different cellular targets and can therefore trigger various signaling pathways in cells. As such, the type of cell death they induce can also vary. Although apoptosis has generally been regarded as an immunologically silent event, ICD often occurs as a type of

immunogenic apoptosis, for example in cells treated with anthracyclines (87). ICD can also appear as necroptosis or necrosis (93, 94). Common for all inducers of ICD is that they cause cancer cell death and the simultaneous release and exposure of DAMPs that are specifically associated with ICD (58, 95).

There are three danger signals that have classically been defined as the hallmarks of ICD. They are cell surface exposure of calreticulin, release of adenosine triphosphate (ATP), and release of high mobility group box 1 (HMGB1) (96). However, more recent research has identified further DAMPs that also contribute to ICD. For example, ERp57, heat shock protein 70 kDa (HSP70), and heat shock protein 90 kDa (HSP90) can also be exposed on the plasma membrane along with calreticulin (95). The release of type I interferon (IFN), CXC-chemokine ligand 10 (CXCL10), and annexin A1 (ANXA1) is also associated with ICD.

When not secreted or exposed, the DAMP molecules have other important roles within cells. In the lumen of the ER, calreticulin acts as a protein folding chaperone and it regulates calcium homeostasis (97). Calreticulin is also one of the components of the peptide loading complex, which loads peptide antigens onto MHC class I molecules before transportation to the cell surface. During ICD, calreticulin is translocated from the ER to the cell surface, where it functions as an "eat me" signal for immune cells in the tumor microenvironment (87). This is something that occurs early in the course of cell death, before plasma membrane rupture. Through binding to the low-density lipoprotein receptor-related protein 1 (LRP1, also known as CD91) on dendritic cells, cell surface calreticulin promotes the phagocytosis of dying cells and dead cell-associated antigens (95, 98). The translocation of calreticulin to the plasma membrane depends on the activation of the integrated stress response, which manifests with the phosphorylation of the eukaryotic initiation factor 2α (eIF2α) (95, 99).

Intracellularly, ATP stores and provides energy, but when released into the tumor microenvironment it also has recruiting effects on immune cells, functioning as a "find me" signal (100). ATP binds to purinergic receptors, such as P2RX7 and P2RY2 on dendritic cells (101). In living cells, HMGB1 binds to DNA and is therefore located in the nucleus (96). HMGB1 released into the tumor microenvironment can bind to Toll-like receptor 4 (TLR4) on dendritic cells. This binding stimulates tumor antigen processing and cross-presentation to naïve CD8 T cells (102). Both HMGB1 and ATP, when bound to their respective receptors, also stimulate the activation of the inflammasome in dendritic cells, which leads to activation of caspase 1, in turn stimulating the release of IL-1β from dendritic cells (101). IL-1β stimulates activation of γδ T cells, which produce IL-17. IL-1β and IL-17 both contribute to the priming

of naïve CD8 T cells to become mature tumor-specific IFNγ-producing cytotoxic T cells, which perform further tumor cell lysis (Figure 7) (101).

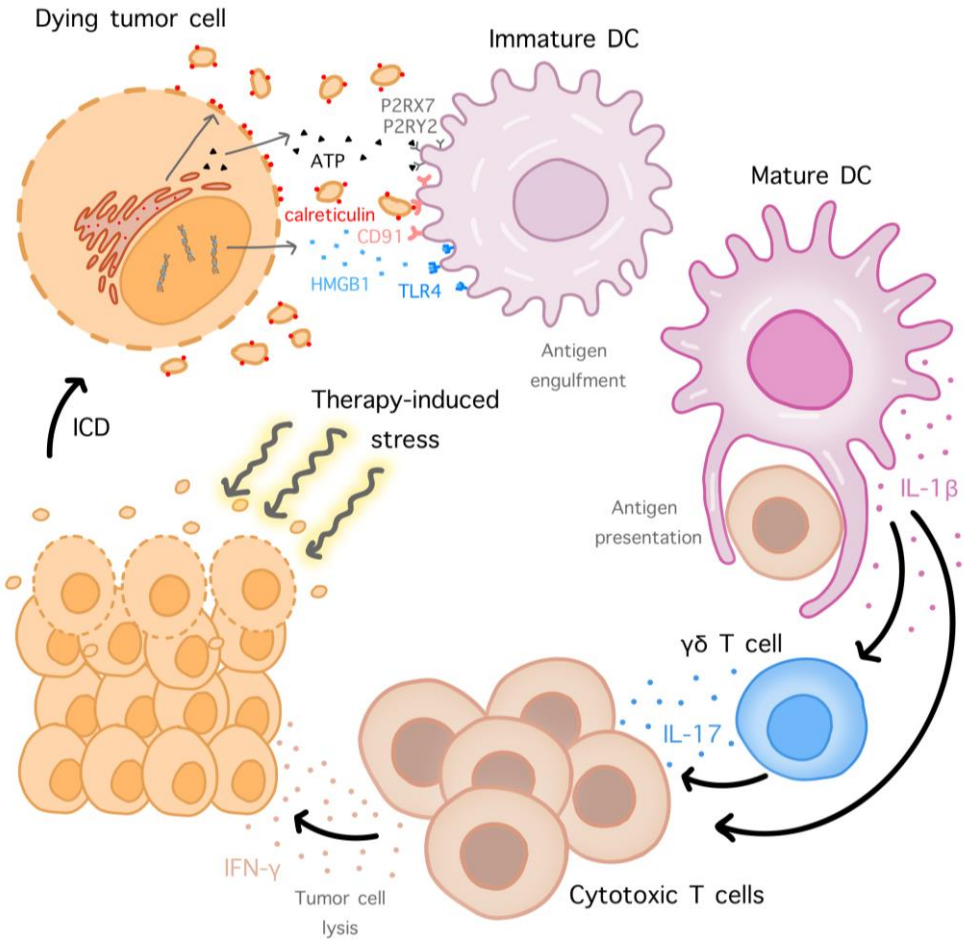

Figure 7 The course of immunogenic cell death (ICD). Treatments that induce ICD in cancer cells cause these cells to expose and release damage-associated molecular patterns (DAMPs). Cell surface calreticulin, released ATP, and released HMGB1 can all bind to receptors on dendritic cells. This stimulates the uptake and cross-presentation of tumor antigens to CD8 T cells, as well as maturation of the dendritic cells. Together with γδ T cells, the dendritic cells stimulate the maturation of naïve CD8 T cells to become tumor-specific IFNγ-producing cytotoxic T cells, which contribute to further tumor cell lysis. Figure produced with inspiration from (96).

1.7.4 Lysosomal Cell Death

Lysosomes are a type of organelle which is present in most cells. They are membrane-bound, have a low internal pH (<5), and contain hydrolytic enzymes which can break down several different types of molecules (103). The main function of lysosomes is to digest or recycle material that is taken up by the cells or that they don't need any more. As such, lysosomes can be viewed as the stomachs of the cell. However, the discoverer of lysosomes, Christian de Duve, also nick-named the lysosomes "suicide bags". This was due to the possibility that lysosomal content could leak into the cytoplasm in case of lysosomal membrane

rupture and cause harm to the cell. Although many of the hydrolytic enzymes only function at low pH, some of them, including cathepsin B, D, and L, also function at neutral pH and can therefore cause uncontrolled degradation of cellular components (104). Cathepsins can also activate caspases, triggering the onset of apoptosis. Moreover, extensive lysosomal membrane rupture can cause acidification of the cytosol and subsequent necrosis. Cell death which occurs as a consequence of lysosomal membrane rupture is referred to as lysosomal cell death, and can be similar to either apoptosis or necrosis (103).

Lysosomal cell death can be induced by lysosomotropic compounds. These are typically weak bases which contain hydrophobic parts. Interestingly, the pharmacophore for small antimicrobial peptides is strikingly similar to the description of lysosomotropic compounds (12, 105). Lysosomotropic compounds exist in an equilibrium between protonated and neutral molecules. The neutral molecules can diffuse freely through cellular membranes, but once they enter a lysosome, the low pH there causes them to become protonated and unable to leave again. This causes accumulation of lysosomotropic compounds in lysosomes, and above a certain threshold concentration they may acquire detergent-like properties, which causes disruption of the lysosomal membrane and subsequent cell death (104).

Interestingly, many chemotherapeutic agents and other commonly used drugs are naturally lysosomotropic even though induction of lysosomal cell death is not their main mechanism of action. This includes for example the chemotherapeutic drugs doxorubicin and tamoxifen (105, 106). Their main targets are DNA and estrogen receptors, respectively. Thus, lysosomal trapping of these drugs may hinder them from reaching their main site of action. This has been suggested as a mechanism for cancer cells to harbor resistance to some chemotherapeutic agents (106). On the other hand, cancer cells often have less acidic lysosomes than normal cells, potentially making them more sensitive to lysosomotropic drugs which exert their main mechanism of action in the cytoplasm or nucleus (106-109).

1.8 Autophagy

Autophagy, which is Greek for “self-eating”, is a process where cells degrade some of their organelles or other cellular content (110). There exists different types of autophagy, but this section will mainly describe macroautophagy, hereafter referred to as *autophagy*. The process of autophagy starts with the initial formation of an autophagosome, which is a double membrane vesicle that encapsulates the content which is targeted for degradation. Next, the autophagosome fuses with a lysosome, forming an autolysosome, which contains hydrolytic enzymes that break down the cellular content (Figure 8). Autophagy is regulated by several

autophagy-related proteins (ATGs). For instance, ATG3 and ATG7 are involved in the conjugation of LC3-I to phosphatidylethanolamine (PE) to form LC3-II, which forms part of the phagophore and autophagosome membranes. Autophagy can be non-specific, or it can selectively target for example damaged organelles or proteins, or invading bacteria. In the case of selective autophagy, autophagy receptors recognize and bind to the cargo intended for degradation. One of the most well-studied autophagy receptors is p62, which binds to ubiquitinated cargo as well as to LC3-II to bring the cargo to the inside of the autophagosome (111).

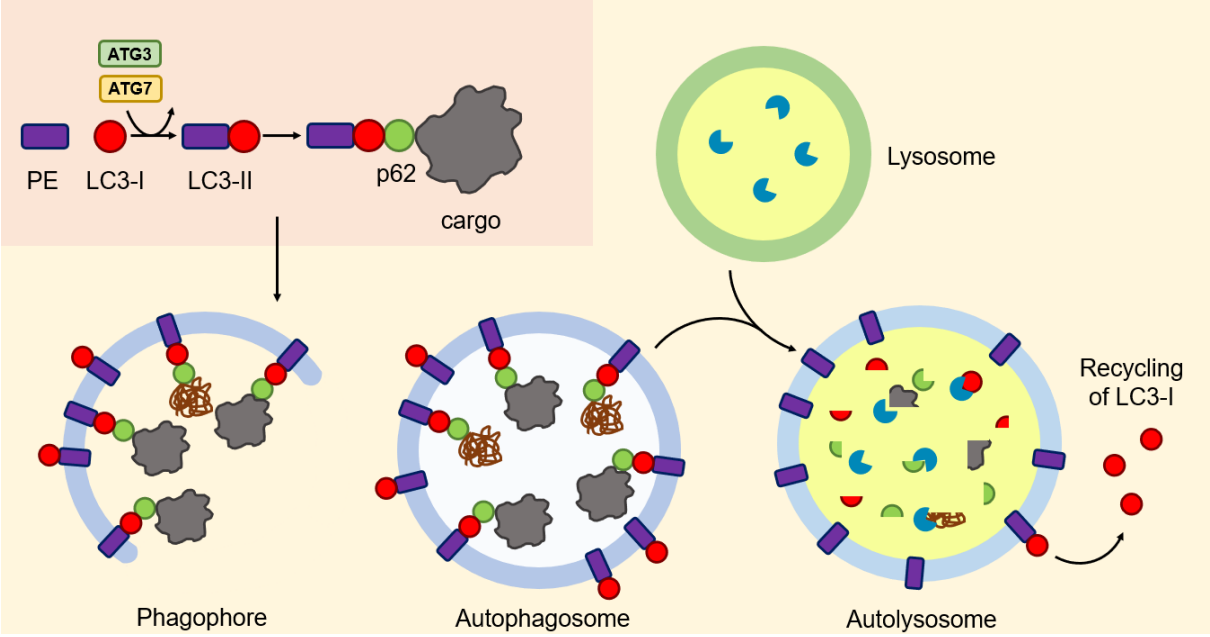

Figure 8 General overview of selective autophagy. LC3-I is the cytosolic form of LC3, which can be conjugated to the phospholipid phosphatidylethanolamine (PE) in a process which relies on ATG3 and ATG7. This forms LC3-II. LC3-II can then bind to p62, which recognizes and binds to cargo that should be degraded. This complex can then form part of a vesicle that traps the cargo on the inside, creating a double membrane autophagosome. The autophagosome then fuses with a lysosome, creating an autolysosome which contains hydrolytic enzymes that degrade the engulfed content, including p62 and LC3. LC3 on the outside of the autolysosome is recycled.

Autophagic degradation provides nutrients and energy for the cell during periods of fasting or stress (110). It can be viewed as a recycling system. As such, it is an important process for most cells, including cancer cells. During homeostasis, autophagy is a way for cells to get rid of toxins or other potentially harmful components that may have entered the cells. Thus, if there is something wrong with the autophagic machinery, this can lead to accumulation of harmful content which in turn may harm the cells. In some cases, this can cause DNA damage and the formation of mutations. Before tumorigenesis, autophagy is thus believed to be tumor suppressive (110). However, during later stages of cancer progression, when tumor cells are

growing and proliferating rapidly, many use autophagy as a way to acquire enough energy to keep up the growth. At this stage, active autophagy can be very important for the survival of cancer cells. For this reason, autophagy has been suggested and explored as a potential target for cancer treatment (112). On the other hand, autophagy has been associated with the active release of both ATP and HMGB1 during immunogenic cell death (100, 113). Thus, activation of autophagy may also be beneficial in certain contexts of cancer treatment.

Sometimes, dying cells have a morphology which is characterized by massive vacuolization, caused by autophagy. Such cell death has often been referred to as autophagic cell death, and was long considered a third main form of cell death, in addition to apoptosis and necrosis (114). However, in many cases of such cell death, it is unclear whether autophagy is the cause of death, or whether it is induced as a way for the cell to try to avoid death. Autophagic cell death is not defined as a distinct form of cell death in the recommendations by the Nomenclature Committee on cell death (76). However, autophagy-dependent cell death, which is a specific form of regulated cell death that is dependent on autophagy, is listed as a distinct form of cell death.

2 Aims

The current PhD research project was born from the discovery of the marine natural product mimic MPM-1 as a potent anticancer agent. The cytotoxic activity of MPM-1 against a small selection of cancer cell lines as well as its lack of effect on red blood cells made this compound interesting to study further. Moreover, the unique marine background of MPM-1 and the knowledge that it shares structural similarity with other promising anticancer agents also contributed to the great interest in MPM-1. By studying the anticancer activity and mechanism of action of MPM-1 and structurally related compounds (MPMs), this project aimed to explore the clinical potential of amphipathic barbiturates in cancer treatment.

Specifically, the following research questions were asked:

- Through which mechanism does the marine natural product mimic MPM-1 induce cell death? (**Paper I**)
- Can the molecular structure of MPM-1 be optimized to create novel amphipathic barbiturates with improved anticancer qualities? (**Paper II**)
- Do the MPMs induce hallmarks of ICD in vitro? (**Paper I and II**)
- Does MPM-1 induce ICD in vivo? (**Paper III**)

3 Results – Summary of Papers

Paper I – The marine natural product mimic MPM-1 is cytolytic and induces DAMP release from human cancer cell lines.

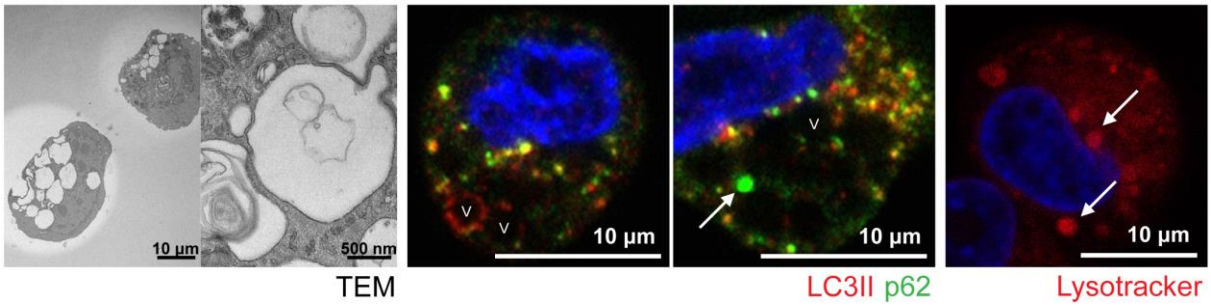

HSC-3 cells treated with 8.5 µM MPM-1 (1xIC50). Both transmission electron microscopy (TEM) and confocal microscopy demonstrated the presence of large intracellular vacuoles (V).

In **Paper I**, the development of MPM-1 as a novel natural product mimic inspired by eusynstyelamide D was described and its synthesis presented. We showed that MPM-1 was cytotoxic to a variety of different cell lines with IC_{50} values ranging from 4.13 to 18.54 µM among the tested cell lines. There was no selectivity towards cancer cells over healthy cells. Yet, MPM-1 had no cytotoxic effect on red blood cells, suggesting an intracellular mechanism of action. Using different methods such as flow cytometry and microscopy, we showed that MPM-1 induced a form of cell death which was similar to necrosis in the oral cancer cell line HSC-3 and the B cell lymphoma cell line Ramos. Simultaneously, MPM-1 caused the appearance of large intracellular vacuoles in HSC-3 cells. Based on this, we hypothesized that MPM-1 affected some part of the cells' vesicular transport or degradation systems. By the use of confocal microscopy, it was shown that MPM-1 caused perturbation of the autophagic machinery, as accumulation of both LC3II and p62 was seen upon treatment of HSC-3 cells with MPM-1. However, the large vacuoles did not appear to be autophagosomes as the majority of them were not associated with LC3II. Instead, MPM-1 caused the enlargement of lysosomes, which suggested that MPM-1 affected the function of lysosomes. Taken together, these results, along with the chemical structure of MPM-1, indicated that MPM-1 is a lysosomotropic compound. Interestingly, when cells were treated with Bafilomycin A1 (BafA1) to decrease the accumulation of MPM-1 in lysosomes, the potency of MPM-1 was increased. This suggested that the main target of MPM-1 is not lysosomes, but some other intracellular structure. Lastly, it was shown that MPM-1 caused the release of DAMPs associated with immunogenic cell death from HSC-3 cells. This included HMGB1 and ATP, and the cell surface exposure of calreticulin.

Paper II – Amphipathic barbiturates as marine product mimics with cytolytic and immunogenic effects on head and neck squamous cell carcinoma cell lines

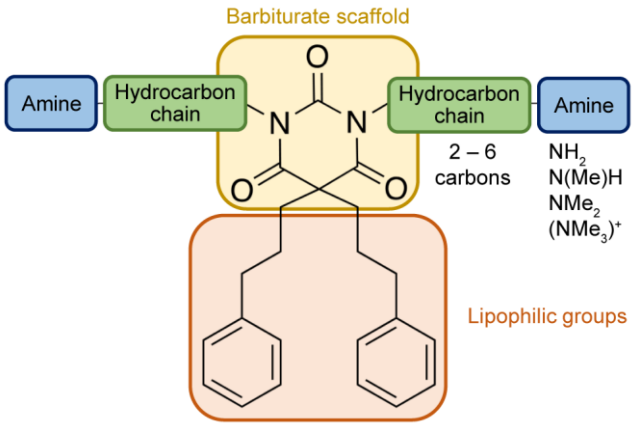

The general structure of the amphipathic barbiturates referred to as MPMs. Attached to the barbiturate scaffold, the MPMs all have the same two lipophilic groups as well as two hydrocarbon chains each containing an amine group.

In **Paper II**, a panel of nine new amphipathic barbiturates, further inspired by MPM-1, was presented. These compounds were collectively referred to as MPMs. To study the potency of the novel MPMs, a high throughput drug screening was performed on a panel of seven HNSCC cell lines and one normal oral fibroblast (NOF) cell line. The screening demonstrated that all new MPMs except one, MPM-4:3, were more potent than the original MPM-1. The potency of the MPMs against the different cell lines, including the NOFs, was of a similar magnitude. By increasing the pH of the cell culture media that was used to treat cells with the MPMs, which causes fewer compounds to be protonated, the potency of the MPMs was increased. MPM-4:3, which was the only MPM to contain a quaternary amine group, causing it to be permanently protonated, was found to be completely inactive by the screening. This indicated that protonation inhibited the effect of the MPMs, most likely because it inhibits them from penetrating through the cell membrane. The MPMs were also found to have minimal effects on red blood cells and bacteria, further suggesting that they have an intracellular mechanism of action.

The four MPMs found to be the most potent by the screening (MPM-2:0, MPM-6:0, MPM-3:2, and MPM-4:2) were included in further studies on HSC-3 and UT-SCC-24A cells. Studies on the mode of death induced by the MPMs revealed that they all caused activation of caspase 3/7, which is associated with apoptosis. However, the pan-caspase inhibitor z-VAD-FMK provided minimal protection from the MPMs and flow cytometric analysis did not reveal the presence of an apoptotic population in MPM treated cells. Instead, the MPMs were found to cause rapid plasma membrane rupture and BafA1 was found to increase the viability of MPM treated cells more than z-VAD-FMK. The latter suggested that the MPMs could be

lysosomotropic. This hypothesis was also supported by the physiochemical properties of the MPMs, which are typical for lysosomotropic compounds. Furthermore, staining of lysosomes with the fluorescent dye Lysotracker revealed that MPM treated cells had visibly enlarged lysosomes as compared to untreated cells, a feature which is associated with cells that have been treated with lysosomotropic compounds.

Lastly, the induction of hallmarks of immunogenic cell death was studied in MPM treated HSC-3 and UT-SCC-24A cells. It was found that the MPMs could induce phosphorylation of eIF2α, cell surface exposure of calreticulin, release of ATP and release of HMGB1, suggesting they could have the ability to cause immunogenic cell death.

Paper III – Intratumoral injection with the marine natural product mimic MPM-1 causes complete remission of B16F1 Melanoma

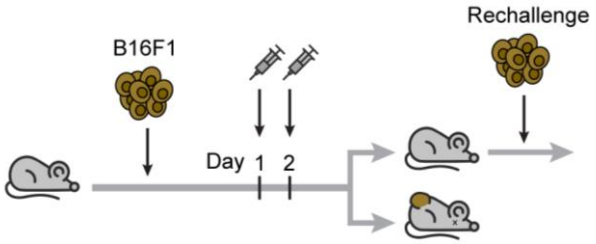

Schematic overview of the rechallenge study.

In **Paper III**, the aim was to investigate the ability of MPM-1 to induce ICD in vivo in a B16F1 melanoma mouse model. To verify that the mode of death induced by MPM-1 in B16F1 cells was of a similar nature as that previously demonstrated in HSC-3 cells, flow cytometric analysis was employed. It was demonstrated that MPM-1 caused rapid plasma membrane permeabilization as well as cell surface exposure of calreticulin in B16F1 cells with intact plasma membranes. Next, B16F1 tumors were established subcutaneously on the flank of C57BL/6 mice. When the tumors became palpable, they were treated with two consecutive injections with 0.5 mg MPM-1 and tumor growth was monitored. In all treated mice, the tumors were completely eradicated, while in control mice treated with PBS, the tumors continued to grow. Mice that were treated by MPM-1 were then subjected to a rechallenge with B16F1 cells to determine whether the initial treatment had induced ICD and thereby established long term immunological memory and protection against the B16F1 cells. However, tumor growth was observed in 8/10 animals, suggesting it had not. Another in vivo study was performed where tumors were established and treated the same way, but the mice were euthanized at set time points after treatment to allow for histological analyses of the tumors. Blood samples were also acquired throughout this study and demonstrated that there was an increase in blood neutrophils and lymphocytes on days 9/10 and 15, respectively. Histological analysis of the tumors and tumor stroma demonstrated that MPM-1 induced local inflammation, as seen by the presence of neutrophils. However, immunohistochemistry staining of CD4 and CD8 demonstrated that there was little infiltration of $CD4^+$ and $CD8^+$ cells in the tumor area, indicating that this was the reason for the modest vaccination effect of intratumoral treatment with MPM-1.

4 Discussion

4.1 Methodological Considerations

The methods used to acquire the results included in this thesis have been described in detail in the papers they belong to. The current section will focus on discussing some selected methods, considerations that were made during the selection of methods to use, as well as considerations that should be made during the planning of future studies.

4.1.1 Compound Screening Design

When starting a research project that aims to identify novel drug candidates, one of the first experiments that should be performed is normally an activity screening. This is something that can be done in a number of different ways, meaning that several important decisions have to be made. Factors like the number of cells seeded, the length of the incubation period, the range of compound concentrations, the cell culture media used, and the assay used for monitoring viability or degree of inhibition can all affect the achieved results and should therefore be carefully considered. In addition, it must be decided whether the screening should be performed manually or include the use of more advanced robotic systems.

In **Paper I**, a small-scale screening of only the compound MPM-1 on different cell lines was performed. MPM-1 had been selected for inclusion in this screening based on previous results showing that it had activity against selected cancer cell lines but not against red blood cells or bacteria. The MPM-1 screening was performed manually by seeding a high number of cells (20 000/well in 96-well plates) and letting them adhere overnight. The next day, the cells were treated with MPM-1 in a two-fold dilution series ranging from 0.5 μg/ml to 128 μg/ml for four hours before viability was monitored by use of the MTS assay, which measures metabolic activity. Four hours is often considered a too short incubation period in a drug screening as many well-known drugs require longer to exert their effect. However, based on previous results with MPM-1 and similar compounds, it was known that MPM-1 could induce cell death quickly. Four-hour incubations have previously been used for screening purposes in similar studies (115-117). Nevertheless, live cell imaging studies, also performed in **Paper I**, clearly showed that concentrations lower than the IC50 value also could cause complete cell death if incubated long enough. Thus, had a longer incubation been chosen for the screening, the achieved IC50 values would have been lower. Similarly, it was demonstrated that the number of seeded cells also affected the rate of cell death. Consequently, a lower number of seeded cells would also have resulted in lower IC50 values.

Manual screening as performed in **Paper I** is extremely time consuming and labor intensive. To make the screening in **Paper II** more efficient, an established high throughput screening platform was used to evaluate the cytotoxic effects of the novel MPMs. This platform allowed for the screening of 11 compounds against 8 different cell lines in a significantly shorter time than it took to perform the smaller screening in **Paper I**. The setup used was adapted from a setup originally developed for the screening of drugs on acute myeloid leukemia patient samples with the goal of providing personalized treatment (118). This original setup used 187 different approved and investigational drugs. Many of these were conventional chemotherapeutics, which do not kill the cells directly but rather inhibit growth or cause the cells to undergo apoptosis. These are effects that take long to see. Thus, the setup used a 72-hour incubation period. In this time, the untreated control cells manage to proliferate extensively, meaning that the initial number of seeded cells had to be quite low. As discussed, this may significantly affect the sensitivity of the cells to drug treatment.

While the screening setup from **Paper I** can analyze direct cell killing by measuring metabolic activity, the setup from **Paper II** analyzes cell death more indirectly by measuring the number of live cells remaining in a well after drug treatment. A low number of cells does not necessarily mean that cells have been killed. It could also be the result of inhibited proliferation. A 72-hour incubation is therefore more sensitive to picking up on such less cytotoxic effects. On the other hand, the results from a 72-hour incubation may be more sensitive to inaccuracies in cell seeding and treatment.

Taken together, virtually all variables in a drug screening setup can greatly influence the measured outcome. It is therefore important to be aware of these effects, both when designing compound screens and when reading reports on screenings performed by others. In abstracts and results sections of papers, IC50 values are often presented as absolute values with no additional information about the setup used to determine them. To find this information, one generally has to actively seek up the methods section, but even then, not all studies report all the relevant information in the methods section either. Thus, it is important to be aware that IC50 values generally cannot be compared between different studies.

4.1.2 Measuring the Viability of Cells

As briefly mentioned, the MTS assay was used to measure viability of cells in the activity screening performed in **Paper I**. In **Paper II**, the MTS assay was also used to measure viability upon co-treatment of cells with MPMs and BafA1 or z-VAD-fmk, as well as after treatment with MPMs in different media and pH. The MTS assay has a simple add-mix-measure

protocol, which makes it faster and easier to use than the related MTT assay, which is also widely used (119). The MTS assay is based on the conversion of a tetrazolium salt into a formazan product with a brown-red color which can be quantified by measuring absorbance at 490 nm. This conversion only happens in metabolically active cells. Thus, the MTS assay results are a measurement of metabolic activity and not viability, per se. This does mean that treatments which affect metabolism without causing direct cell death can skew the results of an MTS assay. One study of the MTT assay, which is similarly based on metabolic activity, found that it could not be used to study the effects of radiation on growth inhibition as radiation simultaneously caused mitochondrial biogenesis and metabolic hyperactivation (120).

In **Paper II**, the viability assay CellTiter-Glo was used in the compound screening. Similar to the MTS assay, the CellTiter-Glo assay also has an add-mix-measure protocol, which makes it comparably easy to use. However, the readout is based on the number of ATP molecules present in the cells, which produce a luminescence signal when the CellTiter-Glo reagent is added. The amount of ATP is directly proportional to the luminescence signal and the number of living cells. CellTiter-Glo has been reported to be more sensitive than other viability assays, such as the MTS assay (121).

4.1.3 In Vitro Cell Culture and Media

Cell culture is an essential part of most biomedical research, and many of the procedures and reagents involved in cell culture are so routinely employed that they are often not given much consideration. In the current PhD project, it was discovered that the pH of the cell culture media greatly affected the potency of the MPMs. Knowing that the MPMs are weak bases, this effect can be logically explained and could have been predicted (biological effects are discussed in greater detail in section 4.2.2). However, these considerations were not made during the early work on this project and may have affected some results. Most notably, the compound screening performed in **Paper II** showed that the control cell line NOF was more sensitive to the MPMs than the cancer cell lines. In hindsight, it seems likely that this was a side effect of the different medias used to plate out these cells.

The main challenge related to pH is that commonly used cell culture medias do not maintain a stable pH. Dulbecco's modification of Eagle's medium (DMEM), which is commonly used to culture cancer cell lines, employs a sodium bicarbonate buffer system, which should hold a physiological pH of around 7.2 to 7.4 when the concentration of CO_2 is 10% (122). However, most cell incubators, including those used to culture the cells in the current project, are set to 5% CO_2. Moreover, the concentration of CO_2 in normal air is only around

0.03-0.04%. Low concentrations of CO_2 cause the pH of DMEM to increase. This is especially noticeable (by judging from the color of phenol red containing media) when working with smaller aliquots of media where the surface-to-volume ratio is large, for example when preparing drug dilution series in microcentrifuge tubes. Some cell culture media, including the DMEM/F-12 used in **Paper II**, are supplemented with HEPES buffer, which is a much stronger buffer than the sodium bicarbonate system at physiological pH (122). This media was therefore found to maintain a stable pH more efficiently than DMEM. However, the sodium bicarbonate system occurs naturally in the human body and is therefore less toxic than HEPES (122). Nevertheless, DMEM/F-12 was judged as the better alternative for the cell culture studies in **Paper II**. When working with drugs and other substances in cell culture, it can be important to consider whether pH may influence the results.

4.1.4 Flow Cytometry

Flow cytometry was used in all three papers to study both apoptosis and cell surface exposure of calreticulin. Flow cytometry is a very useful method as it is relatively simple and allows for the rapid analysis of several thousand individual cells in each assay. Double staining of cells with fluorescently labeled annexin V and propidium iodide (PI), or another viability dye, is a very popular method of studying apoptosis in drug treated cells (123). Annexin V binds to PS, which is only exposed on the outer leaflet of the plasma membrane in apoptotic cells, thus allowing for their identification. However, Annexin V can also bind to PS on the inside of cells with ruptured cell membranes. Therefore, PI, which only penetrates and stains cells that have lost membrane integrity, is added to discriminate between cells with intact and ruptured plasma membranes. However, flow cytometry can be prone to subjective analysis mostly related to the drawing of analysis gates. In the papers belonging to this thesis, the gates were initially drawn in the untreated sample close to the main population in these samples, which should represent unaffected living cells. Any cells falling outside of this gate were considered apoptotic or necrotic depending on their Annexin V and PI fluorescence. This is generally how the gating of these assays is recommended to be performed (123, 124). However, when looking at plots of Annexin V and PI fluorescence presented in different articles, it is evident that different researchers often set gates differently. It is important to be aware that this can greatly affect the outcome of the analysis. Interestingly, many descriptions of the Annexin V and PI apoptosis assay mainly focus on distinguishing alive (Annexin V-/PI-), apoptotic (Annexin V+/PI-), and late apoptotic/necrotic (Annexin V+/PI+) cells (123, 124). The fourth population, Annexin V-/PI+ cells, is often not seen because cells which have lost their plasma membrane

integrity should also be bound by Annexin V. However, MPM treated cells often displayed a clear Annexin V-/PI+ population. The PI staining indicates that the plasma membrane is ruptured in these cells but there is a possibility that the holes in the membrane are still so small that PI can penetrate through them but Annexin V, which is significantly larger, cannot. Several studies refer to this population as necrotic cells (125-127).

When studying the cell surface exposure of calreticulin in **Paper I**, a fluorescently labeled antibody recognizing calreticulin was used. Although an increase in fluorescence was observed in MPM-1 treated cells, the increase appeared to be relatively small. However, this is consistent with what other in vitro studies on ICD often show (91, 128-130). Still, in **Paper II** and **III**, an improved protocol for flow cytometric analysis of cell surface calreticulin was employed. This protocol was directly inspired by a published method, where a primary and secondary antibody was used (131). By using a fluorescently labeled secondary antibody instead of a single fluorochrome conjugated antibody, the fluorescence signal can be amplified as multiple secondary antibodies bind to each primary antibody. For the analysis of cell surface calreticulin, this approach made the CALR+/Zombie Violet- population more easily distinguishable from the other populations, likely resulting in more accurate gating and analysis.

4.1.5 Immunogenic Cell Death In Vivo

When developing novel chemotherapeutic agents, it is often interesting to study whether they have the potential to induce ICD or not. Although in vitro experiments can be used to evaluate the ability of a compound to induce release and exposure of DAMPs associated with ICD, the general consensus is that only in vivo experiments can verify if a compound is a bona fide ICD-inducer (58). A gold-standard method for the evaluation of ICD in vivo has been developed (132). This method is a vaccination assay where cancer cells that are treated with the potential ICD-inducer in vitro are injected subcutaneously into one flank of a mouse (132). The cells should be syngeneic to the host and treated with a concentration and incubation time which causes around 50-70% cell death. One week after the injection of treated cells, live cells of the same type are injected on the opposite flank. If this causes no or reduced tumor growth, the conclusion drawn is that the tested compound is a true ICD-inducer.

In **Paper III**, an in vivo assay was performed to study whether MPM-1 could be an ICD-inducer. The model chosen to for this purpose was not the gold-standard method. Instead, a different vaccination model was employed where B16F1 tumors were established subcutaneously in syngeneic C57BL/6 mice before being subjected to intratumoral injections

with MPM-1 or PBS (control). MPM-1 treated mice who became tumor free were rechallenged with the same B16F1 cells injected on the opposite flank upon being tumor free for at least four weeks. Again, reduced tumor growth was interpreted as though MPM-1 had induced ICD and activated an adaptive anti-tumor immune response. There are some disadvantages to this model which are mainly related to the fact that it is difficult to control the compound exposure. Even though the same number of cancer cells is injected into each mouse, the rate of tumor growth can vary between individual mice, making it difficult to time the injections. The measurement of tumor size was also done by calipers, which is not necessarily completely accurate. Potential differences in size between treated tumors means that the level of exposure of each tumor to injected compound may vary significantly. This could give inconsistent results. Furthermore, determining the appropriate dose for intratumoral injections can be challenging. For MPM-1, it was possible to estimate an appropriate dose by looking at similar studies performed with LTX-401, which has a similar structure and potency to MPM-1 (92). In addition, a pilot study was performed where three different doses (0.25, 0.5, or 1 mg) were tested before the main assays were performed. The results from the pilot study do not form part of **Paper III** but indicated that 0.25 mg was too low to cause tumor remission and 1 mg caused too much necrosis to healthy tissue surrounding the tumor. By treating a fixed number of cancer cells in vitro before injection, the level of compound exposure can be controlled more precisely than when intratumoral injections are performed. The time frame for performing the gold standard assay is also much shorter than the intratumoral injections model. Nevertheless, the latter was chosen for the current study because it has successfully been employed when studying similar compounds previously (117). Moreover, the intratumoral injections model better mimics how MPMs would likely be administered if they ever reach clinical trials. LTX-315 has previously been administered via intratumoral injections in humans (60, 63).

4.1.6 Histological Analysis of B16F1 Tumors

Many melanoma cells, including B16F1, naturally contain the pigment melanin, which typically has a brown-black color (133). When studying immunohistochemistry sections of B16F1 tumors from MPM-1 treated mice in **Paper III**, it was discovered that the 3,3'-diaminobenzidine tetra-hydrochloride (DAB) staining used to visualize antibody binding was very similar in color to the melanin naturally present in the B16F1 melanoma cells. This could be seen from the fact that tumor sections stained with hematoxylin and eosin (H&E) contained large areas of brown cells (Figure 9). When sections from the same tumor were stained with antibodies targeting CD4 or CD8 and DAB, the brown color of the melanin became even more

prominent. This made it very difficult to distinguish between specific antibody staining and the natural color of the B16F1 cells. The staining pattern of the antibodies and the melanin was somewhat different, making it possible to distinguish some cells that were most likely specifically stained. However, it was concluded that both automatic and manual scoring of the staining would likely produce inaccurate results. Therefore, a decision to not include the actual tumor area in the scoring of CD4 and CD8 positive staining was made. This is unfortunate as it is common to analyze infiltration of immune cells into the tumor when studying ICD (61, 116, 134, 135). In the tumor stroma, melanin contamination was not an issue, making it possible to perform reliable scoring of immunohistochemistry staining there. Fortunately, the majority of cells staining positive for CD4 and CD8 in MPM-1 treated B16F1 tumors seemed to be located in the stroma and less so intratumorally. Thus, focusing the scoring on the stroma could still provide some valuable results.

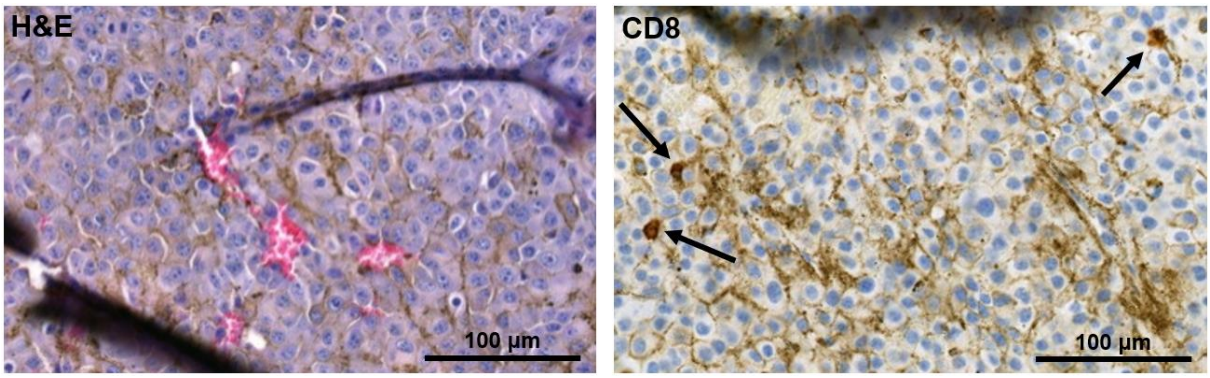

Figure 9 Example of the same area of a PBS treated B16F1 tumor stained with H&E (left) or a CD8-specific antibody and DAB (right). Arrows point to cells which appear to be stained specifically.

The problems associated with immunohistochemistry staining of melanin containing tissues are well-known (133). Nevertheless, some articles still report using DAB to study infiltration of immune cells in melanoma tumors (116, 117, 134). However, different methods have been developed to circumvent the problems associated with melanin. One option is to bleach the melanin, for example using hydrogen peroxide, before staining (133). Another option is to not use DAB, but other chromogens which produce colors that are more distinguishable from melanin. One example is VIP peroxidase, which has a purple color. Lastly, it is possible to use immunofluorescent staining of the tissues instead of chromogens. For future histological studies of immunogenic cell death in the B16F1 melanoma model, one of these options should be considered.

4.2 General Discussion

4.2.1 Amphipathic Barbiturates and their Original Inspiration from Antimicrobial Compounds

As described in the introduction to this thesis, the development of the amphipathic barbiturates studied in the current PhD project was very much inspired by antimicrobial compounds. Different types of amphipathic compounds, and especially the naturally occurring AMPs, are known for having the ability to disrupt biological membranes. The negative charge of bacterial membranes causes the positively charged AMPs to selectively target bacteria and not healthy mammalian cells (9). Antimicrobial activity of amphipathic barbiturates has also been related to electrostatic interactions between the positively charged part of these compounds and the negatively charged bacterial membrane, in turn causing membrane disruption (15).

Conveniently, many cancer cells have the same Achille's heel as bacteria; they too contain a high number of negatively charged phospholipids in their plasma membrane (136, 137). As such, the same electrostatic interactions can occur between AMPs and cancer cell membranes as between AMPs and bacterial membranes. Consequently, AMPs can cause depolarization and disruption of cancer cell membranes and subsequent cell death (138). The oncolytic peptide LTX-315 has an amphipathic structure and is believed to cause cancer cell death in this way (139). LTX-315 has also been reported to selectively target cancer cells over non-malignant cells because of its positive charge (139, 140).

The fact that several antimicrobial and anticancer compounds are positively charged is thus highly important for their function. Based on this, it would be logical to assume that the permanently protonated (positively charged) compound MPM-4:3, introduced in **Paper II**, would be more potent than the other MPMs, which exist in an equilibrium between protonated and unprotonated compounds. However, the opposite was observed. MPM-4:3 had no cytotoxic activity against any cell lines tested, while the other MPMs all effectively reduced cell viability. Moreover, increasing the pH of the cell culture media, which shifts the equilibrium between protonated and unprotonated compounds towards the unprotonated form, increased potency of the MPMs. This indicated that positive charge inhibited the cytotoxic effect of the MPMs and that their mechanism of inducing cancer cell death is fundamentally different from that of for example LTX-315.

A likely explanation why positive charge has an inhibitory effect on the MPMs is that they have an intracellular target and that they are unable to penetrate through the plasma

membrane in their protonated form. In their unprotonated form, the MPMs are rather lipophilic and should therefore be able to penetrate through phospholipid membranes easily.

In both **Paper I** and **Paper II**, the cytotoxic effect of the MPMs was hypothesized to be coupled to lysosomotropism. This hypothesis was based on several factors. For instance, amphipathicity and the ability to shift between protonated and unprotonated forms is a prerequisite of lysosomotropic compounds (105, 141). In addition, the MPMs had minimal effects on red blood cells, which do not contain lysosomes. The potency of the MPMs was also affected by pretreatment of cells with BafA1, which inhibits lysosomal trapping of compounds. Lastly, MPM-1, MPM-2:0, MPM-6:0, MPM-3:2 and MPM-4:2 all induced enlargement of lysosomes, an effect which is also coupled to lysosomotropism (141). However, it can not be absolutely concluded from the results presented in **Paper I** or **II** whether lysosomotropism is the direct or only cause of cell death.

Nevertheless, the results do strongly indicate that the MPMs have an intracellular target and do not disrupt the plasma membrane directly. This hypothesis is also supported by the fact that the MPMs were generally found to have low activity against bacteria. If the MPMs do not directly interact with the plasma membrane, except for passively diffusing through it, this is a likely explanation why the MPMs were not found to selectively target cancer cells over healthy cells despite being positively charged.

Taken together, it is curious to consider how the development of the amphipathic barbiturates was directly inspired by AMPs but turned out to generate compounds with anticancer activity and likely a very different mechanism of action.

4.2.2 Influence of pKa on Membrane Penetration and Potency

As already mentioned, the pH of the solution that the MPMs are in affects the equilibrium between protonated and unprotonated compounds. The equilibrium is also directly related to the negative logarithm of the acid dissociation constant (pKa) of the compounds. The Henderson-Hasselbalch equation is commonly used to estimate the pH of a buffer solution (142). However, by rearranging the equation, it can also be used to calculate the ratio of protonated to neutral compounds at different pH levels, based on the pKa of the compound. For **Paper II**, the pKa of all the MPMs was calculated and the results showed that it varied between 8.06 for MPM-3:2 to 10.24 for MPM-6:0. A graph based on the rearranged Henderson-Hasselbalch equation demonstrates that the difference in pKa values has a significant impact on the effect of pH on the different MPMs (Figure 10). The graph only demonstrates the ratios between pH 7 and 8 but the differences are nevertheless substantial. At pH 7, only one out of

1738 MPM-6:0 molecules (0.06%) will be unprotonated and likely able to penetrate through a plasma membrane, while at pH 8, the number is one out of 174 (0.6%). This effect is very likely the reason why increased potency of the MPMs was observed when cells were treated in cell culture media with increased pH in **Paper II**. For the two compounds with the lowest pKa values, MPM-2:0 and MPM-3:2, the difference in the ratio between protonated and unprotonated molecules at pH 7 compared to pH 8 is very little. At pH 8 the ratio is close to 1:1, meaning that almost 50% of compounds are neutral. This seems like a probable explanation as to why these two compounds were found to be some of the most potent. On the other hand, MPM-6:0 was also found to be one of the most potent MPMs despite having the highest pKa value. In **Paper II**, we speculate that the reason for this may be that MPM-6:0 in fact does have some membrane disrupting abilities unlike the other MPMs due to its long hydrocarbon chains, which make it the most lipophilic MPM. This in turn may make it more able to interact with a biological membrane in a detergent-like manner, compensating for its reduced ability to passively diffuse through the membrane (143). Indeed, MPM-6:0 did have some cytotoxic effect against red blood cells as well as significant antimicrobial effects. However, these theories are only speculations which have not been confirmed.

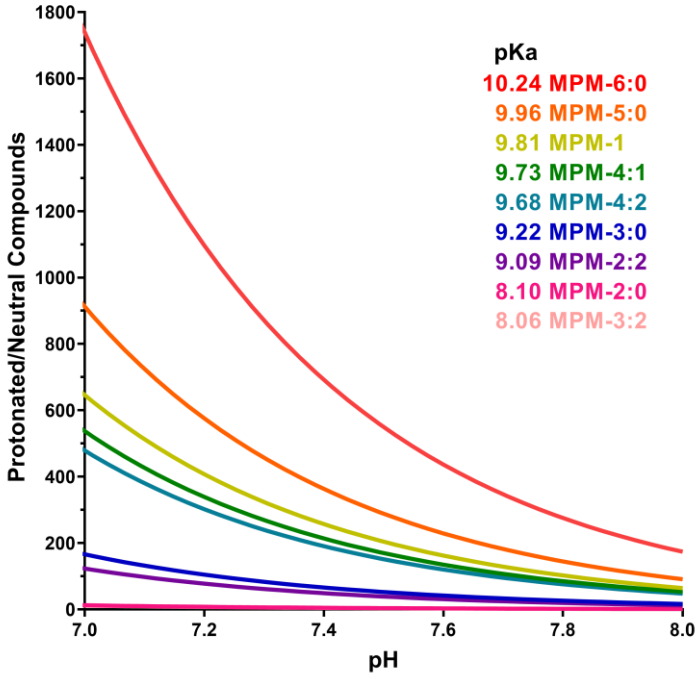

Figure 10 Graph demonstrating the effect of pH on the ratio between protonated and neutral compounds. The numbers are based on the rearranged Henderson-Hasselbalch equation (protonated/neutral compounds = $1/(10^{pH-pKa})$) and the calculated pKa for the MPMs.

While calculated pKa values can provide useful insight about how compounds may behave in different contexts, it should be noted that theoretical calculation is not always completely representative of reality (142). Nevertheless, it is important to be aware of the impact pH can have on drug efficacy. With the Henderson-Hasselbalch equation in mind and knowing that the TME typically has a lower pH than healthy tissues due to the Warburg effect, it seems apparent that these factors can influence how certain drugs interact with cancer cells. It is known that in the same way as lysosomotropic compounds become trapped inside lysosomes due to their low internal pH, many weak base drugs can be trapped on the outside of cancer cells due to the low pH in the TME (30). They are therefore inhibited from affecting the cancer cells. This phenomenon has been demonstrated for several well-known chemotherapeutics such as doxorubicin, mitoxantrone and paclitaxel, which are all lysosomotropic (144, 145). It is thus highly likely that the MPMs would be affected by a low pH in the TME in the same way. However, it should be considered that in the in vivo assay performed with MPM-1 in **Paper III**, a very high concentration of MPM-1, solved in a buffered solution, was administered directly inside the tumor. This may have limited the possible effects of a low pH. Still, it is relevant to consider these matters when planning both in vitro and in vivo studies.

4.2.3 Lysosomotropism and Subcellular Distribution of the MPMs

Continuing the topic of pH-dependent distribution of compounds, this section will focus on the intracellular distribution of the MPMs. By treating cells with BafA1, the subcellular distribution of lysosomotropic compounds can be altered. BafA1 is an inhibitor of the V-ATPase, which normally pumps H+ into the lysosomal lumen to keep the lysosomal pH low (146). By inhibiting the V-ATPase, the lysosomal pH rises, and less drug is accumulated (Figure 11). This phenomenon has been demonstrated for doxorubicin, which is naturally fluorescent, allowing for the direct observation of its distribution within cells by confocal microscopy (106). Upon treatment of cells with BafA1, doxorubicin was redistributed to the nucleus, where its main target, DNA, is located (106). Consequently, the cells became more sensitive to doxorubicin. Similarly, when treating HSC-3 cells with BafA1 in **Paper I**, they became more sensitive to MPM-1. This suggests that the same phenomenon is applicable to MPM-1 and that its main target is located outside of the lysosomes. Surprisingly, BafA1 had the opposite effect on MPM-2:0, MPM-6:0, MPM-3:2 and MPM-4:2 when a similar experiment was performed in **Paper II**. HSC-3 and UT-SCC-24A cells became less sensitive to treatment with these compounds when co-treated with BafA1. This suggested that for these compounds, their accumulation in lysosomes is a central part of their mechanism of inducing cell death.

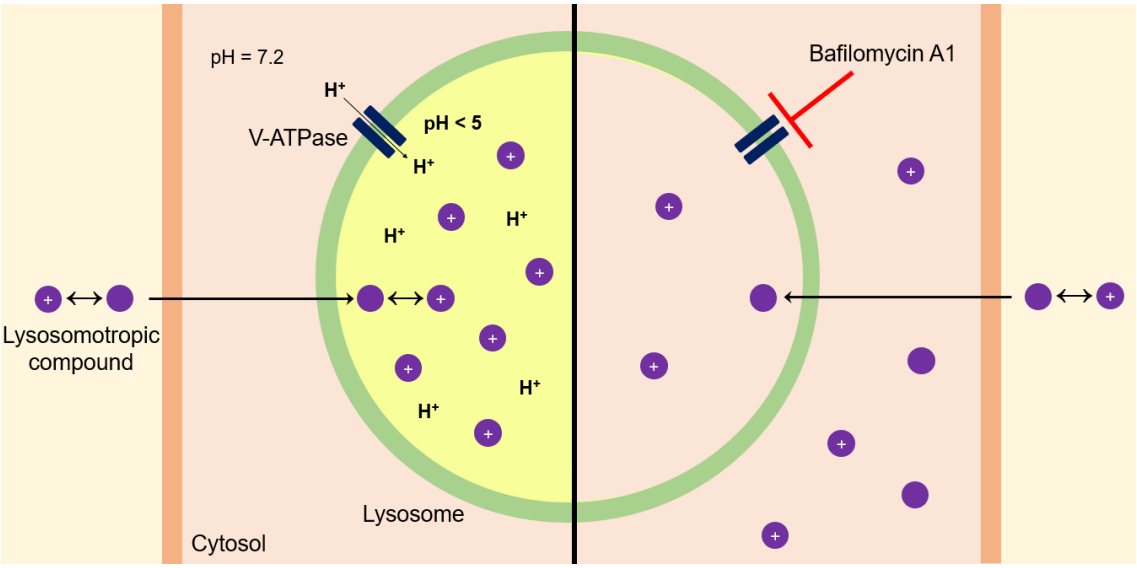

Figure 11 Under normal conditions, the V-ATPase functions to pump protons into lysosomes to keep the internal pH of the lysosomes under 5. The big difference in pH between the inside of the lysosomes and the cytosol causes lysosomotropic compounds to be sequestered in the lysosomes (left). Bafilomycin A1 is an inhibitor of the V-ATPase, which therefore causes the pH inside the lysosomes to increase. Consequently, lysosomotropic compounds are not as readily sequestered by the lysosomes and instead distribute throughout the cytosol (right).

It is not clear why BafA1 had the opposite effect on MPM-1 and the other MPMs tested. From the drug screening performed in **Paper II**, it was demonstrated that MPM-1 was also markedly less potent than all the other MPMs (except for the completely inactive MPM-4:3), which in general had quite similar potencies. These results could suggest that MPM-1 has a different mechanism of action than the other MPMs. However, by looking at the chemical structure of MPM-1 and the other MPMs, it is difficult to understand why MPM-1 should stand out as the only compound with a markedly different mechanism of action as it is not more unique than any of the other MPMs. Nevertheless, as mentioned, there is a possibility that MPM-2:0, MPM-6:0, MPM-3:2 and MPM-4:2 mainly target lysosomes while MPM-1 has a different main target.

Even though the results from **Paper I** indicate that MPM-1 is also lysosomotropic, there are other compartments within cells that could potentially sequester MPM-1 to a greater extent. For example the mitochondrial matrix is known for being able to trap lipophilic cationic drugs due to the negative charge in this part of the organelle (141, 147). This trapping is independent of the V-ATPase, supporting the idea that reducing lysosomal trapping with BafA1 could lead to more mitochondrial trapping and potentially increased cytotoxicity. Interestingly, LTX-315, despite being reported to induce cell death via direct plasma membrane rupture, has also been shown to preferentially accumulate in the mitochondria of cells (148). This was demonstrated using subcellular fractionation of LTX-315 treated cells followed by mass spectrometric quantification. The same type of analysis has demonstrated that LTX-401 preferentially accumulates in the Golgi apparatus and cytosol, and not in mitochondria (128). A pure

lysosomal fraction was not included in this analysis. However, the V-ATPase is present in the membrane of the trans-Golgi, as well as in endosomes and secretory granules, causing these compartments to be acidic and capable of trapping compounds due to protonation like lysosomes (141). This could therefore be the mechanism behind the accumulation of LTX-401 in the Golgi apparatus. Independently of which organelle oncolytic compounds accumulate in, a common mechanism of inducing cell death is disruption of the membrane of the targeted organelle (59). LTX-401 has been shown to cause disruption of the Golgi apparatus, and LTX-315 has been shown to disrupt mitochondrial morphology and cause mitochondrial membrane permeabilization (94, 128, 148).

It has not been confirmed that the mechanism behind MPM induced cell death is disruption of the lysosomal membranes. However, lysosomotropic compounds which contain a hydrophobic part, like the MPMs do, are expected to work as so-called lysosomotropic detergents (141). To verify that the MPMs actually cause lysosomal membrane disruption, one option is to study the release of lysosomal proteins, for example cathepsins, into the cytosol upon treatment of cells with the MPMs (104). However, In **Paper II**, the pan-caspase inhibitor z-VAD-fmk was utilized to study the involvement of caspases in MPM-mediated cell death. The results demonstrated that z-VAD-fmk had some protective effects, but the protective effects of BafA1 were generally greater, supporting the hypothesis that lysosomotropism is at least a part of the mechanism behind the cell death induced by MPM-2:0, MPM-6:0, MPM-3:2, and MPM-4:2. Interestingly, z-VAD-fmk has been found to not only inhibit caspases, but also several different cathepsins (149, 150). Thus, there is a possibility that the protective effects of z-VAD-fmk are mainly related to their inhibitory effect on cathepsins and not the caspases.

4.2.4 The Mode of Cell Death Induced by MPMs

Lysosomal cell death represents one distinct cell death modality. However, as briefly discussed in the introduction to this thesis, different cell death pathways can often be interconnected with each other and activated at the same time (76). Through the in vitro studies performed in **Paper I** and **II**, hallmarks of necrosis, apoptosis and ICD were studied. **Paper I** presented several indications that at least MPM-1 did not cause classic apoptosis but instead induced morphological and biochemical features typically associated with necrosis. From **Paper II**, where the compounds MPM-2:0, MPM-6:0, MPM-3:2, and MPM-4:2 were studied, the results were somewhat more conflicting. Both live cell imaging of caspase 3/7 activation and viability assays with z-VAD-fmk indicated that there was some caspase activity in MPM treated cells. As caspase activity is typically associated with apoptosis, this could mean that

MPMs have the ability to induce some apoptotic pathways. However, as mentioned, the protective effects of z-VAD-fmk could be related to cathepsin inhibition instead. Cathepsins can also activate caspases, suggesting they could be the explanation for the observed caspase 3/7 activation as well (104). Flow cytometric analysis of cell surface exposure of PS and membrane integrity, from all three papers, demonstrated that the MPMs induced rapid membrane permeabilization, which is not typical for apoptotic cells (76, 151). Moreover, MPM treatment did not cause cell surface exposure of PS in cells with intact plasma membranes. There are thus several indications that the MPMs generally induce a more necrosis like death.

Regardless of whether MPM induced cell death is more similar to necrosis or apoptosis, what is perhaps more interesting, is whether they can induce ICD, as that is the aim of intratumoral treatment with MPMs. Results from both **Paper I** and **II** demonstrate that the MPMs do induce hallmarks of ICD. The finding that the MPMs induced translocation of calreticulin form the ER to the cell surface was especially intriguing as this process requires regulated signaling (98, 99). Secretion of ATP and HMGB1 can be actively regulated as well, which is important during immunogenic apoptosis, but they can also be passively released from necrotic cells (86, 152).

Studying the characteristics of different modes of cell death in vitro is important because it can give interesting implications about the mechanism of action of novel compounds as well as about their potential effects in vivo. However, as previously discussed, the induction of hallmarks of ICD by a compound in vitro does not necessarily mean that the same compound is able to activate an adaptive anti-tumor immune response in vivo.

4.2.5 In Vivo Results and Clinical Potential of the MPMs

In **Paper III**, the results from an in vivo study with MPM-1 are presented. Based on these results it is difficult to say much about the clinical potential of the MPMs. The modest vaccination effect seen in the rechallenge study was somewhat discouraging. Only 20% of mice initially cured by intratumoral injections with MPM-1 remained tumor free upon the rechallenge. Similar studies with LTX-315, LTX-401, DTT-205 and DTT-304 have seen protection against rechallenge tumors in 60-100% of previously cured animals (61, 64, 115, 117). However, as discussed in **Paper III**, the reason for the modest effect may be related to the treatment dose used. Since complete remission of the primary tumors, which were injected with MPM-1, was seen in all animals, it seems unlikely that the selected dose was too low. In this study, the tumors were treated with two consecutive injections of 0.5 mg MPM-1 in 50 µl PBS, which gives a concentration of 13 600 µM. This concentration is considerably higher than

the concentrations used to study the effect of MPM-1 on cells in vitro in **Paper I**. The number of cancer cells in a palpable tumor is evidently also considerably higher than the number of cells treated in cell culture plates thus warranting the increased concentration used in in vivo studies. However, it is difficult to estimate the exact ratio between cells and compound in vivo. If the concentration used was too high, there is a possibility that the cells died in a different manner than what was demonstrated in the in vitro studies. A very high concentration may cause instant lysis of cells. This may still cause the release of the DAMPs ATP and HMGB1, but for instance cell surface exposure of calreticulin must occur in cells that still have intact plasma membranes to be able to contribute to the immunogenicity of cell death (59).

It has previously been described that oncolytic chemotherapies aiming to induce ICD in vivo should induce complete necrosis at the center of the tumor but leave a "halo" around the center, where the cancer cells are killed in a less acute manner (59). It is in this halo area that cancer cells should be expressing cell surface calreticulin and other membrane bound DAMPs, and that the highest degree of immune cell infiltration is expected to occur (59). Non-small cell lung cancer tumors resected from patients treated with radiofrequency ablation, which is a form of oncolytic treatment, demonstrated that these tumors were characterized by tissue damage and necrosis in the central parts but a high degree of immune cell infiltration in the surrounding area (153). Total destruction of the whole tumor is thus believed not to be ideal. Dosing and scheduling of the treatment should therefore be optimized to achieve an appropriate amount of tumor cell death. In a clinical setting, the tumor burden can vary significantly between different individuals, indicating that determining the optimal dose for a specific patient might be very challenging.

Another challenge which may be especially pronounced in clinical settings, is the influence of the TME on treatment success. Many tumors have immunosuppressive microenvironments which inhibit anti-tumor immune responses. While oncolytic therapies may contribute to elimination of immunosuppressive cells through their direct lysis, immunosuppression could still pose a problem, especially for untreated metastatic lesions (59). Combining treatments that induce ICD with immune checkpoint inhibitors has therefore been shown to improve treatment outcomes (154). In one mouse study on breast cancer, where two separate tumors were established but only one was subjected to irradiation, it was demonstrated that irradiation alone or immune checkpoint inhibitors alone did not significantly affect the growth of the untreated tumor (155). However, when irradiation was combined with administration of an antibody binding to CTLA4, the abscopal effects were significantly improved. Similarly, in a study of intratumoral injections with LTX-401 which also employed

dual tumors and treatment of only one of them, the abscopal effects were limited without checkpoint inhibitors but significantly improved when antibodies against PD-1 and CTLA4 were also given (92). A similar study also found that CTLA4 antibodies improved the abscopal effects of intratumoral injections with LTX-315, but only when administered in advance of treatment with LTX-315 (156).

The clinical potential of the MPMs depends on several factors. Normally, a certain level of selectivity for cancer cells over healthy cells is a quality which is deemed indispensable for novel cancer drugs (157). However, by confining the area of administration to the tumor by use of direct intratumoral injection, side effects related to damage to healthy cells can be limited. The in vivo study from **Paper III** indicated that the intratumoral treatment with MPM-1 was safe. In fact, the unselective nature of the MPMs may indicate that they have the potential to be used in treatment of several different forms of cancer as well as on drug resistant cells. However, a prerequisite for treatment with any form of intratumoral injection is that the tumor lesions are solid and accessible for injection, either directly or with the help of imaging techniques and/or endoscopy (158). In addition, the success of treatments that aim to induce ICD depends on the presence of tumor antigens (58, 59). This could mean that a higher tumor mutational load may be beneficial for treatment with MPMs. In **Paper I** and **II**, the focus was on HNSCC cell lines, which represent solid tumors that often have a medium to high tumor mutational burden, indicating that they could be good candidates for MPM treatment (159). Since immunologically cold HNSCC tumors are associated with unfavorable prognosis, and since treatment with ICD inducers may contribute to turning cold tumors hot, HNSCC tumors with limited immune cell infiltration may benefit especially well from treatment with MPMs. A clinical trial with LTX-315 included HNSCC patients, but generally saw more favorable outcomes in other cancers, such as melanoma (60). LTX-401 has shown promising results in pre-clinical models of liver cancer (61).

In addition to oncolytic and ICD inducing effects, which have been the main focus of all three papers, **Paper I** also demonstrated that MPM-1 had the ability to cause perturbation of the autophagic flux in HSC-3 cells. This was seen by the fact that treated cells contained an increased number of autophagosomes as well as p62 aggregates. This is an effect which is commonly associated with lysosomal dysfunction and lysosomotropic compounds (112). It is therefore likely that the other MPMs would have this effect as well. However, this has not been confirmed. As autophagy has been associated with the progression of cancer, drugs that cause inhibition of autophagy have been implicated in cancer treatment before (112, 160, 161). The lysosomotropic drugs chloroquine and hydroxychloroquine, originally antimalarial agents,

have been included in several clinical trials for cancer treatment although with mixed results (112, 162). In a pre-clinical study of pancreatic cancer, it was demonstrated that cancer cells actively employed autophagy to break down MHC I molecules, thereby escaping anti-tumor immune responses (163). Upon treatment with chloroquine, the expression of MHC I was increased, and tumor burden decreased. Since the higher concentrations of the MPMs cause complete cell lysis, the potential benefit from effects on autophagy are likely most relevant for cells exposed to lower concentrations, possibly those present in the previously described "halo" area of a tumor treated with oncolytic therapy. Chloroquine and hydroxychloroquine are believed to cause inhibition of autophagy by causing lysosomal dysfunction. Like the MPMs, chloroquine and hydroxychloroquine have also been found to cause activation of the integrated stress response through phosphorylation of eIF2α (164). Interestingly, the phosphorylation of eIF2α was subsequently found to induce autophagy, as inhibition of its phosphorylation caused a decreased number of autophagosomes to be present in cells treated with chloroquine and hydroxychloroquine (164). As phosphorylation of eIF2α is highly associated with ICD, especially the cell surface exposure of calreticulin, this highlights the fact that multiple cellular processes are often interconnected with each other. As mentioned in the introduction, autophagy is also associated with release of ATP and HMGB1 from cells dying of ICD (100, 113). Taken together, whether the effects of MPMs on autophagy could have implications for their clinical potential remains an open question.

5 Conclusions and Future Perspectives

The work presented in the current thesis has shown that amphipathic barbiturates, designed with inspiration from the marine natural products eusynstyelamides and AMPs, are potent anticancer compounds. It has been demonstrated that these compounds, referred to as MPMs, can kill a broad range of different cancer cells both in vitro and in vivo. Notably, the MPMs did induce cell death in non-malignant cells as well, underlining the fact that they should not be administered systemically but rather directly intratumorally.

Results from **Paper I** indicated that the cell death induced by MPM-1 shared several traits with necrosis. From **Paper II**, it was not equally apparent which cell death mode was induced by the compounds MPM-2:0, MPM-6:0, MPM-3:2, and MPM-4:2. As such, it would be interesting to follow up on this question, for example by acquiring electron microscopy images of cells treated with the mentioned compounds to allow for more detailed studies of the morphological changes induced by these compounds. Additionally, it could be useful to study the activation of further signaling molecules associated with different cell death pathways, such as apoptosis or necroptosis, to better understand the intracellular mechanisms induced by the MPMs.

The chemical structures of the MPMs, as well as results from the first two papers, strongly indicated that the MPMs are lysosomotropic. However, it would be useful to confirm whether the MPMs also induce lysosomal membrane permeabilization and whether this is the direct cause of MPM induced cell death. This could be achieved by studying the involvement of cathepsins, for example by analyzing their release into the cytosol, or by studying the effects on cell death of specific cathepsin inhibitors. Also related to lysosomotropism, it could be interesting to study the origin of the large vacuoles observed in electron microscopy images of MPM-1 treated cells. It was assumed that these vacuoles were of lysosomal origin as that correlates with the hypothesis of lysosomotropism, and lysotracker staining also demonstrated the presence of enlarged lysosomes. However, further analysis, for example through staining of specific lysosome markers or markers of other vesicular organelles could provide more in-depth information.

While the in vitro results from **Paper I** and **II** demonstrated that MPMs could induce hallmarks of ICD, the study presented in **Paper III** did not confirm that MPM-1 had this ability in vivo. To further understand the mechanisms behind this, it could be useful to study the release and exposure of further DAMPs not evaluated in this project, such as ERp57, HSP70, HSP90

type I IFN, CXCL10, and ANXA1. The expression or release of molecules with potential inhibitory effects on DAMPs could also be relevant to study.

In **Paper III**, blood samples from mice treated with MPM-1 were analyzed for cellular composition. However, analysis of cytokines present in the plasma of these samples is also planned. Moreover, splenocytes have been collected from the mice included in the in vivo studies and could be used in further analyses of the immune response to MPM-1 treatment. For example, it could be interesting to study the splenocytes from the two mice who remained tumor free upon rechallenge to try to determine if they contain tumor specific $CD8^+$ T cells. This could for example be achieved by performing proliferation assays or T cell receptor sequencing.

It was hypothesized that the reason for the modest vaccination effect seen in **Paper III** could be related to the selected dose or scheduling of the treatment with MPM-1. Thus, it could be worthwhile to test other treatment regimens. Positive results in pre-clinical studies are vital for the further development of amphipathic barbiturates as candidates for future oncolytic cancer therapy.

References

1. Hughes JP, Rees S, Kalindjian SB, Philpott KL. Principles of early drug discovery. Br J Pharmacol. 2011;162(6):1239-49.
2. Miethke M, Pieroni M, Weber T, Brönstrup M, Hammann P, Halby L, et al. Towards the sustainable discovery and development of new antibiotics. Nature Reviews Chemistry. 2021;5(10):726-49.
3. Ligon BL. Penicillin: its discovery and early development. Semin Pediatr Infect Dis. 2004;15(1):52-7.
4. Newman DJ, Cragg GM. Natural Products as Sources of New Drugs over the Nearly Four Decades from 01/1981 to 09/2019. Journal of natural products. 2020;83(3):770-803.
5. Harvey AL, Edrada-Ebel R, Quinn RJ. The re-emergence of natural products for drug discovery in the genomics era. Nature Reviews Drug Discovery. 2015;14(2):111-29.
6. Newman DJ, Cragg GM. Drugs and Drug Candidates from Marine Sources: An Assessment of the Current "State of Play". Planta Med. 2016;82(09/10):775-89.
7. Tadesse M, Tabudravu JN, Jaspars M, Strom MB, Hansen E, Andersen JH, et al. The antibacterial ent-eusynstyelamide B and eusynstyelamides D, E, and F from the Arctic bryozoan Tegella cf. spitzbergensis. J Nat Prod. 2011;74(4):837-41.
8. Tapiolas DM, Bowden BF, Abou-Mansour E, Willis RH, Doyle JR, Muirhead AN, et al. Eusynstyelamides A, B, and C, nNOS Inhibitors, from the Ascidian Eusynstyela latericius. Journal of natural products. 2009;72(6):1115-20.
9. Zasloff M. Antimicrobial peptides of multicellular organisms. Nature. 2002;415(6870):389-95.
10. Brender J, McHenry A, Ramamoorthy A. Does Cholesterol Play a Role in the Bacterial Selectivity of Antimicrobial Peptides? Frontiers in Immunology. 2012;3.
11. Kumar P, Kizhakkedathu JN, Straus SK. Antimicrobial Peptides: Diversity, Mechanism of Action and Strategies to Improve the Activity and Biocompatibility In Vivo. Biomolecules [Internet]. 2018; 8(1).
12. Strøm MB, Haug BE, Skar ML, Stensen W, Stiberg T, Svendsen JS. The pharmacophore of short cationic antibacterial peptides. J Med Chem. 2003;46(9):1567-70.
13. Strøm MB, Bayer A, Engqvist SOM, Paulsen MH, Ausbacher D. 2018. Barbituric acid derivatives comprising cationic and lipophilic groups. WO/2018/178198. PCT/EP2018/058011.
14. Barykina OV, Snider BB. Synthesis of (±)-Eusynstyelamide A. Organic Letters. 2010;12(11):2664-7.
15. Paulsen MH, Engqvist M, Ausbacher D, Anderssen T, Langer MK, Haug T, et al. Amphipathic barbiturates as mimics of antimicrobial peptides and the marine natural products eusynstyelamides with activity against multi-resistant clinical isolates. J Med Chem. 2021;64(15):11395-417.
16. Langer MK, Rahman A, Dey H, Anderssen T, Zilioli F, Haug T, et al. A concise SAR-analysis of antimicrobial cationic amphipathic barbiturates for an improved activity-toxicity profile. Eur J Med Chem. 2022;241:114632.
17. Ausbacher D, Svineng G, Hansen T, Strøm MB. Anticancer mechanisms of action of two small amphipathic β(2,2)-amino acid derivatives derived from antimicrobial peptides. Biochim Biophys Acta. 2012;1818(11):2917-25.
18. Hanahan D, Weinberg RA. The hallmarks of cancer. Cell. 2000;100(1):57-70.
19. Hanahan D, Weinberg RA. Hallmarks of cancer: the next generation. Cell. 2011;144(5):646-74.

20. Hanahan D. Hallmarks of Cancer: New Dimensions. Cancer Discovery. 2022;12(1):31-46.
21. Hanahan D, Coussens Lisa M. Accessories to the Crime: Functions of Cells Recruited to the Tumor Microenvironment. Cancer Cell. 2012;21(3):309-22.
22. Saharinen P, Eklund L, Pulkki K, Bono P, Alitalo K. VEGF and angiopoietin signaling in tumor angiogenesis and metastasis. Trends in Molecular Medicine. 2011;17(7):347-62.
23. Fiori ME, Di Franco S, Villanova L, Bianca P, Stassi G, De Maria R. Cancer-associated fibroblasts as abettors of tumor progression at the crossroads of EMT and therapy resistance. Molecular Cancer. 2019;18(1):70.
24. Mantovani A, Allavena P, Sica A. Tumour-associated macrophages as a prototypic type II polarised phagocyte population: role in tumour progression. European Journal of Cancer. 2004;40(11):1660-7.
25. Zhang J, Veeramachaneni N. Targeting interleukin-1β and inflammation in lung cancer. Biomarker Research. 2022;10(1):5.
26. Li Y, Zhao L, Li XF. Hypoxia and the Tumor Microenvironment. Technol Cancer Res Treat. 2021;20:15330338211036304.
27. Apostolova P, Pearce EL. Lactic acid and lactate: revisiting the physiological roles in the tumor microenvironment. Trends in Immunology. 2022;43(12):969-77.
28. Warburg O, Wind F, Negelein E. THE METABOLISM OF TUMORS IN THE BODY. J Gen Physiol. 1927;8(6):519-30.
29. Watson MJ, Vignali PDA, Mullett SJ, Overacre-Delgoffe AE, Peralta RM, Grebinoski S, et al. Metabolic support of tumour-infiltrating regulatory T cells by lactic acid. Nature. 2021;591(7851):645-51.
30. Wojtkowiak JW, Verduzco D, Schramm KJ, Gillies RJ. Drug Resistance and Cellular Adaptation to Tumor Acidic pH Microenvironment. Molecular Pharmaceutics. 2011;8(6):2032-8.
31. Chen Daniel S, Mellman I. Oncology Meets Immunology: The Cancer-Immunity Cycle. Immunity. 2013;39(1):1-10.
32. Boon T, Cerottini JC, Van den Eynde B, van der Bruggen P, Van Pel A. Tumor antigens recognized by T lymphocytes. Annual review of immunology. 1994;12:337-65.
33. Dunn GP, Bruce AT, Ikeda H, Old LJ, Schreiber RD. Cancer immunoediting: from immunosurveillance to tumor escape. Nature Immunology. 2002;3(11):991-8.
34. Yarchoan M, Johnson BA, Lutz ER, Laheru DA, Jaffee EM. Targeting neoantigens to augment antitumour immunity. Nature Reviews Cancer. 2017;17(4):209-22.
35. Garrido F, Cabrera T, Concha A, Glew S, Ruiz-Cabello F, Stern PL. Natural history of HLA expression during tumour development. Immunology today. 1993;14(10):491-9.
36. Tang S, Ning Q, Yang L, Mo Z, Tang S. Mechanisms of immune escape in the cancer immune cycle. International Immunopharmacology. 2020;86:106700.
37. Binnewies M, Roberts EW, Kersten K, Chan V, Fearon DF, Merad M, et al. Understanding the tumor immune microenvironment (TIME) for effective therapy. Nature medicine. 2018;24(5):541-50.
38. Joyce JA, Fearon DT. T cell exclusion, immune privilege, and the tumor microenvironment. Science. 2015;348(6230):74-80.
39. Bonaventura P, Shekarian T, Alcazer V, Valladeau-Guilemond J, Valsesia-Wittmann S, Amigorena S, et al. Cold Tumors: A Therapeutic Challenge for Immunotherapy. Frontiers in Immunology. 2019;10.
40. Zhang J, Huang D, Saw PE, Song E. Turning cold tumors hot: from molecular mechanisms to clinical applications. Trends in Immunology. 2022;43(7):523-45.

41. Arruebo M, Vilaboa N, Sáez-Gutierrez B, Lambea J, Tres A, Valladares M, et al. Assessment of the Evolution of Cancer Treatment Therapies. Cancers (Basel) [Internet]. 2011; 3(3):[3279-330 pp.].
42. Wyld L, Audisio RA, Poston GJ. The evolution of cancer surgery and future perspectives. Nature Reviews Clinical Oncology. 2015;12(2):115-24.
43. Baskar R, Lee KA, Yeo R, Yeoh KW. Cancer and radiation therapy: current advances and future directions. Int J Med Sci. 2012;9(3):193-9.
44. Thariat J, Hannoun-Levi J-M, Sun Myint A, Vuong T, Gérard J-P. Past, present, and future of radiotherapy for the benefit of patients. Nature Reviews Clinical Oncology. 2013;10(1):52-60.
45. Galluzzi L, Kepp O, Kroemer G. Immunogenic cell death in radiation therapy. Oncoimmunology. 2013;2(10):e26536.
46. DeVita VT, Jr., Chu E. A History of Cancer Chemotherapy. Cancer Research. 2008;68(21):8643-53.
47. Behranvand N, Nasri F, Zolfaghari Emameh R, Khani P, Hosseini A, Garssen J, et al. Chemotherapy: a double-edged sword in cancer treatment. Cancer Immunology, Immunotherapy. 2022;71(3):507-26.
48. Roos WP, Kaina B. DNA damage-induced cell death by apoptosis. Trends in Molecular Medicine. 2006;12(9):440-50.
49. Nitiss JL. Targeting DNA topoisomerase II in cancer chemotherapy. Nature Reviews Cancer. 2009;9(5):338-50.
50. Malhotra V, Perry MC. Classical Chemotherapy: Mechanisms, Toxicities and the Therapeutc Window. Cancer Biology & Therapy. 2003;2(sup1):1-3.
51. Zugazagoitia J, Guedes C, Ponce S, Ferrer I, Molina-Pinelo S, Paz-Ares L. Current Challenges in Cancer Treatment. Clinical Therapeutics. 2016;38(7):1551-66.
52. Oiseth SJ, Aziz MS. Cancer immunotherapy: a brief review of the history, possibilities, and challenges ahead. Journal of Cancer Metastasis and Treatment. 2017;3:250-61.
53. McCarthy EF. The toxins of William B. Coley and the treatment of bone and soft-tissue sarcomas. Iowa Orthop J. 2006;26:154-8.
54. Waldman AD, Fritz JM, Lenardo MJ. A guide to cancer immunotherapy: from T cell basic science to clinical practice. Nature Reviews Immunology. 2020;20(11):651-68.
55. Pardoll DM. The blockade of immune checkpoints in cancer immunotherapy. Nature reviews Cancer. 2012;12(4):252-64.
56. Maleki Vareki S. High and low mutational burden tumors versus immunologically hot and cold tumors and response to immune checkpoint inhibitors. Journal for ImmunoTherapy of Cancer. 2018;6(1):157.
57. Vitale I, Yamazaki T, Wennerberg E, Sveinbjornsson B, Rekdal O, Demaria S, et al. Targeting cancer heterogeneity with immune responses driven by oncolytic peptides. Trends Cancer. 2021;7(6):557-72.
58. Galluzzi L, Vitale I, Warren S, Adjemian S, Agostinis P, Martinez AB, et al. Consensus guidelines for the definition, detection and interpretation of immunogenic cell death. J Immunother Cancer. 2020;8(1).
59. Kepp O, Marabelle A, Zitvogel L, Kroemer G. Oncolysis without viruses — inducing systemic anticancer immune responses with local therapies. Nature Reviews Clinical Oncology. 2020;17(1):49-64.
60. Spicer J, Marabelle A, Baurain J-F, Jebsen NL, Jøssang DE, Awada A, et al. Safety, Antitumor Activity, and T-cell Responses in a Dose-Ranging Phase I Trial of the Oncolytic Peptide LTX-315 in Patients with Solid Tumors. Clinical Cancer Research. 2021;27(10):2755-63.

61. Mauseth B, Camilio KA, Shi J, Hammarstrom CL, Rekdal O, Sveinbjornsson B, et al. The novel oncolytic compound LTX-401 induces antitumor immune responses in experimental hepatocellular carcinoma. Mol Ther Oncolytics. 2019;14:139-48.
62. Pol J, Kroemer G, Galluzzi L. First oncolytic virus approved for melanoma immunotherapy. Oncoimmunology. 2016;5(1):e1115641.
63. Jebsen NL, Apelseth TO, Haugland HK, Rekdal Ø, Patel H, Gjertsen BT, et al. Enhanced T-lymphocyte infiltration in a desmoid tumor of the thoracic wall in a young woman treated with intratumoral injections of the oncolytic peptide LTX-315: a case report. Journal of Medical Case Reports. 2019;13(1):177.
64. Zhou H, Mondragón L, Xie W, Mauseth B, Leduc M, Sauvat A, et al. Oncolysis with DTT-205 and DTT-304 generates immunological memory in cured animals. Cell Death & Disease. 2018;9(11):1086.
65. Pasquereau-Kotula E, Habault J, Kroemer G, Poyet JL. The anticancer peptide RT53 induces immunogenic cell death. PloS one. 2018;13(8):e0201220.
66. Johnson DE, Burtness B, Leemans CR, Lui VWY, Bauman JE, Grandis JR. Head and neck squamous cell carcinoma. Nature Reviews Disease Primers. 2020;6(1):92.
67. Johnson N. Tobacco Use and Oral Cancer: A Global Perspective. Journal of Dental Education. 2001;65(4):328-39.
68. Sung H, Ferlay J, Siegel RL, Laversanne M, Soerjomataram I, Jemal A, et al. Global cancer statistics 2020: GLOBOCAN estimates of incidence and mortality worldwide for 36 cancers in 185 countries. CA Cancer J Clin. 2021;71(3):209-49.
69. Gillison ML, Chaturvedi AK, Anderson WF, Fakhry C. Epidemiology of Human Papillomavirus-Positive Head and Neck Squamous Cell Carcinoma. J Clin Oncol. 2015;33(29):3235-42.
70. Tsentemeidou A, Fyrmpas G, Stavrakas M, Vlachtsis K, Sotiriou E, Poutoglidis A, et al. Human Papillomavirus Vaccine to End Oropharyngeal Cancer. A Systematic Review and Meta-Analysis. Sexually Transmitted Diseases. 2021;48(9).
71. Gameiro SF, Ghasemi F, Barrett JW, Koropatnick J, Nichols AC, Mymryk JS, et al. Treatment-naïve HPV+ head and neck cancers display a T-cell-inflamed phenotype distinct from their HPV- counterparts that has implications for immunotherapy. Oncoimmunology. 2018;7(10):e1498439.
72. Ribbat-Idel J, Perner S, Kuppler P, Klapper L, Krupar R, Watermann C, et al. Immunologic “Cold” Squamous Cell Carcinomas of the Head and Neck Are Associated With an Unfavorable Prognosis. Frontiers in Medicine. 2021;8.
73. Heijnen BJ, Speyer R, Kertscher B, Cordier R, Koetsenruijter KWJ, Swan K, et al. Dysphagia, Speech, Voice, and Trismus following Radiotherapy and/or Chemotherapy in Patients with Head and Neck Carcinoma: Review of the Literature. BioMed Research International. 2016;2016:6086894.
74. Wang C, Liu XQ, Hou JS, Wang JN, Huang HZ. Molecular Mechanisms of Chemoresistance in Oral Cancer. Chin J Dent Res. 2016;19(1):25-33.
75. Andreassen R, Jönsson B, Hadler-Olsen E. Oral health related quality of life in long-term survivors of head and neck cancer compared to a general population from the seventh Tromsø study. BMC Oral Health. 2022;22(1):100.
76. Galluzzi L, Vitale I, Aaronson SA, Abrams JM, Adam D, Agostinis P, et al. Molecular mechanisms of cell death: recommendations of the Nomenclature Committee on Cell Death 2018. Cell Death Differ. 2018;25(3):486-541.
77. Danial NN, Korsmeyer SJ. Cell Death: Critical Control Points. Cell. 2004;116(2):205-19.
78. Cao X, Hou J, An Q, Assaraf YG, Wang X. Towards the overcoming of anticancer drug resistance mediated by p53 mutations. Drug Resistance Updates. 2020;49:100671.

79. Kroemer G, Martin SJ. Caspase-independent cell death. Nature medicine. 2005;11(7):725-30.
80. Segawa K, Nagata S. An Apoptotic 'Eat Me' Signal: Phosphatidylserine Exposure. Trends in Cell Biology. 2015;25(11):639-50.
81. Birge RB, Boeltz S, Kumar S, Carlson J, Wanderley J, Calianese D, et al. Phosphatidylserine is a global immunosuppressive signal in efferocytosis, infectious disease, and cancer. Cell Death Differ. 2016;23(6):962-78.
82. Fuchs Y, Steller H. Live to die another way: modes of programmed cell death and the signals emanating from dying cells. Nature Reviews Molecular Cell Biology. 2015;16(6):329-44.
83. Vanden Berghe T, Vanlangenakker N, Parthoens E, Deckers W, Devos M, Festjens N, et al. Necroptosis, necrosis and secondary necrosis converge on similar cellular disintegration features. Cell Death Differ. 2010;17(6):922-30.
84. Conrad M, Angeli JPF, Vandenabeele P, Stockwell BR. Regulated necrosis: disease relevance and therapeutic opportunities. Nature Reviews Drug Discovery. 2016;15(5):348-66.
85. Krysko O, Aaes TL, Kagan VE, D'Herde K, Bachert C, Leybaert L, et al. Necroptotic cell death in anti-cancer therapy. Immunol Rev. 2017;280(1):207-19.
86. Scaffidi P, Misteli T, Bianchi ME. Release of chromatin protein HMGB1 by necrotic cells triggers inflammation. Nature. 2002;418(6894):191-5.
87. Obeid M, Tesniere A, Ghiringhelli F, Fimia GM, Apetoh L, Perfettini JL, et al. Calreticulin exposure dictates the immunogenicity of cancer cell death. Nat Med. 2007;13(1):54-61.
88. Casares N, Pequignot MO, Tesniere A, Ghiringhelli F, Roux S, Chaput N, et al. Caspase-dependent immunogenicity of doxorubicin-induced tumor cell death. J Exp Med. 2005;202(12):1691-701.
89. Pozzi C, Cuomo A, Spadoni I, Magni E, Silvola A, Conte A, et al. The EGFR-specific antibody cetuximab combined with chemotherapy triggers immunogenic cell death. Nat Med. 2016;22(6):624-31.
90. Donnelly OG, Errington-Mais F, Steele L, Hadac E, Jennings V, Scott K, et al. Measles virus causes immunogenic cell death in human melanoma. Gene Ther. 2013;20(1):7-15.
91. Zhou H, Forveille S, Sauvat A, Yamazaki T, Senovilla L, Ma Y, et al. The oncolytic peptide LTX-315 triggers immunogenic cell death. Cell Death Dis. 2016;7(3):e2134.
92. Xie W, Mondragón L, Mauseth B, Wang Y, Pol J, Lévesque S, et al. Tumor lysis with LTX-401 creates anticancer immunity. Oncoimmunology. 2019;8(7):1594555.
93. Yang H, Ma Y, Chen G, Zhou H, Yamazaki T, Klein C, et al. Contribution of RIP3 and MLKL to immunogenic cell death signaling in cancer chemotherapy. Oncoimmunology. 2016;5(6):e1149673.
94. Forveille S, Zhou H, Sauvat A, Bezu L, Muller K, Liu P, et al. The oncolytic peptide LTX-315 triggers necrotic cell death. Cell cycle (Georgetown, Tex). 2015;14(21):3506-12.
95. Galluzzi L, Buque A, Kepp O, Zitvogel L, Kroemer G. Immunogenic cell death in cancer and infectious disease. Nat Rev Immunol. 2017;17(2):97-111.
96. Kroemer G, Galluzzi L, Kepp O, Zitvogel L. Immunogenic cell death in cancer therapy. Annu Rev Immunol. 2013;31:51-72.
97. Johnson S, Michalak M, Opas M, Eggleton P. The ins and outs of calreticulin: from the ER lumen to the extracellular space. Trends in Cell Biology. 2001;11(3):122-9.
98. Garg AD, Krysko DV, Verfaillie T, Kaczmarek A, Ferreira GB, Marysael T, et al. A novel pathway combining calreticulin exposure and ATP secretion in immunogenic cancer cell death. EMBO J. 2012;31(5):1062-79.

99. Bezu L, Sauvat A, Humeau J, Gomes-da-Silva LC, Iribarren K, Forveille S, et al. eIF2α phosphorylation is pathognomonic for immunogenic cell death. Cell Death & Differentiation. 2018;25(8):1375-93.
100. Michaud M, Martins I, Sukkurwala AQ, Adjemian S, Ma Y, Pellegatti P, et al. Autophagy-Dependent Anticancer Immune Responses Induced by Chemotherapeutic Agents in Mice. Science. 2011;334(6062):1573.
101. Ghiringhelli F, Apetoh L, Tesniere A, Aymeric L, Ma Y, Ortiz C, et al. Activation of the NLRP3 inflammasome in dendritic cells induces IL-1β–dependent adaptive immunity against tumors. Nature medicine. 2009;15(10):1170-8.
102. Apetoh L, Ghiringhelli F, Tesniere A, Obeid M, Ortiz C, Criollo A, et al. Toll-like receptor 4-dependent contribution of the immune system to anticancer chemotherapy and radiotherapy. Nat Med. 2007;13(9):1050-9.
103. Aits S, Jäättelä M. Lysosomal cell death at a glance. Journal of Cell Science. 2013;126(9):1905-12.
104. Boya P, Kroemer G. Lysosomal membrane permeabilization in cell death. Oncogene. 2008;27(50):6434-51.
105. Nadanaciva S, Lu S, Gebhard DF, Jessen BA, Pennie WD, Will Y. A high content screening assay for identifying lysosomotropic compounds. Toxicol In Vitro. 2011;25(3):715-23.
106. Altan N, Chen Y, Schindler M, Simon SM. Defective acidification in human breast tumor cells and implications for chemotherapy. J Exp Med. 1998;187(10):1583-98.
107. Ndolo RA, Forrest ML, Krise JP. The role of lysosomes in limiting drug toxicity in mice. J Pharmacol Exp Ther. 2010;333(1):120-8.
108. Zhitomirsky B, Assaraf YG. Lysosomes as mediators of drug resistance in cancer. Drug Resistance Updates. 2016;24:23-33.
109. Jiang LW, Maher VM, McCormick JJ, Schindler M. Alkalinization of the lysosomes is correlated with ras transformation of murine and human fibroblasts. Journal of Biological Chemistry. 1990;265(9):4775-7.
110. Dikic I, Elazar Z. Mechanism and medical implications of mammalian autophagy. Nature Reviews Molecular Cell Biology. 2018;19(6):349-64.
111. Pankiv S, Clausen TH, Lamark T, Brech A, Bruun J-A, Outzen H, et al. p62/SQSTM1 binds directly to Atg8/LC3 to facilitate degradation of ubiquitinated protein aggregates by autophagy. Journal of biological chemistry. 2007;282(33):24131-45.
112. Solitro AR, MacKeigan JP. Leaving the lysosome behind: novel developments in autophagy inhibition. Future Med Chem. 2016;8(1):73-86.
113. Kim YH, Kwak MS, Lee B, Shin JM, Aum S, Park IH, et al. Secretory autophagy machinery and vesicular trafficking are involved in HMGB1 secretion. Autophagy. 2021;17(9):2345-62.
114. Kroemer G, Levine B. Autophagic cell death: the story of a misnomer. Nat Rev Mol Cell Biol. 2008;9(12):1004-10.
115. Fleten KG, Eksteen JJ, Mauseth B, Camilio KA, Vasskog T, Sveinbjørnsson B, et al. Oncolytic peptides DTT-205 and DTT-304 induce complete regression and protective immune response in experimental murine colorectal cancer. Scientific Reports. 2021;11(1):6731.
116. Eike LM, Mauseth B, Camilio KA, Rekdal Ø, Sveinbjørnsson B. The Cytolytic Amphipathic β(2,2)-Amino Acid LTX-401 Induces DAMP Release in Melanoma Cells and Causes Complete Regression of B16 Melanoma. PloS one. 2016;11(2):e0148980.
117. Camilio KA, Berge G, Ravuri CS, Rekdal O, Sveinbjørnsson B. Complete regression and systemic protective immune responses obtained in B16 melanomas after treatment with LTX-315. Cancer Immunol Immunother. 2014;63(6):601-13.

118. Pemovska T, Kontro M, Yadav B, Edgren H, Eldfors S, Szwajda A, et al. Individualized Systems Medicine Strategy to Tailor Treatments for Patients with Chemorefractory Acute Myeloid Leukemia. Cancer Discovery. 2013;3(12):1416-29.
119. Wang L, Sun J, Horvat M, Koutalistras N, Johnston B, Ross Sheil AG. Evaluation of MTS, XTT, MTT and3HTdR incorporation for assessing hepatocyte density, viability and proliferation. Methods in Cell Science. 1996;18(3):249-55.
120. Rai Y, Pathak R, Kumari N, Sah DK, Pandey S, Kalra N, et al. Mitochondrial biogenesis and metabolic hyperactivation limits the application of MTT assay in the estimation of radiation induced growth inhibition. Sci Rep. 2018;8(1):1531.
121. Nowak E, Kammerer S, Küpper J-H. ATP-based cell viability assay is superior to trypan blue exclusion and XTT assay in measuring cytotoxicity of anticancer drugs Taxol and Imatinib, and proteasome inhibitor MG-132 on human hepatoma cell line HepG2. Clinical Hemorheology and Microcirculation. 2018;69:327-36.
122. Freshney IA. Defined Media and Supplements. Culture of Animal Cells2010. p. 99-114.
123. Vermes I, Haanen C, Steffens-Nakken H, Reutellingsperger C. A novel assay for apoptosis Flow cytometric detection of phosphatidylserine expression on early apoptotic cells using fluorescein labelled Annexin V. Journal of Immunological Methods. 1995;184(1):39-51.
124. Adan A, Alizada G, Kiraz Y, Baran Y, Nalbant A. Flow cytometry: basic principles and applications. Critical Reviews in Biotechnology. 2017;37(2):163-76.
125. Viola G, Grobelny P, Linardi MA, Salvador A, Basso G, Mielcarek J, et al. The Phototoxicity of Fluvastatin, an HMG-CoA Reductase Inhibitor, Is Mediated by the formation of a Benzocarbazole-Like Photoproduct. Toxicological Sciences. 2010;118(1):236-50.
126. Jalilzadeh N, Samadi N, Salehi R, Dehghan G, Iranshahi M, Dadpour MR, et al. Novel nano-vehicle for delivery and efficiency of anticancer auraptene against colon cancer cells. Scientific Reports. 2020;10(1):1606.
127. Gu X, Wang Z, Gao J, Han D, Zhang L, Chen P, et al. SIRT1 suppresses p53-dependent apoptosis by modulation of p21 in osteoblast-like MC3T3-E1 cells exposed to fluoride. Toxicology in Vitro. 2019;57:28-38.
128. Zhou H, Sauvat A, Gomes-da-Silva LC, Durand S, Forveille S, Iribarren K, et al. The oncolytic compound LTX-401 targets the Golgi apparatus. Cell Death Differ. 2016;23(12):2031-41.
129. Liu CC, Leclair P, Monajemi M, Sly LM, Reid GS, Lim CJ. α-Integrin expression and function modulates presentation of cell surface calreticulin. Cell Death & Disease. 2016;7(6):e2268-e.
130. Zhang Y, Yang S, Yang Y, Liu T. Resveratrol induces immunogenic cell death of human and murine ovarian carcinoma cells. Infectious Agents and Cancer. 2019;14(1):27.
131. Liu P, Zhao L, Kepp O, Kroemer G. Quantitation of calreticulin exposure associated with immunogenic cell death. Methods in enzymology. 2020;632:1-13.
132. Humeau J, Lévesque S, Kroemer G, Pol JG. Gold Standard Assessment of Immunogenic Cell Death in Oncological Mouse Models. In: López-Soto A, Folgueras AR, editors. Cancer Immunosurveillance: Methods and Protocols. New York, NY: Springer New York; 2019. p. 297-315.
133. Liu CH, Lin CH, Tsai MJ, Chen YH, Yang SF, Tsai KB. Melanin Bleaching With Warm Hydrogen Peroxide and Integrated Immunohistochemical Analysis: An Automated Platform. Int J Surg Pathol. 2018;26(5):410-6.

134. Zhou H, Tu C, Yang P, Li J, Kepp O, Li H, et al. Carbon ion radiotherapy triggers immunogenic cell death and sensitizes melanoma to anti-PD-1 therapy in mice. Oncoimmunology. 2022;11(1):2057892.
135. Camilio KA, Wang M-Y, Mauseth B, Waagene S, Kvalheim G, Rekdal Ø, et al. Combining the oncolytic peptide LTX-315 with doxorubicin demonstrates therapeutic potential in a triple-negative breast cancer model. Breast Cancer Research. 2019;21(1):9.
136. Utsugi T, Schroit AJ, Connor J, Bucana CD, Fidler IJ. Elevated expression of phosphatidylserine in the outer membrane leaflet of human tumor cells and recognition by activated human blood monocytes. Cancer Res. 1991;51(11):3062-6.
137. Hilton KLF, Manwani C, Boles JE, White LJ, Ozturk S, Garrett MD, et al. The phospholipid membrane compositions of bacterial cells, cancer cell lines and biological samples from cancer patients. Chem Sci. 2021;12(40):13273-82.
138. Boohaker RJ, Lee MW, Vishnubhotla P, Perez JM, Khaled AR. The use of therapeutic peptides to target and to kill cancer cells. Curr Med Chem. 2012;19(22):3794-804.
139. Sveinbjørnsson B, Camilio KA, Haug BE, Rekdal Ø. LTX-315: a first-in-class oncolytic peptide that reprograms the tumor microenvironment. Future Medicinal Chemistry. 2017;9(12):1339-44.
140. Klaiss-Luna MC, Jemioła-Rzemińska M, Strzałka K, Manrique-Moreno M. Understanding the Biophysical Interaction of LTX-315 with Tumoral Model Membranes. Int J Mol Sci. 2022;24(1).
141. Marceau F, Bawolak MT, Lodge R, Bouthillier J, Gagne-Henley A, Gaudreault RC, et al. Cation trapping by cellular acidic compartments: beyond the concept of lysosomotropic drugs. Toxicol Appl Pharmacol. 2012;259(1):1-12.
142. Völgyi G, Baka E, Box KJ, Comer JEA, Takács-Novák K. Study of pH-dependent solubility of organic bases. Revisit of Henderson-Hasselbalch relationship. Analytica Chimica Acta. 2010;673(1):40-6.
143. Bechinger B, Lohner K. Detergent-like actions of linear amphipathic cationic antimicrobial peptides. Biochimica et Biophysica Acta (BBA) - Biomembranes. 2006;1758(9):1529-39.
144. Vukovic V, Tannock IF. Influence of low pH on cytotoxicity of paclitaxel, mitoxantrone and topotecan. Br J Cancer. 1997;75(8):1167-72.
145. Gerweck LE, Vijayappa S, Kozin S. Tumor pH controls the in vivo efficacy of weak acid and base chemotherapeutics. Molecular Cancer Therapeutics. 2006;5(5):1275-9.
146. Yoshimori T, Yamamoto A, Moriyama Y, Futai M, Tashiro Y. Bafilomycin A1, a specific inhibitor of vacuolar-type H(+)-ATPase, inhibits acidification and protein degradation in lysosomes of cultured cells. Journal of Biological Chemistry. 1991;266(26):17707-12.
147. Modica-Napolitano JS, Aprille JR. Delocalized lipophilic cations selectively target the mitochondria of carcinoma cells. Advanced Drug Delivery Reviews. 2001;49(1):63-70.
148. Zhou H, Forveille S, Sauvat A, Sica V, Izzo V, Durand S, et al. The oncolytic peptide LTX-315 kills cancer cells through Bax/Bak-regulated mitochondrial membrane permeabilization. Oncotarget. 2015;6(29):26599-614.
149. Schotte P, Declercq W, Van Huffel S, Vandenabeele P, Beyaert R. Non-specific effects of methyl ketone peptide inhibitors of caspases. FEBS Lett. 1999;442(1):117-21.
150. Rozman-Pungerčar J, Kopitar-Jerala N, Bogyo M, Turk D, Vasiljeva O, Štefe I, et al. Inhibition of papain-like cysteine proteases and legumain by caspase-specific inhibitors: when reaction mechanism is more important than specificity. Cell Death & Differentiation. 2003;10(8):881-8.

151. Taylor RC, Cullen SP, Martin SJ. Apoptosis: controlled demolition at the cellular level. Nature Reviews Molecular Cell Biology. 2008;9(3):231-41.
152. Iyer SS, Pulskens WP, Sadler JJ, Butter LM, Teske GJ, Ulland TK, et al. Necrotic cells trigger a sterile inflammatory response through the Nlrp3 inflammasome. Proceedings of the National Academy of Sciences of the United States of America. 2009;106(48):20388-93.
153. Schneider T, Hoffmann H, Dienemann H, Herpel E, Heussel CP, Enk AH, et al. Immune Response After Radiofrequency Ablation and Surgical Resection in Nonsmall Cell Lung Cancer. Seminars in Thoracic and Cardiovascular Surgery. 2016;28(2):585-92.
154. Kepp O, Zitvogel L, Kroemer G. Clinical evidence that immunogenic cell death sensitizes to PD-1/PD-L1 blockade. Oncoimmunology. 2019;8(10):e1637188.
155. Dewan MZ, Galloway AE, Kawashima N, Dewyngaert JK, Babb JS, Formenti SC, et al. Fractionated but not single-dose radiotherapy induces an immune-mediated abscopal effect when combined with anti-CTLA-4 antibody. Clin Cancer Res. 2009;15(17):5379-88.
156. Yamazaki T, Pitt JM, Vétizou M, Marabelle A, Flores C, Rekdal Ø, et al. The oncolytic peptide LTX-315 overcomes resistance of cancers to immunotherapy with CTLA4 checkpoint blockade. Cell Death & Differentiation. 2016;23(6):1004-15.
157. Kamb A, Wee S, Lengauer C. Why is cancer drug discovery so difficult? Nature Reviews Drug Discovery. 2007;6(2):115-20.
158. Marabelle A, Andtbacka R, Harrington K, Melero I, Leidner R, de Baere T, et al. Starting the fight in the tumor: expert recommendations for the development of human intratumoral immunotherapy (HIT-IT). Ann Oncol. 2018;29(11):2163-74.
159. Sha D, Jin Z, Budczies J, Kluck K, Stenzinger A, Sinicrope FA. Tumor Mutational Burden as a Predictive Biomarker in Solid Tumors. Cancer Discovery. 2020;10(12):1808-25.
160. Galluzzi L, Pietrocola F, Bravo-San Pedro JM, Amaravadi RK, Baehrecke EH, Cecconi F, et al. Autophagy in malignant transformation and cancer progression. EMBO J. 2015;34(7):856-80.
161. Lazova R, Camp RL, Klump V, Siddiqui SF, Amaravadi RK, Pawelek JM. Punctate LC3B Expression Is a Common Feature of Solid Tumors and Associated with Proliferation, Metastasis, and Poor Outcome. Clinical Cancer Research. 2012;18(2):370-9.
162. Manic G, Obrist F, Kroemer G, Vitale I, Galluzzi L. Chloroquine and hydroxychloroquine for cancer therapy. Molecular & Cellular Oncology. 2014;1(1):e29911.
163. Yamamoto K, Venida A, Yano J, Biancur DE, Kakiuchi M, Gupta S, et al. Autophagy promotes immune evasion of pancreatic cancer by degrading MHC-I. Nature. 2020;581(7806):100-5.
164. Tian A-L, Wu Q, Liu P, Zhao L, Martins I, Kepp O, et al. Lysosomotropic agents including azithromycin, chloroquine and hydroxychloroquine activate the integrated stress response. Cell Death Dis. 2021;12(1):6.

Paper I

scientific reports

Check for updates

OPEN

The marine natural product mimic MPM-1 is cytolytic and induces DAMP release from human cancer cell lines

Susannah von Hofsten[1]✉, Marianne Hagensen Paulsen[2], Synnøve Norvoll Magnussen[1], Dominik Ausbacher[2], Mathias Kranz[3], Annette Bayer[4], Morten B. Strøm[2] & Gerd Berge[1]

Bioprospecting contributes to the discovery of new molecules with anticancer properties. Compounds with cytolytic activity and the ability to induce immunogenic cell death can be administered as intratumoral injections with the aim to activate anti-tumor immune responses by causing the release of tumor antigens as well as damage-associated molecular patterns (DAMPs) from dying cancer cells. In the present study, we report the cytolytic and DAMP-releasing effects of a new natural product mimic termed MPM-1 that was inspired by the marine *Eusynstyelamides*. We found that MPM-1 rapidly killed cancer cells in vitro by inducing a necrosis-like death, which was accompanied by lysosomal swelling and perturbation of autophagy in HSC-3 (human oral squamous cell carcinoma) cells. MPM-1 also induced release of the DAMPs adenosine triphosphate (ATP) and high mobility group box 1 (HMGB1) from Ramos (B-cell lymphoma) and HSC-3 cells, as well as cell surface expression of calreticulin in HSC-3 cells. This indicates that MPM-1 has the ability to induce immunogenic cell death, further suggesting that it may have potential as a novel anticancer compound.

Cancer remains one of the leading causes of death worldwide despite major advances within the field of cancer treatment during recent years[1]. In addition to drug resistance and severe side effects, intratumoral heterogeneity is becoming recognized as a major obstacle for development of novel effective therapies. In this context, cytolytic therapies inducing immunogenic cell death, a specific type of cell death that activates immune responses, are rising as promising new therapeutic tools[2]. Treatment with cytolytic compounds is a novel and attractive option since these can be administered intratumorally, minimizing the effect on healthy cells, while causing the release of tumor antigens from dying cancer cells. Cytolytic compounds that induce immunogenic cell death cause release of damage-associated molecular patterns (DAMPs) into the tumor microenvironment, triggering an immune response. Specifically, surface expression of calreticulin, release of ATP and release of high mobility group box 1 (HMGB1) are generally considered the hallmarks of immunogenic cell death[3]. These DAMPs have recruiting and activating effects on cells of the innate immune system, which can recognize the released tumor antigens. Among these are dendritic cells and macrophages, which upon activation can initiate an adaptive immune response, ultimately leading to the activation of cytotoxic $CD8^+$ T cells that recognize and kill cancer cells.

Immunogenic cell death can be induced by several different types of compounds and other cell stressors, which may have different cellular targets. This includes for example conventional DNA-binding agents such as doxorubicin and mitoxantrone[4,5], some targeted anti-cancer therapies[6], therapeutic oncolytic viruses[7], and physical stressors such as ionizing radiation[8]. We have previously shown that the cytolytic peptides LTX-302 and LTX-315 are able to activate adaptive anti-tumor immune responses in mice[9,10]. We have also reported on the cytolytic activity of the ultra-short peptidomimetic LTX-401 (initially reported as BAA-1)[11], which was recently shown to induce immunogenic cell death in vivo[12,13]. In the present study, we have investigated the cytolytic and immunogenic effects of the novel marine natural product mimic MPM-1.

MPM-1 is a synthetic and simplified mimic of a group of marine bioactive compounds referred to as the *eusynstyelamides,* which have previously been isolated from arctic bryozoans (Fig. 1)[14]. The *eusynstyelamides* mainly show antimicrobial activity, and fulfill the minimum pharmacophore model of small cationic

[1]Department of Medical Biology, Faculty of Health Sciences, UiT The Arctic University of Norway, 9037 Tromsø, Norway. [2]Department of Pharmacy, Faculty of Health Sciences, UiT The Arctic University of Norway, 9037 Tromsø, Norway. [3]PET Imaging Center Tromsø, University Hospital of North Norway, 9019 Tromsø, Norway. [4]Department of Chemistry, UiT The Arctic University of Norway, 9037 Tromsø, Norway. ✉email: susannah.hofsten@uit.no

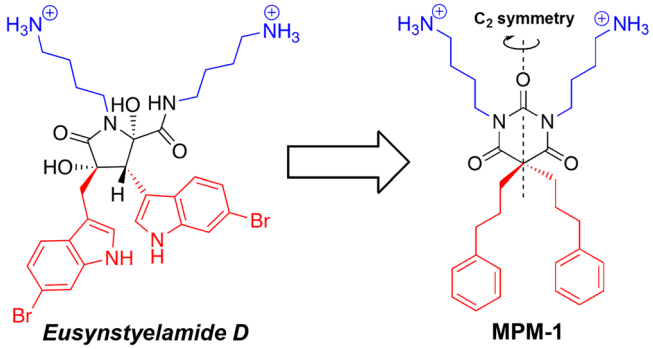

Figure 1. Molecular structures of the marine antimicrobial *Eusynstyelamide D* and the novel marine natural product mimic MPM-1. Cationic groups are colored blue and lipophilic groups are colored red to highlight the amphipathic arrangement in both molecules.

antimicrobial peptides by having an amphipathic structure consisting of two cationic and two lipophilic/bulky groups[15]. However, the *eusynstyelamides* are challenging to synthesize due to the complex five-membered dihydroxybutyrolactam ring. Recently, we have reported a class of simplified mimics of the *eusynstyelamides*, where the complex dihydroxybutyrolactam ring is replaced by a barbiturate scaffold[16,17]. This scaffold is rigid and can easily be modified with different cationic and lipophilic groups. Moreover, the barbiturate scaffold has C_2 symmetry and no stereogenic centers, which implies that synthesis of these compounds will not produce any unwanted stereoisomers of the intended compound. A library of barbiturate *eusynstyelamide* mimics including MPM-1 was created, originally intended as antimicrobial agents. However, during pilot screening experiments, MPM-1 stood out from the other compounds by being able to kill selected cancer cell lines efficiently while showing negligible antimicrobial activity (Bayer and Strøm, unpublished results).

The aim of the present study was to perform an expanded screening of the anti-cancer effect of MPM-1 in addition to studying its mechanism-of-action and ability to induce DAMP release. This represents the first step in elucidating the clinical potential of MPM-1 as a cytolytic compound intended for intratumoral immunotherapy.

Results

Synthesis of MPM-1. MPM-1 was synthesized based on a procedure previously developed by our group, with some modifications (Fig. 2)[16]. The overall strategy for synthesis of MPM-1 involved dialkylation of malonate ester **1** to attach the lipophilic side chains (giving **2** or **3** as described below), reaction with urea to form the barbiturate scaffold (**4**), *N*-alkylation of the barbiturate (**5**), followed by azide conversion (**6**), and final reduction of the azide groups to give MPM-1.

Two different alkylation reagents were tested to give the dialkylated malonate ester **3**; 1-bromo-3-phenylpropane and 3-bromo-1-phenyl-1-propene. Dialkylation of the malonate ester **1** with 1-bromo-3-phenylpropane gave a mixture of starting material, mono and dialkylated malonate ester (**3**), which proved difficult to separate using flash chromatography. Both the weak base potassium carbonate (K_2CO_3) and the stronger base sodium hydride (NaH) were tested as a base in the reaction. Neither of the two bases gave satisfying amounts of the dialkylated malonate ester **3,** so an alternative route was explored. In the second route we used 3-bromo-1-phenyl-1-propene as the alkylating agent, which gave the dialkylated malonate ester **2** in high yield (97%) but involved an additional hydrogenation step to achieve **3** (67% overall yield). The dialkylated malonate ester (**3**) was further condensed with urea to give barbiturate **4** (65% yield). *N*,*N*-Dialkylation of **4** using an excess of 1,4-dibromobutane under basic conditions gave **5** in 70% yield. The *N*,*N*′-dialkylated barbiturate **5** was converted to the corresponding azide derivative **6** using sodium azide (NaN_3) (99% yield). Reduction of the azide groups in **6** with a catalytic amount of propane-1,3-dithiol and sodium borohydride ($NaBH_4$), and subsequent Boc-protection with Boc_2O and Boc deprotection with 2,2,2-trifluoroacetic acid (TFA) gave the target molecule MPM-1 in 53% yield. Of note, the Boc-protection and Boc-deprotection steps were necessary in order to ease purification by flash chromatography and increasing the purity of MPM-1. NMR data for the synthesis can be found as Supplementary Data S1.

MPM-1 is cytotoxic to a large selection of cancer cell lines. The cytotoxic effect of MPM-1 was assessed by determining its IC50 value for a panel of cell lines (Table 1 and Supplementary Fig. S1). The panel represented a selection of cancerous, non-cancerous, adherent, non-adherent, and multidrug resistant cells. As a preliminary measurement of drug toxicity, the hemolytic activity of MPM-1 was also measured. MPM-1 had no hemolytic activity against human red blood cells (IC50 > 500 μM), but effectively killed all other cell types tested. The obtained IC50 values were of similar magnitude, ranging from 4.13 μM for PBMCs to 18.54 μM for MRC-5. Apart from the lack of hemolysis of human red blood cells, there was no trend towards selectivity for cancerous over non-cancerous cell lines. For this reason, our subsequent studies focused mainly on the oral cancer cell line HSC-3, which represents a solid tumor. However, the mean IC50 value for suspension cells was significantly lower than for adherent cell lines (6.09 ± 1.76 vs. 14.00 ± 3.12, $p = 0.002$). Since this could be indicative of MPM-1's mode of action, one adherent (HSC-3) and one suspension (Ramos) cell line was included in

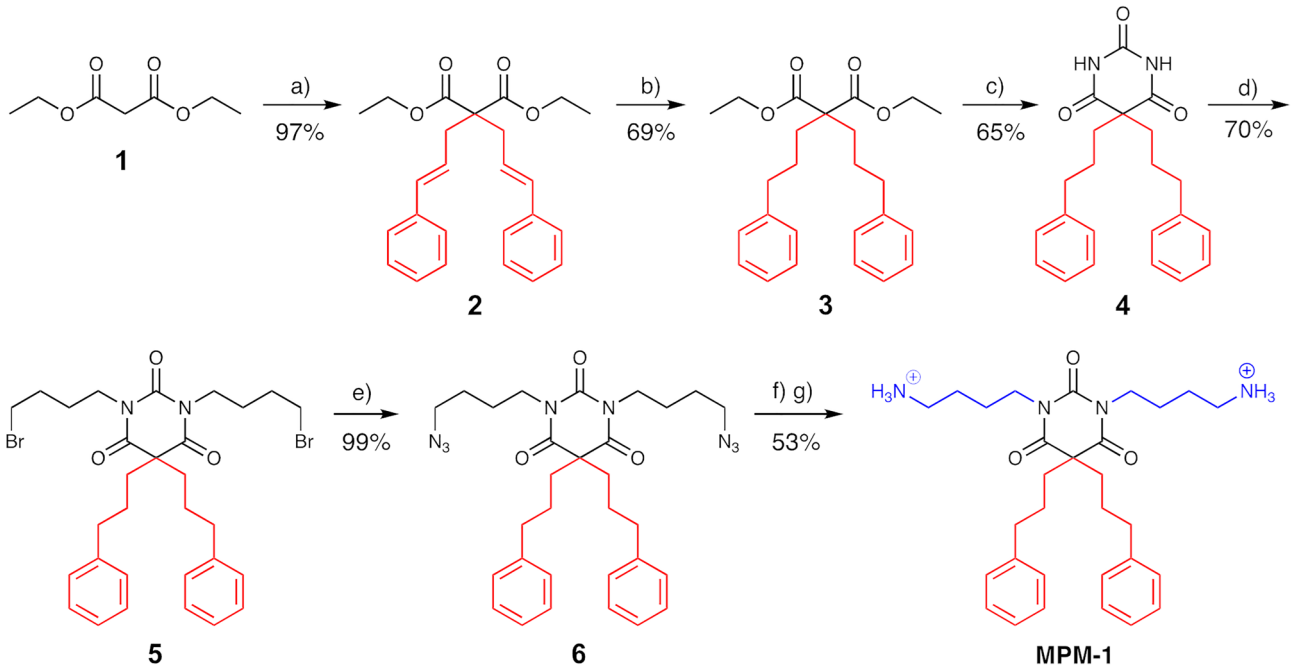

Figure 2. Synthesis of the amphipathic barbiturate MPM-1. Conditions: (**a**) 3-bromo-1-phenyl-1-propene, NaH, DMF, r.t.; (**b**) Pd/C, H_2 (10 bar), r.t.; (**c**) 10 equiv. urea (dry), NaH, DMF (dry), r.t.; (**d**) 10 equiv. 1,4-dibromobutane, 4 equiv. K_2CO_3, DMF (dry), r.t., 18–48 h; (**e**) 3 equiv. NaN_3, DMF (dry); (**f**) i. $NaBH_4$, 1,3-propanedithiol, THF:isopropanol 1:1, r.t.; ii. Boc_2O, r.t.; (**g**) TFA, CH_2Cl_2.

Cell line	Type[a]	Site of origin	IC50 (μM) ± SD
A375	A	Human melanoma	14.52 ± 0.22
HepG2	A	Human hepatocellular carcinoma	17.26 ± 2.50
HSC-3	A	Human oral squamous cell carcinoma	8.53 ± 0.57
HT-29	A	Human colorectal adenocarcinoma	15.68 ± 0.33
SK-N-AS	A	Human neuroblastoma	15.94 ± 0.23
MCF-7	A	Human breast adenocarcinoma (multidrug resistant)	14.06 ± 2.71
Jurkat	S	Human T cell leukemia	6.62 ± 1.60
Ramos	S	Human B cell lymphoma	7.53 ± 2.01
B16F1	A	Murine melanoma	13.72 ± 0.61
GL261-Luc2	A	Murine glioblastoma	11.04 ± 2.88
MRC-5	A	Non-cancerous human lung fibroblast	18.54 ± 2.68
HUVEC	A	Non-cancerous human umbilical endothelium	10.73 ± 3.63
PBMC	S	Human peripheral blood mononuclear cells	4.13 ± 0.31

Table 1. MPM-1 IC50 values obtained from MTS cytotoxicity assays after four hours of incubation. The values represent the mean from three independent experiments ± standard deviation. [a]A = Adherent cells, S = Suspension cells.

several of the mechanistic studies. In these studies, the cells were treated with concentrations of MPM-1 equal to their respective IC50 values or multiples thereof.

The cytotoxicity of MPM-1 is dependent on compound concentration and cell density. To study the effect of treating cells with MPM-1 in different concentrations as well as with different cell densities, live cell imaging of HSC-3 cells treated with MPM-1 was performed. It was found that the density of cells seeded for experiments with MPM-1 greatly affected the cytotoxicity of MPM-1. At approximately 80% confluence (7.5×10^4 cells/cm^2), HSC-3 cells appeared to be dead after six hours when treated with 1xIC50 MPM-1 (Fig. 3). This could be seen from the cells' changed morphology. They became rounded, stopped moving and by 6 h looked completely damaged (Supplementary Video S1). When decreasing the number of cells per well to 5×10^4 cells/cm^2, cell death appeared after only three hours with the same concentration of MPM-1. Increasing the concentration of MPM-1 to 2xIC50, but keeping the original number of cells per well (7.5×10^4 cells/cm^2), also greatly accelerated the rate of cell death, which occurred after only two hours. In contrast, when decreasing

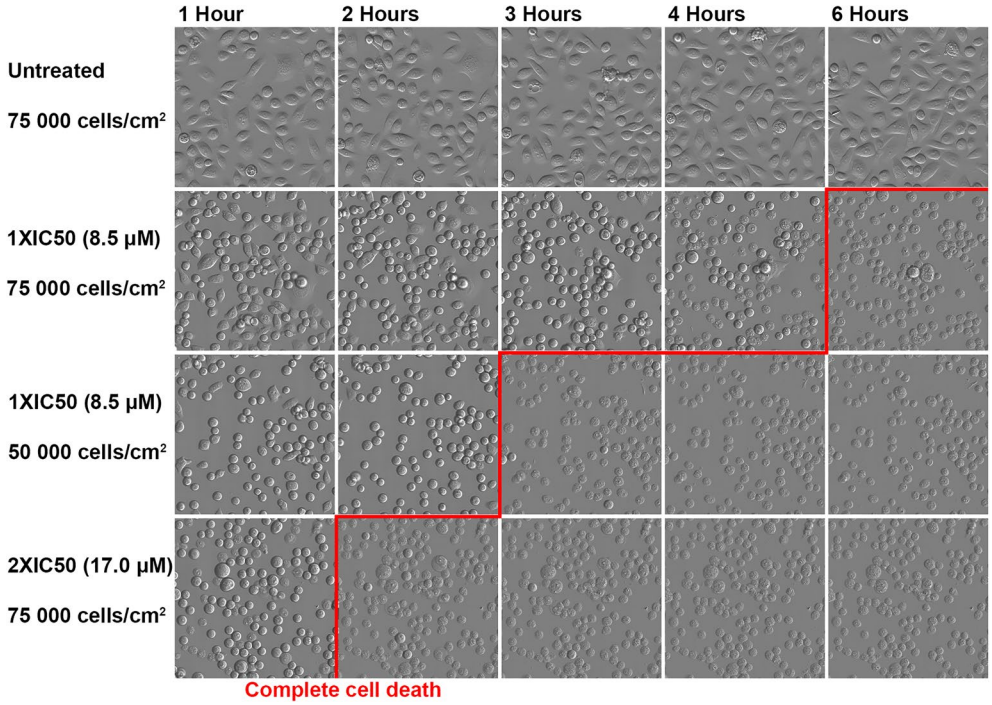

Figure 3. The rate at which MPM-1 kills cells is dependent on concentration and cell density. HSC-3 cells were seeded at different densities, treated with 1xIC50 or 2xIC50 MPM-1, and subsequently imaged continuously.

the concentration of MPM-1 to ½xIC50, reaching complete cell death took approximately 15 h (Supplementary Video S2). This indicates that the cytotoxicity of MPM-1 is directly related to the number of available molecules per cell.

MPM-1 causes vacuolization and necrosis. To study the mode of death induced by MPM-1, HSC-3 and Ramos cells were analyzed for the cell surface exposure of phosphatidylserine (PS), which characterizes apoptosis. This can be detected by staining with fluorescently labeled Annexin V, which binds to PS, and propidium iodide (PI), which only penetrates cells with ruptured cell membranes. Treatment of HSC-3 and Ramos cells with known inducers of apoptosis (Staurosporine and TBTC) resulted in the appearance of a large annexin V^+/PI^- apoptotic population, whereas treatment of cells with MPM-1 did not result in the formation of such a population (Fig. 4a). However, the percentage of PI^+ events did increase, indicating that cells had died, but not from apoptosis.

The mitochondrial membrane potential in cells treated with MPM-1 was also analyzed by flow cytometry, using the fluorescent dye tetramethylrhodamine (TMRE) (Fig. 4b). In healthy cells, the mitochondrial intermembrane space is positively charged, while the mitochondrial matrix is negatively charged. This proton gradient creates a potential, which is referred to as the mitochondrial membrane potential. TMRE is positively charged and therefore accumulates in the mitochondrial matrix[18]. An early sign of apoptosis is a collapse of the mitochondrial membrane potential, also referred to as a depolarized mitochondrial membrane potential, which causes the mitochondrial matrix to be less negatively charged. This in turn causes less TMRE to be sequestered by the mitochondria, which could be observed when Ramos and HSC-3 cells were treated with their respective apoptosis controls (Fig. 4b). When cells were treated with MPM-1, the TMRE fluorescence increased instead, indicating that the mitochondrial matrix had become more negatively charged, i.e. that the mitochondrial membrane potential was hyperpolarized. This effect was especially prominent in Ramos cells, but a slight increase in fluorescence could be seen for HSC-3 cells as well. Hyperpolarization of the mitochondrial membrane potential is typical for necrotic cells[19]. Taken together, the flow cytometric analyses indicate that MPM-1 causes cells to undergo a form of necrosis.

To further study the morphological changes induced in HSC-3 cells treated with MPM-1, scanning and transmission electron microscopy (SEM/TEM) images were acquired (Fig. 4c). No typical signs of apoptosis, such as chromatin condensation or distorted mitochondria, could be observed upon treatment with MPM-1. Both nuclei and mitochondria were unaffected, indicating a necrotic mode of cell death. Instead, SEM images revealed major structural changes on the cell membrane of HSC-3 cells. Untreated HSC-3 cells had a rough surface covered with microvillus-like protrusions. Upon treatment with MPM-1, these protrusions generally disappeared, rendering the membrane surface smoother. Simultaneously, formation of vesicles on the surface of the cell membrane could be observed. TEM images demonstrated the formation of large intracellular single-membraned vesicles or vacuoles.

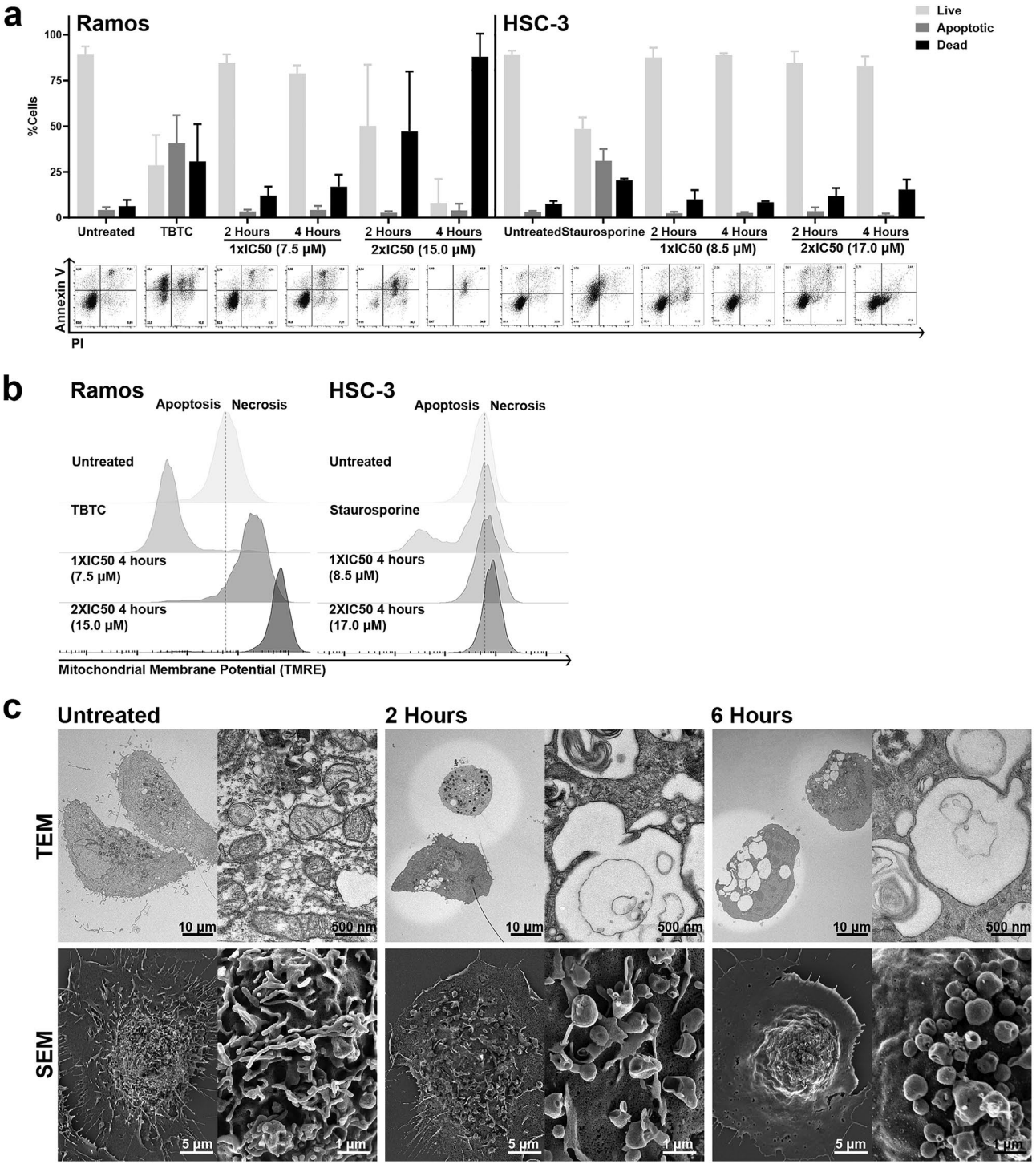

Figure 4. MPM-1 causes necrosis and vacuolization. (**a**) Ramos and HSC-3 cells were analyzed by flow cytometry for cell surface exposure of Annexin V. Cells were treated with 1xIC50 or 2xIC50 MPM-1 for 2 or 4 h. TBTC (2 µM, 2 h) and Staurosporine (100 nM, 24 h) were used as apoptosis controls for Ramos and HSC-3 cells, respectively. The graph shows the percentage of live (PI^-/Annexin V^-), apoptotic (PI^-/Annexin V^+), and dead (PI^+) cells for each condition, determined from three independent experiments, with error bars representing the standard deviation. (**b**) The mitochondrial membrane potential in Ramos and HSC-3 cells treated with 1xIC50 or 2xIC50 MPM-1 for four hours was assessed by flow cytometric analysis of TMRE fluorescence. The graph illustrates the results from three independent experiments. (**c**) Transmission (TEM) and scanning (SEM) electron microscopy images of untreated HSC-3 cells and HSC-3 cells treated with 1xIC50 MPM-1 for 2 or 6 h.

Effect of MPM-1 on autophagy and lysosomes. Increased autophagy has been suggested as a survival mechanism for drug-treated cells, and it has also been coupled to vacuolization of dying cells[20]. Autophagy is a process that cells use to degrade and reuse cellular content. A double-membraned autophagosome forms around the content that should be degraded and subsequently fuses with a lysosome, creating a single-membraned autolysosome where lysosomal enzymes degrade the content[21]. We hypothesized that the large vesicles observed in Fig. 4c upon treatment of HSC-3 cells with MPM-1 might be coupled to autophagy or other lysosomal degradation pathways.

MPM-1 treated HSC-3 cells were stained for the autophagy markers p62 (green) and LC3B (red), and immunofluorescence confocal microscopy images were acquired. Normally, LC3B coats the membrane of autophagosomes, while p62 is involved in sequestering the content to be degraded. Co-localization of p62 and LC3B (yellow) can therefore be used as a marker of autophagosomes[22]. The staining with p62 and LC3B revealed the presence of the same large vesicles as were seen in the electron microscopy images, here seen as empty black circles (Fig. 5a). Overall, it was not possible to determine whether the vesicles were specifically connected to the presence of LC3B or p62. With a few exceptions, the large vesicles were not coated by LC3B or p62, indicating that they were not autophagosomes. It is however worth mentioning that a small selection of vesicles were clearly coated by LC3B, as can be seen in one of the images acquired after four hours of treatment (Fig. 5b). A number of smaller autophagosomes (yellow dots) could be seen in both untreated and MPM-1 treated cells. Quantification of the number of co-localized p62 and LC3B dots per cell revealed that MPM-1 treated cells on average contained a higher number of autophagosomes (Fig. 5c). There was also a significant increase in the total number of only green (p62) or only red (LC3B) dots in MPM-1 treated cells. The appearance of large, green dots was especially prominent, and revealed that aggregates of p62 had been formed. Since p62 is a substrate of autophagy, the total amount of it is expected to decrease in cells where the autophagic activity (autophagic flux) is high. Accumulation of p62 and of autophagosomes instead often occurs when autophagy is inhibited, indicating that this might be an effect of MPM-1[22].

Since autophagy related protein 7 (ATG7) knockout HeLa cells were readily available to us, we used these to study whether the process of autophagy could affect the sensitivity of cells towards MPM-1. The ATG7 KO cells are not able to perform autophagy because ATG7 is essential for the formation of autophagosomes[21]. The IC50-value of MPM-1 was determined for wild type (WT) HeLa cells and the ATG7 knockout HeLa cells. There was no significant difference between the IC50-value obtained for WT and ATG7 KO HeLa cells (24.30 ± 1.73 µg/ml vs. 22.97 ± 0.35 µg/ml, $p = 0.3$) (Supplementary Fig. S2), indicating that autophagy could not protect the HeLa cells from MPM-1.

However, we further studied the role of autophagy by treating HSC-3 cells with MPM-1 in the presence of the late-stage autophagy inhibitor bafilomycin A1 to see if this would affect the cytotoxicity of MPM-1. Bafilomycin A1 is an inhibitor of the V-ATPase which is present on lysosomes and keeps their internal pH low. Bafilomycin A1 therefore causes the lysosomal pH to increase, in turn causing lysosomal dysfunction and inhibition of fusion between autophagosomes and lysosomes[23]. Bafilomycin A1 alone was not cytotoxic during the time span of the assay, but the results revealed that cells were more sensitive to MPM-1 in the presence of bafilomycin A1 than in its absence (Fig. 5d). The same tendency was observed for both WT and ATG7 KO HeLa cells as well (Supplementary Fig. S3).

To study the effect of MPM-1 on lysosomes, HSC-3 cells were stained with the fluorescent dye Lysotracker Deep Red, which stains lysosomes and other acidic cellular compartments, and confocal microscopy images were acquired (Fig. 5e). Untreated cells contained a high number of small and acidic lysosomes, as seen by the bright lysotracker signal. In cells treated with MPM-1 the distribution of the lysotracker dye was more diffuse and less intense, making it difficult to distinguish individual lysosomes from each other. Thus, it was not possible to perform automatic identification of lysosomes and quantification of size and lysotracker intensity. However, it was evident that MPM-1 influenced lysosomal morphology. Several of the MPM-1 treated cells contained lysosomes that were visibly enlarged as compared to the lysosomes in untreated cells. The enlarged lysosomes generally seemed to have a relatively weak lysotracker signal, indicating that their internal pH was higher than the pH of lysosomes in untreated cells. Taken together, these results reveal that MPM-1 has an effect on lysosomes, which in turn may be the reason for the observed accumulation of autophagosomes and p62.

MPM-1 induces release and exposure of DAMPs. To study the immunogenic potential of MPM-1, we tested whether the cell death induced by MPM-1 caused release and exposure of DAMPs specifically related to immunogenic cell death. Flow cytometry was used to detect cell surface calreticulin in Ramos and HSC-3 cells treated with MPM-1. For Ramos cells, only a very small and statistically insignificant increase in cell surface calreticulin was observed after treatment with MPM-1. However, HSC-3 cells treated with 2xIC50 MPM-1 for four hours showed a significantly increased amount of cell surface calreticulin, as compared to untreated cells (Fig. 6a). Release of ATP into the cell media by cells treated with MPM-1 was analyzed with a firefly luminescence-based assay. For Ramos cells treated with MPM-1, only a small amount of ATP could be detected in the supernatant. The same was observed for HSC-3 cells treated with 1xIC50 MPM-1, but with 2xIC50 MPM-1, the ATP levels increased significantly (Fig. 6b). Release of HMGB1 was analyzed by Western blot and demonstrated that for Ramos cells, HMGB1 release occurred rapidly upon treatment with MPM-1 (Fig. 6c). The supernatant of untreated Ramos cells already contained detectable levels of HMGB1, but upon treatment with 1xIC50 MPM-1, the amount of HMGB1 in the supernatant gradually increased with time. For HSC-3 cells, no HMGB1 was detectable in the supernatant of untreated cells, but upon treatment with 2xIC50 MPM-1, HMGB1 was released. In summary, these results demonstrate that MPM-1 does induce the release and exposure of DAMPs related to immunogenic cell death.

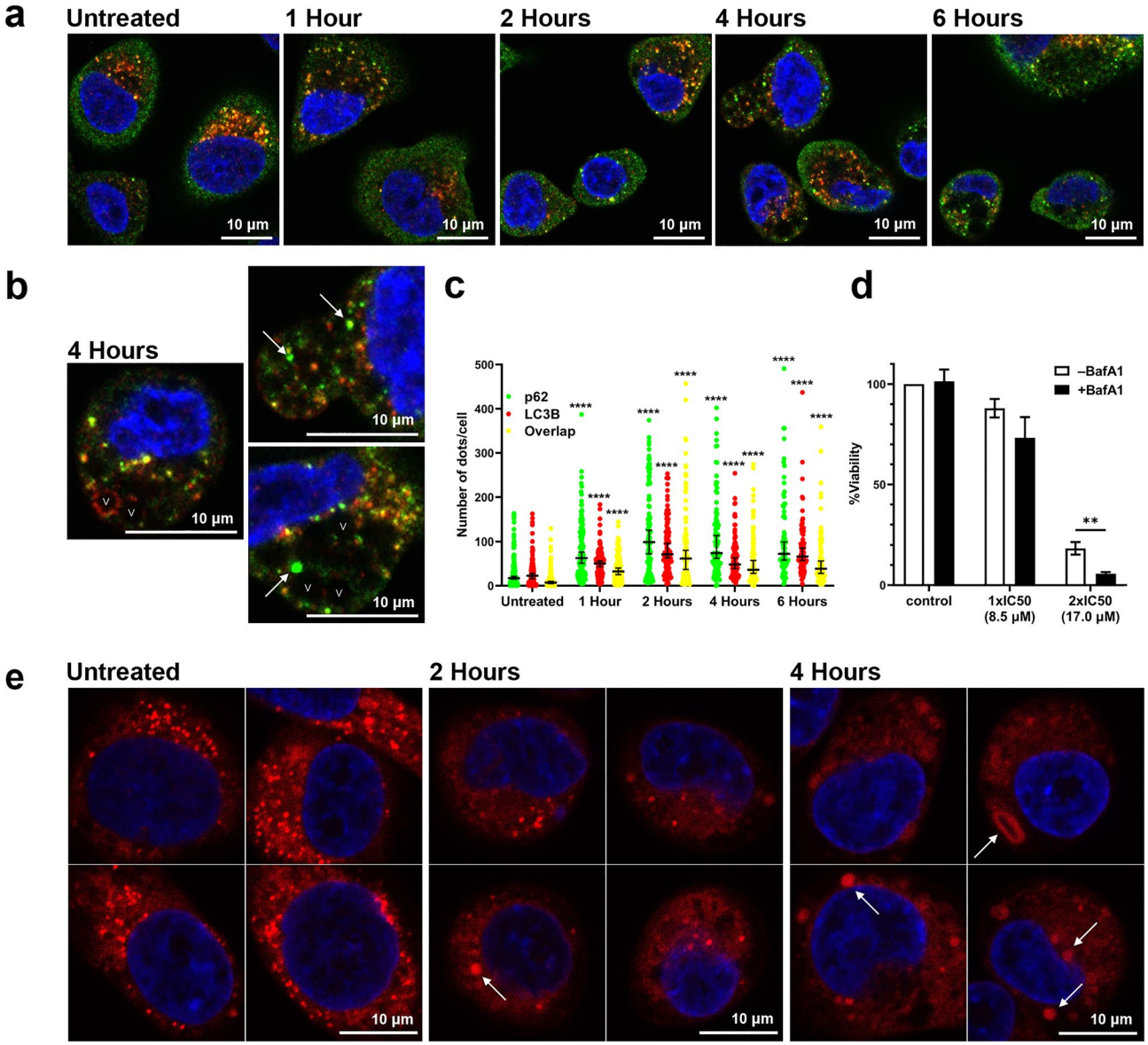

Figure 5. MPM-1 causes perturbation of autophagy and lysosomal swelling. (**a**) Immunofluorescence microscopy images of untreated HSC-3 cells and HSC-3 cells treated with 1xIC50 MPM-1 for 1, 2, 4 or 6 h before being stained for presence of p62 (green) and LC3B (red). Examples of vesicles (V) and p62 aggregates (arrows) are shown in images taken after 4 h of treatment (**b**). The number of p62/LC3B/overlapping dots per cell was counted in > 80 cells for each condition and the results are visualized in (**c**). Horizontal lines denote the median and error bars show 95% CI. Significant differences between treated and untreated groups were determined by separate Kruskal–Wallis tests with Dunn's post-hoc for the p62, LC3B, and overlap data. (**d**) Viability of HSC-3 cells after treatment with 1xIC50 or 2xIC50 MPM-1 in the presence or absence of bafilomycin A1 (BafA1) (100 nM) was determined by the MTS assay. Bars represent the mean from three independent experiments with error bars denoting the standard deviation. Significant differences were determined by unpaired t-test (**e**) Immunofluorescence microscopy images of untreated HSC-3 cells and HSC-3 cells treated with 1xIC50 MPM-1 for 2 or 4 h before being stained with Lysotracker Deep Red. Arrows indicate enlarged lysosomes.

Discussion

Our results demonstrate that the newly developed marine natural product mimic MPM-1 may have potential as an intratumoral immunotherapy. MPM-1 is clearly cytolytic and rapidly induced cell death in all cell lines tested. This included the multi-drug resistant breast adenocarcinoma cell line MCF-7. This non-selective killing of cells indicates that MPM-1 likely targets a site of action that is present in most cells. Inevitably, this means that also non-malignant cells can be killed by MPM-1 in an in vivo setting. However, the ability to target, and thereby release antigens from, any cell in a heterogenic tumor is the main goal of cancer treatment with cytolytic

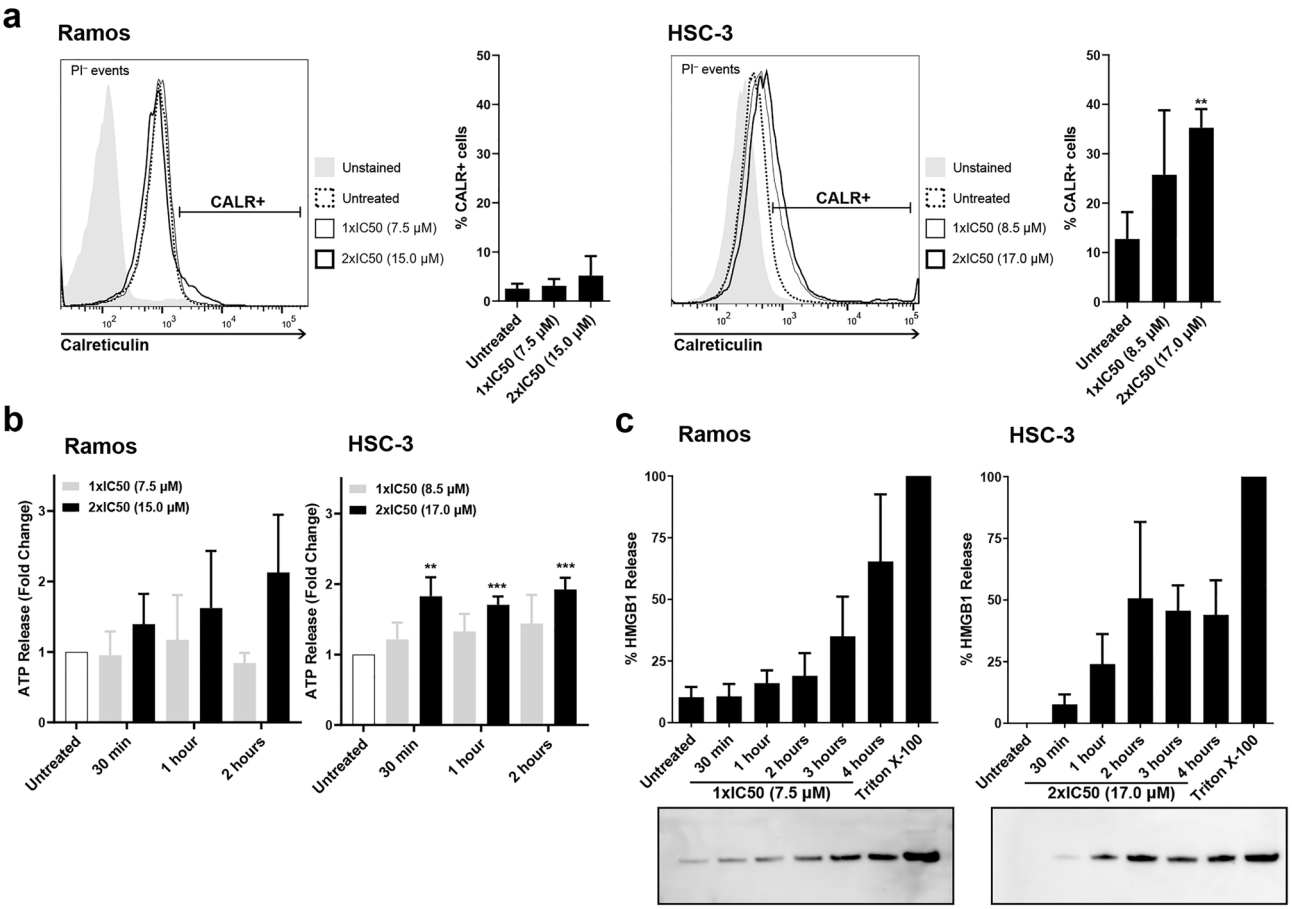

Figure 6. MPM-1 induces the release and exposure of DAMPs related to immunogenic cell death. (**a**) Cell surface exposure of calreticulin by Ramos and HSC-3 cells treated with 1xIC50 or 2xIC50 MPM-1 for four hours was assessed by flow cytometry. Calreticulin expressing cells were identified among live (PI negative) cells. The bar graph shows the mean percentage of calreticulin expressing cells from three separate experiments with error bars denoting the standard deviation. Significant differences between treated and untreated groups were determined by unequal variances t-test. (**b**) Release of ATP from Ramos and HSC-3 cells treated with MPM-1 was assessed by a firefly luminescence assay. Bars represent the mean ATP release from five individual experiments, expressed as fold increase relative to untreated (control) cells. Significant differences between treated and untreated groups were determined by repeated measures ANOVA and Dunnett's post-hoc. (**c**) Release of high mobility group box 1 (HMGB1) from cells treated with MPM-1 was assessed by Western blotting. Untreated and Triton X-100 treated cells served as negative and positive control, respectively. Bars represent the mean from three independent experiments with error bars denoting the standard deviation. The blots have been cropped for presentation in this figure. Original blots are presented in Supplementary Fig. S4.

compounds. Moreover, the intended administration route for MPM-1 is as an intratumoral injection, which can help limit the amount of damage to non-malignant healthy cells.

It is worth emphasizing that human red blood cells were not affected by treatment with MPM-1. This finding suggests that MPM-1's primary target is an intracellular structure. Unlike most other cells, red blood cells do not possess organelles or a nucleus. The electron microscopy images of HSC-3 cells treated with MPM-1 showed that large intracellular vesicles had been formed and suggests that MPM-1 affects some part of vesicular transport or degradation. MPM-1 is a small, weakly basic and amphipathic compound. This means that it fits the description of *lysosomotropic compounds*, which induce cell death by causing lysosomal dysfunction[24,25]. Lysosomotropic compounds are also known not to lyse red blood cells, since they do not possess lysosomes. Lysosomotropic compounds have lipophilic features that allow them to cross through the lipid cell membrane in their neutral (deprotonated) form, while their basic nature leads them to accumulate within the acidic lysosomes. Due to the basic features of MPM-1, the majority of molecules are expected to be fully protonated at physiological pH and not able to cross a lipophilic cell membrane. However, due to the equilibrium between protonated and neutral molecules, a small fraction of neutral molecules will be present and likely able to diffuse into cells and their organelles. The acidic environment inside the lysosomes will then cause MPM-1 to become protonated and thereby trapped within the lysosomes. This is the accepted mechanism of action for lysosomotropic compounds[24]. As more and more molecules become trapped, osmotic pressure causes water to diffuse into the lysosomes, which then adopt the appearance of large vacuoles. The influx of water into lysosomes makes the lysosomal pH higher and causes biological dysfunction of the lysosomes. Additionally, the trapped molecules

can function as detergents, causing disruption of the lysosomal membrane, leakage of lysosomal enzymes, and subsequent cell death[24].

The imaging results obtained in the present study, which demonstrated the appearance of large empty vacuoles in HSC-3 cells treated with MPM-1, support the idea that MPM-1 is a lysosomotropic compound. Moreover, since lysosomes play a central role in autophagy, their dysfunction is expected to disturb the autophagic flux. Again, this fits well with the observed results for MPM-1. Accumulation of autophagosomes, as well as LC3B and p62 aggregates is a well-known effect of disrupted fusion of autophagosomes with lysosomes[25]. Interestingly, a few of the large vesicles were clearly coated by LC3B, suggesting that they were of autophagic origin. A possibility is that the LC3B coated vesicles were autolysosomes, which are also acidic and therefore might trap MPM-1 in the same way as other lysosomes. This also fits the electron imaging results, which showed that the large vesicles had single membranes.

For some lysosomotropic compounds, including the well-studied antimalarial drug chloroquine, their main mechanism of inducing cell death is thought to be via their accumulation in lysosomes[25]. It has been demonstrated that bafilomycin A1 can protect cells from chloroquine induced cell death, an effect which may partially be due to decreased sequestration of chloroquine in lysosomes when the lysosomal pH is increased[27]. However, many well-known drugs and cytotoxic compounds are lysosomotropic even though their main target is located in other parts of the cell. For such compounds, increased lysosomal pH causes less compound to be sequestered in lysosomes and more to reach the main target. One example is the DNA intercalating agent doxorubicin, which has been shown to accumulate in lysosomes[28]. Upon treatment with bafilomycin A1 to increase the lysosomal pH, it was demonstrated that doxorubicin re-located from the lysosomes to a more diffuse distribution in the whole cell and subsequently induced more cell death[28]. Similarly, when HSC-3 cells were treated with bafilomycin A1, they became more sensitive to treatment with MPM-1. Since bafilomycin A1 itself was not cytotoxic, this indicates that the effect was synergistic. Furthermore, this result suggests that the main target for MPM-1 may not be lysosomes but possibly another organelle or structure located in the cytoplasm or nucleus.

We hypothesized that autophagy could affect the sensitivity of cells towards MPM-1. The fact that inhibition of autophagy with bafilomycin A1 caused increased cell death by MPM-1 supports this hypothesis. However, the results obtained with the HeLa cells, which showed that there was no difference in sensitivity towards MPM-1 between WT and autophagy deficient ATG7 KO HeLa cells, does not. Despite the fact that treatment with bafilomycin A1 and knockout of ATG7 both cause inhibition of autophagy, it is important to note that they do so through different mechanisms. Bafilomycin A1 indirectly inhibits autophagy by causing lysosomal dysfunction which subsequently inhibits the fusion of autophagosomes with lysosomes. Knockout of ATG7 directly inhibits autophagy by inhibiting the formation of autophagosomes without affecting lysosomes. These results thus suggest that it is the dysfunction of lysosomes which sensitizes cells towards MPM-1 rather than the inhibition of autophagy per se. Consequently, the ATG7 KO HeLa cells were equally sensitive to MPM-1 as WT HeLa cells. The same phenomenon is observed for WT and ATG7 silenced cells treated with chloroquine[26]. Nevertheless, autophagy is a complex process, and it cannot be ruled out that it may play some role in cells' response to treatment with MPM-1 or that the disturbance of the autophagic flux seen upon treatment of HSC-3 cells with MPM-1 may have implications for its potential as an anticancer compound.

Autophagy is considered an instrumental cellular process for most cancer cells. For this reason, lysosomotropic compounds such as chloroquine and hydroxychloroquine have been tested as anti-cancer agents in several studies and clinical trials, with some showing promising results[25]. Chloroquine is usually given as a systemic treatment, which means that it can affect many different cell types in the body. The intratumoral injection route suggested for MPM-1 thus represents an alternative treatment mode for lysosomotropic compounds, which could be used to target cancer cells more specifically.

The live cell imaging of HSC-3 cells indicated that the potency of MPM-1 was not directly related to concentration of the compound per se, but rather to the exact number of molecules available per cell. This was demonstrated by the fact that it took longer to reach cell death when the cell density was higher, and that low concentrations of MPM-1 needed more time to cause cell death as compared to high concentrations. This phenomenon is often referred to as the inoculum effect, and it has been demonstrated to apply for several types of compounds, including doxorubicin[29]. The fact that the suspension cell lines had significantly lower IC50 values compared to adherent cells may be due to the lack of adherence to a surface, making their entire cell membrane available for penetration by MPM-1, possibly resulting in a high intracellular drug concentration being reached sooner. This phenomenon could be relevant for several types of compounds, indicating that when planning drug screening projects, the types of cell lines that are included and compared with each other should be carefully considered.

Many chemotherapeutic and lysosomotropic agents cause cell death by inducing apoptosis[4,30]. However, MPM-1 did not induce any of the signs that are typically associated with apoptosis, such as exposure of phosphatidylserine, chromatin condensation or depolarized mitochondrial membrane potential. Instead, the death induced by MPM-1 was accompanied by morphological and biochemical features typical of necrosis. Historically, necrosis has been regarded as an accidental form of cell death, but the number of recognized modes of cell death has greatly expanded over the last few decades and now includes regulated forms of necrosis as well[31]. Inducing regulated forms of necrosis has been suggested as a potentially more beneficial approach to cancer therapy than inducing immunogenic apoptosis[32]. The reason for this being that many tumors have developed resistance to apoptosis and therefore do not respond to apoptosis inducing chemotherapies[32]. In addition, apoptotic cells express phosphatidylserine, which is immunosuppressive. Phosphatidylserine promotes removal of apoptotic cells while simultaneously inhibiting unnecessary inflammation. It is also reported that phosphatidylserine plays a role in the tumor microenvironment, where it has immunosuppressive functions on immune cells[33]. Since the goal of intratumoral immunotherapy is to activate immune responses, the fact that MPM-1 does not induce expression of phosphatidylserine is promising.

The exposure of calreticulin on the surface of MPM-1 treated HSC-3 cells supports the idea that the cell death induced by MPM-1 is regulated. HMGB1 and ATP can be released from cells dying of accidental necrosis, but exposure of calreticulin requires regulated signaling and is not typically associated with necrotic cells[34]. The fact that no cell surface calreticulin was detected in MPM-1 treated Ramos cells may indicate that MPM-1 caused a more classical type of necrosis in these cells. However, since Ramos cells do not originate from a solid tumor, they do not represent the type of cancer that would benefit from intratumoral injection with MPM-1. Thus, the finding that MPM-1 could cause translocation of calreticulin to the outside of HSC-3 cells, which do originate from a type of solid tumor, was particularly interesting.

Together with the release of HMGB1 and ATP, the exposure of calreticulin on HSC-3 cells indicates that MPM-1 may have the ability to induce immunogenic cell death. Cell surface calreticulin functions as an "eat me" signal, which is important for the effective phagocytosis of dying cancer cells by cells of the innate immune system and their subsequent cross-presentation of tumor antigens to cells of the adaptive immune system[4]. Exposed calreticulin binds to CD91, mainly expressed by dendritic cells and macrophages[35]. Release of ATP functions as a "find me" signal. By binding to the purinergic receptors P2RY2 and P2RX7 on dendritic cells and macrophages, ATP stimulates their recruitment and activation[36,37]. HMGB1 can bind different receptors, including Toll-like receptor 4 (TLR4) on dendritic cells, which is most relevant for immunogenic cell death. Upon binding to TLR4, HMGB1 promotes antigen processing and cross-presentation of tumor antigens[38].

A widely accepted notion is that whether a compound truly has the ability to induce immunogenic cell death or not, can only be determined through in vivo experiments[37]. We have previously used a model where tumors are established subcutaneously in immunocompetent mice and then treated by intratumoral injections[10]. Mice with complete tumor regression are then given a secondary challenge with the same tumor cells. Absent or slow tumor growth is interpreted as a sign that the compound used for treatment did induce immunogenic cell death. We are currently performing extensive in vivo studies of this type with MPM-1.

The present study is the first report on the cytolytic and mechanistic effects of MPM-1. We have shown that MPM-1 effectively kills many different cancer cells, while affecting autophagy and causing the release and exposure of DAMPs related to immunogenic cell death. Moreover, the unique marine background of MPM-1 highlights the fact that there is still much unexplored potential in molecules derived from arctic marine species.

Methods

Reagents and equipment. MPM-1 (Mw 734.74) was synthesized as described below and dissolved in 10 mM Tris–HCl buffer (pH 7.4) to 1 mg/ml. In all cell-based assays, MPM-1 was further diluted in cell culture medium. Tributylchlorotin (TBTC) was from Sigma-Aldrich (St. Louis, MO, USA), and Staurosporine was from Abcam (Cambridge, UK).

Synthesis of MPM-1. The synthesis of MPM-1 was similar to that described in our original report on amphipathic barbiturates[16]. All reagents and solvents were purchased from commercial sources and used as supplied. Anhydrous DMF was prepared by storage over 4 Å molecular sieves. The hydrogenation with Pd/C at higher pressure (8–10 bar) were carried out on a Parr Instrument, Series 4590 Micro Stirred reactor, 50 ml, attached to a Parr 4843 Modular Controller. Reactions were monitored by thin-layer chromatography (TLC) with Merck pre-coated silica gel plates (60 F_{254}). Visualization was accomplished with either UV light or by immersion in potassium permanganate or phosphomolybdic acid (PMA) followed by light heating with a heating gun. Purifications using normal phase flash chromatography were either done by normal column chromatography using Normalsil 60, 40–63 mm silica gel or by automated normal phase flash chromatography (Heptane/EtOAc) with the sample preloaded on a Samplet® cartridge belonging to a Biotage SP-1. Purification of reactions by reversed phase (RP) C_{18} column chromatography (water with 0.1% TFA/acetonitrile with 0.1% TFA) was also executed on an automated purification module with the sample preloaded on a Samplet® cartridge. The sample used for biological testing were determined to be of > 95% purity. NMR spectra were obtained on a 400 MHz Bruker Avance III HD equipped with a 5 mm SmartProbe BB/^{1}H (BB = ^{19}F, ^{31}P–^{15}N). Data are represented as follows: chemical shift, multiplicity (s = singlet, d = doublet, t = triplet, q = quartet, p = pentet, h = heptet, m = multiplet), coupling constant (*J*, Hz) and integration. Chemical shifts (δ) are reported in ppm relative to the residual solvent peak ($CDCl_3$: δ_H 7.26 and/or 1.56, and δ_C 77.16; CD_3OD: δ_H 3.31 and δ_C 49.00). Positive and negative ion electrospray ionization mass spectrometry (ESI–MS) was conducted on a Thermo electron LTQ Orbitrap XL spectrometer.

Diethyl 2,2-dicinnamylmalonate (**2**). To a stirred solution of diethyl malonate (2.0 g, 1.89 ml, 12.48 mmol) in DMF (20 ml) at 0°C, NaH (630 mg, 26.22 mmol, 2.1 equiv.) was added slowly. A solution of 3-bromo-1-phenyl-1-propene (5.16 g, 26.22 mmol, 2.1 equiv.) in DMF (25 ml) was then added. The reaction was kept stirring at RT over night. The reaction mixture was diluted with EtOAc (100 ml), water (20 ml) and 10% citric acid (20 ml). The layers were separated and the organic phase was washed with water (4 × 50 ml) and brine. The organic phase was dried over Na_2SO_4, filtered and concentrated. The crude product was dissolved in $CHCl_3$, and adsorbed on Celite. The product was purified on a silica column using 0–5% EtOAc/pentane as mobile phase to give **2** (4.801 g, 97%) as a white powder. ^{1}H NMR (400 MHz, Chloroform-*d*) δ 7.37 – 7.27 (m, 8H), 7.25–7.18 (m, 2H), 6.46 (d, 2H), 6.10 (dt, *J* = 15.5, 7.5 Hz, 2H), 4.22 (q, *J* = 7.1 Hz, 4H), 2.85 (dd, *J* = 7.5, 1.4 Hz, 4H), 1.26 (t, *J* = 7.1 Hz, 6H). HRMS-ESI: $C_{25}H_{28}NaO_4^+[M+Na]^+$ calcd: 415.1880, found: 415.1868.

Diethyl 2,2-bis(3-phenylpropyl)malonate (**3**). The procedure was performed in a Parr hydrogenation apparatus under pressure (10 bar). Pd/C was weighted out in a test tube, soaked in EtOH (3 ml) and poured into the "bomb". **1a** (2.5 g, 6.4 mmol) was dissolved in EtOH and added to the "bomb". The bomb was mounted on the Parr hydrogenation apparatus, evacuated and refilled 6 times with H_2 and stirred at r.t. for 48 h. After purging, the reaction mixture was filtered through a pad of celite and concentrated. The resulting brown oil was dissolved

in 40 ml $CHCl_3$ and concentrated to remove remaining EtOH. Adding heptane revealed some Pd/C particles so the solution was filtered through a pad of celite with a filter paper on top. The filtrate was concentrated and turned solid overnight. TLC and NMR revealed only minor impurities and the crude (1.256 g, 69%) was used without further purification. ^{1}H NMR (400 MHz, Chloroform-*d*) δ 7.30–7.24 (m, 8H), 7.21–7.10 (m, 2H), 4.13 (q, *J* = 7.1 Hz, 4H), 2.59 (t, *J* = 7.5 Hz, 4H), 1.98–1.79 (m, 4H), 1.45 (tdd, *J* = 8.8, 6.0, 4.3 Hz, 4H), 1.19 (t, *J* = 7.1 Hz, 6H). ^{13}C NMR (101 MHz, Chloroform-*d*) δ 171.8, 141.9, 128.5, 128.4, 126.0, 61.2, 57.5, 36.0, 31.8, 25.8, 14.2. HRMS-ESI: $C_{25}H_{32}NaO_4^+$ $[M+Na]^+$ calcd: 419.2193, found: 419.2166.

5,5-bis(3-phenylpropyl)pyrimidine-2,4,6(1H,3H,5H)-trione (**4**). To a solution of urea (1.51 g, 25.22 mmol) in anhydrous DMF (10 ml) was slowly added NaH (151 mg, 6.3 mmol) and the resulting solution was stirred for 10 min before a solution of **3** (1.0 g, 2.522 mmol) in DMF (8 ml) was added. The resulting mixture was stirred overnight. The reaction was diluted with EtOAc (50 ml), washed with 10% citric acid sol. (3 × 30 ml), 10% $NaHCO_3$ sol. (2 × 20 ml), and brine (30 ml). The organic phase was dried over Na_2SO_4, filtered and concentrated. The crude product was dissolved in $CHCl_3$ and purified on automated flash chromatography affording **4** (595 mg, 65%) as a white powder. ^{1}H NMR (400 MHz, $CDCl_3$): δ 9.02 (s, 2H), 7.30–7.23 (m, 4H), 7.19 (t, *J* = 7.2 Hz, 2H), 7.11 (d, *J* = 7.4 Hz, 4H), 2.57 (t, *J* = 7.3 Hz, 4H), 2.25–1.87 (m, 4H), 1.73–1.15 (m, 4H). ^{13}C NMR (101 MHz, DMSO-d_6) δ 173.0, 149.8, 141.2, 128.3, 128.2, 125.9, 54.8, 37.7, 34.8, 26.4. HRMS-ESI: $C_{22}H_{23}N_2O_3^-$ $[M-H]^-$ calcd: 363.1714, found: 363.1706.

1,3-bis(4-bromobutyl)-5,5-bis(3-phenylpropyl)pyrimidine-2,4,6(1H,3H,5H)-trione (**5**). To a stirred solution of **3** (0.582 g, 1.6 mmol) in DMF (15 mL) was added Na_2CO_3 (1.32 g, 1.2 mmol, 6 equiv.) and 1,4-dibromobutane (1.88 mL, 1.6 mmol, 10 equiv.). The reaction mixture was stirred for 48 h, diluted with EtOAc (50 mL) and washed with 10% citric acid sol. (3 × 25 mL), 10% $NaHCO_3$ sol. (2 × 25 mL), and brine (25 mL). The organic phase was dried over Na_2SO_4, filtered and concentrated. The crude product was purified on automated flash chromatography affording **5** (0.705 g, 70%) as a white powder. ^{1}H NMR (400 MHz, $CDCl_3$): δ ^{1}H NMR (400 MHz, Chloroform-*d*) δ 7.26 (dd, *J* = 8.0, 6.6 Hz, 4H), 7.21–7.14 (m, 2H), 7.12–7.05 (m, 4H), 3.90 (t, *J* = 7.2 Hz, 4H), 3.38 (t, *J* = 6.5 Hz, 4H), 2.54 (t, *J* = 7.7 Hz, 4H), 2.10–1.97 (m, 4H), 1.85 (dq, *J* = 8.8, 6.0 Hz, 4H), 1.79–1.66 (m, 4H), 1.48–1.30 (m, 4H).^{13}C NMR (101 MHz, $CDCl_3$): δ ^{13}C NMR (101 MHz, Chloroform-*d*) δ 171.6, 150.6, 141.1, 128.6, 128.3, 126.2, 56.5, 41.2, 39.7, 35.7, 32.8, 30.0, 27.1, 26.8. HRMS-ESI: $C_{30}H_{38}{}^{79}Br^{81}Br_2N_2O_3$ $[M+Br^{81}]^-$ calcd: 715.0397, found: 715.0388.

1,3-bis(4-azidobutyl)-5,5-bis(3-phenylpropyl)pyrimidine-2,4,6(1H,3H,5H)-trione (**6**). To a stirred solution of **5** (690 mg, 1.1 mmol) in 10 mL DMF was added NaN_3 (210 g, 3.2 mmol, 3 equiv.) and stirred for 18 h. The reaction mixture was diluted with EtOAc (30 mL), washed with water (3 × 50 mL) and brine. The organic phase was dried over Na_2SO_4, filtered and concentrated to give the crude product **6** as white crystals (0.602 g, 99%). ^{1}H NMR (400 MHz, $CDCl_3$): δ 7.29–7.22 (m, 4H), 7.21–7.15 (m, 2H), 7.10–7.05 (m, 4H), 3.89 (t, *J* = 7.1 Hz, 4H), 3.27 (t, *J* = 6.6 Hz, 4H), 2.54 (t, *J* = 7.7 Hz, 4H), 2.07–1.97 (m, 4H), 1.71–1.51 (m, 8H), 1.43–1.32 (m, 4H). ^{13}C NMR (101 MHz, $CDCl_3$): δ 171.6, 150.5, 141.1, 128.5, 128.3, 126.2, 56.5, 50.9, 41.5, 39.7, 35.7, 27.0, 26.3, 25.3. HRMS-ESI: $C_{30}H_{38}N_8NaO_3^+$ $[M+Na]^+$ calcd: 581.2959, found: 581.2961.

4,4′-(2,4,6-trioxo-5,5-bis(3-phenylpropyl)dihydropyrimidine-1,3(2H,4H)-diyl)bis(butan-1-aminium) (MPM-1). To a stirred solution of 6 (574 mg, 1.03 mmol) and Et_3N (0.30 mL, 2.1 equiv.) in i-PrOH:THF (1:1, 6 mL) was added 1,3-propanedithiol (0.212 mL, 2.05 equiv.). The mixture was stirred for 5 min before addition of $NaBH_4$ (78 mg, 2 equiv.). After 48 h reaction time, Boc_2O (90 mg, 0.41 mmol, 4 equiv.) was added and the reaction was stirred for 18 h and evaporated, before EtOAc (20 mL) and water (15 mL) were added and stirred for 1 h. The two phases were filtered using a glass funnel filter with a sinter glass disc. The organic phase was washed with water (3 × 15 mL) and brine (15 mL) and concentrated. The resulting crude was purified by automated flash chromatography and evaporated. The Boc-protected intermediate was deprotected with TFA (2 mL, 26 mmol) in CH_2Cl_2 (5 mL) for 18 h. The reaction mixture was concentrated, and the crude product purified by RP automated flash chromatography and lyophilized to give MPM-1 (268 mg, 53%) as the TFA-salt. ^{1}H NMR (400 MHz, CD_3OD): δ 7.27–7.21 (m, 4H), 7.18–7.13 (m, 2H), 7.11–7.07 (m, 4H), 3.95–3.87 (m, 4H), 2.97–2.90 (m, 4H), 2.54 (t, *J* = 7.4 Hz, 4H), 2.00–1.92 (m, 4H), 1.65 (p, *J* = 3.7 Hz, 7H), 1.40 (dq, *J* = 12.1, 7.6 Hz, 4H). ^{13}C NMR (101 MHz, $CDCl_3$): δ 172.9, 151.9, 142.5, 129.5, 129.3, 127.1, 57.6, 42.2, 40.3, 40.2, 36.4, 27.9, 26.0, 25.9. HRMS-ESI: $C_{30}H_{43}N_4O_3^+$ $[M+H]^+$ calcd: 507.3330, found: 507.3329.

Cell lines and cell culture. The glioblastoma GL261-Luc2 cell line was kindly gifted by Dr. Adrienne Scheck. Wild type HeLa and ATG7 KO HeLa cells were a kind gift from Professor Terje Johansen. A375 (RRID:CVCL_0132) was obtained from Public Health England (PHE Culture Collection, London, UK). HSC-3 (RRID: CVCL_1288) was obtained from the Japanese Collection of Research Bioresources Cell Bank (JCRB Cell Bank, Osaka, Japan). PBMCs were isolated from blood samples from randomized anonymous healthy volunteers. The remaining cell lines, B16F1 (RRID:CVCL_0158), HepG2 (RRID:CVCL_0027), Jurkat (RRID:CVCL_0367), Ramos (RRID:CVCL_0597), HT-29 (RRID: CVCL_0320), MCF-7 (RRID: CVCL_0031), SK-N-AS (RRID:CVCL_1700), HUVEC (RRID:CVCL_2959) and MRC-5 (RRID:CVCL_0440) were all obtained from the American Type Culture Collection (ATCC, Manassas, VA, USA). Cells were kept at 37°C with 5% CO_2 and cultured in complete medium unless otherwise stated. For A375, B16F1, GL261-Luc2, HepG2, HeLa (wild type and ATG7 KO) and HSC-3 this consisted of high glucose Dulbecco's Modified Eagle's Medium (DMEM, Sigma-Aldrich) supplemented with 10% fetal bovine serum (FBS) and 1% L-glutamine (Sigma-Aldrich). Jurkat, Ramos, PBMCs, HT-29, MCF-7 and SK-N-AS were kept in RPMI-1640 (Sigma-Aldrich) supplemented with 10% FBS. MRC-5 was kept in Minimum Essential Medium Eagle (MEM, Sigma-Aldrich) with 10% FBS and HUVEC was kept in complete EGM™-2 Endothelial Cell Growth Medium-2 BulletKit™ (Lonza, Basel, Switzerland).

MTS cytotoxicity assay. A colorimetric proliferation assay, based on the conversion of a tetrazolium compound (3-(4,5-dimethylthiazol-2-yl)-5-(3-carboxymethoxyphenyl)-2-(4-sulfophenyl)-2H-tetrazolium, inner salt; MTS) to a formazan product, was used to assess the cytotoxic effect of MPM-1. Cells were seeded at approximately 80% confluence in flat-bottom 96-well plates. For adherent cell lines, this corresponded to 2×10^4 cells/well, which were left to adhere overnight. HeLa cells (wild type and ATG7 KO) were seeded at 1.5×10^4 cells/well. Before treatment with MPM-1, cells were washed twice with serum free medium. Suspension cells were seeded on the same day as the experiment, in serum free medium. For Ramos and Jurkat, 8×10^4 cells were seeded/well, and for PBMCs, 15×10^4 were seeded/well. For determination of IC50 values, all cells were treated with MPM-1 in 100 µL serum free medium in a two-fold serial dilution series with concentrations ranging from 128 µg/µL to 0.125 µg/µL. For the viability assays with Bafilomycin A1, HSC-3 cells were pre-treated with 50 µL Bafilomycin A1 (100 nM) (Merck, Darmstadt, Germany) for one hour. Next, 50 µL of MPM-1 diluted in Bafilomycin A1 containing media was added to yield a final volume of 100 µL and a final concentration of MPM-1 of 8.5 or 17 µM. Serum free medium ± 1% Triton X-100 functioned as positive and negative controls, respectively. After four hours of incubation, 20 µL of MTS solution (CellTiter 96® Aqueous One Solution, Promega, Madison, WI, USA) was added to each well and the plate was incubated for another 75 min. Absorbance was measured at 490 nm with a VersaMax™ Microplate reader (Molecular Devices, San Jose, CA, USA). The percentage of live cells was determined according to the formula:

$$\% = \frac{\text{Abs treated sample} - \text{Abs positive control}}{\text{Abs negative control} - \text{Abs positive control}} \times 100.$$

Each experiment was run three times with triplicate wells and the mean IC50 value was calculated for each cell line.

Hemolysis assay. The hemolytic effect of MPM-1 was determined by the use of a hemolysis assay as previously described[39]. Briefly, human red blood cells were isolated and resuspended in PBS. Next, they were mixed with MPM-1 in PBS at varying concentrations. The concentration of red blood cells was 1% and the concentrations of MPM-1 ranged up to 500 µM. 0.1% Triton X-100 and pure PBS were used as positive and negative controls, respectively. After 1 h of incubation at 37 °C with agitation, the samples were centrifuged at 4000 rpm for 5 min and the supernatant was collected. The absorption of the supernatant was measured at 405 nm and the percentage of hemolysis was calculated using the same formula as for the MTS assay.

Live cell imaging. HSC-3 cells were seeded, 1×10^5 or 1.5×10^5 cells per well, on glass-bottom 24-well plates that had been pre-coated with fibronectin and left to adhere overnight. This corresponded to 50,000 and 75,000 cells/cm^2, respectively. Cells were washed in complete DMEM and stimulated with MPM-1 diluted in complete DMEM to 4.3, 8.5 or 17.0 µM. Upon addition of MPM-1 to the cells, the culture plate was incubated in a Celldiscoverer 7 (Zeiss, Oberkochen, Germany), which was set to take pictures of each well approximately every three minutes for a total of 23 h.

Transmission electron microscopy. HSC-3 cells were seeded, 3×10^5 cells per dish, in 35 mm dishes with a 14 mm gridded coverslip (MatTek, Ashland, MA, USA) that had been pre-coated with fibronectin and left to adhere overnight. Cells were washed in complete DMEM and stimulated with MPM-1 diluted in complete DMEM to 8.5 µM for 2 h or 6 h. One well was left untreated in complete DMEM alone. All processing was done in a microwave processor with a temperature control unit (Ted Pella, Redding, CA, USA). The cells were fixed for 14 min in a fixative containing 4% formaldehyde, 0.5% glutaraldehyde, and 0.05% malachite green in PHEM buffer (60 mM PIPES, 25 mM HEPES, 10 mM EGTA, 4 mM $MgSO_4 \cdot 7H2O$) (2 min vacuum on–off-on–off-on–off–on, 100 W) and subsequently washed twice with PHEM buffer. Post-fixation was done with 1% Osmium tetroxide and 1% $K_3Fe(CN)_6$ in 0.1 M cacodylic acid buffer. The cells were post-stained with 1% tannic acid and 1% uranyl acetate. Samples were then dehydrated in an increasing ethanol series (30–60–96–100%) and embedded in an epon equivalent (Agar). 70 nm sections were cut using a diamond knife (DiATOME, USA) on a UC7 ultramicrotome (Leica Microsystems, Wetzlar, Germany) and picked up on formvar-coated cupper grids. Sections were imaged using a Hitatchi HT7800 Transmission Electron Microscopy (Hitachi, Tokyo, Japan) with a XAROSA camera (EMSIS GmbH, Münster, Germany).

Scanning electron microscopy. HSC-3 cells were seeded at 1.5×10^5 cells per well, on fibronectin coated glass coverslips that were placed at the bottom of a 24-well plate. Cells were washed in complete DMEM and stimulated with MPM-1 diluted in complete DMEM to 8.5 µM for 2 or 6 h. One well was left untreated in complete DMEM alone. Processing was performed as described for the transmission electron microscopy samples up until the last step of the dehydration series (100% ethanol). At this point, samples were dehydrated by incubation 3 × 2 min in hexamethyldisilazane (Sigma-Aldrich). The samples were mounted on specimen holders and coated with gold–palladium in a Polaron Sputter Coater (Quorum Technologies, Lewes, UK) before being imaged on a GeminiSEM 360 (Zeiss).

Confocal microscopy. HSC-3 cells were seeded at 5×10^4 cells/well, in an 8-well chambered coverglass that had been pre-coated with fibronectin. The following day, cells were washed once in complete medium and then treated with 8.5 µM MPM-1 in 350 µL for 1 h, 2 h, 4 h or 6 h. One well was left untreated.

For staining of p62 and LC3B, cells were fixed in 4% formaldehyde in PHEM buffer and left at 4 °C until the next day. Cells were permeabilized by incubating them in 5% methanol in PBS for 5 min on ice. Next, cells were

washed twice in PBS and blocked by 45 min incubation in PBS 3% goat serum before they were incubated for 60 min with primary antibodies targeting p62 (#GP62-C, guinea pig polyclonal, Progen, diluted 1:2000) and LC3B (#L7543, rabbit polyclonal, Sigma-Aldrich, diluted 1:1000) in PBS 1% goat serum. The cells were then washed 6 × 2 min in PBS before being incubated with secondary antibodies (Alexa Fluor Plus 555 conjugated goat anti-rabbit (#A32732, Thermo Fisher), and Alexa Fluor 488 conjugated goat anti-guinea pig (#A11073, Thermo Fisher) diluted 1:1000 for 30 min. The cells were then washed 4 × 2 min in PBS before being incubated with DAPI (Thermo Fisher) (1 µg/mL in PBS) for 5 min followed by 2 × 2 min washing in PBS.

For staining of lysosomes, lysotracker Deep Red (L12492, Thermo Fisher) was included in each well for the last 30 min of incubation at a final concentration of 50 nM. Cells were then fixed in 4% formaldehyde for 15 min at room temperature. Next, cells were washed 4 × 2 min in PBS before being incubated with DAPI (1 µg/mL in PBS) for 5 min followed by 2 × 2 min washing in PBS.

Imaging was performed on a LSM 780 confocal microscope (Zeiss) and analysis was performed in Volocity ver 6.3 (PerkinElmer).

Flow cytometric apoptosis detection. The mode of death induced by MPM-1 was investigated with an apoptosis detection kit (88-8005-74, Thermo Fisher Scientific, Waltham, MA, USA), which combines staining with FITC-labeled Annexin V and propidium iodide (PI). HSC-3 cells were seeded, 4×10^5 cells/well in 6-well plates, and left to adhere overnight. The following day, one well was treated with 100 nM Staurosporine. On day two, the remaining wells were treated with 8.5 or 17.0 µM MPM-1 for up to four hours. To retain cells that could have detached from the well, the supernatant from each well was transferred to microcentrifuge tubes. The remaining cells were trypsinized and mixed with their respective supernatants. Ramos cells were seeded on the day of analysis, 6×10^5 cells/well in 24-well plates. Cells were treated with 2 µM TBTC for 2 h, or 7.5 or 15 µM MPM-1 for up to four hours. HSC-3 and Ramos cells were centrifuged and washed in binding buffer before being stained with the Annexin V-FITC antibody at 1:20 dilution for 15 min. Next, cells were washed in binding buffer again and transferred to flow cytometry tubes, before being stained with PI at 1:150 dilution for at least five minutes before analysis.

Flow cytometric analysis of mitochondrial membrane potential. Changes in the mitochondrial membrane potential were analyzed with the fluorescent mitochondrial dye TMRE (T669, Thermo Fisher Scientific). HSC-3 cells were seeded, 6×10^5 cells/well in 6-well plates, and left to adhere overnight. Cells were washed in serum free RPMI and treated with 1 µM staurosporine for four hours, or 8.5 or 17.0 µM MPM-1 for up to four hours. Ramos cells were seeded on the day of the experiment, 6×10^5 cells/well in serum free RPMI in 24-well plates, and treated with 2 µM TBTC for two hours, or 7.5 or 15 µM MPM-1 for up to four hours. 20 min before incubation was ended, TMRE was added to a final concentration of 5 nM for both cell lines. HSC-3 cells were washed in PBS, trypsinized and resuspended in PBS 2% FBS before analysis. Ramos cells were washed in PBS 2% FBS and analyzed directly.

Flow cytometric detection of calreticulin exposure. For detection of cell surface exposure of calreticulin, HSC-3 cells were seeded at 1.5×10^5 cells/well in a 24-well plate and left to adhere overnight. Cells were washed in complete DMEM and stimulated with MPM-1 diluted in complete DMEM to 8.5 or 17 µM for 4 h. Next, the cells were washed in PBS, trypsinized and resuspended in PBS 2% FBS before being stained with an Alexa Fluor 647 conjugated anti-calreticulin antibody (#ab196159, Abcam, Cambridge, United Kingdom) at 1:50 dilution. After 40 min incubation, cells were washed and resuspended in PBS 2% FBS, stained with PI at 1:150 dilution for at least five minutes, and immediately analyzed by flow cytometry.

All flow cytometric analyses in the present study were performed on a BD LSRFortessa™ (Becton Dickinson, Franklin Lakes, NJ, USA). Analyses were performed in FlowJo™ v.10 (https://www.flowjo.com/).

Luminescence based detection of ATP release. Release of ATP from cells treated with MPM-1 was detected with an ATP determination kit (A22066, Thermo Fisher Scientific) according to the manufacturer's protocol. HSC-3 cells were seeded at 2×10^4 cells/well in flat-bottom 96-well plates and left to adhere overnight. Before treatment with MPM-1, cells were washed twice with serum free RPMI. Ramos cells were seeded on the same day as the experiment at 8×10^4 cells/well in serum free RPMI in flat-bottom 96-well plates. HSC-3 and Ramos cells were stimulated with 8.5 or 17.0 µM (HSC-3) or 7.5 or 15 µM (Ramos) MPM-1 in a total volume of 100 µL for 30 min, 1 h or 2 h. After stimulation, 70 µL of the supernatant was carefully removed from each well and mixed well before 10 µL was transferred to wells on a white flat-bottom 96-well plate. The plate was inserted into the CLARIOstar microplate reader (BMG LABTECH, Ortenberg, Germany), which was set to add 90 µL of pre-made reaction buffer to each well and subsequently record luminescence. Luminescence was measured at 555–570 nm for 10 s. ATP release was expressed as fold increase of the luminescence in untreated samples.

Detection of HMGB1 release by western blotting. Release of HMGB1 from cells treated with MPM-1 was detected by Western blotting. Ramos cells were suspended in serum free RPMI and seeded at 6×10^5 cells/well, in a 24-well plate before being treated with 7.5 µM MPM-1 in a total volume of 750 µL. HSC-3 cells were seeded at 4×10^5 cells/well, in a 6-well plate, and left to adhere overnight. Cells were then washed once with serum free RPMI and treated with 17 µM MPM-1 in a total volume of 1 mL. Ramos and HSC-3 cells were treated for 0.5, 1, 2, 3 or 4 h in separate wells. Serum free medium ± 1% Triton X-100 functioned as positive and negative controls, respectively. After treatment, supernatants were collected and centrifuged to remove cell debris before being mixed with DTT and sample buffer. The samples were boiled for 5 min and loaded on a NuPAGE® 10% Bis–Tris Gel (Thermo Fisher Scientific) before being electro-transferred to a polyvindiline dilfluoride (PVDF)

immobilon-P membrane (Merck, Darmstadt, Germany). The membrane was blocked for 1 h with 5% non-fat dry milk in TBST and then incubated overnight at 4 °C with the primary antibody targeting HMGB1 (Abcam, #ab18256) diluted 1:1000 in 5% non-fat dry milk in TBST. Next, the membrane was washed and incubated with a horseradish peroxidase-conjugated goat anti-rabbit secondary antibody (Southern Biotech, Birmingham, AL, USA, Cat #4050-05) diluted 1:2000 in 5% non-fat dry milk in TBST for 1 h. After washing, the membrane was incubated for 5 min with 5 mL pre-mixed chemiluminescent peroxidase substrate-3 (Merck) and subsequently imaged on an ImageQuant LAS 3000 (GE Healthcare, Chicago, IL, USA). Band intensities were analyzed in Image Studio Lite Ver 5.2 (https://www.licor.com/bio/image-studio-lite/). HMGB1 release was expressed as percentage of release relative to the positive control sample.

Statistical analyses. Statistical analyses were performed in GraphPad Prism 9.0 (https://www.graphpad.com/). A p-value of < 0.05 was considered statistically significant. In all graphs, asterisks indicate significant differences: $^{*}p < 0.05$, $^{**}p < 0.01$, $^{***}p < 0.001$, $^{****}p < 0.0001$.

Ethical considerations. All use of human material was according to national guidelines. Blood samples from randomized anonymous healthy volunteers were obtained from the blood bank at the University Hospital North Norway in Tromsø, which is officially approved by the Norwegian Directorate of Health. Donors had given written informed consent for use of their blood for research, in accordance with the Declaration of Helsinki. Additional ethical approval for the use of anonymous blood samples for research was not required according to the Norwegian Health Research Act.

Data availability

The datasets generated and analyzed during the current study are available from the corresponding author on reasonable request.

Received: 22 December 2021; Accepted: 31 August 2022
Published online: 16 September 2022

References

1. Sung, H. *et al.* Global cancer statistics 2020: GLOBOCAN estimates of incidence and mortality worldwide for 36 cancers in 185 countries. *CA Cancer J. Clin.* **71**, 209–249 (2021).
2. Vitale, I. *et al.* Targeting cancer heterogeneity with immune responses driven by oncolytic peptides. *Trends Cancer* **7**, 557–572 (2021).
3. Galluzzi, L., Buque, A., Kepp, O., Zitvogel, L. & Kroemer, G. Immunogenic cell death in cancer and infectious disease. *Nat. Rev. Immunol.* **17**, 97–111 (2017).
4. Obeid, M. *et al.* Calreticulin exposure dictates the immunogenicity of cancer cell death. *Nat. Med.* **13**, 54–61 (2007).
5. Casares, N. *et al.* Caspase-dependent immunogenicity of doxorubicin-induced tumor cell death. *J. Exp. Med.* **202**, 1691–1701 (2005).
6. Pozzi, C. *et al.* The EGFR-specific antibody cetuximab combined with chemotherapy triggers immunogenic cell death. *Nat. Med.* **22**, 624–631 (2016).
7. Donnelly, O. G. *et al.* Measles virus causes immunogenic cell death in human melanoma. *Gene Ther.* **20**, 7–15 (2013).
8. Galluzzi, L., Kepp, O. & Kroemer, G. Immunogenic cell death in radiation therapy. *Oncoimmunology* **2**, e26536 (2013).
9. Berge, G. *et al.* Therapeutic vaccination against a murine lymphoma by intratumoral injection of a cationic anticancer peptide. *Cancer Immunol. Immunother.* **59**, 1285–1294 (2010).
10. Camilio, K. A., Berge, G., Ravuri, C. S., Rekdal, O. & Sveinbjørnsson, B. Complete regression and systemic protective immune responses obtained in B16 melanomas after treatment with LTX-315. *Cancer Immunol. Immunother.* **63**, 601–613 (2014).
11. Ausbacher, D., Svineng, G., Hansen, T. & Strøm, M. B. Anticancer mechanisms of action of two small amphipathic β(2,2)-amino acid derivatives derived from antimicrobial peptides. *Biochim. Biophys. Acta* **1818**, 2917–2925 (2012).
12. Mauseth, B. *et al.* The novel oncolytic compound LTX-401 induces antitumor immune responses in experimental hepatocellular carcinoma. *Mol. Ther. Oncolytics* **14**, 139–148 (2019).
13. Xie, W. *et al.* Tumor lysis with LTX-401 creates anticancer immunity. *Oncoimmunology* **8**, 1594555 (2019).
14. Tadesse, M. *et al.* The antibacterial ent-eusynstyelamide B and eusynstyelamides D, E, and F from the Arctic bryozoan Tegella cf. spitzbergensis. *J. Nat. Prod.* **74**, 837–841 (2011).
15. Strøm, M. B. *et al.* The pharmacophore of short cationic antibacterial peptides. *J. Med. Chem.* **46**, 1567–1570 (2003).
16. Paulsen, M. H. *et al.* Amphipathic barbiturates as mimics of antimicrobial peptides and the marine natural products eusynstyelamides with activity against multi-resistant clinical isolates. *J. Med. Chem.* **64**, 11395–11417 (2021).
17. Strøm, M. B., Bayer, A., Engqvist, S. O. M., Paulsen, M. H. & Ausbacher, D. Barbituric acid derivatives comprising cationic and lipophilic groups. WO/2018/178198. PCT/EP2018/058011 (2018).
18. Perry, S. W., Norman, J. P., Barbieri, J., Brown, E. B. & Gelbard, H. A. Mitochondrial membrane potential probes and the proton gradient: A practical usage guide. *Biotechniques* **50**, 98–115 (2011).
19. Vanden Berghe, T. *et al.* Necroptosis, necrosis and secondary necrosis converge on similar cellular disintegration features. *Cell Death Differ.* **17**, 922–930 (2010).
20. Kroemer, G. & Levine, B. Autophagic cell death: The story of a misnomer. *Nat. Rev. Mol. Cell Biol.* **9**, 1004–1010 (2008).
21. Dikic, I. & Elazar, Z. Mechanism and medical implications of mammalian autophagy. *Nat. Rev. Mol. Cell Biol.* **19**, 349–364 (2018).
22. Klionsky, D. J. *et al.* Guidelines for the use and interpretation of assays for monitoring autophagy (3rd edition). *Autophagy* **12**, 1–222 (2016).
23. Yoshimori, T., Yamamoto, A., Moriyama, Y., Futai, M. & Tashiro, Y. Bafilomycin A1, a specific inhibitor of vacuolar-type H(+)-ATPase, inhibits acidification and protein degradation in lysosomes of cultured cells. *J. Biol. Chem.* **266**, 17707–17712 (1991).
24. Boya, P. & Kroemer, G. Lysosomal membrane permeabilization in cell death. *Oncogene* **27**, 6434–6451 (2008).
25. Solitro, A. R. & MacKeigan, J. P. Leaving the lysosome behind: Novel developments in autophagy inhibition. *Future Med. Chem.* **8**, 73–86 (2016).
26. Gallagher, L. E. *et al.* Lysosomotropism depends on glucose: A chloroquine resistance mechanism. *Cell Death Dis.* **8**, e3014–e3014 (2017).
27. Shacka, J. J. *et al.* Bafilomycin A1 inhibits chloroquine-induced death of cerebellar granule neurons. *Mol. Pharmacol.* **69**, 1125–1136 (2006).

28. Altan, N., Chen, Y., Schindler, M. & Simon, S. M. Defective acidification in human breast tumor cells and implications for chemotherapy. *J. Exp. Med.* **187**, 1583–1598 (1998).
29. Kobayashi, H., Takemura, Y. & Ohnuma, T. Relationship between tumor cell density and drug concentration and the cytotoxic effects of doxorubicin or vincristine: Mechanism of inoculum effects. *Cancer Chemother. Pharmacol.* **31**, 6–10 (1992).
30. Tian, A.-L. *et al.* Lysosomotropic agents including azithromycin, chloroquine and hydroxychloroquine activate the integrated stress response. *Cell Death Dis.* **12**, 6 (2021).
31. Galluzzi, L. *et al.* Molecular mechanisms of cell death: Recommendations of the Nomenclature Committee on Cell Death 2018. *Cell Death Differ.* **25**, 486–541 (2018).
32. Krysko, O. *et al.* Necroptotic cell death in anti-cancer therapy. *Immunol. Rev.* **280**, 207–219 (2017).
33. Birge, R. B. *et al.* Phosphatidylserine is a global immunosuppressive signal in efferocytosis, infectious disease, and cancer. *Cell Death Differ.* **23**, 962–978 (2016).
34. Inoue, H. & Tani, K. Multimodal immunogenic cancer cell death as a consequence of anticancer cytotoxic treatments. *Cell Death Differ.* **21**, 39–49 (2014).
35. Kroemer, G., Galluzzi, L., Kepp, O. & Zitvogel, L. Immunogenic cell death in cancer therapy. *Annu. Rev. Immunol.* **31**, 51–72 (2013).
36. Elliott, M. R. *et al.* Nucleotides released by apoptotic cells act as a find-me signal to promote phagocytic clearance. *Nature* **461**, 282–286 (2009).
37. Galluzzi, L. *et al.* Consensus guidelines for the definition, detection and interpretation of immunogenic cell death. *J. Immunother. Cancer* **8** (2020).
38. Apetoh, L. *et al.* Toll-like receptor 4-dependent contribution of the immune system to anticancer chemotherapy and radiotherapy. *Nat. Med.* **13**, 1050–1059 (2007).
39. Hansen, T., Alst, T., Havelkova, M. & Strøm, M. B. Antimicrobial activity of small beta-peptidomimetics based on the pharmacophore model of short cationic antimicrobial peptides. *J. Med. Chem.* **53**, 595–606 (2010).

Acknowledgements

This study received funding from the MABIT program (Grant no. BS0086). The publication charges for this article have been funded by a grant from the publication fund of UiT The Arctic University of Norway. The authors thank Peter McCourt for linguistic revision of the manuscript as well as Dr. Adrienne Scheck and Professor Terje Johansen for donation of cell lines. We would also like to thank the blood bank at the University Hospital North Norway in Tromsø for providing blood samples. Further, we would like to thank the Advanced Microscopy Core Facility (AMCF) at UiT, especially Kenneth Bowitz Larsen and Randi Olsen, for providing excellent technical assistance and participating in discussions.

Author contributions

S.H. performed all mechanistic studies of MPM-1, analyzed the results and wrote the manuscript. M.H.P., A.B. and M.B.S. invented the synthesis procedure for the molecule MPM-1. M.H.P. synthesized all MPM-1 used in the current study and wrote parts of the manuscript. G.B., S.N.M., M.B.S., D.A. and M.K. contributed to the acquisition and analysis of results. All authors have contributed substantially to the revision of the manuscript and have approved the final submitted version.

Funding

Open access funding provided by UiT The Arctic University of Norway (incl University Hospital of North Norway).

Competing interests

The authors declare no competing interests.

Additional information

Supplementary Information The online version contains supplementary material available at https://doi.org/10.1038/s41598-022-19597-4.

Correspondence and requests for materials should be addressed to S.H.

Reprints and permissions information is available at www.nature.com/reprints.

Publisher's note Springer Nature remains neutral with regard to jurisdictional claims in published maps and institutional affiliations.

The Marine Natural Product Mimic MPM-1 is Cytolytic and Induces DAMP Release from Human Cancer Cell Lines

Susannah von Hofsten[1*], Marianne Hagensen Paulsen[2], Synnøve Norvoll Magnussen[1], Dominik Ausbacher[2], Mathias Kranz[3], Annette Bayer[4], Morten B. Strøm[2] and Gerd Berge[1]

[1]Department of Medical Biology, Faculty of Health Sciences, UiT The Arctic University of Norway, 9037 Tromsø, Norway. [2]Department of Pharmacy, Faculty of Health Sciences, UiT The Arctic University of Norway, 9037 Tromsø, Norway. [3]PET Imaging Center Tromsø, University Hospital of North Norway, 9019 Tromsø, Norway. [4]Department of Chemistry, UiT The Arctic University of Norway, 9037 Tromsø, Norway. *email: susannah.hofsten@uit.no

Supplementary Figures and Legends

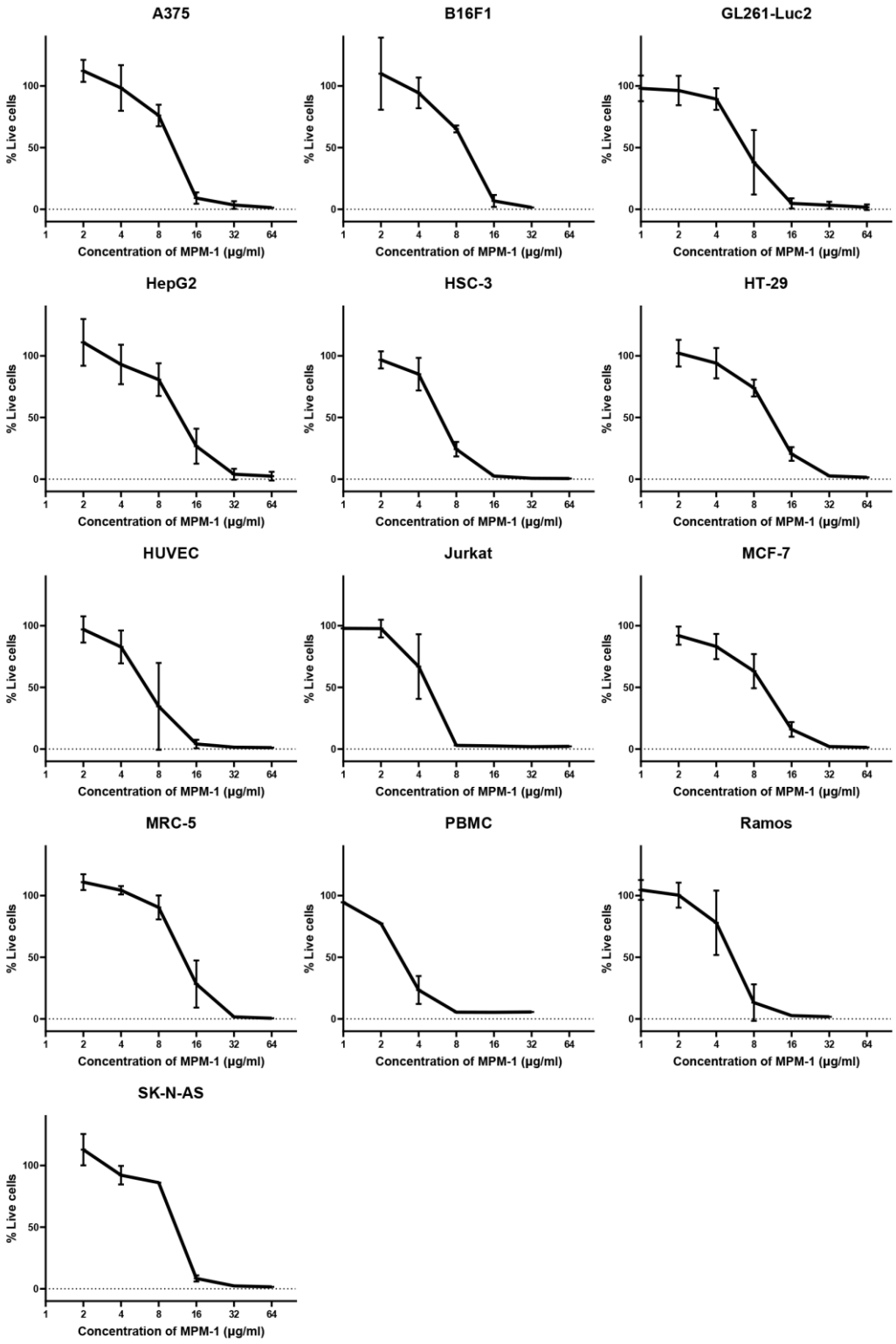

Supplementary Figure S1. Dose-response curves for all cell lines tested against MPM-1. The data is based on three independent MTS experiments, and error bars represent the standard deviation.

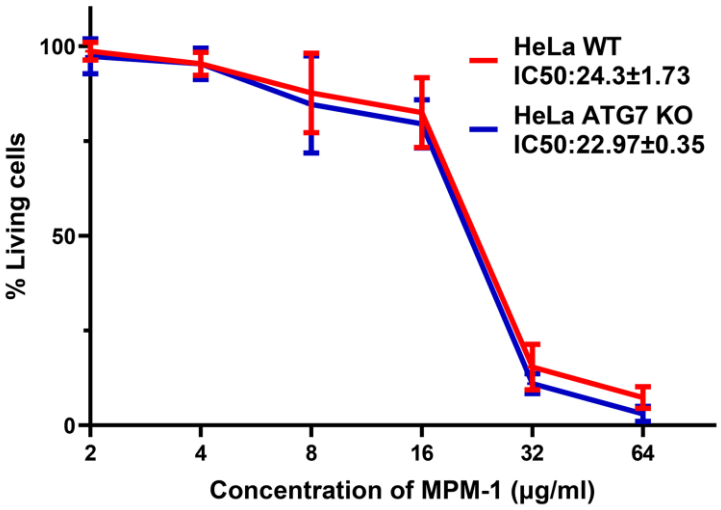

Supplementary Figure S2. Dose-response curves for wild type HeLa cells and ATG7 knockout HeLa cells treated with MPM-1. The data is based on three independent MTS experiments, and error bars represent the standard deviation.

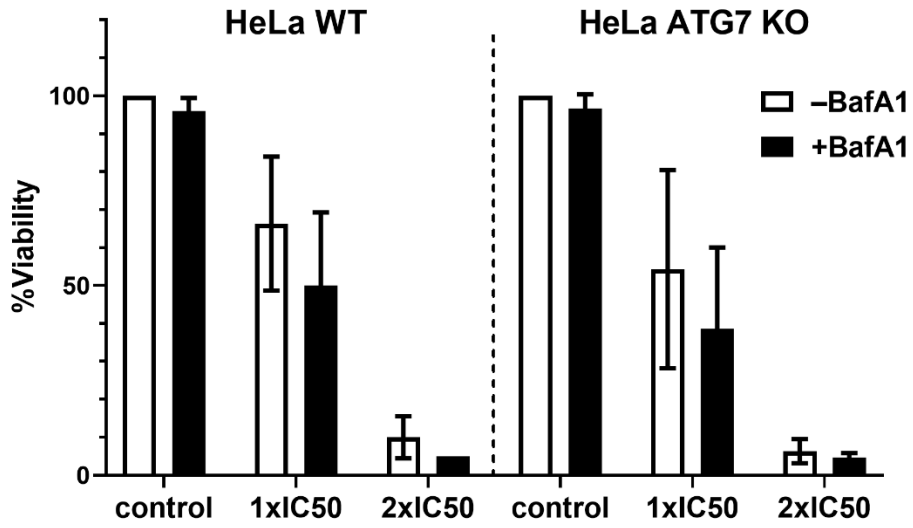

Supplementary Figure S3. Viability of wild type HeLa cells and ATG7 knockout HeLa cells was measured upon treatment with MPM-1 in the presence or absence of Bafilomycin A1 (100 nM). The concentration of MPM-1 was equal to 1xIC50 (23 µg/ml) or 2xIC50 (46 µg/ml). The data is based on three independent MTS experiments, and error bars represent the standard deviation.

Ramos

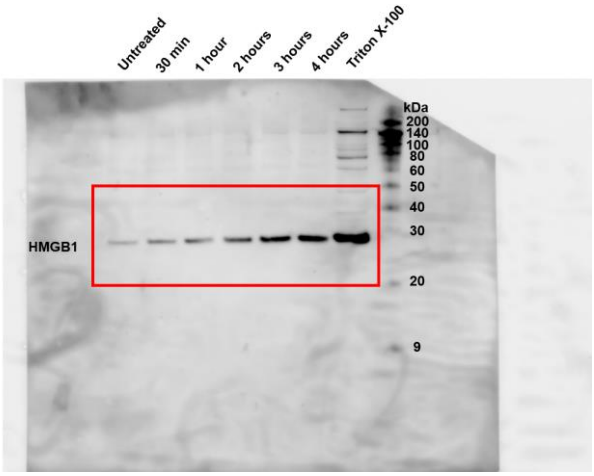

Ramos

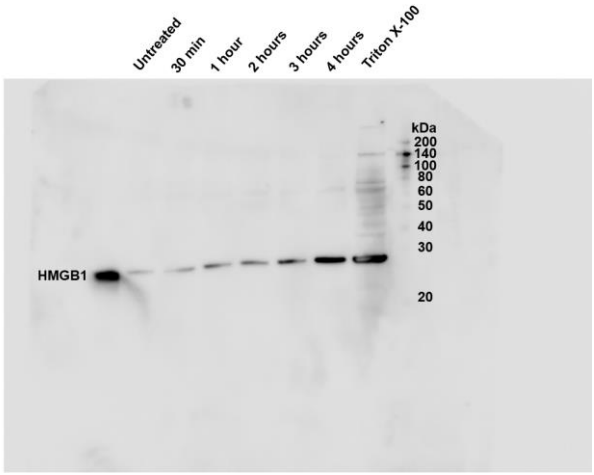

Ramos

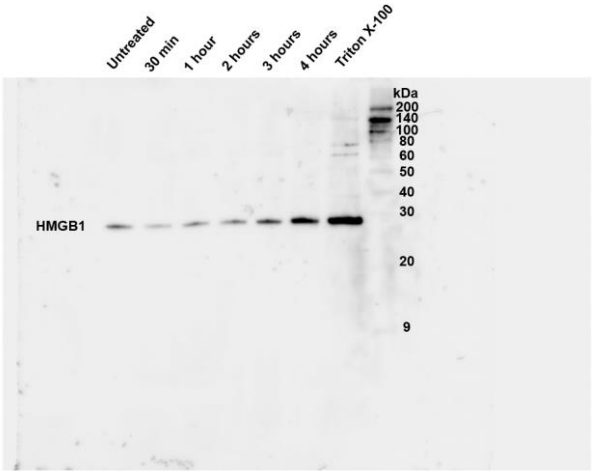

HSC-3

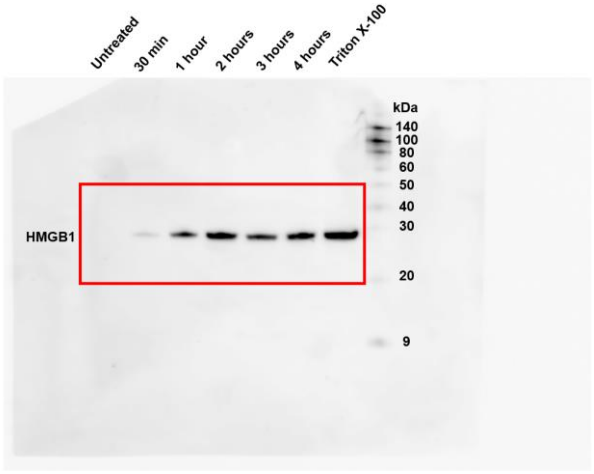

HSC-3

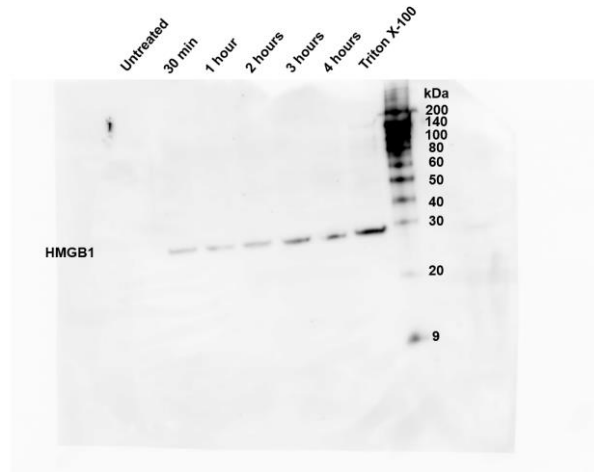

HSC-3

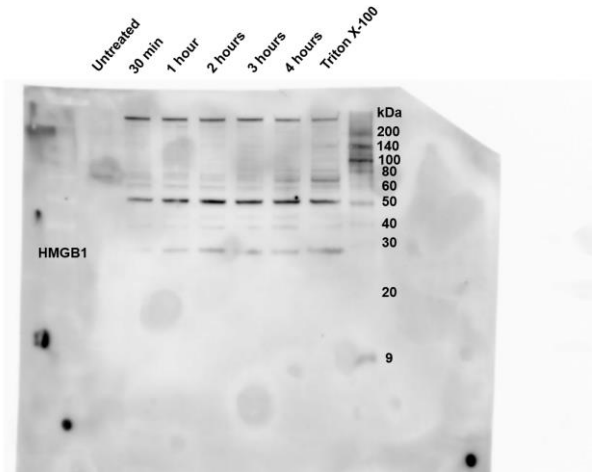

Supplementary Figure S4. Uncropped images of blots presented in Figure 6c in the main article as well as the two additional replicates.

Supplementary Video S1. HSC-3 cells treated with 1xIC50 (8.5 µM) MPM-1.

Supplementary Video S2. HSC-3 cells treated with ½xIC50 (4.25 µM) MPM-1.

Supplementary Data S1

NMR for all intermediate molecules produced during the synthesis of the target compound MPM-1.

Compound 2

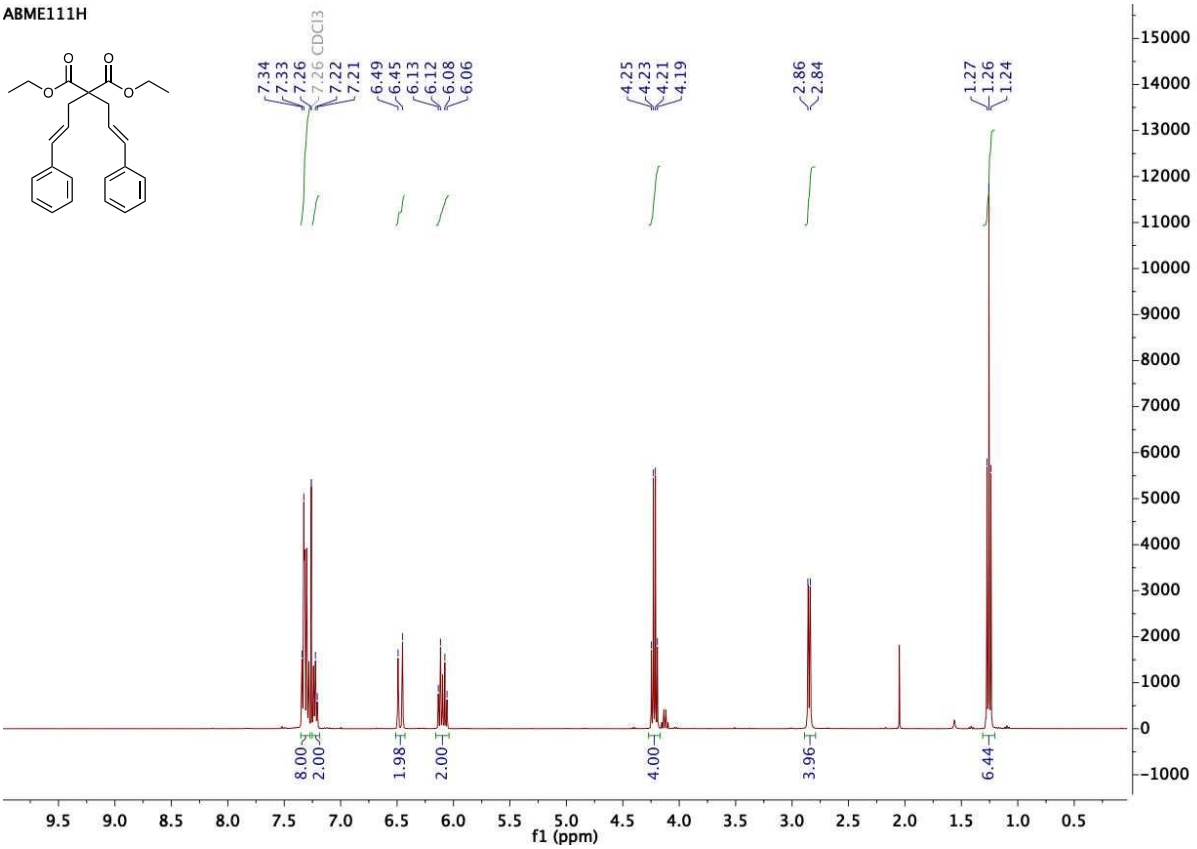

Compound 3

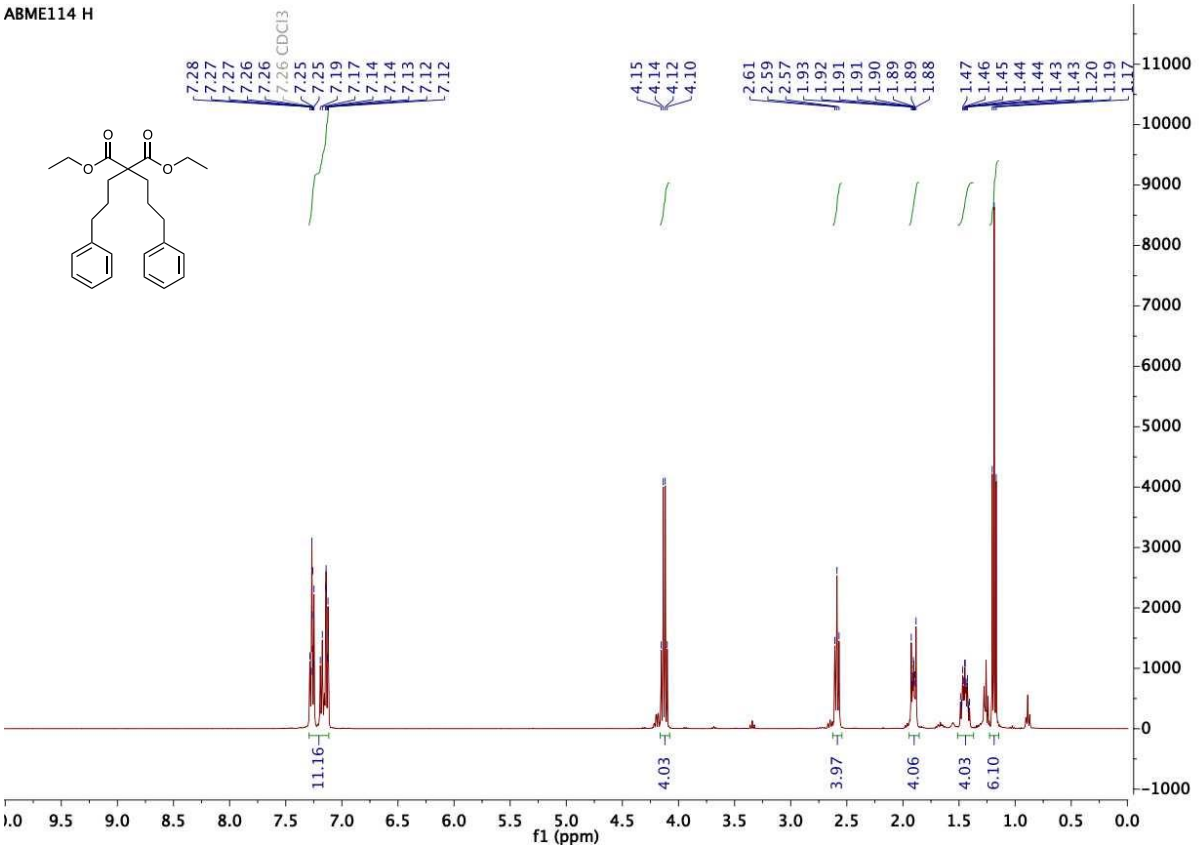
ABME114 H
7.28
7.27
7.27
7.26
7.26
7.26 CDCl3
7.25
7.25
7.19
7.17
7.14
7.14
7.13
7.12
7.12
4.15
4.14
4.12
4.10
2.61
2.59
2.57
1.93
1.92
1.91
1.91
1.90
1.89
1.89
1.88
1.47
1.46
1.45
1.44
1.44
1.43
1.43
1.20
1.19
1.17
11.16
4.03
3.97
4.06
4.03
6.10
f1 (ppm)

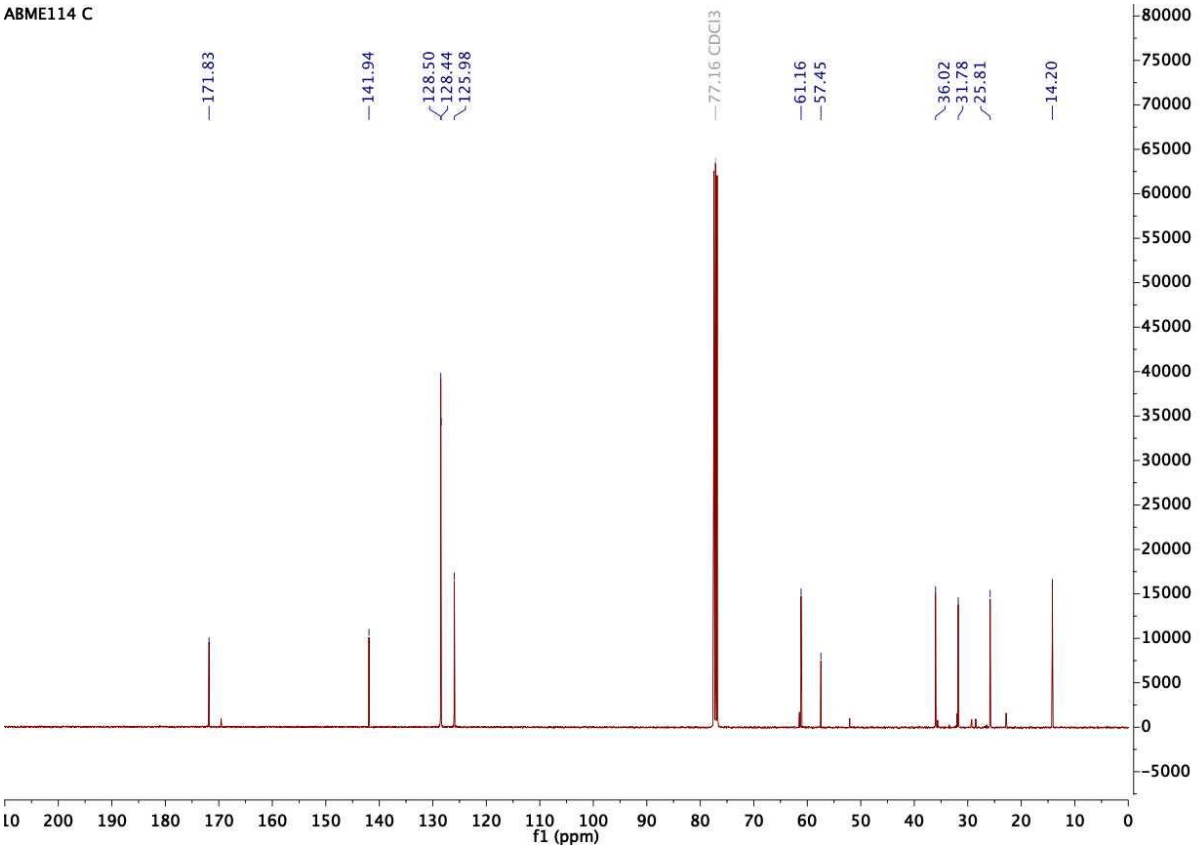
ABME114 C
171.83
141.94
128.50
128.44
125.98
77.16 CDCl3
61.16
57.45
36.02
31.78
25.81
14.20
f1 (ppm)

Compound 4

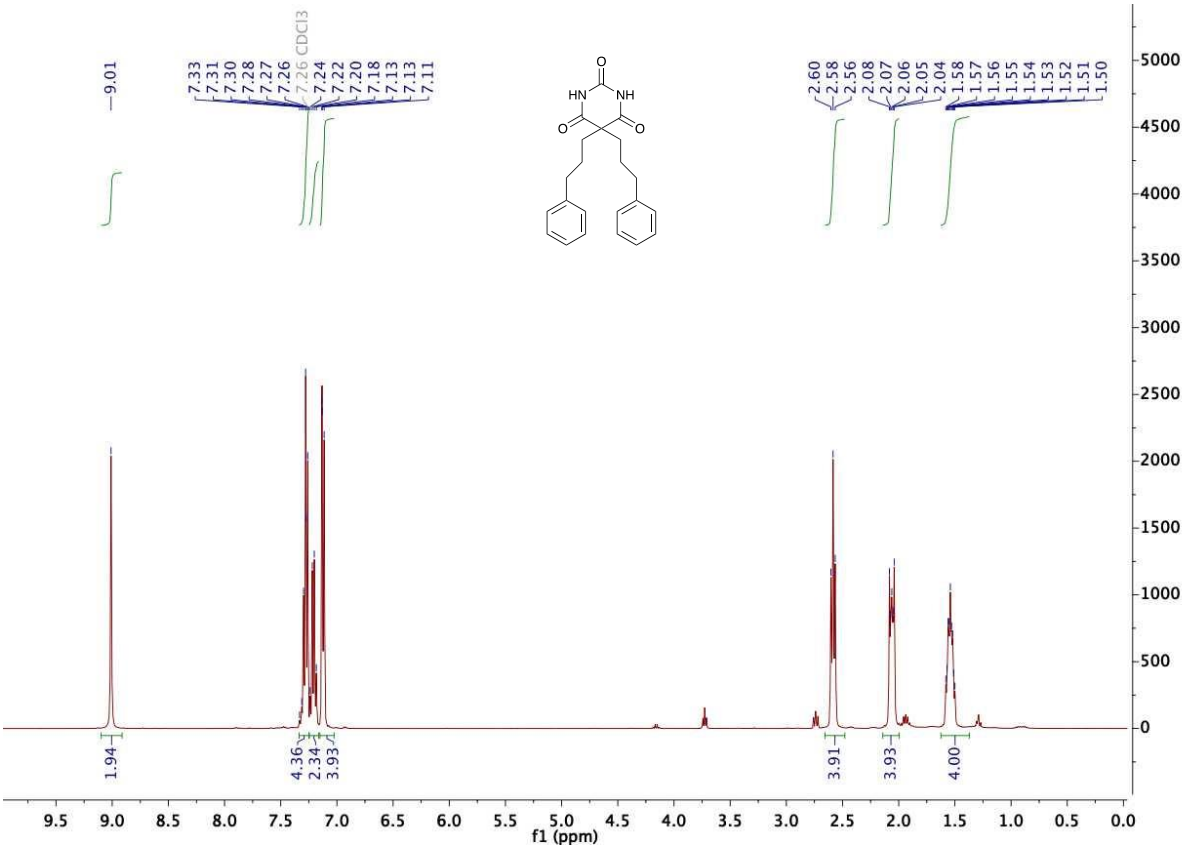
9.01
7.33
7.31
7.30
7.28
7.27
7.26
7.26 CDCl3
7.24
7.22
7.20
7.18
7.13
7.11
2.60
2.58
2.56
2.08
2.07
2.06
2.05
2.04
1.58
1.57
1.56
1.55
1.54
1.53
1.52
1.51
1.50
HN
NH
O
O
O
1.94
4.36
2.34
3.93
3.91
3.93
4.00
f1 (ppm)

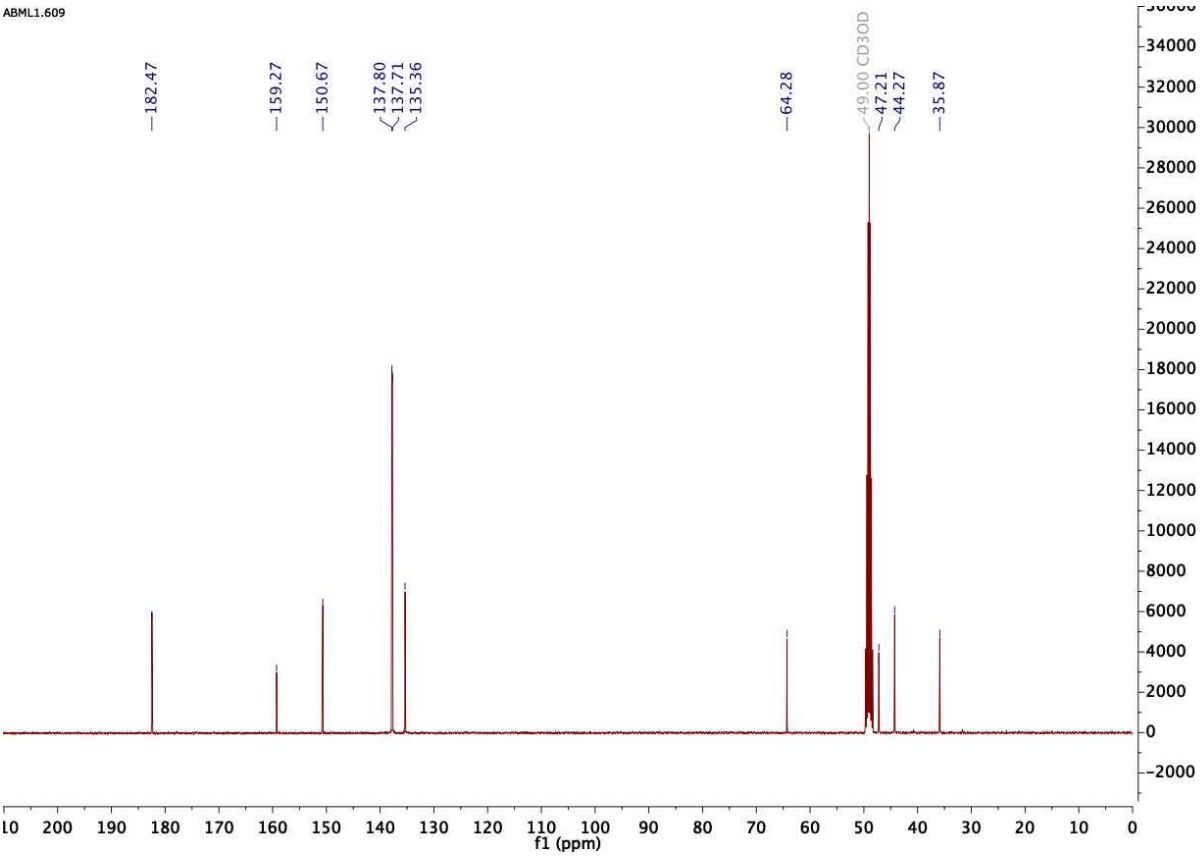
ABML1.609
182.47
159.27
150.67
137.80
137.71
135.36
64.28
49.00 CD3OD
47.21
44.27
35.87
f1 (ppm)

Compound 5

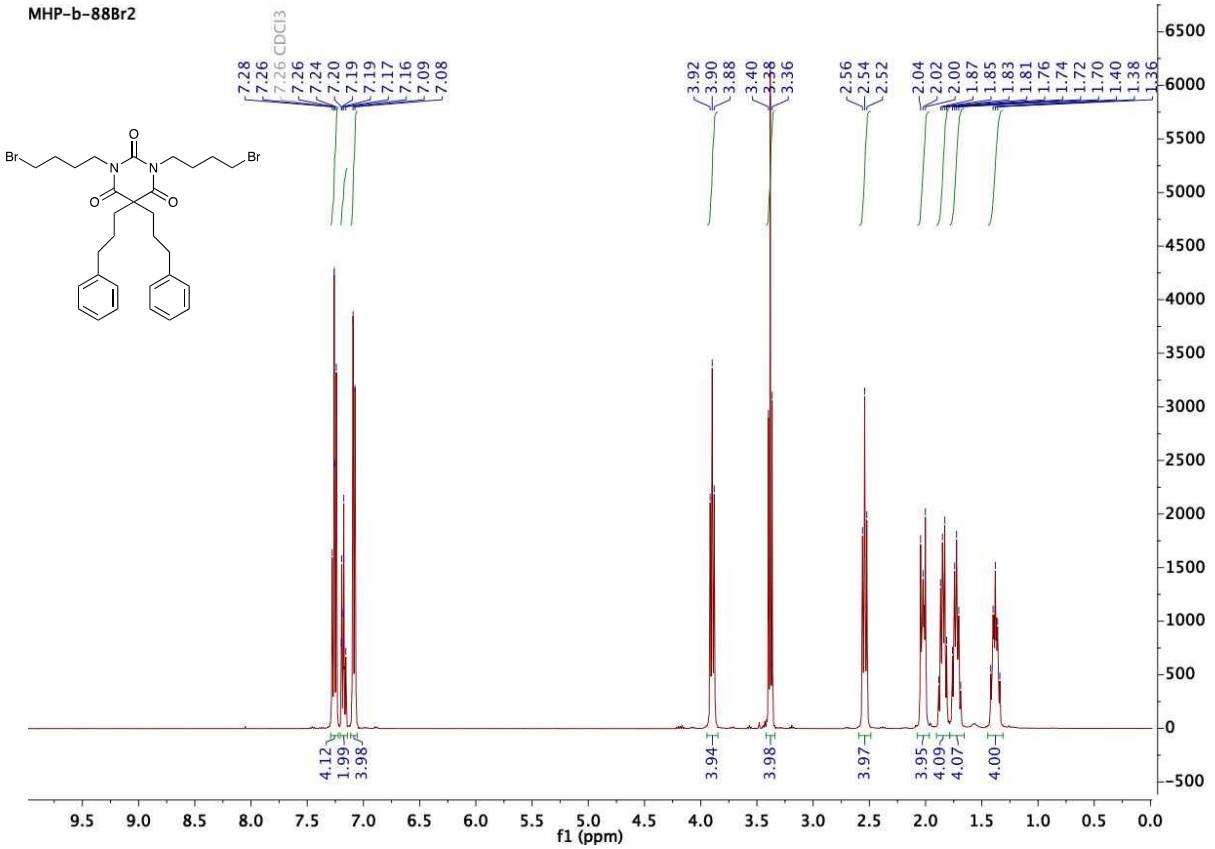
MHP-b-88Br2
Br
Br
O
O
O
O
N
N
7.28
7.26
7.26 CDCl3
7.24
7.20
7.19
7.19
7.17
7.16
7.09
7.08
3.92
3.90
3.88
3.40
3.38
3.36
2.56
2.54
2.52
2.04
2.02
2.00
1.87
1.85
1.83
1.81
1.76
1.74
1.72
1.70
1.40
1.38
1.36
4.12
1.99
3.98
3.94
3.98
3.97
3.95
4.09
4.07
4.00
f1 (ppm)

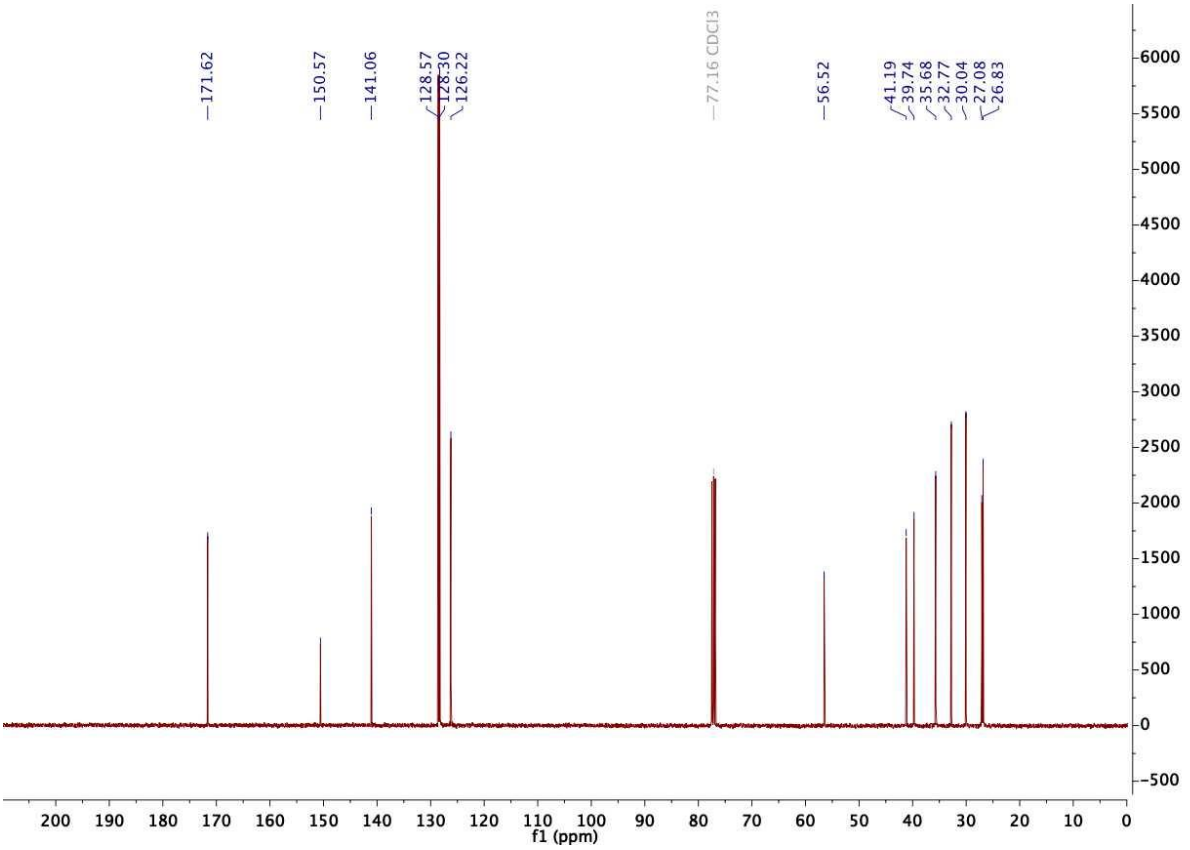
171.62
150.57
141.06
128.57
128.30
126.22
77.16 CDCl3
56.52
41.19
39.74
35.68
32.77
30.04
27.08
26.83
f1 (ppm)

Compound 6

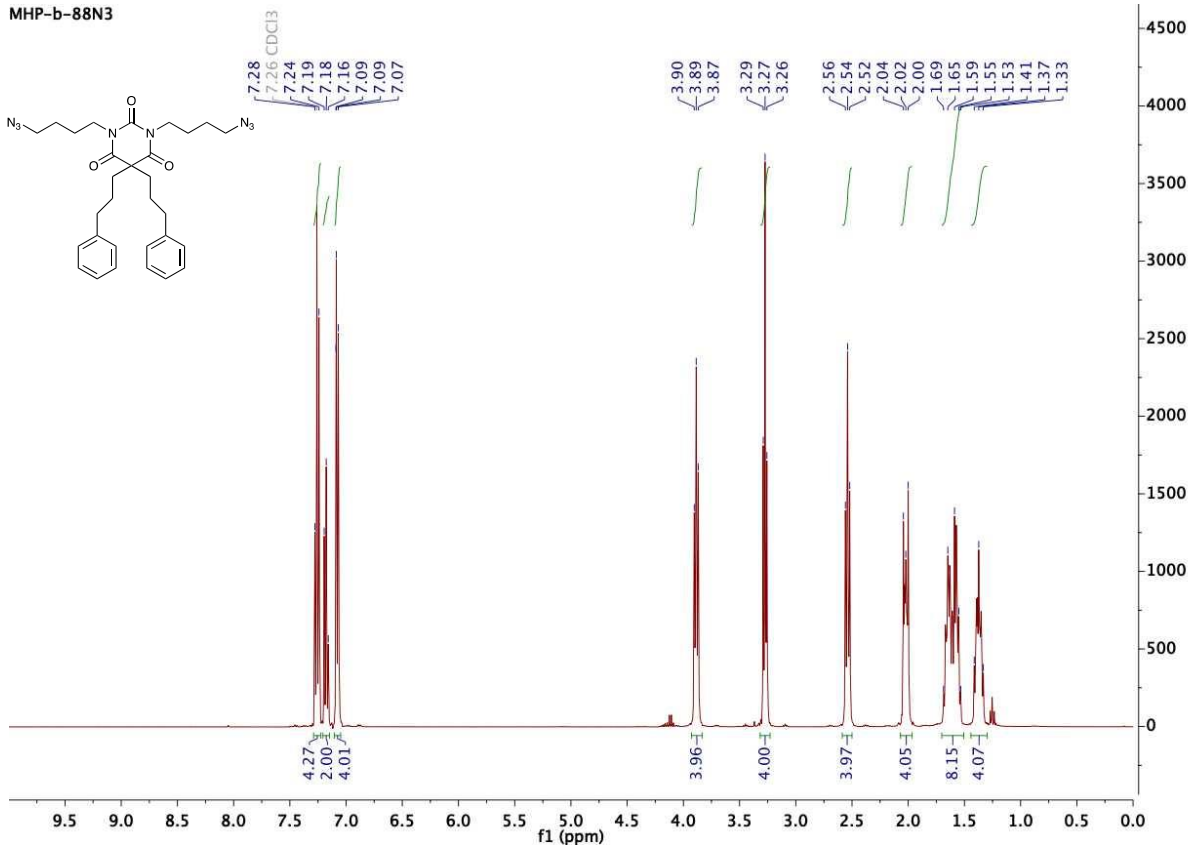
MHP-b-88N3
7.28
7.26 CDCl3
7.24
7.19
7.18
7.16
7.09
7.09
7.07
3.90
3.89
3.87
3.29
3.27
3.26
2.56
2.54
2.52
2.04
2.02
2.00
1.69
1.65
1.59
1.55
1.53
1.41
1.37
1.33
4.27
2.00
4.01
3.96
4.00
3.97
4.05
8.15
4.07
f1 (ppm)

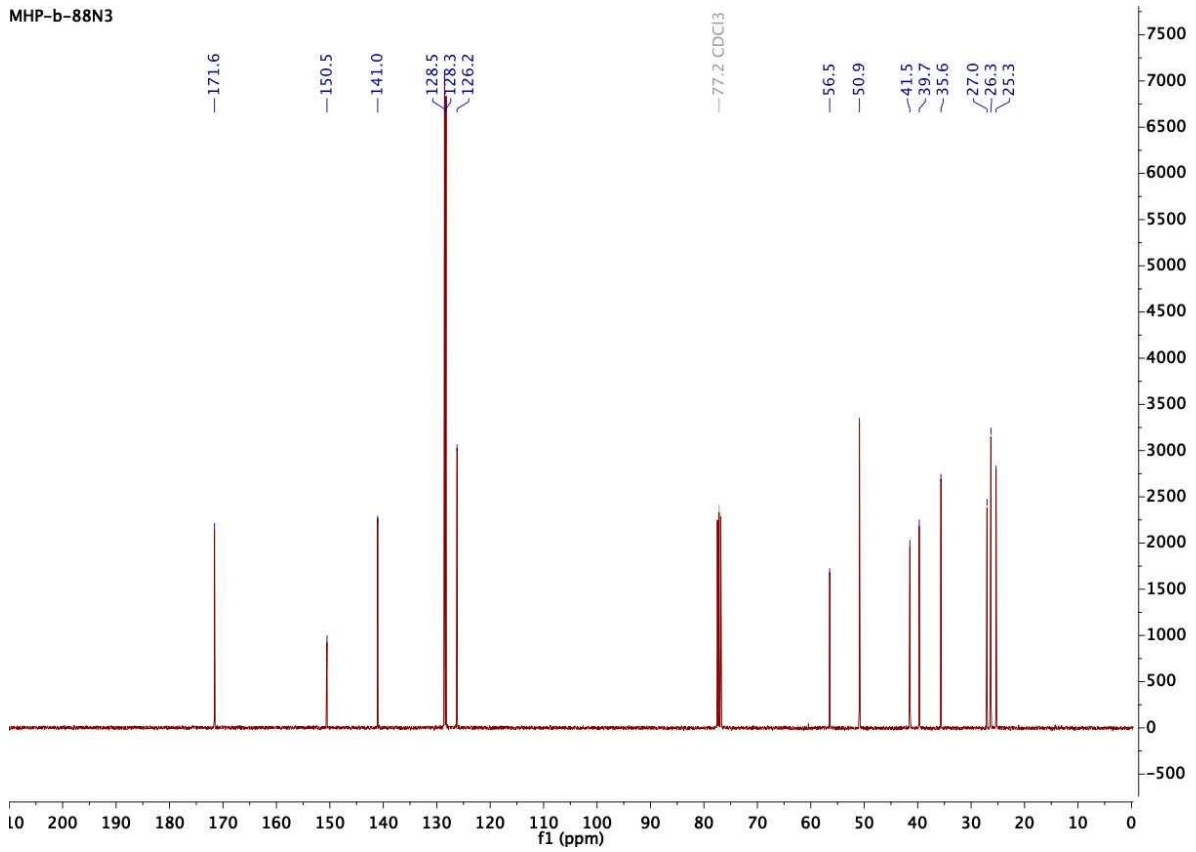
MHP-b-88N3
171.6
150.5
141.0
128.5
128.3
126.2
77.2 CDCl3
56.5
50.9
41.5
39.7
35.6
27.0
26.3
25.3
f1 (ppm)

MPM-1

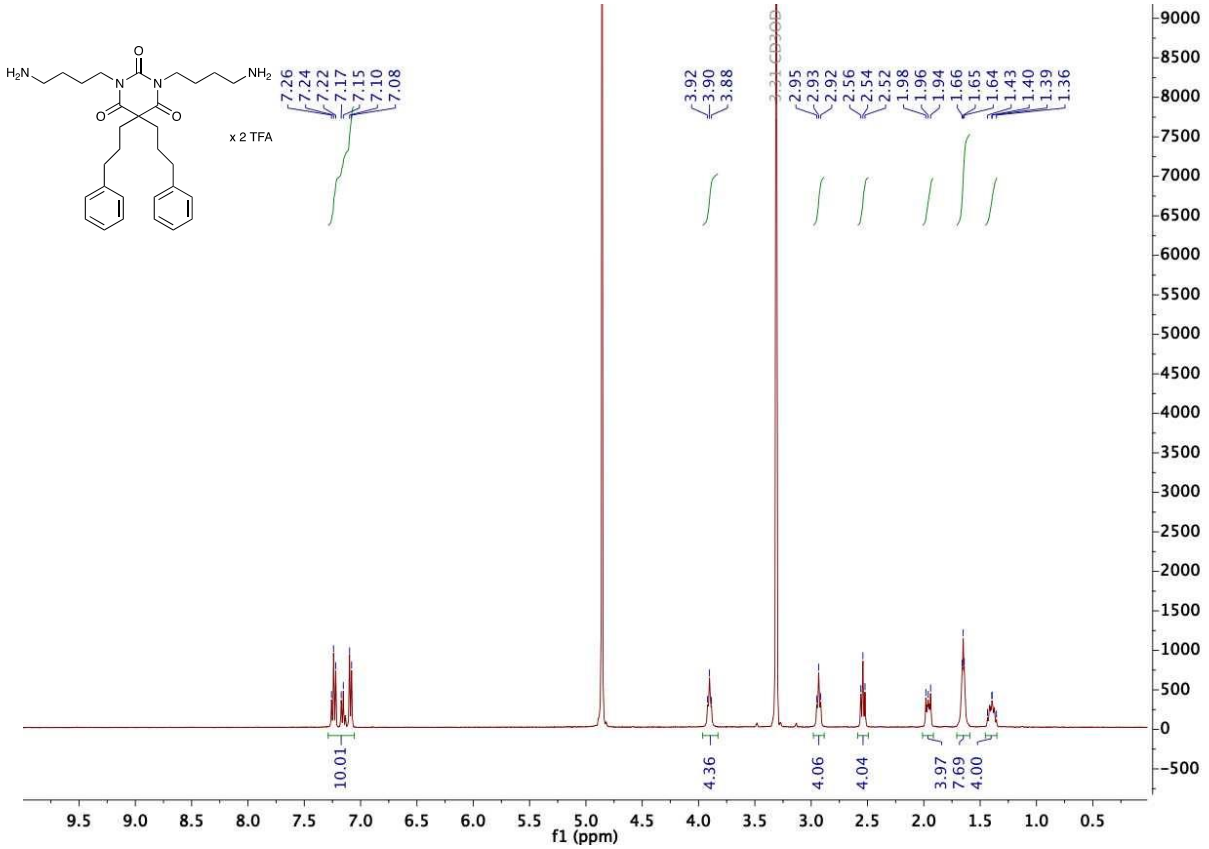
x 2 TFA
7.26
7.24
7.22
7.17
7.15
7.10
7.08
3.92
3.90
3.88
2.95
2.93
2.92
2.56
2.54
2.52
1.98
1.96
1.94
1.66
1.65
1.64
1.43
1.40
1.39
1.36
10.01
4.36
4.06
4.04
3.97
7.69
4.00
f1 (ppm)

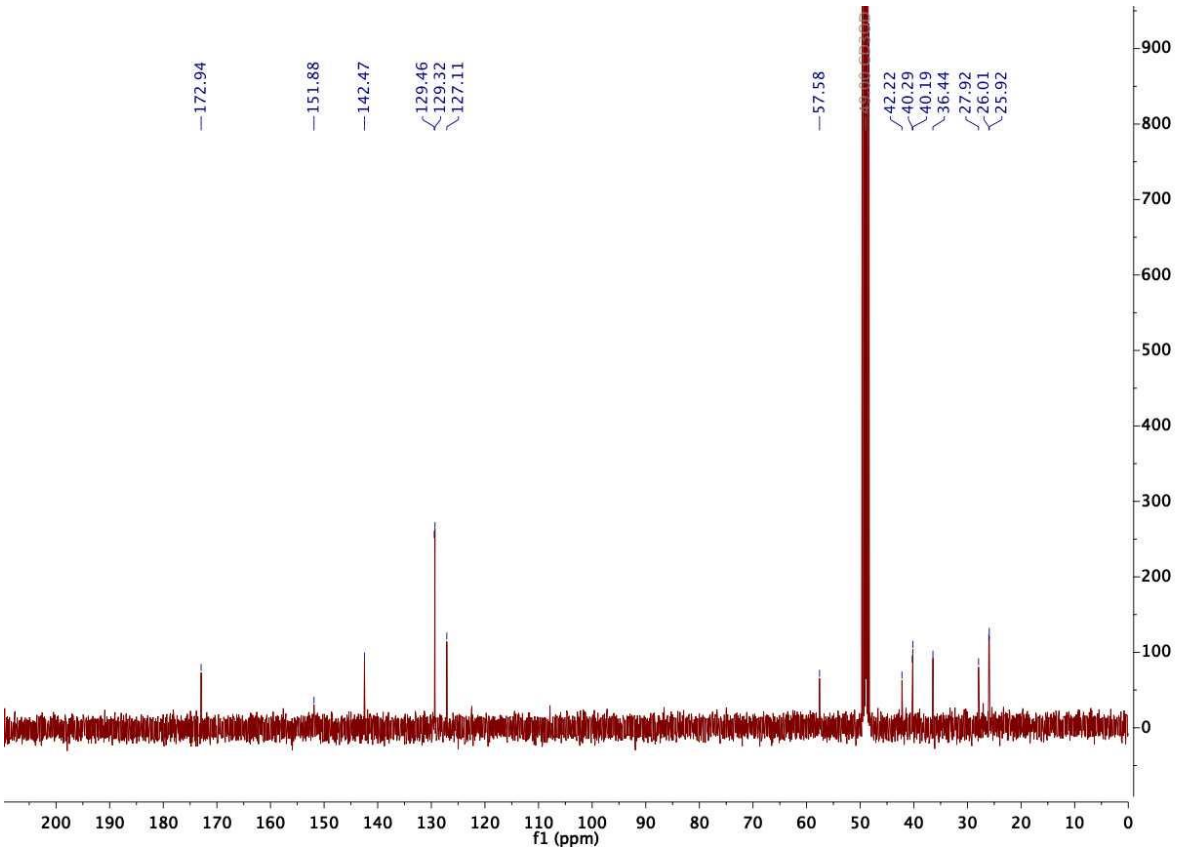
172.94
151.88
142.47
129.46
129.32
127.11
57.58
42.22
40.29
40.19
36.44
27.92
26.01
25.92
f1 (ppm)

Purity SFC^2

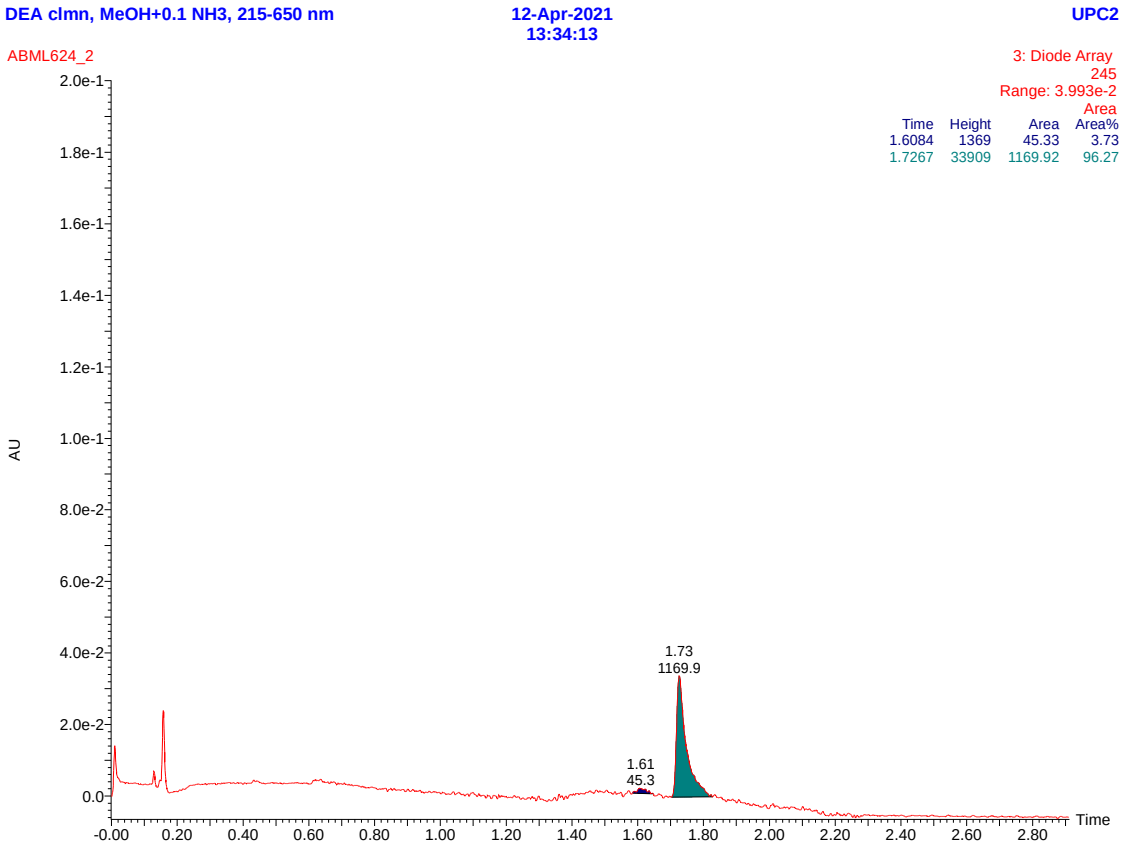
DEA clmn, MeOH+0.1 NH3, 215-650 nm
12-Apr-2021
13:34:13
UPC2
ABML624_2
3: Diode Array
245
Range: 3.993e-2
Area
Time Height Area Area%
1.6084 1369 45.33 3.73
1.7267 33909 1169.92 96.27
AU
2.0e-1
1.8e-1
1.6e-1
1.4e-1
1.2e-1
1.0e-1
8.0e-2
6.0e-2
4.0e-2
2.0e-2
0.0
1.73
1169.9
1.61
45.3
-0.00 0.20 0.40 0.60 0.80 1.00 1.20 1.40 1.60 1.80 2.00 2.20 2.40 2.60 2.80
Time

Paper II

frontiers | Frontiers in Pharmacology

TYPE Original Research
PUBLISHED 30 March 2023
DOI 10.3389/fphar.2023.1141669

OPEN ACCESS

EDITED BY
Letizia Polito,
Diagnostic and Specialty Medicine—Alma Mater Studiorum—University of Bologna, Italy

REVIEWED BY
Karin Bartel,
Ludwig Maximilian University of Munich, Germany
Cátia Santos-Pereira,
University of Minho, Portugal
Tatiana Viktorovna Denisenko,
Lomonosov Moscow State University, Russia

*CORRESPONDENCE
Annette Bayer,
annette.bayer@uit.no
Gerd Berge,
gerd.berge@uit.no

SPECIALTY SECTION
This article was submitted to Experimental Pharmacology and Drug Discovery, a section of the journal Frontiers in Pharmacology

RECEIVED 10 January 2023
ACCEPTED 17 March 2023
PUBLISHED 30 March 2023

CITATION
von Hofsten S, Langer MK, Korelin K, Magnussen S, Ausbacher D, Anderssen T, Salo T, Strøm MB, Bayer A, Al-Samadi A and Berge G (2023), Amphipathic barbiturates as marine product mimics with cytolytic and immunogenic effects on head and neck squamous cell carcinoma cell lines.
Front. Pharmacol. 14:1141669.
doi: 10.3389/fphar.2023.1141669

Amphipathic barbiturates as marine product mimics with cytolytic and immunogenic effects on head and neck squamous cell carcinoma cell lines

Susannah von Hofsten[1], Manuel K. Langer[2], Katja Korelin[3,4], Synnøve Magnussen[1], Dominik Ausbacher[5], Trude Anderssen[5], Tuula Salo[3,4], Morten B. Strøm[5], Annette Bayer[2]*, Ahmed Al-Samadi[3,4] and Gerd Berge[1]*

[1]Department of Medical Biology, Faculty of Health Sciences, UiT—The Arctic University of Norway, Tromsø, Norway, [2]Department of Chemistry, Faculty of Science and Technology, UiT—The Arctic University of Norway, Tromsø, Norway, [3]Department of Oral and Maxillofacial Diseases, University of Helsinki, Helsinki, Finland, [4]Translational Immunology Research Program (TRIMM), University of Helsinki, Helsinki, Finland, [5]Department of Pharmacy, Faculty of Health Sciences, UiT—The Arctic University of Norway, Tromsø, Norway

The incidence of head and neck squamous cell carcinoma (HNSCC) is increasing and the conventional treatments for this form of cancer can be tough. Despite the success of existing immunotherapies in some HNSCC patients, many do not respond to this type of treatment. Thus, the development of novel anti-cancer therapies should be prioritized. In the current study, the anticancer activity of a panel of novel compounds, herein termed marine product mimics (MPMs), against HNSCC cell lines is explored. The previously reported compound MPM-1, which is structurally related to the novel MPMs, was shown to have promising effects on the HNSCC cell line HSC-3. The results from the current study indicate that the novel MPMs are more potent than MPM-1 but cause a similar type of cell death. The results indicated that the MPMs must cross through the cell membrane to exert their action and that they are lysosomotropic. Further experiments showed that some of the MPMs could induce phosphorylation of eukaryotic initiation factor 2α (eIF2α) in HSC-3 and UT-SCC-24A cells, which indicates that they can activate the integrated stress response that is strongly associated with immunogenic cell death. Cell surface expression of calreticulin and release of HMGB1 and ATP, which are all hallmarks of immunogenic cell death, was also demonstrated in HSC-3 and UT-SCC-24A cells treated with MPMs. This suggests that the MPMs are interesting candidates for future HNSCC cancer therapies.

KEYWORDS

cancer, lysosomotropic, calreticulin, immunogenic cell death, head and neck squamous cell cancer (HNSCC), drug development

1 Introduction

Head and neck squamous cell carcinoma (HNSCC) (which includes all cancers of the lip and oral cavity, salivary glands, oropharynx, nasopharynx, hypopharynx, and larynx) is the cancer with the seventh highest incidence worldwide, and the incidence is increasing (Sung et al., 2021). Standard treatment of HNSCC involves surgery and irradiation or chemoradiotherapy with cisplatin and 5-fluorouracil (Johnson et al., 2020). The epidermal growth factor receptor (EGFR) inhibitor cetuximab can also be used. However, resistance to chemotherapy and targeted therapy is a frequent concern in HNSCC patients (Wang et al., 2016). During recent years, immunotherapy in the form of programmed cell death protein 1 (PD-1) inhibitors has also been approved as treatment for patients with recurrent or metastatic HNSCC in several countries (Johnson et al., 2020).

The emergence of different forms of immunotherapy has revolutionized cancer treatment during recent years.In particular, checkpoint inhibitors have been very successful in certain cancers and patient groups (Waldman et al., 2020). Nevertheless, there are still many patients who do not respond to treatment with existing immunotherapies. Thus, the need for the development of novel therapies persists.

The effect of immunotherapy relies on the ability of the patient's own immune system to recognize and kill cancer cells. The recognition of cancer cells is dependent on the cancer cells' presentation of cancer-related antigens on major histocompatibility complex molecules (MHC) (Waldman et al., 2020). Typically, these are neoantigens which emerge due to the mutations that occur in cancer cells during tumor progression. Thus, cancer types with a high mutational burden are often those that respond best to immunotherapy (Sha et al., 2020). HNSCC generally has a medium to high tumor mutational burden and studies have indicated that those HNSCC patients who have a higher tumor mutational burden do respond better to immunotherapy than those with a lower mutational burden (Sha et al., 2020).

A high mutational burden is not only beneficial for treatment with immune checkpoint inhibitors, but also for other immunotherapies. A promising form of immunotherapy for solid tumors consists of the intratumoral injection of oncolytic compounds that induce immunogenic cell death in cancer cells (Vitale et al., 2021). The induction of immunogenic cell death causes the release of tumor antigens as well as damage-associated molecular patterns (DAMPs) such as high mobility group box 1 (HMGB1) and adenosine triphosphate (ATP) (Galluzzi et al., 2017). Cell surface expression of calreticulin, which functions as an "eat-me" signal for immune cells, is also considered a hallmark of immunogenic cell death. Cancer cells succumbing to immunogenic cell death can cause the activation of an anti-tumor immune response, which leads to the infiltration of immune cells to the tumor area and the killing of more cancer cells.

We have previously reported on the cytolytic marine natural product mimic MPM-1 (von Hofsten et al., 2022). MPM-1 is a simplified mimic of the natural product *eusynstyelamide D*, which has been isolated from an arctic bryozoan (Tadesse et al., 2011). Instead of the five-membered dihydroxybutyrolactam ring which serves as the scaffold in *eusynstyelamide D*, MPM-1 is built on a symmetrical barbiturate scaffold, which makes it easier to synthesize. In addition, both *eusynstyelamide D* and MPM-1 contain two cationic and two lipophilic groups, which makes these compounds amphipathic. Our previous study suggested that MPM-1 was able to induce immunogenic cell death in the HNSCC cell line HSC-3 (von Hofsten et al., 2022). In the present study, we explore the anti-cancer and immunogenic effects of an extended panel of compounds which are structurally related to MPM-1. We study the mechanism of action of these compounds as well as the mode of death that they induce in HNSCC cell lines.

2 Materials and methods

2.1 Compounds

The MPMs were manufactured in-house and dissolved in DMSO to a concentration of 100 mM. Further dilutions were performed in cell culture media. The synthesis of the MPMs is described in detail in the Supplementary Data.S1

2.2 Cell culture

HSC-3 (RRID: CVCL_1288) was obtained from the Japanese Collection of Research Bioresources Cell Bank (JCRB Cell Bank, Osaka, Japan). The UT-SCC-8, UT-SCC-24A, UT-SCC-24B, UT-SCC-42A, UT-SCC-42B and UT-SCC-106A cell lines were all established at and obtained from Turku University Hospital and Prof. Grénman's laboratory. All cancer cell lines were cultured in 1:1 DMEM/F-12 (#31330-038, Thermo Fisher Scientific, Waltham, MA, United States) supplemented with 10% fetal bovine serum (FBS), 1% ascorbic acid, 1% PenStrep, 0.1% amphotericin B and 0.01% hydrocortisone. The NOF cell line had been established in a previous study (Sinha et al., 2020). They were cultured in DMEM high glucose (#41965-039, Thermo Fisher Scientific) supplemented with 10% FBS, 1% sodium pyruvate, 1% PenStrep, and 0.1% amphotericin B. In the high throughput drug screening, the live cell apoptosis assay, and the migration and invasion assays, wells were plated with the human tumor-derived matrix "myogel" to provide a more realistic tumor microenvironment and improve the predictability of drug testing (Salo et al., 2018; Tuomainen et al., 2019). The use of human leiomyoma tissue to produce myogel was approved by the Ethics Committee of both Oulu and Helsinki University Hospitals (statement number 2/2017), and all research was performed in accordance with relevant regulations.

2.3 Hemolysis assay

The hemolytic effect of the MPMs was determined using a hemolysis assay as previously described (Paulsen et al., 2021). Briefly, hemolysis was determined using a heparinized fraction (10 IU/mL) of freshly drawn blood. The blood collected in ethylenediaminetetraacetic acid-containing test tubes (Vacutest, KIMA, Arzergrande, Italy) was used for the determination of the hematocrit (hct). The heparinized blood was washed 3 × with pre-warmed phosphate-buffered saline (PBS) and adjusted to a final hct of 4%. MPMs in DMSO (50 mM) were added to a 96-well

polypropylene V-bottom plate (NUNC, Fisher Scientific, Oslo, Norway) and serially diluted. The test concentration range was 4–500 μM with DMSO contents ≤1%. A solution of 1% triton X-100 was used as a positive control for 100% hemolysis. As a negative control, a solution of 1% DMSO in PBS was included. Red blood cells (1% v/v final concentration) were added to the well plate and incubated at 37°C and 800 rpm for 1 h. After centrifugation (5 min, 3000 g), 100 μL from each well was transferred to a 96-well flat-bottomed microtiter plate, and absorbance was measured at 545 nm with a microplate reader (VersaMaxTM, Molecular Devices, Sunnyvale, CA, United States). The percentage of hemolysis was calculated as the ratio of the absorbance in the MPM treated and surfactant-treated samples, corrected for the PBS background. Three independent experiments were performed, and EC50 values are presented as averages.

2.4 High throughput drug screening

The MPMs were screened against a panel of eight different cell lines (HSC-3, UT-SCC-8, UT-SCC-24A, UT-SCC-24B, UT-SCC-42A, UT-SCC-42B and NOF) at the High Throughput Biomedicine Unit (HTB) at the Institute for Molecular Medicine Finland (FIMM). On day 1, black-walled 384-well plates were coated with 5 μl diluted myogel (0.5 mg/ml) per well using an automated reagent dispenser (MultiFlo FX, BioTek, Winooski, VT, United States). On day 2, 500 cells per well were seeded in 20 μl of complete media using the MultiFlo FX (BioTek), and the cells were left to adhere overnight. On day 3, the MPMs, cisplatin, DMSO and Benzethonium chloride were added to the cells using an automatic liquid handler (Echo 550, Labcyte Inc., San Jose, CA, United States). Cisplatin and the MPMs were added to yield five different concentrations in a ten-fold dilution series ranging from 10 to 100,000 nM. Each concentration was tested in triplicate wells. DMSO (0.1%) and benzethonium chloride (100 μM) served as negative and positive control, respectively. Three hours later, some of the plates were irradiated with 2 Gy in a gamma irradiator (OB29/4, STS, Braunschweig, Germany). All plates were taken to the irradiation room to ensure similar handling of the plates. 72 h later, the plates were cooled to room temperature before 25 μl of CellTiter-Glo 2.0 reagent (Promega, Madison, WI, USA) was added to each well using the MultiFlo FX (BioTek). Next, the plates were centrifuged for 5 min at 1,000 rpm before the luminescence signal was measured with the PHERAstar FS HT reader (BMG LABTECH GmbH, Ortenberg, Germany). The raw data was analyzed with the Breeze software (https://breeze.fmm.fi), which normalized the luminescence signal from treated cells against the signal from negative and positive control cells to calculate the percentage of inhibition and generate dose-response curves, which were then used to calculate drug sensitivity scores (DSS). The DSS is a parameter which combines the IC50, the slope of the dose-response curve, and the minimum and maximum responses into a single metric, as previously described (Yadav et al., 2014). Quality control was performed by calculation of the Z′-factor, which was >0.7 for all cell lines, indicating high quality of the assay (Zhang et al., 1999).

2.5 Flow cytometric detection of apoptosis

HSC-3 and UT-SCC-24A cells were seeded, 300,000 cells/well, in 6-well plates and left to adhere overnight. The media was then removed and replaced by 2 ml complete DMEM/F-12 containing 5, 7.5, 10 or 20 μM of MPM-2:0, MPM-6:0, MPM-3:2 or MPM-4:2, or 50 μM cisplatin. Some cells were left untreated. The cells were then incubated for 24 h. Next, the cell supernatants were collected before the cells were trypsinized and spun down with the supernatants. For the staining, an apoptosis detection kit was used (#88-8005-74, Thermo Fisher Scientific). The cells were washed once in PBS and once in 1x binding buffer before being incubated with FITC labeled Annexin V diluted 1:25 in 1 × binding buffer for 15 min. Next the cells were washed in 1 × binding buffer before being incubated with PI diluted 1:100 in 1 × binding buffer for at least 5 min before analysis was performed on the LSR Fortessa (BD Biosciences, CA, United States). Analyses were performed in FlowJo™ v.10 (https://www.flowjo.com/).

2.6 Live cell apoptosis assay

A black-walled 96-well plate (#6005182, PerkinElmer, Waltham, MA, United States) was coated with 50 μl myogel (0.5 mg/ml) per well. The next day, HSC-3 and UT-SCC-24A cells were stained with CellTrace Far Red (Invitrogen, Carlsbad, CA, USA) by resuspending 500,000 cells in 500 μl PBS and adding 0.5 μl of the dye before incubating the cells at 37°C for 20 min. Next, 2.5 ml of complete media was added to the cells, and they were incubated for another 5 min. The cells were then centrifuged and resuspended in complete media. The media remaining in the wells of the 96-well plate after myogel coating was removed and the cells were seeded with 1,000 cells/well in 100 μl of media. The cells were left to adhere overnight, and the following day, the media was replaced with 100 μl of media containing the Incucyte® caspase-3/7 green dye for apoptosis (Sartorius, Göttingen, Germany) (diluted 1:1,000), as well as 5 or 10 μM of the MPMs or 10 μM cisplatin. Control wells only contained media and the caspase-3/7 green dye. The plate was placed in the Incucyte S3 (Sartorius) and imaged at ×10 magnification every 2 hours for 24 h in total. Each condition had triplicate wells, and four images were taken per well. The experiment was conducted three times. The Incucyte software was used to analyze the area of red fluorescence (proliferation) and number of green and red objects (apoptotic cells).

2.7 MTS viability assays with bafilomycin A1 and z-VAD-FMK

HSC-3 and UT-SCC-24A cells were seeded, 10,000 cells/well, in flat bottom 96-well plates and left to adhere overnight. The supernatants were then removed and replaced by 50 μl of complete DMEM/F-12 ± 100 nM BafA1 (#196000, Sigma-Aldrich, St. Louis, MO, United States) or 50 μM z-VAD-FMK (#219007, Sigma-Aldrich). The plate was then incubated for 1 hour before another 50 μl of complete DMEM/F-12 ± 100 nM BafA1 or 50 μM z-VAD-FMK as well as the MPMs or cisplatin was

added. The final concentration of cisplatin was 50 μM and for the MPMs it was 5 or 10 μM for MPM-2:0 and MPM-6:0, and 10 or 20 μM for MPM-3:2 and MPM-4:2, for HSC-3 and UT-SCC-24A cells, respectively. 100 μl of media ± 1% Triton X-100 served as positive and negative controls, respectively. The cells were incubated for 24 h before 20 μl of MTS reagent (CellTiter 96® Aqueous One Solution, Promega, Madison, WI, United States) was added to each well. The plate was then incubated for one more hour before absorbance was measured at 490 nm on a VersaMaxTM Microplate reader (Molecular Devices, San Jose, CA, United States). Viability was calculated using the following formula:

$$\% = \frac{Abs\ treated\ sample - Abs\ positive\ control}{Abs\ negative\ control - Abs\ positive\ control}\ x\ 100$$

At least three independent experiments were performed, with triplicate wells in each experiment.

2.8 Confocal microscopy of lysosomes

HSC-3 and UT-SCC-24A cells were seeded at 5×10^4 cells/well, in an 8-well chambered coverglass that had been pre-coated with Matrigel (#354234, Corning, Somerville, MA, United States). The following day, cells were treated with 5, 10, or 20 μM of MPM-2:0, MPM-6:0, MPM-3:2, or MPM-4:2. One well was left untreated. The cells were incubated for 24 h. 30 min before the end of the incubation period, lysotracker Deep Red (L12492, Thermo Fisher) was added to each well to a final concentration of 50 nM. The media was then removed and cells were fixed in 4% formaldehyde for 15 min at room temperature. Next, cells were washed 4 × 2 min in PBS before being incubated with DAPI (1 μg/mL in PBS) for 5 min followed by 2 × 2 min washing in PBS. Imaging was performed on the LSM 780 confocal microscope (Zeiss, Oberkochen, Germany).

2.9 Western blot for the detection of phosphorylated eIF2α

HSC-3 and UT-SCC-24A cells were seeded, 300,000 cells/well, in 6-well plates and left to adhere overnight. The media was then removed and replaced by 2 ml complete DMEM/F-12 containing 5, 7.5, 10 or 20 μM of MPM-2:0, MPM-6:0, MPM-3:2 or MPM-4:2, or 50 μM cisplatin. Some cells were left untreated. The cells were then incubated for 24 h. Next, the cell supernatants were collected before the cells were trypsinized and spun down with the supernatants. The cells were then washed twice in ice-cold PBS before being resuspended in 100 μl RIPA buffer (25 mM Tris-HCl (pH 7,6), 150 mM NaCl, 0.1% SDS, 0.5% sodium deoxycholate, 1% Triton X-100) containing 1% protease inhibitor (SIGMAFASTTM, #S8830, Sigma-Aldrich) and incubated on a shaker for 30 min. Next, the samples were sonicated and then kept at −70°C before being used. The samples were kept on ice or at 4°C during the whole procedure. The samples were thawed on ice and the protein concentration was measured using the DC Protein Assay kit (#5000111, Bio-Rad Laboratories, Hercules, CA, United States). 8 μg of protein was taken from each sample and mixed with DTT (final concentration 50 mM) and 20% 5 × sample buffer (250 mM Tris-HCl pH 6.8, 10% SDS, 20% Glycerol, 0.01% Bromphenol Blue). Next, the samples were boiled for 5 min and loaded on a NuPAGE® 10% Bis–Tris Gel (Thermo Fisher Scientific) before being electro-transferred to a polyvindiline dilfluoride (PVDF) immobilon-P membrane (Merck, Rahway, NJ, United States). The membrane was blocked for 1 h with 5% BSA in TBST and then incubated overnight at 4°C with the primary antibody targeting phosphorylated eIF2α (#ab32157, Abcam, Cambridge, United Kingdom) diluted 1:1,000 in TBST 5% BSA. Next, the membrane was washed three times in TBST and incubated with an HRP-conjugated goat anti-rabbit secondary antibody (#4050-05, Southern Biotech, Birmingham, AL, United States) diluted 1:2000 in TBST 5% BSA at room temperature for 1 h. The membrane was washed three times in TBST before it was incubated for 5 min with pre-mixed chemiluminescent peroxidase substrate-3 (Sigma-Aldrich) and subsequently imaged on an ImageQuant LAS 4000 (GE Healthcare, Chicago, IL, United States). For detection of non-phosphorylated eIF2α and β-actin, the membrane was first stripped by being incubated with 5 ml 1x stripping buffer (#2502, Merck) for 15 min at room temperature. The membrane was then washed three times in water. Blocking, incubation with antibodies, and detection was then performed as before but with primary antibodies targeting eIF2α (#ab242148, Abcam, diluted 1:2000) and β-actin (#A1978, Sigma-Aldrich, diluted 1:2000). The secondary antibodies were HRP-conjugated goat anti-rabbit (#4050-05, Southern Biotech) diluted 1:2000 and HRP-conjugated goat anti-mouse (#A2554, Sigma-Aldrich) diluted 1:40,000. Analysis of band intensities was performed in Image Studio Lite Ver 5.2 (https://www.licor.com/bio/image-studio-lite/).

2.10 Flow cytometric detection of cell surface calreticulin

This procedure was based on a published method (Liu et al., 2020), but was performed with some modifications. Briefly, HSC-3 and UT-SCC-24A cells were seeded, 300,000 cells/well, in 6-well plates and left to adhere overnight. The media was then removed and replaced by 2 ml complete DMEM/F-12 containing 5, 7.5, 10 or 20 μM of MPM-2:0, MPM-6:0, MPM-3:2 or MPM-4:2, or 50 μM cisplatin. Some cells were left untreated. The cells were then incubated for 24 h. Next, the cell supernatants were collected before the cells were trypsinized and spun down with the supernatants. The cells were then washed in PBS before being incubated with the viability dye Zombie Violet (#423114, BioLegend, San Diego, CA, United States) diluted 1:500 in PBS for 20 min. Next, the cells were incubated with an anti-calreticulin antibody (#ab2907, Abcam) diluted 1:100 in FACS buffer (2%BSA in PBS) for 30 min. The cells were then fixed in 4% formaldehyde for 15 min and washed twice in FACS buffer before being incubated with the secondary antibody (#A11034, Thermo Fisher Scientific) diluted 1:250 in FACS buffer for 30 min. The cells were washed in FACS buffer and analyzed on a LSR Fortessa (BD Biosciences) within 1 week. Analyses were performed in FlowJo™ v.10 (https://www.flowjo.com/).

2.11 Luminescence based detection of extracellular ATP

HSC-3 and UT-SCC-24A cells were seeded, 10,000 cells/well in 100 µl complete media in solid white 96-well plates and left to adhere overnight. The following day, 50 µl of complete media containing either cisplatin, MPM-2:0, MPM-6:0, MPM-3:2, or MPM-4:2 was added along with 50 µl of RealTime-Glo™ Extracellular ATP Assay Substrate (#GA5010, Promega). The final concentration of cisplatin was 50 µM, while the final concentration of MPM-2:0 and MPM-6:0 was either 5 or 10 µM, and the final concentration of MPM-3:2 and MPM-4:2 was 10 or 20 µM. Next, luminescence was read on a CLARIOstar microplate reader (BMG LABTECH) every 30 min for the first 3 h, followed by once every hour until the cells had been stimulated for 8 h, and finally once at 24 h of stimulation. The assay was performed with duplicate wells and three independent experiments were performed.

2.12 Western blot for the detection of extracellular HMGB1

Detection of HMGB1 in the supernatant of MPM treated HSC-3 and UT-SCC-24A cells was performed as previously described (von Hofsten et al., 2022). Briefly, HSC-3 and UT-SCC-24A cells were seeded, 100,000 cells/well in 12-well plates and left to adhere overnight. The following day, the media was removed and replaced with media containing either 50 µM cisplatin, 5 or 10 µM MPM-2:0 or MPM-6:0, or 10 or 20 µM MPM-3:2 or MPM-4:2. The cells were incubated for 24 h before supernatants were collected and centrifuged to remove debris. Supernatant samples were mixed with DTT (final concentration 50 mM) and sample buffer before being boiled for 5 min and loaded on a NuPAGE® 10% Bis–Tris Gel (Thermo Fisher Scientific) before being electro-transferred to a polyvindiline dilfluoride (PVDF) immobilon-P membrane (Merck, Rahway, NJ, United States). The membrane was blocked for 1 h with 5% non-fat dry milk in TBST and then incubated overnight at 4°C with the primary antibody targeting HMGB1 (#ab18256, Abcam) diluted 1:1,000 in TBST 5% non-fat dry milk. Next, the membrane was washed three times in TBST and incubated with an HRP-conjugated goat anti-rabbit secondary antibody (#4050-05, Southern Biotech, Birmingham, AL, United States) diluted 1:2000 in TBST 5% non-fat dry milk at room temperature for 1 h. The membrane was washed three times in TBST before it was incubated for 5 min with pre-mixed chemiluminescent peroxidase substrate-3 (Sigma-Aldrich) and subsequently imaged on an ImageQuant LAS 4000 (GE Healthcare, Chicago, IL, United States). Analysis of band intensities was performed in Image Studio Lite Ver 5.2 (https://www.licor.com/bio/image-studio-lite/).

2.13 Migration and invasion assays

Two Incucyte image lock 96-well plates (#4379, Sartorius) were coated with 50 µl myogel (0.5 mg/ml) per well. The next day, the media remaining in the wells was removed before HSC-3 cells were seeded at a density of 25,000 cells/well in 100 µl. The cells were left to adhere, and the following day, a scratch was made in the middle of each well using the Incucyte 96-pin WoundMaker tool (Sartorius). The wells were then washed once with media. For the migration assay, the media in each well was then replaced with 100 µl of media containing 0.1, 1 or 10 µM of MPM-2:0 or MPM-4:2. For the invasion assay, the media was replaced by 50 µl of a gel consisting of serum-free media, myogel (2.4 mg/ml), type I rat tail collagen (0.8 mg/ml, Corning, NY, USA) and 0.1, 1 or 10 µM of MPM-2:0 or MPM-4:2. The plate was incubated at 37°C for 1 h to let the gel solidify. Next, 100 µl of media, also containing 0.1, 1 or 10 µM of MPM-2:0 or MPM-4:2 was added on top of the gel. Both the migration and invasion plates were placed in the Incucyte S3 (Sartorius) and imaged at ×10 magnification every 2 hours for 24 h in total. The Incucyte software was used to analyze the relative wound density.

2.14 Statistical analysis

Statistical analyses were performed in GraphPad Prism 9.0 (https://www.graphpad.com/). A p-value of <0.05 was considered statistically significant. In all graphs, asterisks indicate significant differences: $*p < 0.05$, $**p < 0.01$, $***p < 0.001$, $****p < 0.0001$.

3 Results

3.1 Synthesis of the MPM library

Based on the structure of the previously reported marine natural product mimic MPM-1 (von Hofsten et al., 2022), a panel of nine structurally related amphipathic barbiturates was developed. All compounds share the same barbiturate scaffold and lipophilic groups that are present in MPM-1 (Figure 1). All new

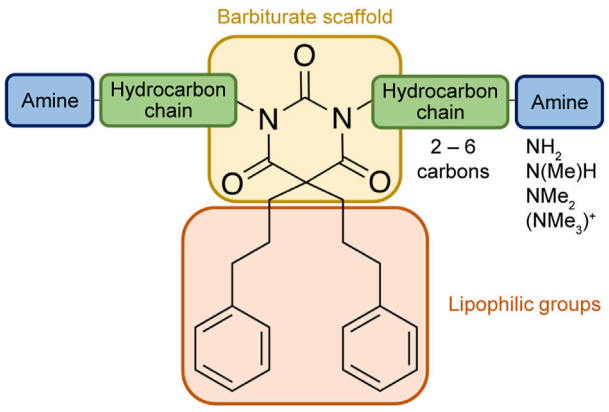

FIGURE 1
General structure of the marine product mimics (MPMs) included in this study. All compounds share the same barbiturate scaffold and lipophilic groups. All compounds also have two identical cationic groups which consist of a hydrocarbon chain of 2–6 carbons and an amine group which is either primary, secondary, tertiary, or quaternary. The cationic groups of the different compounds are demonstrated to the right.

10.3389/fphar.2023.1141669

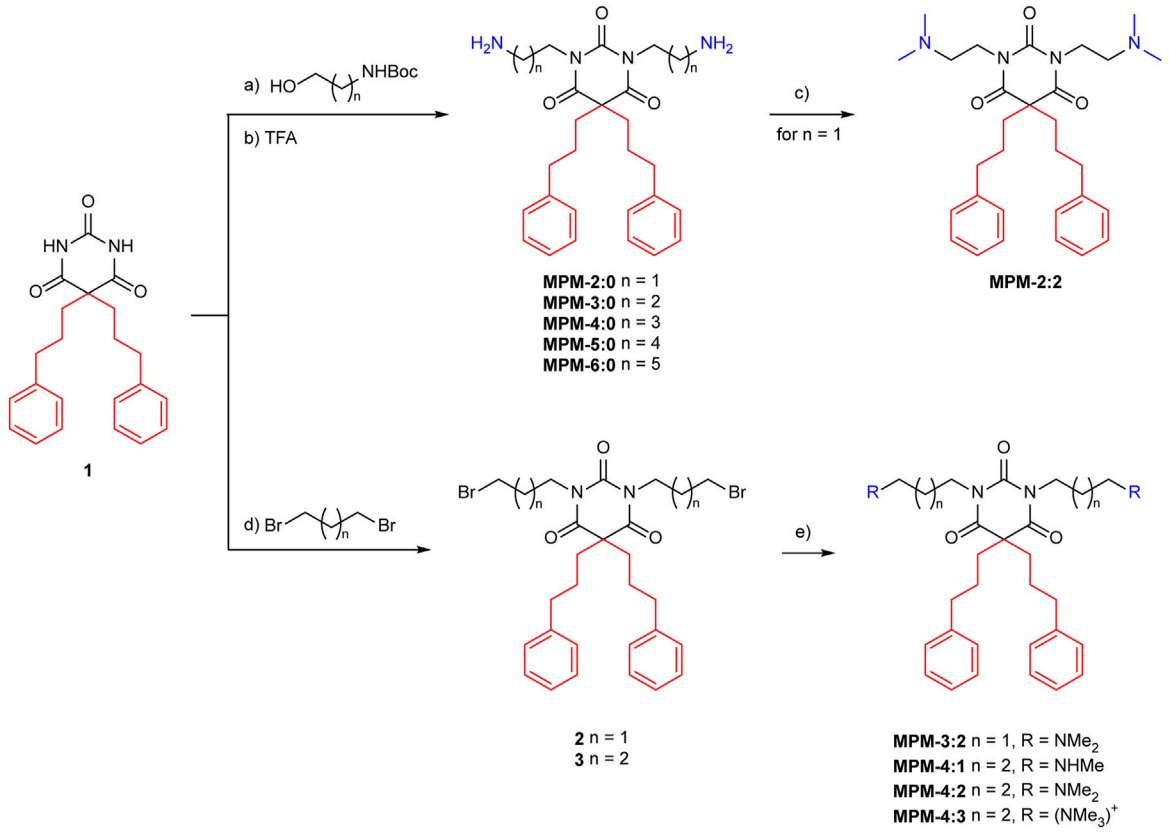

Scheme 1
Synthesis of the MPMs. Conditions: **(A)** DIAD, PPh_3, anhydrous DCM, 0°C to r.t.; **(B)** TFA, DCM, r.t., 51%–93% o2s; **(C)** formaldehyde ($37\%_{(aq)}$), $NaBH_3CN$, AcOH, MeOH, r.t., 96%; **(D)** Cs_2CO_3, acetone, 60°C, 68%–86%; **(E)** NH_2Me or $NH(Me)_2$ or N $(Me)_3$, anhydrous MeCN, 70°C, 63%–97%. All MPMs were obtained as di-TFA salts.

compounds also have two identical hydrocarbon chains that each contain one amine group and represent the cationic parts of the compounds. However, the length of the hydrocarbon chain and the number of methyl groups attached to the amine group varies between the different compounds. All final compounds are referred to as marine product mimics (MPM). The compound codes reflect the chemical structure and are given as follows: MPM-x:y, in which x denotes the number of carbon atoms in each hydrocarbon chain attached to the barbiturate scaffold and y is the number of methyl groups attached to the amine group. According to this system, the previously reported compound MPM-1 would be named MPM-4:0, but to avoid confusion, we will continue to refer to this compound as MPM-1.

Starting from dialkylated barbituric acid 1, all MPMs were synthesized based on modified procedures previously developed in our group (Scheme 1) (Langer et al., 2022; von Hofsten et al., 2022). N,N′-Dialkylation of substituted barbituric acid 1 was easily achieved under standard Mitsunobu conditions, employing diisopropyl azodicarboxylate (DIAD), triphenylphosphine (PPh3) and an aliphatic N-Boc protected amino alcohol of choice in anhydrous dichloromethane (DCM) (Scheme 1, upper pathway). The resulting tetrasubstituted barbituric acids were treated with TFA in DCM to yield MPM-2:0, MPM-3:0, MPM-1, MPM-5:0 and MPM-6:0 as di-TFA salts (51%-93% yield over two steps). For some derivates small amount of reduced DIAD, a byproduct of the Mitsunobu reaction, was observed. The byproduct could be removed by trituration with ice-cold diethyl ether (Et2O). To synthesize the target molecules containing methylated amine groups a different approach was chosen, as free amines did not react under Mitsunobu conditions. Instead, barbituric acid 1 was treated with 1,3-dibromopropane or 1,4-dibromobutane under basic conditions to deliver tetrasubstituted barbiturates 2 and 3 (68% and 86% yield), respectively (Scheme 1, lower pathway). Combining barbiturates 2 and 3 with organic solutions of methylamine, dimethylamine and trimethylamine in anhydrous acetonitrile (MeCN) at elevated temperatures delivered MPM-4:1, MPM-4:2, MPM-4:3 and MPM-3:2 as di-TFA salts after purification by reversed phase chromatography (63%-97% yield). We investigated the same sequence towards MPM-2:2, namely, to alkylate 1 with 1,2-dibromoethane, but no conversion was observed. We therefore chose to di-methylate the primary amines of MPM-2:0 to obtain MPM-2:2. Treatment of MPM-2:0 with an aqueous formaldehyde solution in the presence of sodium cyanoborohydride (NaBH3CN) and acetic acid in methanol (Eschweiler-Clarke conditions) cleanly delivered the di-TFA salt of MPM-2:2 after reversed phase chromatography (96% yield). A detailed description of the experimental data, NMR data and purity analysis can be found in the Supplementary Data.S1

3.2 Biological activity of the MPMs

An overview of the novel MPMs is presented in Table 1. As a measure of the lipophilicity of the compounds, CLogP values were calculated for the compounds. The overall high values demonstrate that all the compounds, except MPM-4:3, are relatively lipophilic. Simultaneously, high pKa values imply that at physiological pH, most of the compounds will have positively charged amine groups. Thus, the MPMs can be described as amphipathic molecules due to lipophilic substituents and hydrophilic side chains. MPM-4:3 contains quaternary amine groups, which remain positively charged at all pH levels, which is why MPM-4:3 has no pKa value and a negative CLogP.

As a preliminary measure of the toxicity of the MPMs, their hemolytic activity was assessed and is expressed as EC_{50} values. Except for MPM-6:0, none of the MPMs showed hemolytic activity against red blood cells. MPM-6:0 had a relatively high EC_{50} of 92 μM. The MPMs were also assessed for antimicrobial activity, which demonstrated that they generally had low activity against bacteria (Supplementary Table S2). However, MPM-6:0 again demonstrated the highest activity against both gram-positive and gram-negative bacteria. Taken together, these results suggest that the MPMs do not have the ability to disrupt biological membranes. However, additional experiments are required to attest this hypothesis.

To study the anti-cancer effects of the MPMs, we performed a high-throughput drug screening. All compounds were screened against a panel of seven HNSCC cell lines and one normal oral fibroblast cell line (NOF), representing healthy cells. The cancer cell lines were selected to represent HNSCC tumors from different locations, as well as both primary and metastatic sites. Clinical and pathological characteristics of the cell lines are summarized in Supplementary Table S1. The UT-SCC cancer cell lines were originally established in the laboratory of Prof. Grénman and have been used in several drug screening studies previously (Lepikhova et al., 2018; Tuomainen et al., 2021). HSC-3 is a commercial cell line which has previously been used to study MPM-1 (von Hofsten et al., 2022). For comparative reasons, the screening included cisplatin in addition to the MPMs. The results from the drug screening were used to calculate drug sensitivity scores (DSS) and are presented as a heat map in Figure 2. Exact DSS can be found in Supplementary Table S3. The DSS is calculated from the dose-response curves for the different compounds and incorporates the slope of the curve, the IC50, and the minimum and maximum responses into a single metric (Yadav et al., 2014). Inactive compounds have a DSS of 0, while the more potent a compound is, the higher the score is (darker color in the heat map).

All compounds except MPM-4:3 effectively reduced the viability of all cell lines, as seen from their high DSS. The compounds were more potent than cisplatin for all cell lines except HSC-3 and UT-SCC-8, for which the potency of cisplatin and the MPMs was similar. Some MPMs were noticeably less potent against the cell lines UT-SCC-42A and UT-SCC-42B than the other cell lines. Overall, the four compounds MPM-2:0, MPM-6:0, MPM-3:2 and MPM-4:2 had the highest DSS and were therefore found to be the most potent. They showed a similar degree of activity against all cell lines, including UT-SCC-42A and UT-SCC-42B.

No compound selectively targeted the cancer cell lines over the NOFs. Surprisingly, there was a slight tendency towards selectivity for the NOFs, which was especially prominent for MPM-1. However, this effect can possibly be explained by the fact that the cancer cell lines and NOFs were cultured in different cell culture medias, which use different buffer systems. To test this hypothesis, MTS viability assays were performed with HSC-3 and UT-SCC-24A cells treated with the different MPMs diluted in three different media. The results revealed that the compounds were generally the least potent in DMEM/F-12, which contains HEPES buffer and should maintain a stable pH of 7.4 (Supplementary Figure S1). The compounds were the most potent in DMEM, which utilizes a sodium bicarbonate buffer system which is sensitive to changes in CO_2 concentration in the surrounding environment, causing the pH to fluctuate. DMEM/F-12 which had been adjusted to a pH of 8 increased the potency of the compounds. According to the relatively high pKa values of the MPMs, increasing the pH above 7.4 would cause a larger proportion of compounds to be unprotonated. This result thus suggests that protonation of the MPMs affects their potency. Despite the fact that the MPMs were the most potent in DMEM, it was decided that all other experiments should be performed in DMEM/F-12 because the lower pH of this media is likely more representative of the microenvironment in a real tumor (Apostolova and Pearce, 2022).

As some chemotherapeutic drugs are known to have synergistic effects with irradiation and since irradiation is part of the standard treatment regimen for HNSCC patients, we also studied the cytotoxic effect of the MPMs when given in combination with irradiation. However, there were no synergistic effects of combining the MPMs with irradiation (Supplementary Table S4).

3.3 Mode of death induced by MPMs

For studies on the mechanism of action and the mode of death induced by the MPMs, the four most potent compounds (MPM-2:0, MPM-6:0, MPM-3:2 and MPM-4:2) were considered the most interesting and were therefore selected for these studies. The 2 cell lines HSC-3 and UT-SCC-24A were also chosen for this objective. HSC-3 was selected because it has previously been used to study the original compound MPM-1 (von Hofsten et al., 2022), and UT-SCC-24A was included to study whether the MPMs would affect different cell lines differently. As could be seen from the screening, MPM-2:0 and MPM-6:0 were somewhat more potent than MPM-3:2 and MPM-4:2. However, due to the design of the high throughput screening, which utilized a 10-fold dilution series of the compounds, it could not differentiate the potency of the different MPMs on the different cell lines at a detailed level. In general, the UT-SCC-24A cell line needed to be treated with higher concentrations of the MPMs as compared to HSC-3, to achieve a similar degree of cell death. In the mechanistic studies, the cells were treated with concentrations which were selected to render the cells heavily affected by the treatment, but not yet completely dead. The same assessment was made regarding cisplatin, which has previously been shown to effectively reduce the viability of both HSC-3 and UT-SCC-24A cells at concentrations ranging between 10 and 100 μM (Mandic et al., 2005; Ahmed et al., 2009). The current compound screening also demonstrated that cisplatin was generally

TABLE 1 Overview of the MPMs and their hemolytic activity against human red blood cells (expressed by the EC_{50} values in μM), as well as their CLogP and pKa values.

Core structure	Comp. ID[a]	R	EC_{50}[b]	CLogP[c]	pKa[d]
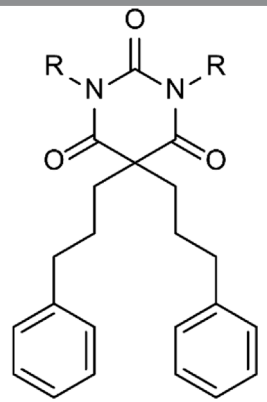	MPM-1	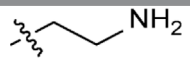	>500[e]	4.45	9.81
	MPM-2:0	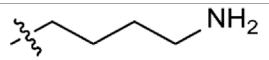	379	2.63	8.10
	MPM-3:0	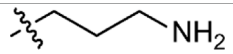	>500	3.54	9.22
	MPM-5:0	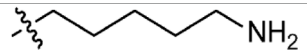	313	5.36	9.96
	MPM-6:0		92	6.27	10.24
	MPM-4:1	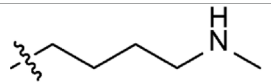	>500	5.15	9.73
	MPM-4:2	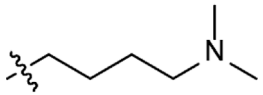	>500	5.69	9.68
	MPM-4:3	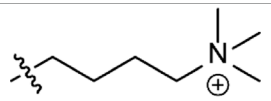	>500	−0.19	–
	MPM-2:2	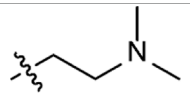	>500	3.60	9.09
	MPM-3:2	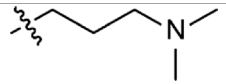	>500	4.78	8.06

[a]Compound codes are constructed as follows: MPM-x:z, where x denotes the number of carbon atoms in the hydrocarbon chains and y is the number of methyl groups on the amine group.

[b]Values given as greater than correspond to the highest concentration (500 μM) tested in the hemolysis assay.

[c]CLogP values were calculated for the neutral molecules, except for MPM-4:3 (calculated with DataWarrior v5.5.0).

[d]Values calculated with ChemBioDraw Ultra v21.0.0.28. –: not calculated.

[e]Value from von Hofsten et al., 2022.

10.3389/fphar.2023.1141669

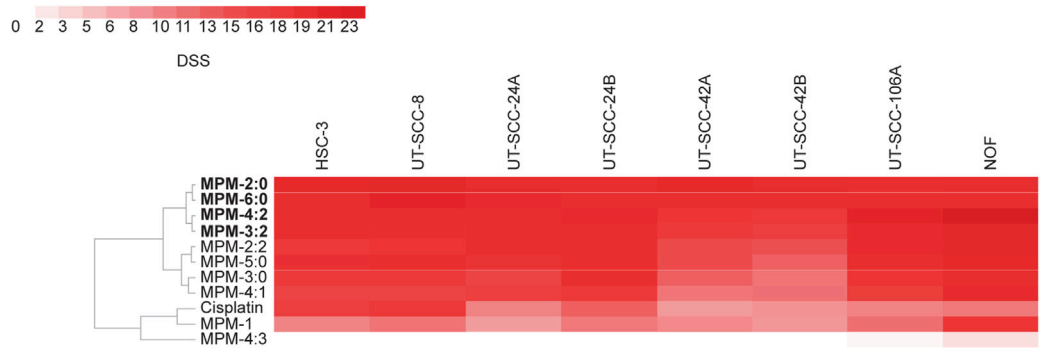

FIGURE 2
The potency of the MPMs was determined against a panel of seven head and neck squamous cell carcinoma cell lines as well as non-malignant normal oral fibroblasts (NOF) in a high throughput drug screening. The drug sensitivity scores (DSS) for each cell line and compound was calculated and presented as a heat map. The higher the DSS, the more potent the drug is. Exact DSS values are presented in Supplementary Table S3.

somewhat less potent than the MPMs and should therefore be used at higher concentrations.

To begin studying the mode of death induced by the MPMs, flow cytometric assessment of the externalization of phosphatidylserine (PS), which is a hallmark for cells in early apoptosis, was performed (Figures 3A,B). HSC-3 and UT-SCC-24A cells were treated with MPM-2:0, MPM-6:0, MPM-3:2, MPM-4:2 or cisplatin and then stained with FITC-labeled Annexin V, which binds to PS. Propidium iodide (PI), which only penetrates and stains cells with a compromised cell membrane, was added for the detection of cells which had lost their plasma membrane integrity. Cisplatin, which is known to trigger apoptosis, caused the appearance of a small, but clearly apoptotic (Annexin V+/PI−) population in both HSC-3 and UT-SCC-24A cells. A similar population was not seen in any of the MPM treated cells. In some HSC-3 samples, a population of Annexin V+ events with low fluorescence intensity for PI was seen. These could represent apoptotic cells. However, the PI fluorescence intensity was noticeably higher in these populations compared to untreated cells or the apoptotic population in cisplatin treated cells, suggesting that there had been some degree of membrane rupture in this population. Moreover, the MPMs also caused the appearance of an Annexin V−/PI + population, which are cells that have lost their membrane integrity but have not externalized PS. These cells were probably not apoptotic.

However, we also performed a live cell imaging apoptosis assay which monitors the activation of caspase 3 and 7. HSC-3 and UT-SCC-24A cells were stained with a red fluorescent marker and treated with MPM-2:0, MPM-6:0, MPM-3:2 or MPM-4:2 in two different concentrations (5 μM and 10 μM). A dye which becomes fluorescent (green) only upon cleavage by caspase 3/7 was also added and the cells were monitored for proliferation and caspase activation for 24 h (Figures 3C,D).

All MPMs caused rapid cell death in both cell lines, as seen by the complete halt of proliferation and movement (Figure 3E). Cisplatin also inhibited proliferation in HSC-3 cells, but not in UT-SCC-24A cells. The MPMs also quickly caused activation of caspase 3/7, which indicates the activation of apoptosis. Cisplatin only induced apoptosis in a minority of HSC-3 cells and in no UT-SCC-24A cells. However, the cisplatin treated cells that did die displayed a morphology which is typical for apoptosis. The formation of apoptotic bodies was clearly visible in these cells. The morphological changes that occurred to the MPM treated cells were generally not reminiscent of apoptosis. Both the HSC-3 and UT-SCC-24A cells treated with MPM-2:0 simply became round. In some cells, such as the UT-SCC-24A cells treated with MPM-4:2, the formation of some bleb-like structures, which could be reminiscent of apoptotic bodies, was seen.

To further study the mode of death induced by the MPMs, MTS viability assays were performed on MPM treated HSC-3 and UT-SCC-24A cells in the presence of the pan-caspase inhibitor z-VAD-FMK or the V-ATPase inhibitor Bafilomycin A1 (BafA1) (Figure 4A). The function of the V-ATPase is to pump protons into acidic cellular compartments like the lysosomes, to keep their internal pH low. By inhibiting the function of the V-ATPase, BafA1 therefore increases the pH inside such compartments. Since the activity of caspase 3/7 had been observed, we hypothesized that the inhibition of caspase activity might rescue cells from cell death induced by the MPMs. Although not statistically significant, z-VAD-FMK seemed to have some protective effects against cisplatin for both cell lines, while BafA1 had the opposite effect. For the MPMs, the results demonstrated that z-VAD-FMK did provide some degree of protection in both cell lines, suggesting that apoptosis may represent some of the MPM induced cell death. However, BafA1 generally increased the viability of MPM treated cells more efficiently than z-VAD-FMK. Only for HSC-3 cells treated with MPM-6:0 did z-VAD-FMK increase viability more than BafA1. Protection by BafA1 indicates that the MPMs may be lysosomotropic compounds (Nadanaciva et al., 2011).

To further study whether the MPMs could be lysosomotropic, the morphology of the lysosomes in HSC-3 and UT-SCC-24A cells treated with MPM-2:0, MPM-6:0, MPM-3:2, and MPM-4:2 was studied by staining the cells with the fluorescent dye lysotracker and imaging the cells using confocal microscopy. Untreated HSC-3 and UT-SCC-24A cells generally contained many small lysosomes (Figure 4B). However, treatment with any of the MPMs drastically changed the lysosomal morphology in both cell lines. Many lysosomes became considerably larger, an effect which is associated with lysosomotropism (Seo et al., 2014).

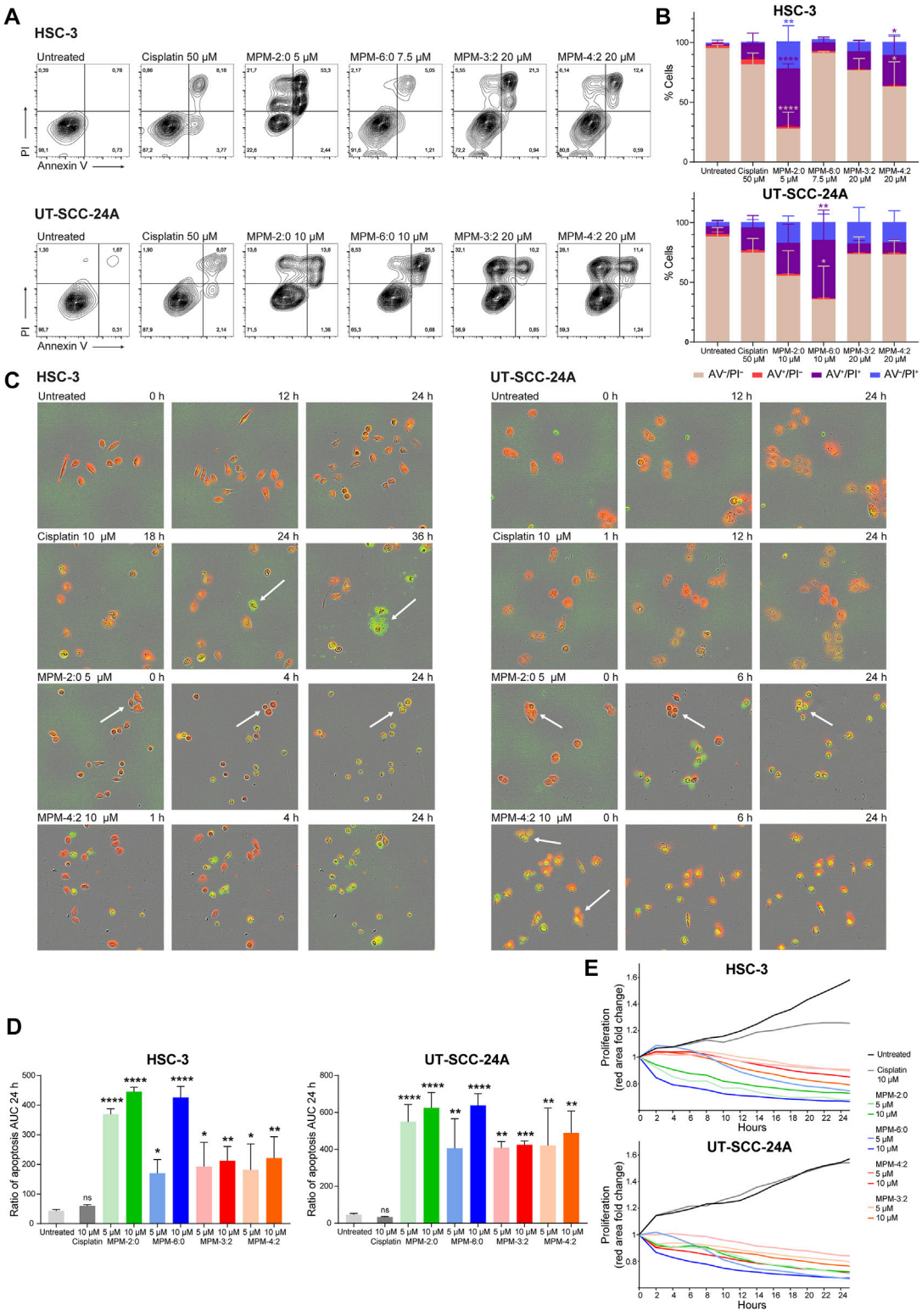

FIGURE 3
The cell surface expression of phosphatidylserine (determined by staining with Annexin V), which characterizes cells in early apoptosis, was analyzed by flow cytometry in HSC-3 and UT-SCC-24A cells treated with MPMs **(A)**. The percentage of Annexin V−/PI−, Annexin V+/PI−, Annexin V−/PI+ and Annexin V+/PI + cells was determined and the mean from three independent experiments is shown in **(B)**. Statistically significant differences, as compared to the untreated cells were determined by one-way ANOVA and Dunnett's *post hoc*. A live cell apoptosis assay was performed where HSC-3 and UT-SCC-24A cells were stained red, treated with MPMs, and a dye which becomes fluorescent (green) upon cleavage by caspase 3/7 was added. Representative images are shown in **(C)**, with arrows pointing to cells referenced in the text. Three independent experiments were performed, and the mean extent of apoptosis was quantified by calculating the area under the curve (AUC) for the ratio of apoptosis (number of green + red objects) for 24 h **(D)**. The statistical differences were determined by one-way ANOVA and Dunnett's *post hoc*. The degree of proliferation was determined by quantifying the area of red fluorescence and is expressed as fold change relative to timepoint 0 **(E)**.

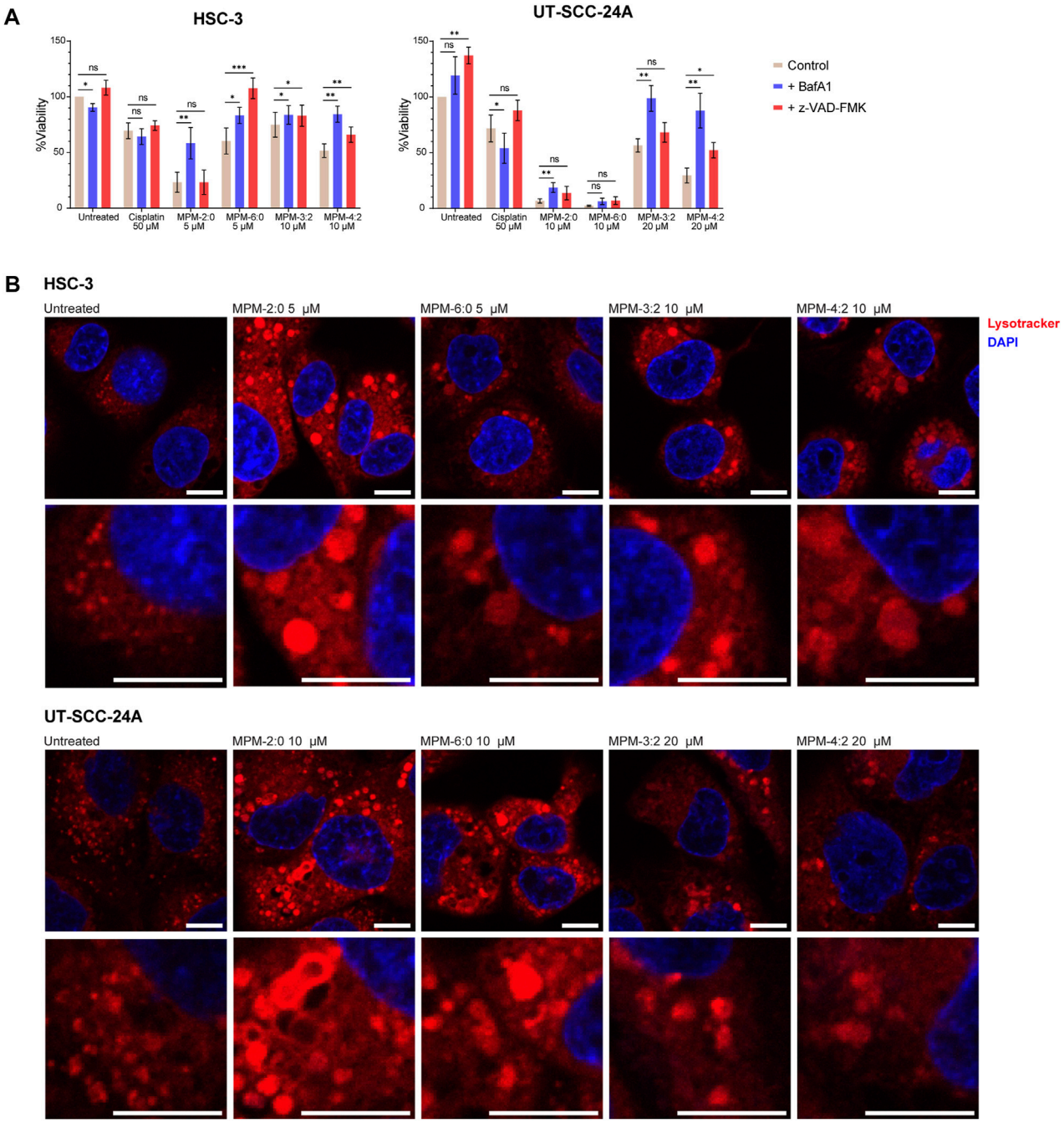

FIGURE 4
The viability of HSC-3 and UT-SCC-24A cells treated with MPMs in the presence of bafilomycin A1 (BafA1) or the pan caspase inhibitor Z-VAD-FMK was determined by means of the MTS assay **(A)**. The graph shows the mean from three independent experiments. Significant differences were determined by paired t-tests. **(B)** HSC-3 and UT-SCC-24A cells were left untreated or were treated with the MPMs for 24 h before being stained with Lysotracker Deep Red and imaged by confocal microscopy. All scale bars are 10 μm.

3.4 Immunogenic potential of the MPMs

To examine the ability of the MPMs to induce immunogenic cell death, we studied their ability to activate the integrated stress response, which is highly associated with immunogenic cell death (Bezu et al., 2018). The integrated stress response is characterized by the phosphorylation of the eukaryotic initiation factor 2α (eIF2α). Western blot analysis of MPM treated HSC-3 and UT-SCC-24A cells demonstrated that some of the MPMs could significantly induce some phosphorylation of eIF2α (Figures 4A,B), indicating that they can activate the integrated stress response.

The expression of calreticulin in MPM treated cells was analyzed by flow cytometry (Figures 5C,D). Since cell surface expression of calreticulin is known to occur early during immunogenic cell death,

10.3389/fphar.2023.1141669

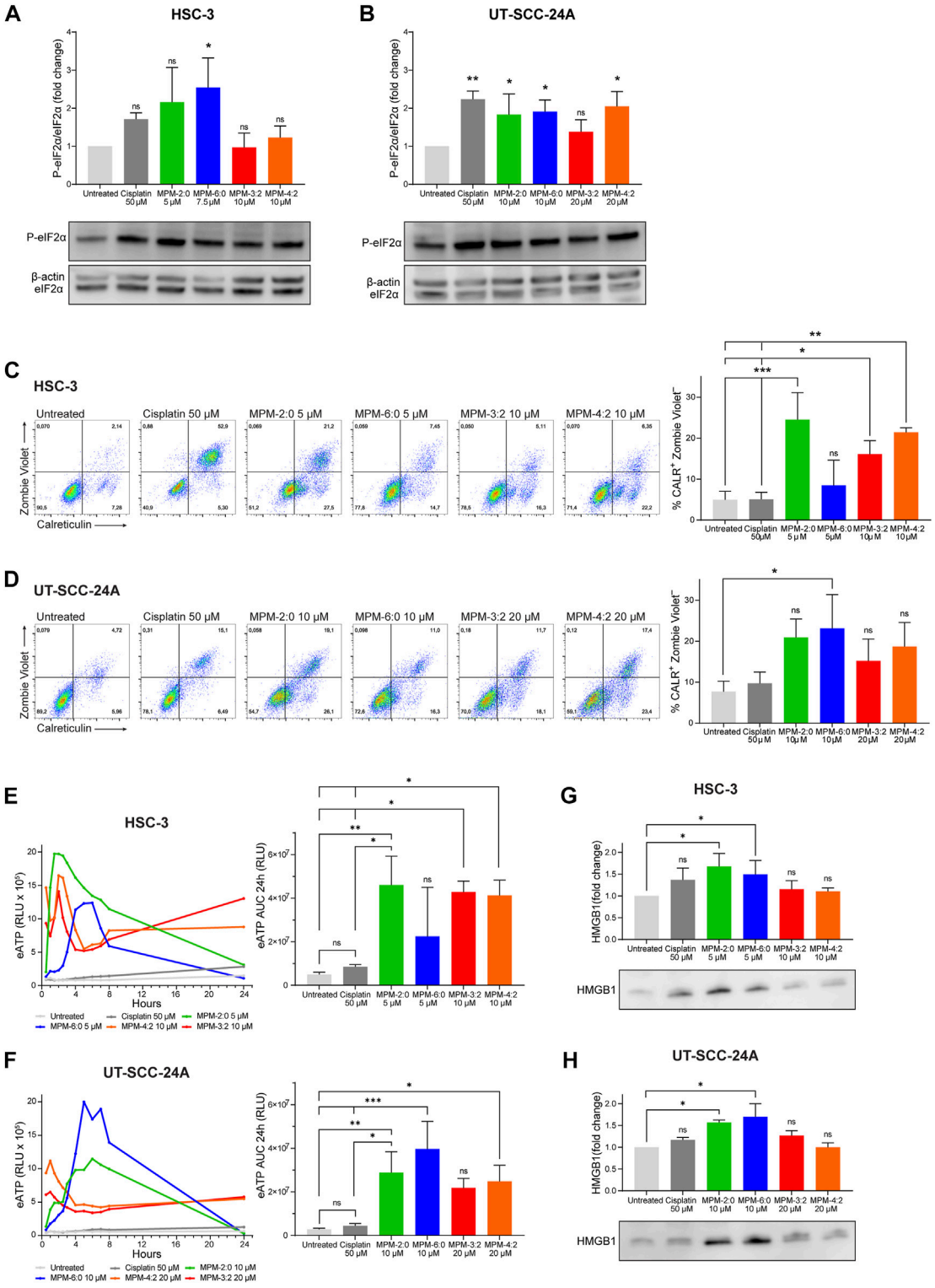

FIGURE 5
The phosphorylation of eIF2α in HSC-3 **(A)** and UT-SCC-24A **(B)** cells treated with MPMs was analyzed by Western blot. Band intensities were quantified and normalized to non-phosphorylated eIF2α. The cell surface expression of calreticulin was analyzed by flow cytometry in HSC-3 **(C)** and UT-SCC-24A **(D)** cells treated with MPMs. The percentage of live cells expressing calreticulin (Zombie Violet−/CALR+) was determined and the graph shows the mean from three independent experiments. Statistical differences were determined by one-way ANOVA and Bonferroni's *post hoc*. Extracellular ATP (eATP) was measured in the supernatant of MPM treated HSC-3 **(E)** and UT-SCC-24A **(F)** cells by means of a luminescence-based assay at several time points over the course of 24 h. The amount of eATP is proportional to the relative luminescence units (RLU). Three independent experiments were performed. The area under the curve (AUC) was calculated and statistical analysis was performed by one-way ANOVA and Bonferroni's *post hoc*. HMGB1 in the supernatant of untreated and MPM treated HSC-3 **(G)** and UT-SCC-24A **(H)** was analyzed by Western blot. Band intensities were quantified and normalized to the untreated sample. Statistical analysis was performed by Kruskal–Wallis test and Dunn's *post hoc*.

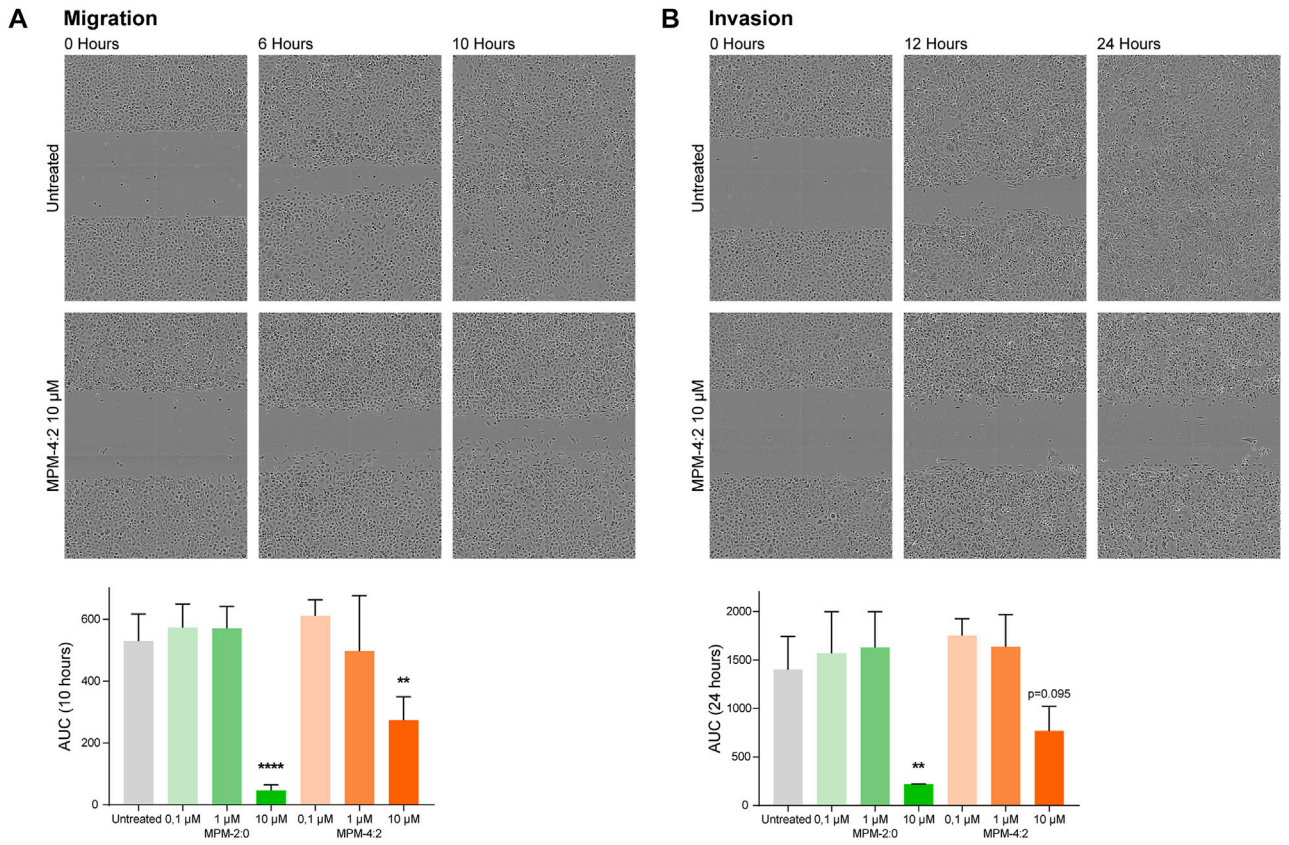

FIGURE 6
The migration and invasion of MPM treated HSC-3 cells was analyzed through scratch wound assays. The cells were left untreated or were treated with 0.1, 1 or 10 µM of MPM-2:0 or MPM-4:2. In the migration assay **(A)**, the wells were only filled with media, and in the invasion assay **(B)**, the scratch was filled with a myogel-collagen mix before the addition of media. The cells were imaged every 2 hours for 24 h. The results were quantified by calculating the area under the curve (AUC) for the relative wound density and statistical differences were calculated by one-way ANOVA and Dunnet's *post hoc*. Four independent migration assays and three independent invasion assays were performed.

before plasma membrane integrity is lost, standard practice is to only analyze calreticulin in cells with intact plasma membranes (Liu et al., 2020). Another reason is that cells which have lost their plasma membrane integrity will also stain positively for intracellular calreticulin, making it impossible to distinguish between cell surface bound and intracellular calreticulin. Cisplatin, which is known to not cause immunogenic cell death, did not induce any cell surface expression of calreticulin. In contrast, all the MPMs could induce cell surface calreticulin. The increase in cell surface calreticulin was statistically significant for HSC-3 cells treated with MPM-2:0, MPM-3:2 and MPM-4:2. For UT-SCC-24A cells, only MPM-6:0 could induce statistically significant levels of cell surface calreticulin. Release of ATP from MPM treated HSC-3 and UT-SCC-24A cells was analyzed by means of a luminescence-based assay, which measured the relative amount of extracellular ATP (eATP) in the supernatant of treated cells at different time points up to 24 h. The results demonstrated that all MPMs could induce release of eATP (Figures 5E,F). Release of HMGB1 from MPM treated HSC-3 and UT-SCC-24A cells was analyzed by Western blot (Figures 5G,H). While all MPMs seemed to cause some release of HMGB1, the results were only statistically significant for MPM-2:0 and MPM-6:0 in both HSC-3 and UT-SCC-24A cells.

3.5 Effects on migration and invasion of HSC-3 cells

The HSC-3 cell line is very aggressive and able to migrate and invade through matrices effectively. Therefore, we wanted to study whether the MPMs could inhibit this ability and at the same time uncover any unwanted side effects relating to treatment-induced increase of migration or invasion of MPM treated cells. A standard scratch wound migration assay where cells were treated with MPM-2:0 or MPM-4:2 in a ten-fold dilution series was performed. The results showed that HSC-3 cells treated with 10 µM MPM-4:2 required more time to close the wound as compared to the untreated control cells in the migration assay (Figure 6A). The morphology of the treated cells suggested that they were heavily affected by the treatment and in the process of dying. However, after 24 h the cells were still moving, indicating that they were not completely dead (Supplementary Video S1). The same trend was

observed in an invasion assay, where the scratch wound was filled with a myogel-collagen mix which the cells had to invade through. In the invasion assay, the control cells needed approximately 24 h to close the wound, whereas the cells treated with 10 μM MPM-4:2 never managed to close the wound (Figure 6B). MPM-2:0 was also included in the migration and invasion assays but at 10 μM it induced cell death so quickly that it was not possible to study the effect on migration or invasion. There was a trend towards faster wound closing for cells treated with the lower concentrations of both MPM-2:0 and MPM-4:2. However, the effect was not statistically significant.

4 Discussion

The current study presents a panel of novel compounds designed for use in cancer treatment *via* intratumoral injection. The structure of these compounds was based on the previously described compound MPM-1, which is a synthetic mimic of a group of natural products called *eusynstyelamides* that have been isolated from marine organisms (Strøm et al., 2018; Tadesse et al., 2011; von Hofsten et al., 2022). While MPM-1 was shown to be a potent anti-cancer compound, the current study demonstrated that, except for MPM-4:3, the novel MPMs were all more potent than MPM-1 against HNSCC cell lines. They were shown to effectively kill a range of different HNSCC cells. Studies on the mechanism of action revealed that overall, the different MPMs had similar effects on HSC-3 and UT-SCC-24A cells. However, despite the small differences in structure, there were some differences in how the compounds affected the cells.

Out of the four most potent compounds, which were selected for inclusion in the mechanistic studies, MPM-3:2 and MPM-4:2 have the most similar structure. They are both tertiary amines and there is only one carbon atom in the hydrocarbon chains that separates them. Unsurprisingly, these two compounds had very similar effects on the cells. For example, they both induced a large population of Annexin V−/PI + UT-SCC-24A cells, as seen by the flow cytometric analysis of PS externalization. Their Annexin V/PI plots for HSC-3 cells were also similar. In addition, the results from the live cell apoptosis assay, the viability assays with BafA1 and z-VAD-FMK, and the analysis of cell surface expression of calreticulin were all very similar for MPM-3:2 and MPM-4:2. This suggests that these two compounds function the same way. However, only by changing the structure slightly more, the properties of the compounds were affected. The structure of MPM-2:0 and MPM-6:0 differs by four carbons, and the results obtained for these compounds were more diverse, both when compared with each other and with MPM-3:2 and MPM-4:2. For example, MPM-6:0 stood out from the other compounds by the fact that it had a noticeably lower EC_{50} against red blood cells and that HSC-3 cells were more protected from it by z-VAD-FMK than by BafA1.

Changing the structure of the compounds also affected their potency against the HNSCC cells, although it was not evident exactly how or why that occurred. For example, the two most potent compounds, MPM-2:0 and MPM-6:0, contained the shortest and the longest hydrocarbon chains out of all the compounds, respectively. Thus, it is difficult to draw conclusions about how the hydrocarbon chain length affects potency. Moreover, MPM-3:2 and MPM-4:2, both have medium length hydrocarbon chains. On a similar note, methylation of the amine groups also seemed to affect potency, although it is unclear how. MPM-2:0 and MPM-6:0 are both primary amines, suggesting that increases potency. On the other hand, the other primary amines in this study, including the original MPM-1, were noticeably less potent than all the tertiary amines, thus indicating that may not be the case. However, we have previously seen that methylation of amine groups decreases both hemolytic and antibacterial activity (Langer et al., 2022). This trend was also seen in the current study, as none of the MPMs containing methylated amine groups had red blood cell (RBC) EC_{50} lower than 500 μM, and they generally had poor effects on bacteria. Contrary to this, both MPM-2:0 and MPM-6:0 were considerably more potent against bacteria and, as previously mentioned, MPM-6:0 was the most hemolytic compound.

Even though there were some clear differences regarding both potency and properties of the different MPMs, overall, their effect on cells was quite similar. Their potency was within the same range and they all induced a type of cell death which is reminiscent of what has previously been demonstrated for MPM-1 (von Hofsten et al., 2022). Originally, the MPMs presented in this study were created as part of a larger library of amphipathic barbiturates. Several of these were found to have antimicrobial activity and their mechanism of action in bacteria has been partly elucidated (Langer et al., 2022). It was found that these compounds could compromise the integrity of the bacterial cell membrane, which caused the bacteria to die. This effect was likely due to the amphipathic barbiturates functioning as detergents which disrupt biological membranes. Interestingly, despite effectively killing the cancer and normal cells, the MPMs generally did not affect bacteria or red blood cells. This indicates that their primary mode of action is not to disrupt the cell membrane. The inactivity of MPM-4:3, which should remain permanently protonated and therefore also permanently amphipathic, also strongly supports this conclusion. Moreover, it makes the MPMs more attractive as potential cancer drugs as they do not represent a threat to the normal flora. However, as discussed, MPM-6:0 did have considerable antimicrobial effects in addition to being the compound with the highest activity against red blood cells. This could indicate that MPM-6:0, unlike the other MPMs, may have some detergent like properties. This could be an effect of MPM-6:0 having the longest hydrocarbon chains, which makes it the most lipophilic and potentially increases its interaction with the lipid bilayer of the cell membrane. Likewise, MPM-5:0 also had relatively high activity against bacteria and the second lowest RBC EC_{50}.

The fact that the MPMs generally did not affect bacteria or red blood cells suggests that their main target is located intracellularly and that they need to cross through the cell membrane to exert their action. The increased potency of the MPMs which was achieved by increasing the pH of the cell media, also supports this conclusion. When the pH is higher, an increased number of molecules are unprotonated, which makes them more lipophilic and likely more able to cross through a cell membrane, resulting in more cell death. The fact that MPM-4:3, which remains protonated at all pH levels, was completely inactive, is also in line with this theory.

The previous study on MPM-1 suggested that it is a lysosomotropic compound, which may partly induce cell death by accumulating in lysosomes and causing their dysfunction (von Hofsten et al., 2022). Lysosomotropic compounds accumulate in

lysosomes because their low internal pH causes such compounds to become protonated and thereby unable to leave the lysosome (Marceau et al., 2012). When the concentration of compound within the lysosomes reaches above a certain threshold, they can act as detergents on the lysosomal membrane, causing its destabilization and the leakage of lysosomal content into the cytosol (Boya and Kroemer, 2008). Accumulation of lysosomotropic compounds in lysosomes can also cause influx of water and swelling of the lysosomes, giving the cells a vacuolated appearance (De Duve et al., 1974; Marceau et al., 2012). Compounds which contain both lipophilic and basic parts tend to be lysosomotropic. A study which looked at characteristics of lysosomotropic compounds found that a ClogP>2 and pKa between 6.5 and 11 were common traits for lysosomotropic compounds (Nadanaciva et al., 2011). This description fits all the MPMs except MPM-4:3. Further results also support the hypothesis that the MPMs are lysosomotropic. For instance, red blood cells do not contain lysosomes and are therefore not affected by lysosomotropic compounds. Accordingly, the MPMs generally had very little effect on red blood cells. In addition, staining of MPM treated HSC-3 and UT-SCC-24A cells with Lysotracker Deep Red demonstrated that the MPMs caused swelling of lysosomes. Furthermore, the fact that the potency of the MPMs was decreased in cells that were co-treated with BafA1 also supports the notion that the MPMs are lysosomotropic. BafA1 inhibits the vacuolar ATPase (V-ATPase), which is present in the lysosomal cell membrane and functions to pump protons into the lysosome to keep the internal pH low. By inhibiting the V-ATPase, BafA1 raises the lysosomal pH, which in turn causes less accumulation of lysosomotropic compounds and consequently less cell death. This phenomenon has been demonstrated for several different lysosomotropic compounds (Marceau et al., 2012).

The fact that the viability of MPM treated cells was significantly increased when they were treated with BafA1 suggests that lysosomotropism is central to their mechanism of inducing cell death. This result is in contrast to what was found for MPM-1, for which the potency was increased in cells treated with BafA1 (von Hofsten et al., 2022). From that result it was presumed that the main reason for MPM-1 induced cell death was not lysosomotropism. Instead, it was believed that MPM-1 may have a different target which it is able to reach in greater concentration when it is not trapped in lysosomes. This is a phenomenon which has been described for some lysosomotropic compounds including doxorubicin (Altan et al., 1998). This curious difference between the novel MPMs and the original MPM-1 highlights the fact that small changes in the structure of these compounds can greatly affect their mechanism of action. As such, *in vitro* mechanism studies are important to perform in order to be able to pick the best lead compounds for further optimization for cancer treatment.

Lysosomotropic compounds have been shown to be able to trigger the phosphorylation of eIF2α, which is a hallmark of the integrated stress response (Tian et al., 2021). Phosphorylation of eIF2α is also highly associated with immunogenic cell death, and specifically with the cell surface expression of calreticulin (Bezu et al., 2018). In line with this, our results demonstrated that the MPMs could induce both the phosphorylation of eIF2α and the cell surface expression of calreticulin in HSC-3 and UT-SCC-24A cells. On the contrary, cisplatin also induced high levels of phosphorylated eIF2α, but no cell surface calreticulin. This is in line with what has been demonstrated in previous studies (Bezu et al., 2018). The MPMs also induced release of ATP and HMGB1 from HSC-3 and UT-SCC-24A cells. Taken together, all of these results suggest that the MPMs may be able to induce immunogenic cell death.

Immunogenic cell death is considered a distinct form of cell death, which is defined by its ability to activate an adaptive immune response (Galluzzi et al., 2018). However, it can appear in different forms. Anthracyclines, which are a group of DNA-intercalating chemotherapeutic agents that are known for their ability to induce immunogenic cell death, trigger a form of immunogenic apoptosis (Obeid et al., 2007). Other compounds, for instance the amphipathic and oncolytic peptide LTX-315, induces a form of immunogenic cell death which is more reminiscent of necrosis (Zhou et al., 2016). Historically, necrosis is known as a proinflammatory type of cell death as the membrane rupture which occurs during necrosis causes the release of DAMPs, such as HMGB1 (Scaffidi et al., 2002).

While the activation of caspase 3/7 that was observed in the live cell apoptosis assay as well as the partial protection of cells from MPM induced cell death by the pan-caspase inhibitor z-VAD-FMK indicates that the MPMs can trigger apoptosis, there are however other factors that suggest that apoptosis is not the main type of cell death induced by the MPMs. For instance, the increase in viability caused by z-VAD-FMK was generally small and statistically insignificant in many cases. In addition, the morphology of the MPM treated cells was not typical for apoptotic cells. The flow cytometric analysis of externalization of PS did not indicate that the cells were undergoing apoptosis. This could be seen by the fact that there was no Annexin V+/PI–population in the MPM treated cells, as there was in the cisplatin treated cells. While some of the MPM treated HSC-3 and UT-SCC-24A cells, especially those treated with MPM-2:0, did appear to have been apoptotic as their PI intensity was relatively low, none of these cells were completely negative for PI, suggesting that membrane rupture happens early during cell death, which is not typical for apoptotic cells. The presence of a large population of Annexin V–/PI+ cells, which was especially prominent in UT-SCC-24A cells treated with MPM-3:2 and MPM-4:2, also supports this notion. Taken together, these results indicate that apoptosis is not the main mode of cell death induced by the MPMs.

Historically, apoptosis and necrosis were known as the two main modes of cell death, representing regulated and accidental cell death, respectively. However, it is now accepted that a variety of different cell death modes exist (Galluzzi et al., 2018). For example, different forms of regulated necrosis exist as well (Galluzzi et al., 2018). The fact that BafA1 and, to a certain extent, z-VAD-FMK, could increase the viability of MPM treated cells indicates that the death that they induce is regulated. The cell surface expression of calreticulin, which is regulated by the phosphorylation of eIF2α, and the activation of caspase 3/7 also indicate the activation of regulated pathways. As previously mentioned, phosphorylation of eIF2α is a reaction to cellular stress, specifically to endoplasmic reticulum stress and the misfolding of proteins (Hetz et al., 2020). This in turn may cause the activation of caspases and subsequent apoptosis.

However, as discussed, it seems like the MPMs do not induce classic apoptosis.

Taken together, this study has demonstrated that amphipathic barbiturates effectively reduce the viability of HNSCC cancer cells by inducing a particular form of cell death, which may be coupled to lysosomotropism. All of the four most potent compounds were able to induce cell surface expression of calreticulin and release of ATP. MPM-2:0 and MPM-6:0 also caused release of HMGB1. These are important hallmarks for immunogenic cell death and therefore makes the MPMs interesting to study further. By making small changes to the structure of the MPMs, their potency could be modified. This is of great interest when designing and selecting compounds for future *in vivo* studies. However, potency is not the only important feature of an anti-cancer compound. Despite MPM-3:2 and MPM-4:2 being somewhat less potent than MPM-2:0 and MPM-6:0, they had a considerably lower effect on red blood cells and bacteria. Therefore, MPM-3:2 and MPM-4:2 may be the most attractive compounds for inclusion in future studies.

Data availability statement

The original contributions presented in the study are included in the article/Supplementary Material, further inquiries can be directed to the corresponding authors.

Ethics statement

The use of human leiomyoma tissue to produce myogel was approved by the Ethics Committee of both Oulu and Helsinki University Hospitals (statement number 2/2017), and all research was performed in accordance with relevant regulations.

Author contributions

GB, SH, ML, AB, and AA-S designed the study. MS, AB, and ML designed the MPMs and ML synthesized all compounds used in the current study. SH, ML, KK, TA, and AA-S performed the mechanistic studies. GB, SM, DA, AA-S, TS, and MS supervised the project. SH and ML wrote the manuscript. All authors were involved in discussions throughout the project and revision of the manuscript. All authors have accepted the final submitted version of the manuscript.

Funding

This work was supported by grants from the Jane and Aatos Erkko Foundation, the Finnish Dental Society Apollonia, and the AKM fund from UiT—The Arctic University of Norway. SH received a travel grant from UiT—The Arctic University of Norway to travel to Helsinki and perform some of the presented work. The publication charges for this article have been funded by a grant from the publication fund of UiT—The Arctic University of Norway.

Acknowledgments

We thank the FIMM High-Throughput Biomedicine Unit (supported by the University of Helsinki and Biocenter Finland), for their technical support. We acknowledge Swapnil Potdar for bioinformatic analysis and Laura Turunen for technical support. The authors thank Peter McCourt for linguistic revision of the manuscript, and the Advanced Microscopy Core Facility (AMCF) at UiT for technical support.

Conflict of interest

The authors declare that the research was conducted in the absence of any commercial or financial relationships that could be construed as a potential conflict of interest.

Publisher's note

Supplementary material

The Supplementary Material for this article can be found online at: https://www.frontiersin.org/articles/10.3389/fphar.2023.1141669/full#supplementary-material

References

Ahmed, Z., Deyama, Y., Yoshimura, Y., and Suzuki, K. (2009). Cisplatin sensitivity of oral squamous carcinoma cells is regulated by Na+,K+-ATPase activity rather than copper-transporting P-type ATPases, ATP7A and ATP7B. *Cancer Chemother. Pharmacol.* 63 (4), 643–650. doi:10.1007/s00280-008-0781-z

Altan, N., Chen, Y., Schindler, M., and Simon, S. M. (1998). Defective acidification in human breast tumor cells and implications for chemotherapy. *J. Exp. Med.* 187 (10), 1583–1598. doi:10.1084/jem.187.10.1583

Apostolova, P., and Pearce, E. L. (2022). Lactic acid and lactate: Revisiting the physiological roles in the tumor microenvironment. *Trends Immunol.* 43 (12), 969–977. doi:10.1016/j.it.2022.10.005

Bezu, L., Sauvat, A., Humeau, J., Gomes-da-Silva, L. C., Iribarren, K., Forveille, S., et al. (2018). eIF2α phosphorylation is pathognomonic for immunogenic cell death. *Cell Death Differ.* 25 (8), 1375–1393. doi:10.1038/s41418-017-0044-9

Boya, P., and Kroemer, G. (2008). Lysosomal membrane permeabilization in cell death. *Oncogene* 27 (50), 6434–6451. doi:10.1038/onc.2008.310

De Duve, C., De Barsy, T., Poole, B., Trouet, A., Tulkens, P., and Van Hoof, F. o. (1974). Commentary. Lysosomotropic agents. *Biochem. Pharmacol.* 23 (18), 2495–2531. doi:10.1016/0006-2952(74)90174-9

Galluzzi, L., Buque, A., Kepp, O., Zitvogel, L., and Kroemer, G. (2017). Immunogenic cell death in cancer and infectious disease. *Nat. Rev. Immunol.* 17 (2), 97–111. doi:10.1038/nri.2016.107

Galluzzi, L., Vitale, I., Aaronson, S. A., Abrams, J. M., Adam, D., Agostinis, P., et al. (2018). Molecular mechanisms of cell death: Recommendations of the nomenclature committee on cell death 2018. *Cell Death Differ.* 25 (3), 486–541. doi:10.1038/s41418-017-0012-4

Hetz, C., Zhang, K., and Kaufman, R. J. (2020). Mechanisms, regulation and functions of the unfolded protein response. *Nat. Rev. Mol. Cell Biol.* 21 (8), 421–438. doi:10.1038/s41580-020-0250-z

Johnson, D. E., Burtness, B., Leemans, C. R., Lui, V. W. Y., Bauman, J. E., and Grandis, J. R. (2020). Head and neck squamous cell carcinoma. *Nat. Rev. Dis. Prim.* 6 (1), 92. doi:10.1038/s41572-020-00224-3

Langer, M. K., Rahman, A., Dey, H., Anderssen, T., Zilioli, F., Haug, T., et al. (2022). A concise SAR-analysis of antimicrobial cationic amphipathic barbiturates for an improved activity-toxicity profile. *Eur. J. Med. Chem.* 241, 114632. doi:10.1016/j.ejmech.2022.114632

Lepikhova, T., Karhemo, P.-R., Louhimo, R., Yadav, B., Murumägi, A., Kulesskiy, E., et al. (2018). Drug-sensitivity screening and genomic characterization of 45 HPV-negative head and neck carcinoma cell lines for novel biomarkers of drug efficacy. *Mol. Cancer Ther.* 17 (9), 2060–2071. doi:10.1158/1535-7163.MCT-17-0733

Liu, P., Zhao, L., Kepp, O., and Kroemer, G. (2020). Quantitation of calreticulin exposure associated with immunogenic cell death. *Methods Enzymol.* 632, 1–13. doi:10.1016/bs.mie.2019.05.011

Mandic, R., Schamberger, C. J., Müller, J. F., Geyer, M., Zhu, L., Carey, T. E., et al. (2005). Reduced cisplatin sensitivity of head and neck squamous cell carcinoma cell lines correlates with mutations affecting the COOH-terminal nuclear localization signal of p53. *Clin. Cancer Res.* 11 (19), 6845–6852. doi:10.1158/1078-0432.CCR-05-0378

Marceau, F., Bawolak, M. T., Lodge, R., Bouthillier, J., Gagne-Henley, A., Gaudreault, R. C., et al. (2012). Cation trapping by cellular acidic compartments: Beyond the concept of lysosomotropic drugs. *Toxicol. Appl. Pharmacol.* 259 (1), 1–12. doi:10.1016/j.taap.2011.12.004

Nadanaciva, S., Lu, S., Gebhard, D. F., Jessen, B. A., Pennie, W. D., and Will, Y. (2011). A high content screening assay for identifying lysosomotropic compounds. *Toxicol Vitro* 25 (3), 715–723. doi:10.1016/j.tiv.2010.12.010

Obeid, M., Tesniere, A., Ghiringhelli, F., Fimia, G. M., Apetoh, L., Perfettini, J. L., et al. (2007). Calreticulin exposure dictates the immunogenicity of cancer cell death. *Nat. Med.* 13 (1), 54–61. doi:10.1038/nm1523

Paulsen, M. H., Engqvist, M., Ausbacher, D., Anderssen, T., Langer, M. K., Haug, T., et al. (2021). Amphipathic barbiturates as mimics of antimicrobial peptides and the marine natural products eusynstyelamides with activity against multi-resistant clinical isolates. *J. Med. Chem.* 64 (15), 11395–11417. doi:10.1021/acs.jmedchem.1c00734

Salo, T., Dourado, M. R., Sundquist, E., Apu, E. H., Alahuhta, I., Tuomainen, K., et al. (2018). Organotypic three-dimensional assays based on human leiomyoma-derived matrices. *Philos. Trans. R. Soc. Lond B Biol. Sci.* 373, 20160482. doi:10.1098/rstb.2016.0482

Scaffidi, P., Misteli, T., and Bianchi, M. E. (2002). Release of chromatin protein HMGB1 by necrotic cells triggers inflammation. *Nature* 418 (6894), 191–195. doi:10.1038/nature00858

Seo, I., Jha, B. K., Lim, J.-G., Suh, S.-I., Suh, M.-H., and Baek, W.-K. (2014). Identification of lysosomotropic compounds based on the distribution and size of lysosomes. *Biochem. Biophysical Res. Commun.* 450 (1), 189–194. doi:10.1016/j.bbrc.2014.05.091

Sha, D., Jin, Z., Budczies, J., Kluck, K., Stenzinger, A., and Sinicrope, F. A. (2020). Tumor mutational burden as a predictive biomarker in solid tumors. *Cancer Discov.* 10 (12), 1808–1825. doi:10.1158/2159-8290.Cd-20-0522

Sinha, S., Narjus-Sterba, M., Tuomainen, K., Kaur, S., Seppanen-Kaijansinkko, R., Salo, T., et al. (2020). Adipose-derived mesenchymal stem cells do not affect the invasion and migration potential of oral squamous carcinoma cells. *Int. J. Mol. Sci.* 21 (18), 6455. doi:10.3390/ijms21186455

Strøm, M. B., Bayer, A., Engqvist, S. O. M., Paulsen, M. H., and Ausbacher, D. (2018). *Barbituric acid derivatives comprising cationic and lipophilic groups*. WO/2018/178198. PCT/EP2018/058011.

Sung, H., Ferlay, J., Siegel, R. L., Laversanne, M., Soerjomataram, I., Jemal, A., et al. (2021). Global cancer statistics 2020: GLOBOCAN estimates of incidence and mortality worldwide for 36 cancers in 185 countries. *CA Cancer J. Clin.* 71 (3), 209–249. doi:10.3322/caac.21660

Tadesse, M., Tabudravu, J. N., Jaspars, M., Strom, M. B., Hansen, E., Andersen, J. H., et al. (2011). The antibacterial ent-eusynstyelamide B and eusynstyelamides D, E, and F from the Arctic bryozoan Tegella cf. spitzbergensis. *J. Nat. Prod.* 74 (4), 837–841. doi:10.1021/np100499c

Tian, A.-L., Wu, Q., Liu, P., Zhao, L., Martins, I., Kepp, O., et al. (2021). Lysosomotropic agents including azithromycin, chloroquine and hydroxychloroquine activate the integrated stress response. *Cell Death Dis.* 12 (1), 6. doi:10.1038/s41419-020-03324-w

Tuomainen, K., Al-Samadi, A., Potdar, S., Turunen, L., Turunen, M., Karhemo, P. R., et al. (2019). Human tumor-derived matrix improves the predictability of head and neck cancer drug testing. *Cancers (Basel)* 12 (1), 92. doi:10.3390/cancers12010092

Tuomainen, K., Hyytiäinen, A., Al-Samadi, A., Ianevski, P., Ianevski, A., Potdar, S., et al. (2021). High-throughput compound screening identifies navitoclax combined with irradiation as a candidate therapy for HPV-negative head and neck squamous cell carcinoma. *Sci. Rep.* 11 (1), 14755. doi:10.1038/s41598-021-94259-5

Vitale, I., Yamazaki, T., Wennerberg, E., Sveinbjornsson, B., Rekdal, O., Demaria, S., et al. (2021). Targeting cancer heterogeneity with immune responses driven by oncolytic peptides. *Trends Cancer* 7 (6), 557–572. doi:10.1016/j.trecan.2020.12.012

von Hofsten, S., Paulsen, M. H., Magnussen, S. N., Ausbacher, D., Kranz, M., Bayer, A., et al. (2022). The marine natural product mimic MPM-1 is cytolytic and induces DAMP release from human cancer cell lines. *Sci. Rep.* 12 (1), 15586. doi:10.1038/s41598-022-19597-4

Waldman, A. D., Fritz, J. M., and Lenardo, M. J. (2020). A guide to cancer immunotherapy: from T cell basic science to clinical practice. *Nat. Rev. Immunol.* 20 (11), 651–668. doi:10.1038/s41577-020-0306-5

Wang, C., Liu, X. Q., Hou, J. S., Wang, J. N., and Huang, H. Z. (2016). Molecular mechanisms of chemoresistance in oral cancer. *Chin. J. Dent. Res.* 19 (1), 25–33. doi:10.3290/j.cjdr.a35694

Yadav, B., Pemovska, T., Szwajda, A., Kulesskiy, E., Kontro, M., Karjalainen, R., et al. (2014). Quantitative scoring of differential drug sensitivity for individually optimized anticancer therapies. *Sci. Rep.* 4 (1), 5193. doi:10.1038/srep05193

Zhang, J.-H., Chung, T. D. Y., and Oldenburg, K. R. (1999). A simple statistical parameter for use in evaluation and validation of high throughput screening assays. *J. Biomol. Screen.* 4 (2), 67–73. doi:10.1177/108705719900400206

Zhou, H., Forveille, S., Sauvat, A., Yamazaki, T., Senovilla, L., Ma, Y., et al. (2016). The oncolytic peptide LTX-315 triggers immunogenic cell death. *Cell Death Dis.* 7 (3), e2134. doi:10.1038/cddis.2016.47

Supplementary Material

Supplementary Table S1: Clinical and pathological characteristics of the cancer cell lines. TNM is based on pathology reports.

CELL LINE	SEX[A]	AGE[B]	TNM	SPECIMEN SITE	TYPE[C]	GRADE	REF
UT-SCC-8	M	42	T2N0M0	larynx	pri	G1	LE* Uni. Turku
UT-SCC-24A	M	41	T2N0M0	tongue	pri	G2	LE* Uni. Turku
UT-SCC-24B	M	41	T2N1M0	neck	met(per)	G2	LE* Uni. Turku
UT-SCC-42A	M	43	T4N3M0	larynx	pri	G3	LE* Uni. Turku
UT-SCC-42B	M	43	T4N3M0	neck	met	G3	LE* Uni. Turku
UT-SCC-106	M	37	T1AN0M	larynx	pri	G1	LE* Uni. Turku
HSC-3	M	64		tongue	met		JCRB Cell Bank

[A]M=MALE, F=FEMALE, [B] AGE IN YEARS, [C] PRI=PRIMARY TUMOR, MET=METASTASIS, PER= PERSISTENT DISEASE, *LOCALLY ESTABLISHED

Supplementary Table S2. Overview of the antimicrobial activity of all MPMs given by their MIC in µg/mL.

Core structure	Comp. ID	R	Antimicrobial activity S. a	B. s	E. c	P. a
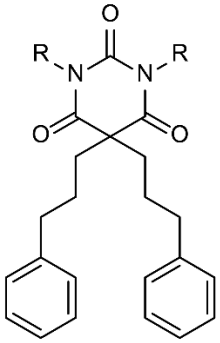	**MPM-1**	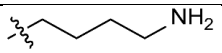				
	MPM-2:0	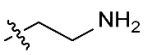	8	8	16	16
	MPM-3:0	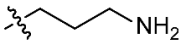	32	16	64	64
	MPM-5:0	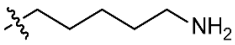	8	4	32	32
	MPM-6:0	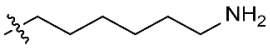	4	2	8	8
	MPM-4:1	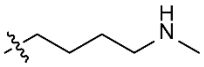	32	8	>64	>64
	MPM-4:2	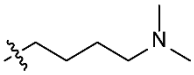	64	16	32	>64
	MPM-4:3	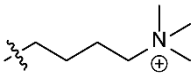	64	>64	64	>64
	MPM-2:2	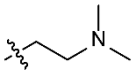	>64	32	32	>64
	MPM-3:2	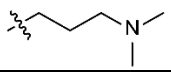	>64	16	32	>64

Bacterial reference strains: S. a – *Staphylococcus aureus* ATCC 9144, B.s – *Bacillus subtilis* 168, E. c – *Escherichia coli* ATCC 25922, and P. a – *Pseudomonas aeruginosa* ATCC 27853. All compounds were tested as di-TFA salts.

Supplementary Table S3. Calculated drug sensitivity scores (DSS) for the MPMs on HNSCC cell lines. The data was obtained from the high throughput drug screening.

	HSC-3	UT-SCC-8	UT-SCC-24A	UT-SCC-24B	UT-SCC-42A	UT-SCC-42B	UT-SCC-106A	NOF
MPM-2:0	19	19,2	18,7	18,3	19	18,7	18	18,3
MPM-6:0	17,8	19,5	18,6	18,3	17,9	18,4	17,9	18
MPM-4:2	18,2	18,1	18,4	18,9	17	16,6	19,5	22,6
MPM-3:2	17,9	17,8	17,9	18,4	16	15,7	18,6	19,3
MPM-2:2	16,8	17	18,1	17,8	13,4	12,9	18,6	19,2
MPM-5:0	17,6	18,1	17,4	18,2	13,5	11,5	17,9	19
MPM-3:0	16,1	16,5	14,3	18	11,7	10,1	17,1	18,3
MPM-4:1	14,8	14,5	15,5	16,4	9,9	10,2	15,8	18,5
Cisplatin	15,6	16,8	8,9	11,6	7,1	7,7	9	9,6
MPM-1	8,8	10	6,9	9,7	8,4	7,4	10,3	17,1
MPM-4:3	0	0	0	0	0,1	0,1	0,5	2,2

Supplementary Table S4. Combined treatment of cells with MPMs and irradiation does not have synergistic or antagonistic effects. The degree of synergy/antagonism was calculated by subtracting the drug sensitivity score (DSS) in non-irradiated cells from the DSS in irradiated (2 Gy) cells, giving a delta DSS (ΔDSS). ΔDSS >5 indicates synergy, while ΔDSS<–5 indicates antagonism.

	HSC-3	UT-SCC-8	UT-SCC-24A	UT-SCC-24B	UT-SCC-42A	UT-SCC-42B	UT-SCC-106A	NOF
MPM-2:0	-0,7	0,6	-0,7	-0,1	-0,7	-0,1	-0,5	-0,7
MPM-6:0	0,7	-0,8	-0,2	0,1	0,3	-0,5	-0,4	-0,3
MPM-4:2	0,3	0,5	-0,6	-0,5	0,4	-0,4	-0,2	1,2
MPM-3:2	-0,2	0,1	-0,2	0,1	0,6	0,3	-0,2	-1,6
MPM-2:2	1,4	0,2	-0,4	-1,5	0,9	-0,4	-1,5	-1,2
MPM-5:0	0,2	0,4	-1,2	-0,5	-0,8	-0,5	-1	-1,2
MPM-3:0	0	-0,6	-1,8	-0,6	-1,1	-0,1	-0,6	-0,6
MPM-4:1	-0,4	0,6	-1,6	-0,5	-0,1	-1,1	-0,8	-0,8
Cisplatin	-0,8	-0,8	-0,9	0,7	-0,1	-0,6	0,3	-1,9
MPM-1	0	-0,8	-1,1	0,5	-0,8	0,6	0,3	0,4
MPM-4:3	0	0	0	0,1	0	-0,1	-0,5	-1,4

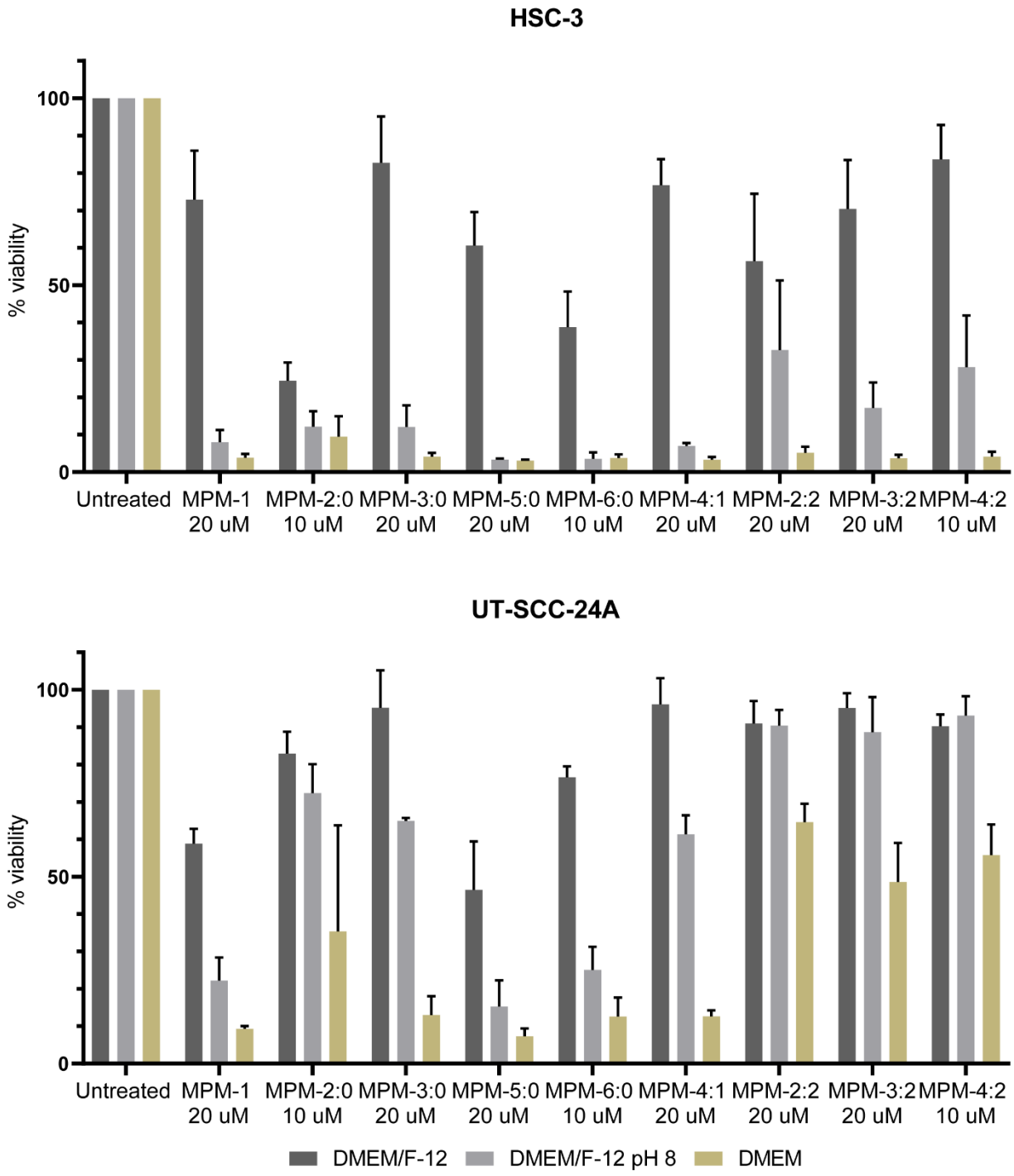

Supplementary Figure S1. The viability of HSC-3 and UT-SCC-24A cells treated with MPMs in different cell culture medias was measured by means of the MTS assay. The cells were seeded in 96-well plates (15 000 cells/well) and treated with MPMs for four hours the following day at 10 or 20 µM according to their potency. The cells were treated in DMEM/F-12, DMEM/F-12 pH 8 (pH adjusted by the addition of NaOH) or DMEM.

Supplementary Methods

Method for determination of bacterial minimum inhibitory concentration (MIC)

Stock solutions of the water-soluble compounds were prepared by dissolving them in ultrapure water (Milli-Q H_2O, Millipore, MA, USA). The less water-soluble compounds were first dissolved in 25 - 50 µL 100% DMSO before further dilution with ultrapure water. The DMSO concentration was always less than 1% in the working concentration of each compound. A modified broth microdilution susceptibility test [1] based on the CLSI M07-A9 protocol, [2] was used to determine minimal inhibitory concentrations (MIC). Briefly, the test compounds were two-fold diluted with ultrapure water in polystyrene 96-well flat-bottom microplates (NUNC, Roskilde, Denmark). The bacterial inoculum was diluted to 2.5 - 3 x 10^4 cells/mL in Mueller-Hinton broth (MHB, Difco Laboratories, USA) and added to the different diluted compounds in a ratio of 1:1. Positive control (ciprofloxacin, Sigma-Aldrich, USA), negative control (bacteria + water), and media control (media + water) were included in each experiment. The microplates were incubated for 48 h at 35 °C in an EnVision microplate reader (PerkinElmer, Waltham, MA, USA). The lowest concentration of compounds that caused no bacterial growth, as determined by optical density (OD_{600}) measurements, was defined as the MIC value. All compounds were tested in 3 technical replicates.

Supplementary Video S1. HSC-3 cells were seeded at 100% confluence and a standard scratch wound migration assay was performed. The cells were imaged every 2 hours for 24 hours. The video shows untreated cells (left) and cells treated with 10 µM MPM-4:2 (right).

References

1. Igumnova EM, Mishchenko E, Haug T, Blencke HM, Sollid JUE, Fredheim EGA, et al. Synthesis and antimicrobial activity of small cationic amphipathic aminobenzamide marine natural product mimics and evaluation of relevance against clinical isolates including ESBL-CARBA producing multi-resistant bacteria. Bioorg Med Chem. 2016;24(22):5884-94.

2. Cockerill FR. Methods for Dilution Antimicrobial Susceptibility Tests for Bacteria That Grow Aerobically. Approved Standard. M07-A9 In: Institut CaLS, editor. 9th ed: Wayne, Pa : Clinical and Laboratory Standards Institut; 2012.

frontiers

Supplementary Material

1 Experimental procedures

1.1 General information

Unless otherwise noted, purchased chemicals were used as received without further purification. Solvents were dried according to standard procedures over molecular sieves of appropriate size. Normal phase flash chromatography was carried out on silica gel 60 (230−400 mesh) or on an interchim® PuriFlash XS420 flash system with the sample preloaded on a Samplet® cartridge belonging to a Biotage SP-1 system. Purification by reversed phase (RP) C18 column chromatography (H_2O with 0.1 % TFA/MeCN with 0.1 % TFA) was performed on an interchim® PuriFlash XS420 flash system with the sample preloaded on a Samplet® cartridge. Thin layer chromatography was carried out using Merck TLC Silica gel 60 F254 and visualized by short-wavelength ultraviolet light or by treatment with an appropriate stain.

NMR spectra were obtained on a 400 MHz Bruker Advance III HD spectrometer equipped with a 5 mm SmartProbe BB/1H (BB = 19F, 31P-15N) at 20 °C. The chemical shifts are reported in ppm relative to the solvent residual peak ($CDCl_3$: δH 7.26 and δC 77.16; Methanol-d4: δH 3.31 and δC 49.00; deuterium oxide: δH 4.79; DMSO-d6 δH 2.51 and δC 39.52). ^{13}C NMR spectra were obtained with ^{1}H decoupling. Data are represented as follows: chemical shift, multiplicity (s = singlet, d = doublet, t = triplet, s = septet, m = multiplet), coupling constant (*J* in Hz) and integration. The raw data was analyzed with MestReNova (Version 14.0.0-23239).

High-resolution mass spectra (HRMS) were recorded from methanol solutions on an LTQ Orbitrap XL (Thermo Scientific) either in negative or in positive electrospray ionization (ESI) mode. The data was analyzed with the Thermo Scientific Xcalibur software.

The purity of all tested compounds was determined to be ≥95%. The analyses were carried out on a Waters ACQUITY UPC^2 system equipped with a Torus™ DEA 130Å, 1.7 µm, 2.1 mm x 50 mm column or a Torus™ 2-PIC 130Å, 1.7 µm, 2.1 mm x 50 mm column. Compounds were detected on a Waters ACQUITY PDA detector spanning wavelengths from 190 to 650 nm, coupled to a Waters ACQUITY QDA detector for low resolution mass (LRMS) detection. The derivatives were eluted with a mobile phase consisting of supercritical CO_2 and MeOH containing 0.1 % NH_3 and a linear gradient of 2 – 40% MeOH over 2 or 4 min followed by isocratic 0.5 min of 40% MeOH. The flow rate was 1.5 mL/min.

Dialkylated barbituric acid **1** was obtained following the procedures described by von Hofsten et al.[1]

General Procedure A: *N,N'*-dialkylation via Mitsunobu reaction

The respective 5,5-disubstituted barbituric acid, *N*-Boc amino alcohol and PPh_3 were mixed with anhydrous DCM in a heat dried vial under an argon atmosphere. The suspension was cooled to 0 °C and upon dropwise addition of DIAD a clear yellow solution was obtained. The mixture was left stirring in the melting ice-water bath until TLC indicated full conversion. Then 10 % $NaHCO_{3(aq)}$ solution and EtOAc were added and the layers were separated. The aqueous layer was

extracted twice with EtOAc and the combined organics were dried over Na_2SO_4, filtered and the solvent was removed under reduced pressure. The crude product was purified by column chromatography on silica gel with EtOAc/heptane as solvents to yield the *N*,*N'*-dialkylated barbiturates.
To the *N*,*N'*-dialkylated barbiturates dissolved in DCM, was added TFA and the mixture was stirred at ambient temperature until HRMS indicated full conversion. The solvent was removed and the crude product was purified on an automated flash system equipped with a C18 column and MeCN/H_2O containing 0.1% TFA as solvents. The product containing fractions were collected, the solvent was removed and the product was lyophilized for 48 h. The obtained solids were triturated three times with Et_2O. The solids were dissolved in MeOH and water was added. The mixture was lyophilized for 48 h to yield the desired amines as di-TFA salts in ≥95% purity.

1.2 Synthesis of intermediates

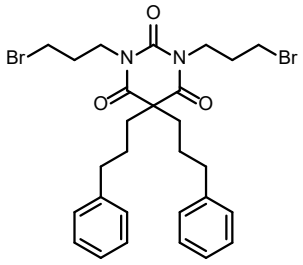

1,3-bis(3-bromopropyl)-5,5-bis(3-phenylpropyl)pyrimidine-2,4,6(1H,3H,5H)-trione **2**.
Compound **1** (100 mg, 0.27 mmol, 1.0 eq) and Cs_2CO_3 (223.5 mg, 0.69 mmol, 2.5 eq) were mixed with acetone (1 mL) and the suspension was stirred for 10 min at ambient temperature. 1,3-dibromopropane (98 µL, 0.96 mmol, 3.5 eq) was added and the suspension was heated to 60 °C for 42 h. The suspension was allowed to cool to ambient temperature, EtOAc and water were added, and the layers were separated. The aqueous layer was extracted with EtOAc twice. The combined organics were dried over $MgSO_4$, filtered and the solvent was removed. After purification by column chromatography on silica gel with 15% EtOAc in heptane compound **2** (113 mg, 0.19 mmol, 68%) was obtained as a colorless oil.

^{1}H NMR (400 MHz, Chloroform-*d*) δ 7.30 – 7.22 (m, 4H), 7.21 – 7.14 (m, 2H), 7.10 – 7.04 (m, 4H), 4.01 (t, *J* = 7.2 Hz, 3H), 3.37 (t, *J* = 6.6 Hz, 4H), 2.53 (t, *J* = 7.7 Hz, 4H), 2.14 (s, *J* = 6.9 Hz, 4H), 2.06 – 1.97 (m, 4H), 1.42 – 1.31 (m, 4H). **^{13}C NMR** (101 MHz, Chloroform-*d*) δ 171.6 (2C), 150.6, 141.0 (2C), 128.7 (4C), 128.4 (4C), 126.3 (2C), 56.7, 41.3 (2C), 39.6 (2C), 35.7 (2C), 31.1 (2C), 29.9 (2C), 27.1 (2C). **HRMS** (ESI): calcd for $C_{28}H_{34}Br_2N_2O_3Na^+$ $[M+H]^+$ 627.0828, found: 627.0821.
Note: Chloroform-d signal overlaps with phenyl rings.

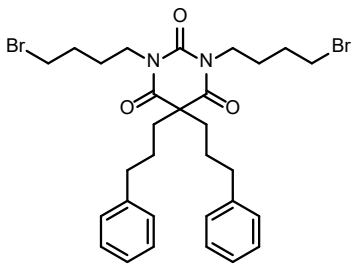

1,3-bis(4-bromobutyl)-5,5-bis(3-phenylpropyl)pyrimidine-2,4,6(1H,3H,5H)-trione **3**.
Compound **1** (243 mg, 0.67 mmol, 1.0 eq) and Cs_2CO_3 (543.1 mg, 1.67 mmol, 2.5 eq) were mixed with acetone (1 mL) and the suspension was stirred for 10 min at ambient temperature. 1,4-dibromobutane (339 µL, 2.33 mmol, 3.5 eq) was added and the suspension was heated to 60 °C for 48 h. The suspension was allowed to cool to ambient temperature, EtOAc and water were added, and the layers were separated. The aqueous layer was extracted with EtOAc twice. The combined organics were dried over $MgSO_4$, filtered and the solvent was removed. After purification on an automated flash system equipped with a silica column and gradient 0-25% EtOAc in heptane compound **3** (364 mg, 0.57 mmol, 86%) was obtained as a colorless oil.

^{1}H NMR (400 MHz, Chloroform-*d*) δ 7.30 – 7.23 (m, 4H), 7.21 – 7.14 (m, 2H), 7.11 – 7.06 (m, 4H), 3.90 (t, *J* = 7.2 Hz, 4H), 3.39 (t, *J* = 6.5 Hz, 4H), 2.54 (t, *J* = 7.7 Hz, 4H), 2.06 – 1.98 (m, 4H),

1.90 – 1.81 (m, 4H), 1.78 – 1.68 (m, 4H), 1.43 – 1.33 (m, 4H). **^{13}C NMR** (101 MHz, Chloroform-*d*) δ 171.7 (2C), 150.6, 141.1 (2), 128.6 (4C), 128.4 (4C), 126.3, 56.6, 41.3 (2C), 39.8 (2C), 35.7 (2C), 32.8 (2C), 30.1 (2C), 27.1 (2C), 26.0 (2C). **HRMS** (ESI): calcd for $C_{30}H_{39}Br_2N_2O_3^+$ $[M+H]^+$ 633.1322, found: 633.1329.
Note: Chloroform-d signal overlaps with signals originating from the phenyl rings.

1.3 Synthesis of final MPMs

The following compounds were prepared according to General Procedure A

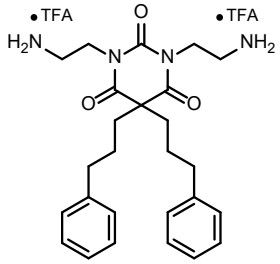

1,3-bis(2-aminoethyl)-5,5-bis(3-phenylpropyl)pyrimidine-2,4,6(1H,3H,5H)-trione **MPM-2:0**.

Compound **1** (75 mg, 206 µmol, 1.0 eq), *tert*-butyl (2-hydroxyethyl)carbamate (83 mg, 515 µmol, 2.5 eq), PPh_3 (162 mg, 617 µmol, 3.0 eq) and DIAD (129 µL, 617 µmol, 3.0 eq) were stirred in anhydrous DCM (1.0 mL) for 4 h. The crude was purified with 10-50% EtOAc in heptane to yield impure Boc-**MPM-2:0** (127 mg, 195 µmol, 95%) as a white solid.

TFA (315 µL, 4.11 mmol, 20.0 eq) and DCM (1.0 mL) were added and the solution was stirred at ambient temperature for 22 h. The crude was purified by RP chromatography with a gradient of 15-50% MeCN in H_2O (both containing 0.1% TFA) to yield the di-TFA salt of **MPM-2:0** (71 mg, 105 µmol, 51% o2s) as a white solid.

^{1}H NMR (400 MHz, Methanol-*d4*) δ 7.27 – 7.19 (m, 4H), 7.18 – 7.07 (m, 7H), 4.18 (t, *J* = 5.7 Hz, 4H), 3.21 (t, *J* = 5.7 Hz, 4H), 2.54 (t, *J* = 7.2 Hz, 4H), 1.96 – 1.87 (m, 4H), 1.54 – 1.42 (m, 4H). **^{13}C NMR** (101 MHz, Methanol-*d4*) δ 172.9 (2C), 153.1, 142.5 (2C), 129.4 (8C), 127.0 (2C), 57.8, 41.0 (2C), 39.5 (2C), 38.7 (2C), 36.4 (2C), 27.3 (2C). **HRMS** (ESI): calcd for $C_{26}H_{35}N_4O_3^+$ $[M+H]^+$ 451.2704, found 451.2694. **SFC**: >99%.

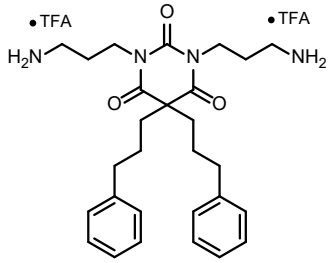

1,3-bis(3-aminopropyl)-5,5-bis(3-phenylpropyl)pyrimidine-2,4,6(1H,3H,5H)-trione **MPM-3:0**.

Compound **1** (75 mg, 206 µmol, 1.0 eq), *tert*-butyl (3-hydroxypropyl)carbamate (90 mg, 515 µmol, 2.5 eq), PPh_3 (162 mg, 617 µmol, 3.0 eq) and DIAD (129 µL, 617 µmol, 3.0 eq) were stirred in anhydrous DCM (1.0 mL) for 4 h. The crude was purified with 10-50% EtOAc in heptane to yield impure Boc-**MPM-3:0** (132 mg, 194 µmol, 95%) as a white solid.

TFA (315 µL, 4.11 mmol, 20.0 eq) and DCM (1.0 mL) were added and the solution was stirred at ambient temperature for 22 h. The crude was purified by RP chromatography with a gradient of 15-50% MeCN in H_2O (both containing 0.1% TFA) to yield the di-TFA salt of **MPM-3:0** (133 mg, 188 µmol, 92% o2s) as a white solid.

^{1}H NMR (400 MHz, Methanol-*d4*) δ 7.28 – 7.20 (m, 4H), 7.24 (dd, *J* = 8.1, 6.7 Hz, 4H), 7.18 – 7.12 (m, 2H), 3.98 (t, *J* = 7.1 Hz, 4H), 2.96 (t, *J* = 7.4 Hz, 3H), 2.55 (t, *J* = 7.4 Hz, 4H), 2.03 – 1.88 (m, 8H), 1.42 (dtd, *J* = 14.9, 7.6, 4.3 Hz, 4H). **^{13}C NMR** (101 MHz, Methanol-*d4*) δ 173.0 (2C), 152.0, 142.4 (2C), 129.4 (4C), 129.3 (4C), 127.1 (2C), 57.7, 40.1 (2C), 40.0 (2C), 38.4 (2C), 36.4 (2C), 27.8 (2C), 27.3 (2C).**HRMS** (ESI): calcd for $C_{28}H_{39}N_4O_3^+$ $[M+H]^+$ 479.3017, found 479.3011. **SFC**: >99%.

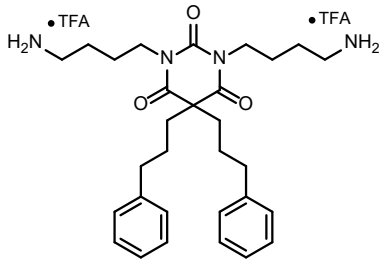

1,3-bis(4-aminobutyl)-5,5-bis(3-phenylpropyl)pyrimidine-2,4,6(1H,3H,5H)-trione **MPM-1**.

Compound **1** (500 mg, 1.37 mmol, 1.0 eq), *tert*-butyl (4-hydroxybutyl)carbamate (597 mg, 3.16 mmol, 2.3 eq), PPh_3 (1.08 g, 4.12 mmol, 3.0 eq) and DIAD (862 µL, 4.12 mmol, 3.0 eq) were stirred in anhydrous DCM (4.0 mL) for 22 h. The crude was purified with 10-50% EtOAc in heptane to yield impure Boc-**MPM-1** (906 mg, 1.28 mmol, 93%) as a white solid.

TFA (2.10 mL, 27.4 mmol, 20.0 eq) and DCM (4.0 mL) were added and the solution was stirred at ambient temperature for 22 h. The crude was purified by RP chromatography with a gradient of 15-50% MeCN in H_2O (both containing 0.1% TFA) to yield the di-TFA salt of **MPM-1** (586 mg, 798 µmol, 58% o2s) as a white solid.

^{1}H NMR (400 MHz, Methanol-*d4*) δ 7.28 – 7.20 (m, 4H), 7.19 – 7.12 (m, 2H), 7.12 – 7.07 (m, 4H), 3.96 – 3.85 (m, 4H), 2.98 – 2.89 (m, 4H), 2.54 (t, *J* = 7.4 Hz, 4H), 2.02 – 1.90 (m, 4H), 1.65 (p, *J* = 3.8 Hz, 8H), 1.47 – 1.34 (m, 4H). **^{13}C NMR** (101 MHz, Methanol-*d4*) δ 172.9 (2C), 151.9, 142.5 (2C), 129.4 (4C), 129.3 (4C), 127.1 (2C), 57.6, 42.2 (2C), 40.2 (4C), 36.4 (2C), 27.9 (2C), 26.0 (2C), 25.9 (2C). **HRMS** (ESI): calcd for $C_{30}H_{43}N_4O_3^+$ $[M+H]^+$ 507.3330, found 507.3324. **SFC:** 96.3%.

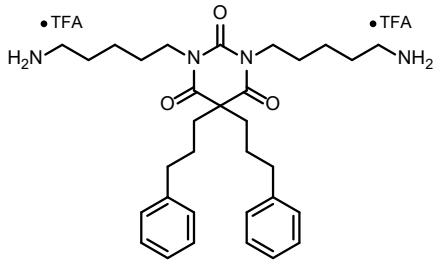

1,3-bis(5-aminopentyl)-5,5-bis(3-phenylpropyl)pyrimidine-2,4,6(1H,3H,5H)-trione **MPM-5:0**\.

Compound **1** (75 mg, 206 µmol, 1.0 eq), *tert*-butyl (5-hydroxypentyl)carbamate (105 mg, 515 µmol, 2.5 eq), PPh_3 (162 mg, 617 µmol, 3.0 eq) and DIAD (129 µL, 617 µmol, 3.0 eq) were stirred in anhydrous DCM (1.0 mL) for 4 h. The crude was purified with 10-45% EtOAc in heptane to yield impure Boc-**MPM-5:0** (185 mg, 252 µmol, 122%) as a colorless solid.

TFA (315 µL, 4.11 mmol, 20.0 eq) and DCM (1.0 mL) were added and the solution was stirred at ambient temperature for 22 h. The crude was purified by RP chromatography with a gradient of 15-50% MeCN in H_2O (both containing 0.1% TFA) to yield the di-TFA salt of **MPM-5:0** (146 mg, 191 µmol, 93% o2s) as a white solid.

^{1}H NMR (400 MHz, Methanol-*d4*) δ 7.28 – 7.20 (m, 4H), 7.19 – 7.12 (m, 2H), 7.12 – 7.06 (m, 4H), 3.93 – 3.85 (m, 4H), 2.93 – 2.81 (m, 4H), 2.53 (t, *J* = 7.5 Hz, 4H), 2.01 – 1.89 (m, 4H), 1.74 – 1.53 (m, 8H), 1.45 – 1.33 (m, 8H). **^{13}C NMR** (101 MHz, Methanol-*d4*) δ 173.0 (2C), 151.8, 142.5, 129.5 (4C), 129.3 (4C), 127.1 (2C), 57.5, 42.5 (2C), 40.5 (2C), 40.4 (2C), 36.5 (2C), 28.4 (2C), 28.0 (4C), 24.7 (2C). **HRMS** (ESI): calcd for $C_{32}H_{47}N_4O_3^+$ $[M+H]^+$ 535.3643, found 535.3637. **SFC:** >99%.

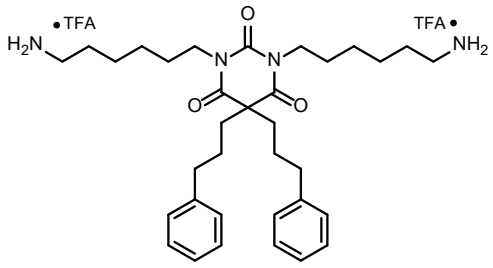

1,3-bis(6-aminohexyl)-5,5-bis(3-phenylpropyl)pyrimidine-2,4,6(1H,3H,5H)-trione **MPM-6:0**.

Compound **1** (75 mg, 206 µmol, 1.0 eq), *tert*-butyl (6-hydroxyhexyl)carbamate (112 mg, 515 µmol, 2.5 eq), PPh_3 (162 mg, 617 µmol, 3.0 eq) and DIAD (129 µL, 617 µmol, 3.0 eq) were stirred in anhydrous DCM (1.0 mL) for 4 h. The crude was purified with 10-45% EtOAc in heptane to yield impure Boc-**MPM-6:0** (161 mg, 211 µmol, 103%) as a colorless oil.

TFA (315 µL, 4.11 mmol, 20.0 eq) and DCM (1.0 mL) were added and the solution was stirred at ambient temperature for 22 h. The crude was purified by RP chromatography with a gradient of 15-50% MeCN in H_2O (both containing 0.1% TFA) to yield the di-TFA salt of **MPM-6:0** (120 mg, 152 µmol, 74% o2s) as a white solid.

^{1}H NMR (400 MHz, Methanol-*d4*) δ 7.28 – 7.20 (m, 4H), 7.19 – 7.12 (m, 2H), 7.11 – 7.04 (m, 4H), 3.91 – 3.84 (m, 4H), 2.93 – 2.84 (m, 4H), 2.53 (t, *J* = 7.5 Hz, 4H), 1.99 – 1.89 (m, 4H), 1.67 – 1.51 (m, 8H), 1.46 – 1.31 (m, 12H). **^{13}C NMR** (101 MHz, Methanol-*d4*) δ 173.0 (2C), 151.9, 142.5 (2C), 129.5 (4C), 129.3 (4C), 127.1 (2C), 57.5, 42.7 (2C), 40.6 (2C), 40.5 (2C), 36.5 (2C), 28.7 (2C), 28.4 (2C), 28.0 (2C), 27.4 (2C), 26.9 (2C). **HRMS** (ESI): calcd for $C_{34}H_{51}N_4O_3^+$ $[M+H]^+$ 563.3956, found 563.3950. **SFC:** >99%.

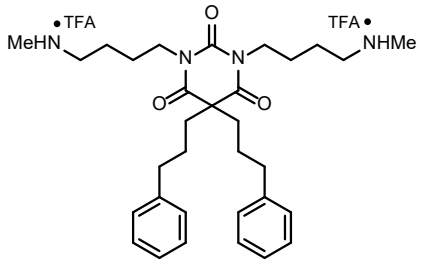

1,3-bis(4-(methylamino)butyl)-5,5-bis(3-phenylpropyl)pyrimidine-2,4,6(1H,3H,5H)-trione **MPM-4:1**.

Compound **3** (86 mg, 136 µmol, 1.0 eq) was taken up in anhydrous acetonitrile (1 mL) and methylamine (542 µL, 1.08 mmol, 8.0 eq; 2M in THF) was added. After heating to 70 °C for 40 h, the mixture was allowed to cool to ambient temperature. The solvent was removed and crude was purified on an automated flash system equipped with a C18 column and gradient 10-55% MeCN in H_2O (both containing 0.1% TFA). The di-TFA salt of **MPM-4:1** (65 mg, 85 µmol, 63%) was obtained as a white solid.

^{1}H NMR (400 MHz, Methanol-*d4*) δ 7.28 – 7.20 (m, 4H), 7.19 – 7.12 (m, 2H), 7.11 – 7.06 (m, 4H), 3.90 (t, *J* = 6.8 Hz, 4H), 3.00 (t, *J* = 7.2 Hz, 4H), 2.67 (s, 6H), 2.54 (t, *J* = 7.4 Hz, 4H), 1.99 – 1.90 (m, 4H), 1.74 – 1.57 (m, 8H), 1.46 – 1.32 (m, 4H). **^{13}C NMR** (101 MHz, Methanol-*d4*) δ 172.9 (2C), 151.9, 142.5 (2C), 129.5 (4C), 129.3 (4C), 127.1 (2C), 57.6, 49.7 (2C) 42.2 (2C), 40.3 (2C), 36.4 (2C), 33.5 (2C), 27.9 (2C), 26.0 (2C), 24.4 (2C). **HRMS** (ESI): calcd for $C_{32}H_{47}N_4O_3^+$ $[M+H]^+$ 535.3643, found: 535.3646. **SFC:** 96.2%.

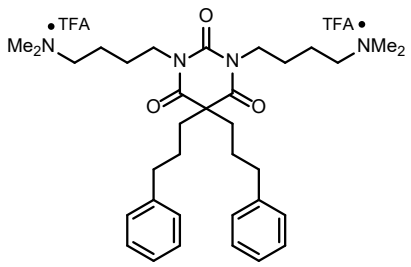

1,3-bis(4-(dimethylamino)butyl)-5,5-bis(3-phenylpropyl)pyrimidine-2,4,6(1H,3H,5H)-trione **MPM-4:2**.

Compound **3** (82 mg, 129 µmol, 1.0 eq) was taken up in anhydrous acetonitrile (1 mL) and dimethylamine (517 µL, 1.03 mmol, 8.0 eq; 2 M in THF) was added. After heating to 70 °C for 40 h, the mixture was allowed to cool to ambient temperature. The solvent was removed and crude was purified on an automated flash system equipped with a C18 column and gradient 10-55% MeCN in H_2O (both containing

0.1% TFA). The di-TFA salt of **MPM-4:2** (99 mg, 125 µmol, 97%) was obtained as a white solid, which became a colorless oil upon standing.

^{1}H NMR (400 MHz, Methanol-*d4*) δ 7.28 – 7.20 (m, 4H), 7.19 – 7.12 (m, 2H), 7.12 – 7.07 (m, 4H), 3.92 (t, *J* = 7.1 Hz, 4H), 3.17 – 3.08 (m, 4H), 2.83 (s, 12H), 2.54 (t, *J* = 7.4 Hz, 4H), 2.00 – 1.91 (m, 4H), 1.77 – 1.57 (m, 8H), 1.46 – 1.33 (m, 4H). **^{13}C NMR** (101 MHz, Methanol-*d4*) δ 172.9 (2C), 151.9, 142.5 (2C), 129.5 (4C), 129.3 (4C), 127.1 (2C), 58.3 (2C), 57.6, 43.4 (4C), 42.1 (2C), 40.3 (2C), 36.5 (2C), 28.0 (2C), 25.9 (2C), 22.9 (2C). **HRMS** (ESI): calcd for $C_{34}H_{51}N_4O_3^+$ $[M+H]^+$ 563.3956, found: 563.3956. **SFC:** >99%.

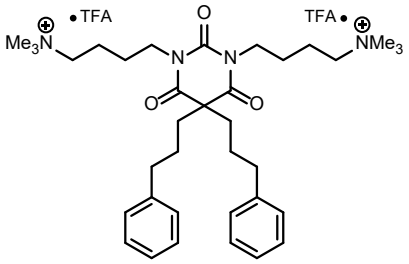

4,4'-(2,4,6-trioxo-5,5-bis(3-phenylpropyl)dihydropyrimi-dine-1,3(2H,4H)-diyl)bis(N,N,N-trimethylbutan-1-aminium) **MPM-4:3**.

Compound **3** (79 mg, 125 µmol, 1.0 eq) was taken up in anhydrous acetonitrile (1 mL) and trimethylamine (996 µL, 1.00 mmol, 8.0 eq; 1 M in THF) was added. After heating to 70 °C for 40 h, the mixture was allowed to cool to ambient temperature. The solvent was removed and crude was purified on an automated flash system equipped with a C18 column and gradient 10-55% MeCN in H_2O (both containing 0.1% TFA). The di-TFA salt of **MPM-4:3** (98 mg, 120 µmol, 96%) was obtained as a white solid, which became a colorless oil upon standing.

^{1}H NMR (400 MHz, Methanol-*d4*) δ 7.29 – 7.21 (m, 4H), 7.20 – 7.13 (m, 2H), 7.12 – 7.07 (m, 4H), 3.98 – 3.83 (m, 4H), 3.40 – 3.33 (m, 4H), 3.08 (s, 18H), 2.54 (t, *J* = 7.5 Hz, 4H), 2.03 – 1.93 (m, 4H), 1.83 – 1.71 (m, 4H), 1.70 – 1.59 (m, 4H), 1.47 – 1.34 (m, 4H). **^{13}C NMR** (101 MHz, Methanol-*d4*) δ 173.0 (2C), 151.8, 142.5 (2C), 129.5 (4C), 129.3 (4C), 127.2 (2C), 67.0 (t, *J* = 2.9 Hz, 2C), 57.6, 53.5 (t, *J* = 3.9 Hz, 6C), 42.1 (2C), 40.4 (2C), 36.5 (2C), 28.0 (2C), 25.7 (2C), 21.3 (2C). **HRMS** (ESI): calcd for $C_{36}H_{56}N_4O_3^{2+}$ $[M]^{2+}$ 296.2171, found: 296.2172. **SFC:** >99%.

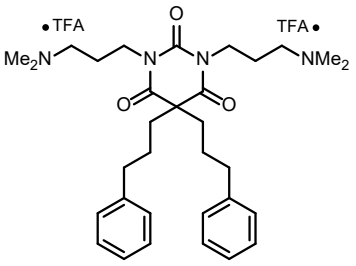

1,3-bis(3-(dimethylamino)propyl)-5,5-bis(3-phenylpropyl)-pyrimidine-2,4,6(1H,3H,5H)-trione **MPM-3:2**.

Compound **2** (113 mg, 186 µmol, 1.0 eq) was taken up in anhydrous acetonitrile (1 mL) and dimethylamine (745 µL, 1.49 mmol, 8.0 eq; 2 M in THF) was added. After heating to 70 °C for 24 h, the mixture was allowed to cool to ambient temperature. The solvent was removed and crude was purified on an automated flash system equipped with a C18 column and gradient 10-50% MeCN in H_2O (both containing 0.1% TFA). The di-TFA salt of **MPM-3:2** (135 mg, 177 µmol, 95%) was obtained as a white powder.

^{1}H NMR (400 MHz, Methanol-*d4*) δ 7.27 – 7.19 (m, 4H), 7.19 – 7.06 (m, 6H), 3.97 (t, *J* = 7.1 Hz, 4H), 3.18 – 3.07 (m, 4H), 2.83 (t, *J* = 1.4 Hz, 12H), 2.55 (t, *J* = 7.4 Hz, 4H), 2.08 – 1.89 (m, 8H), 1.49 – 1.36 (m, 4H). **^{13}C NMR** (101 MHz, Methanol-*d4*) δ 173.0 (2C), 151.9, 142.5 (2C), 129.5 (4C), 129.4 (4C), 127.1 (2C), 57.7, 56.4 (2C), 43.4 (4C), 40.0 (4C), 36.4 (2C), 28.0 (2C), 24.4 (2C). **HRMS** (ESI): calcd for $C_{32}H_{47}N_4O_3^+$ $[M+H]^+$ 535.3643, found: 535.3637. **SFC:** >99%.

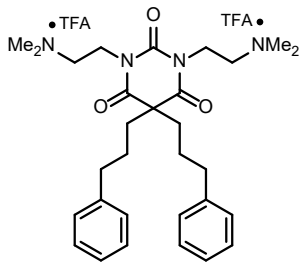

1,3-bis(2-(dimethylamino)ethyl)-5,5-bis(3-phenylpropyl)pyrimidine-2,4,6(1H,3H,5H)-trione **MPM-2:2**.

To **MPM-2:0** (29 mg, 43 µmol, 1.0 eq; TFA salt) and $NaBH_3CN$ (8.1 mg, 128 µmol, 3.0 eq) in MeOH (300 µL), were added acetic acid (9.8 µL, 171 µmol, 4.0 eq) and formaldehyde (19.2 µL, 256 µmol, 6.0 eq; 37% aqueous solution) and the resulting mixture was stirred at ambient temperature for 20 h. Saturated $NaHCO_{3(aq)}$ solution was added, the solvent was removed and the obtained salts were washed with MeOH. The combined organics were filtered over cotton wool and the solvent was removed. The crude was purified on an automated flash system equipped with a C18 column and gradient 15-50% MeCN in H_2O (both containing 0.1% TFA). The di-TFA salt of **MPM-2:2** (30 mg, 41 µmol, 96%) was obtained as a white foam.

^{1}H NMR (400 MHz, Methanol-*d4*) δ 7.27 – 7.19 (dd, *J* = 8.0, 6.6 Hz, 4H), 7.18 – 7.08 (m, 6H), 4.24 (t, *J* = 6.2 Hz, 4H), 3.40 (t, *J* = 6.1 Hz, 4H), 2.96 (s, 12H), 2.54 (t, *J* = 7.3 Hz, 4H), 1.99 – 1.89 (m, 4H), 1.56 – 1.43 (m, 4H). **^{13}C NMR** (101 MHz, Methanol-*d4*) δ 172.8 (2C), 152.7, 142.6 (2C), 129.4 (8C), 127.0 (2C), 57.8, 56.5 (2C), 43.9 (4C), 38.5 (2C), 38.4 (2C), 36.4 (2C), 27.4 (2C). **HRMS** (ESI): calcd for $C_{30}H_{43}N_4O_3^+$ $[M+H]^+$ 507.3330, found: 507.3326. **SFC:** *not obtained*.

2 NMR spectra

2.1 Starting materials for barbituric acid

1,3-bis(3-bromopropyl)-5,5-bis(3-phenylpropyl)pyrimidine-2,4,6(1H,3H,5H)-trione **2**.

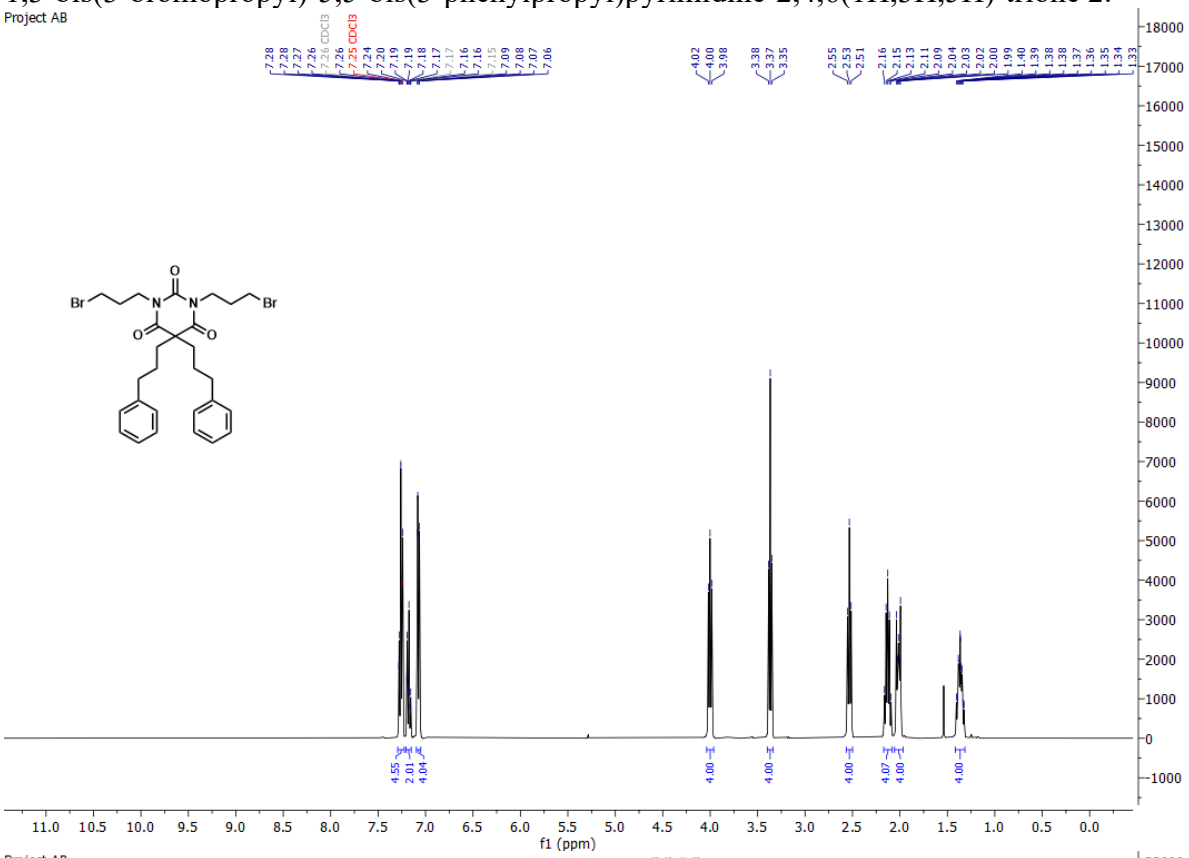

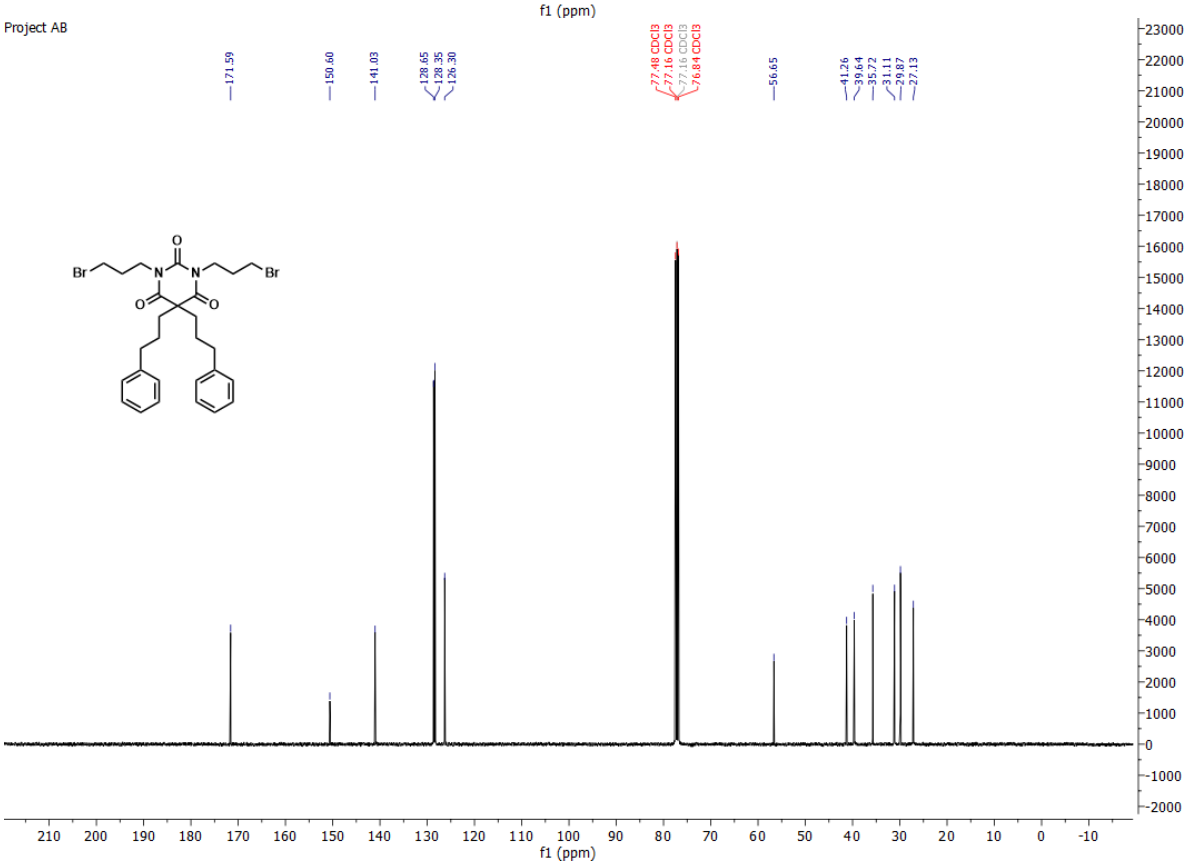

1,3-bis(4-bromobutyl)-5,5-bis(3-phenylpropyl)pyrimidine-2,4,6(1H,3H,5H)-trione **3**.

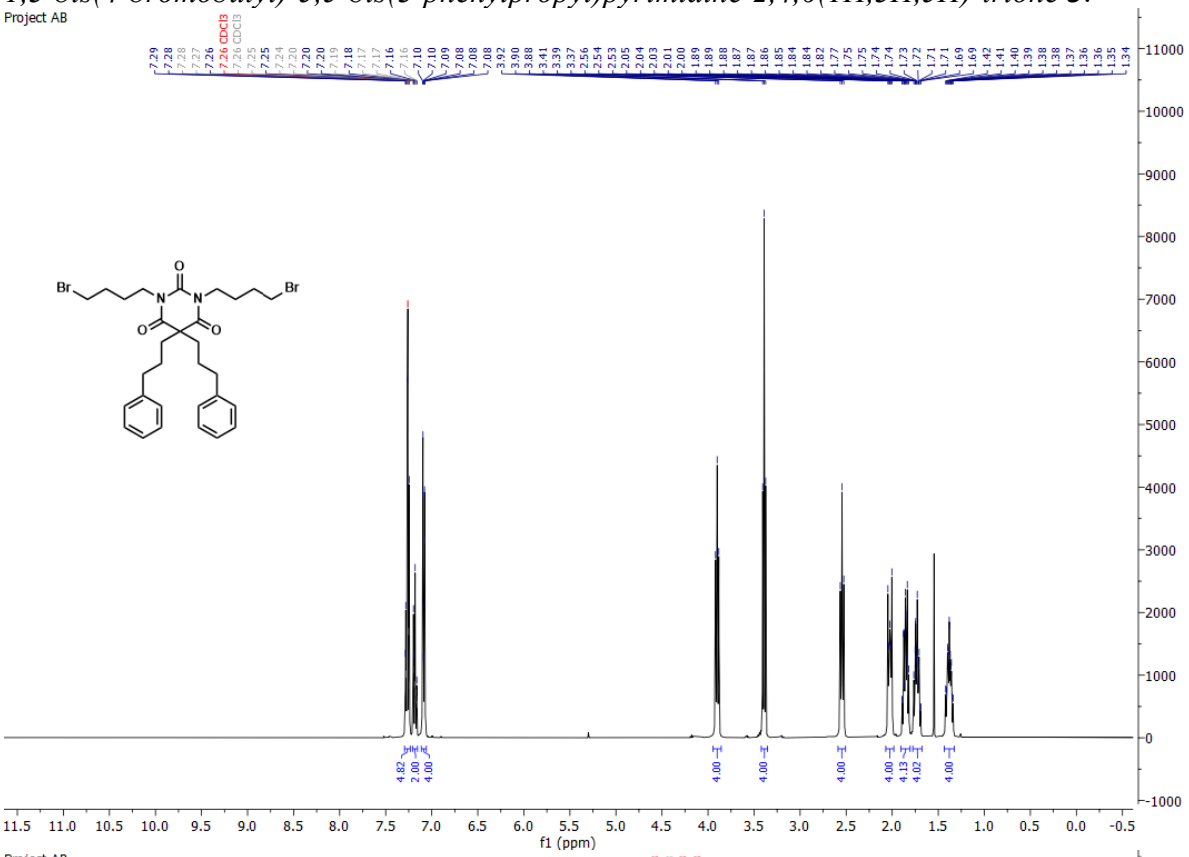

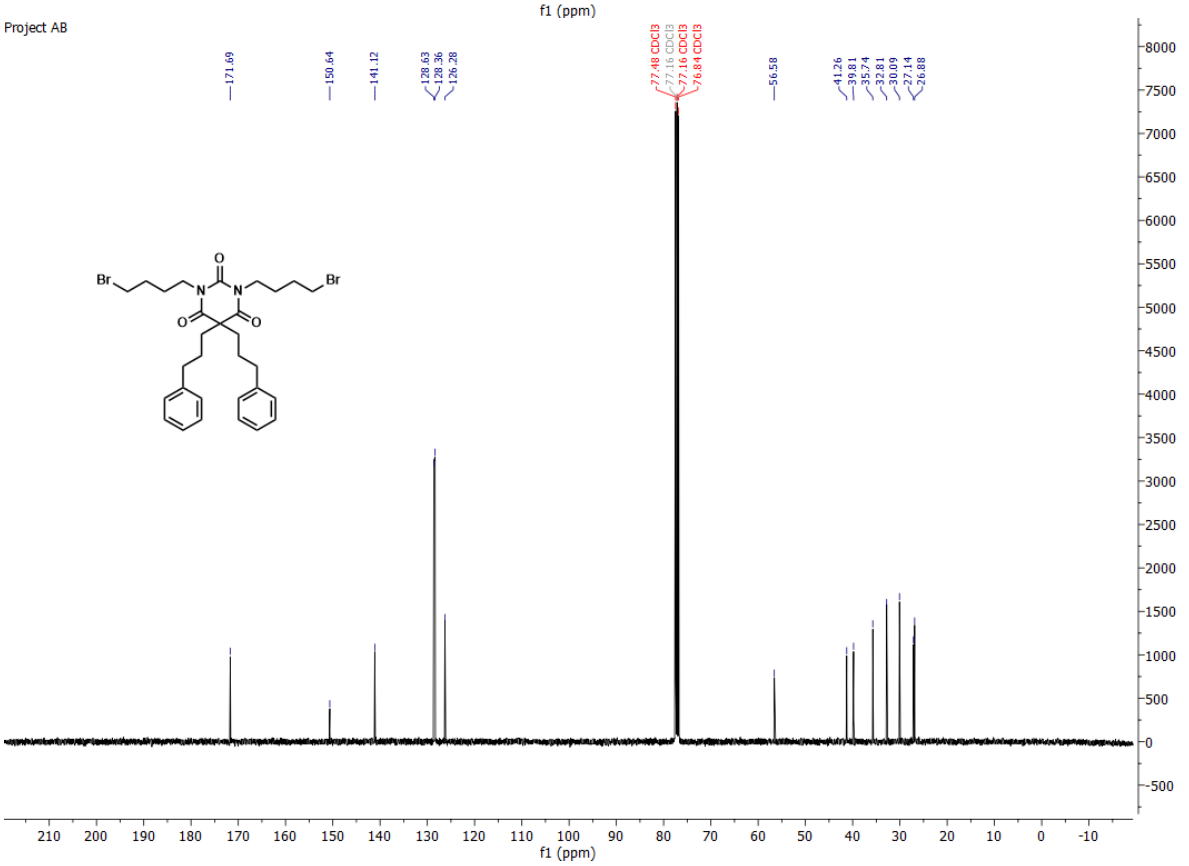

2.2 Final MPMs

1,3-bis(2-aminoethyl)-5,5-bis(3-phenylpropyl)pyrimidine-2,4,6(1H,3H,5H)-trione **MPM-2:0**.

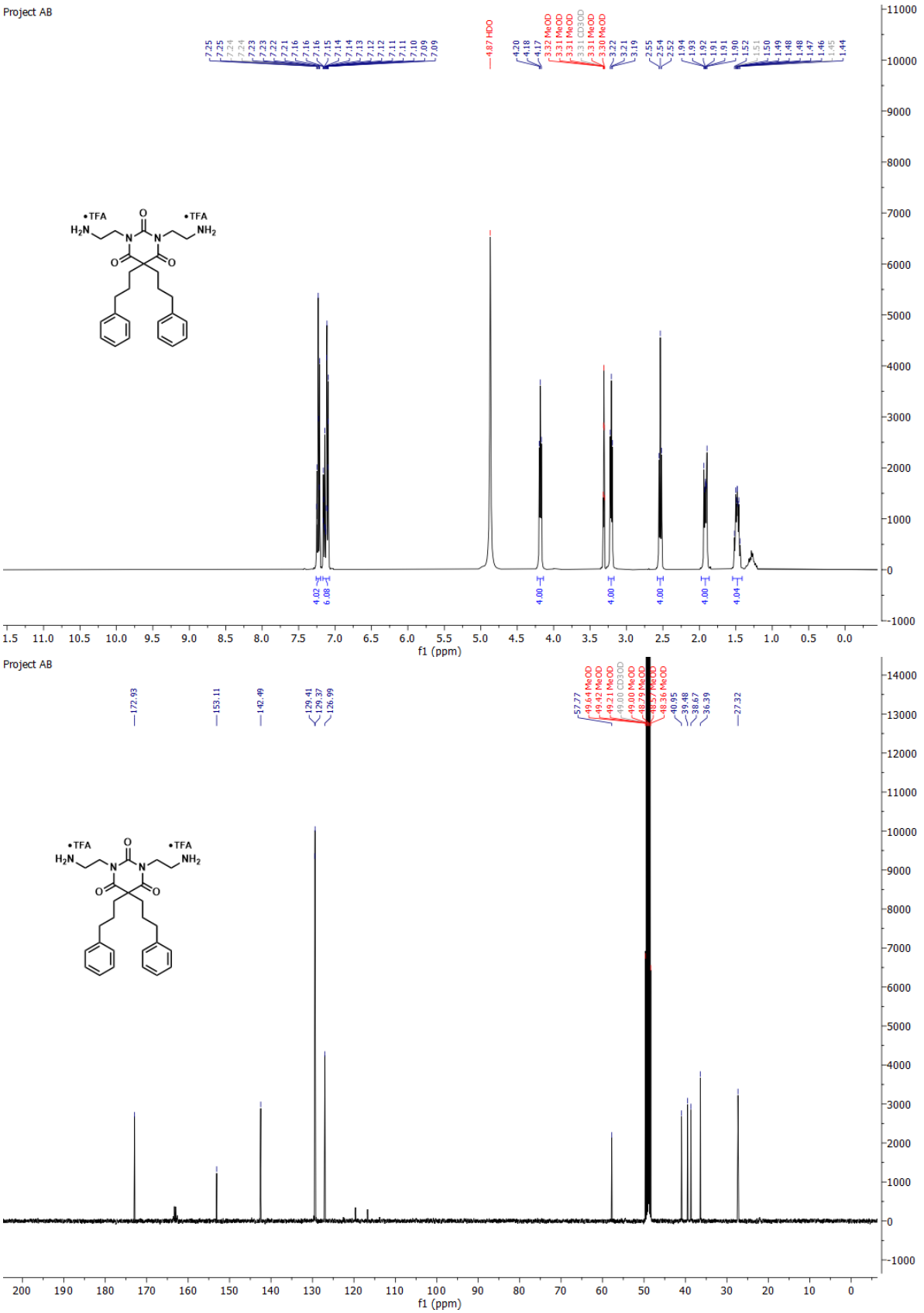

1,3-bis(3-aminopropyl)-5,5-bis(3-phenylpropyl)pyrimidine-2,4,6(1H,3H,5H)-trione **MPM-3:0**.

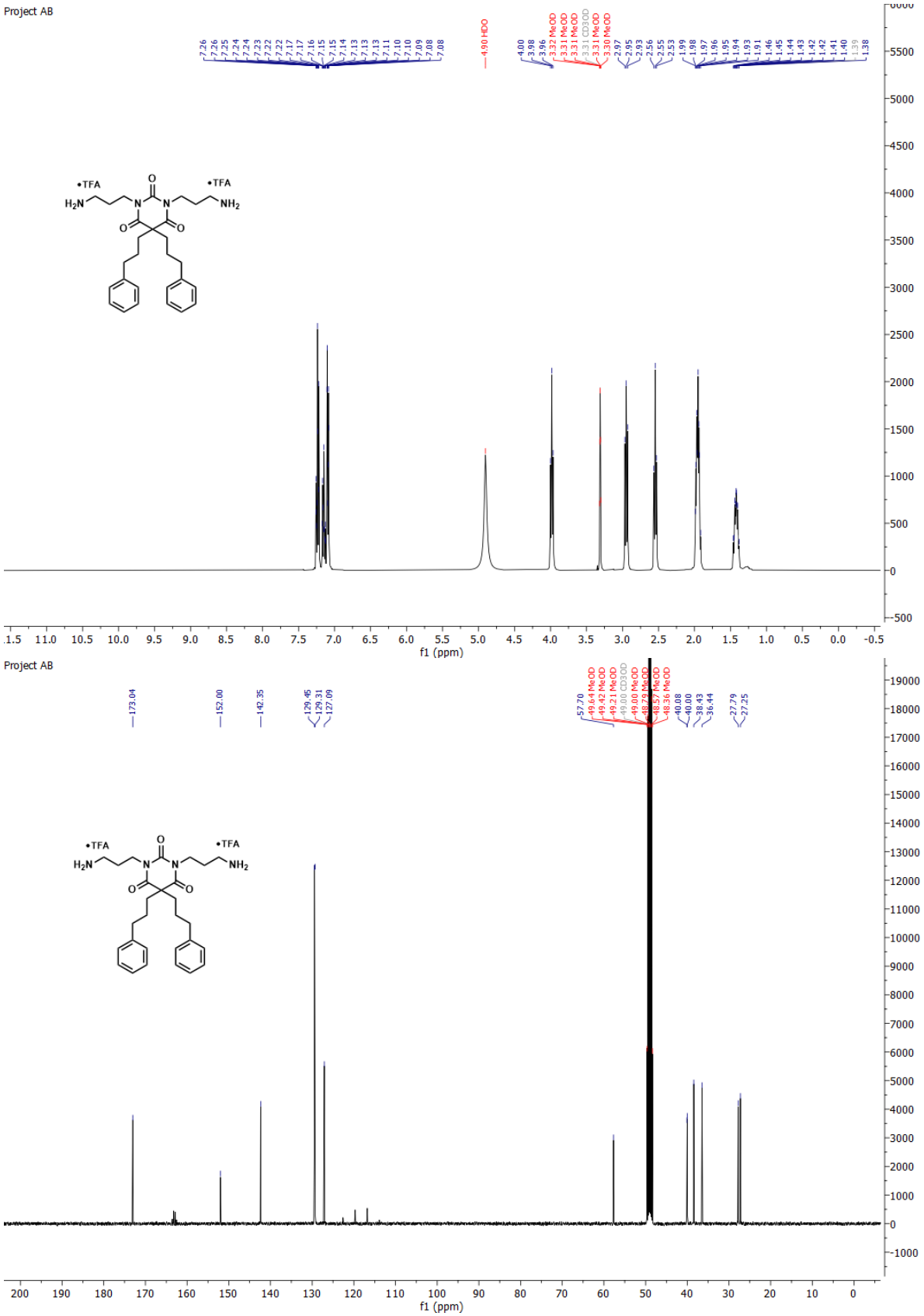

1,3-bis(4-aminobutyl)-5,5-bis(3-phenylpropyl)pyrimidine-2,4,6(1H,3H,5H)-trione **MPM-1**.

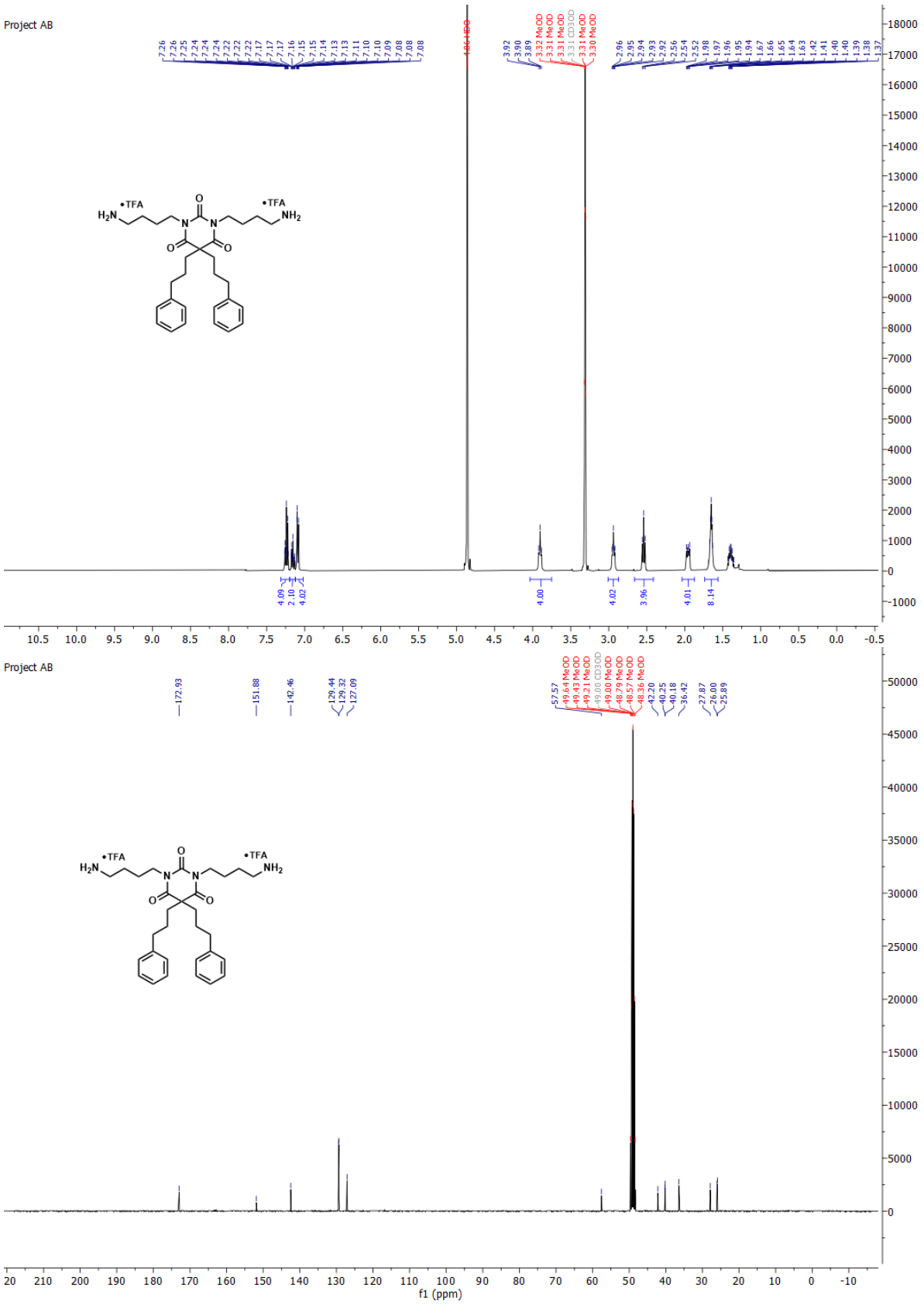

1,3-bis(5-aminopentyl)-5,5-bis(3-phenylpropyl)pyrimidine-2,4,6(1H,3H,5H)-trione **MPM-5:0**.

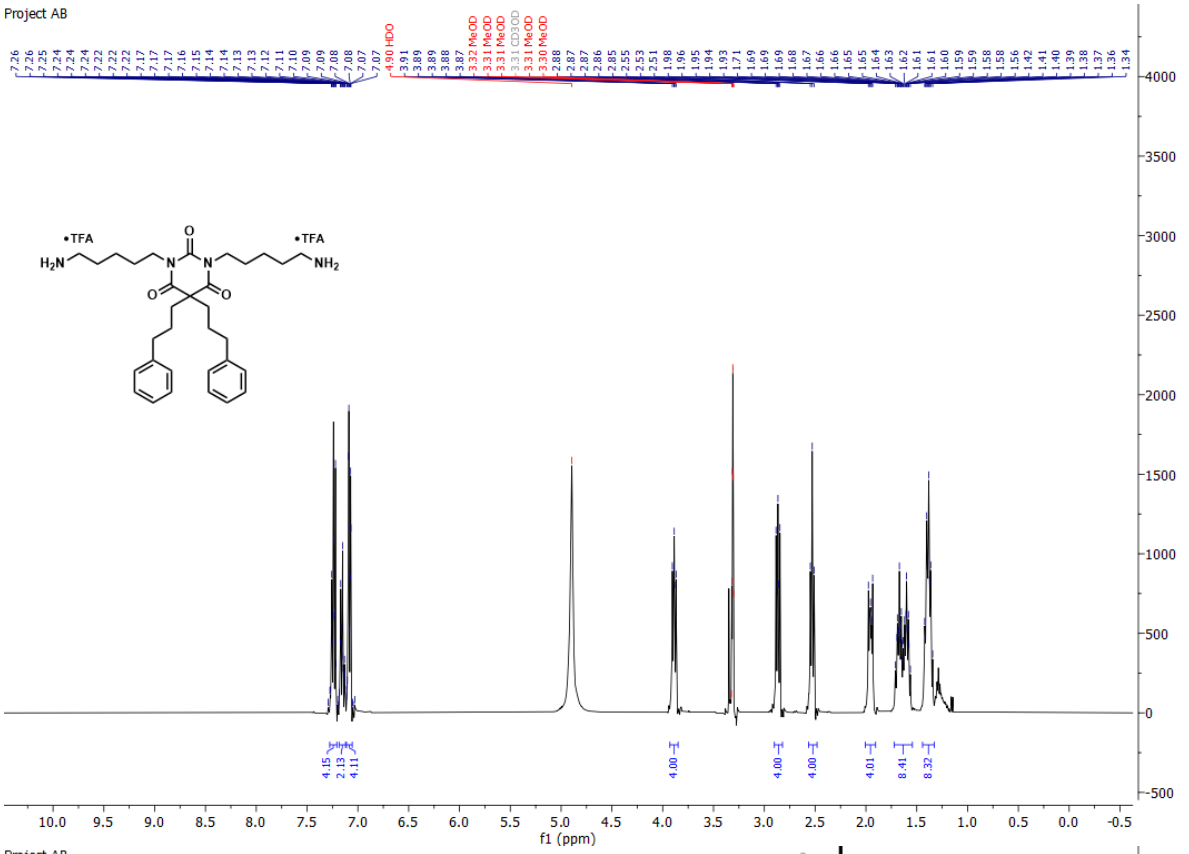
Project AB
•TFA
•TFA
f1 (ppm)

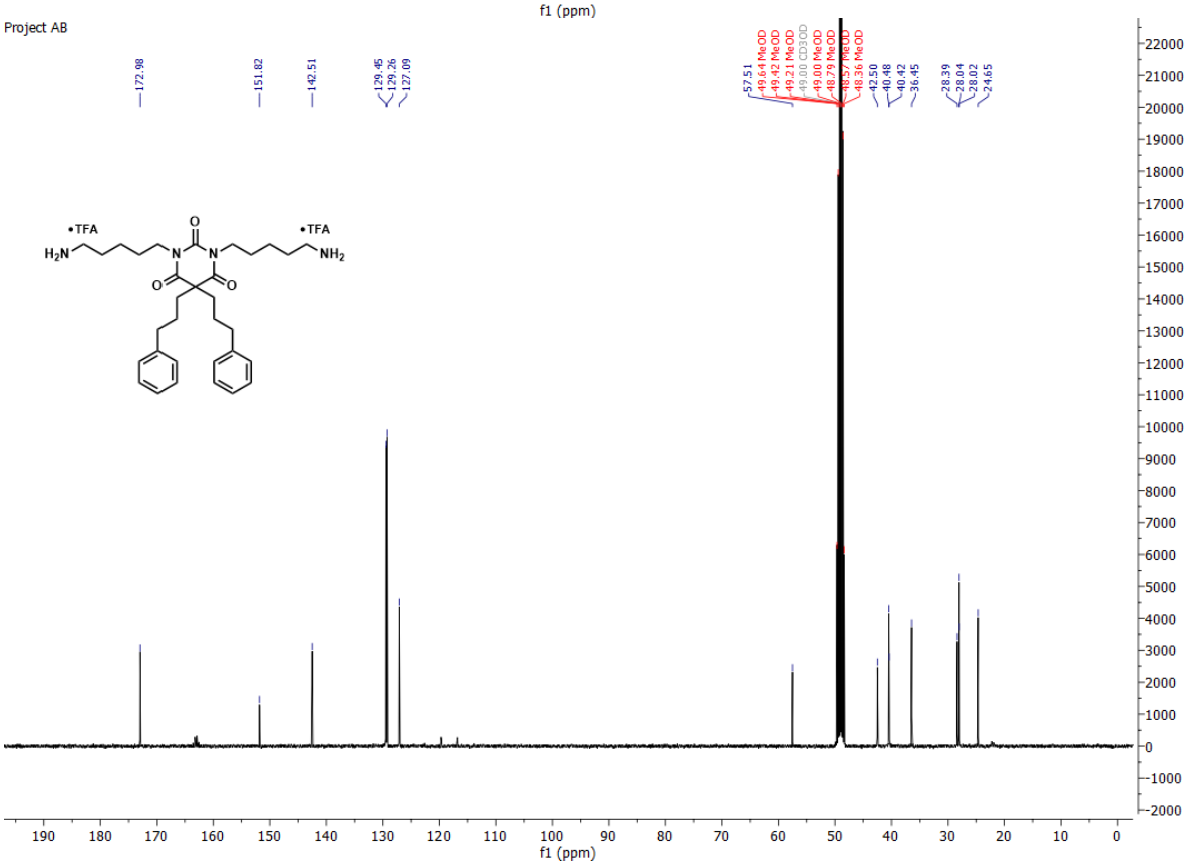
Project AB
•TFA
•TFA
f1 (ppm)

1,3-bis(6-aminohexyl)-5,5-bis(3-phenylpropyl)pyrimidine-2,4,6(1H,3H,5H)-trione **MPM-6:0**.

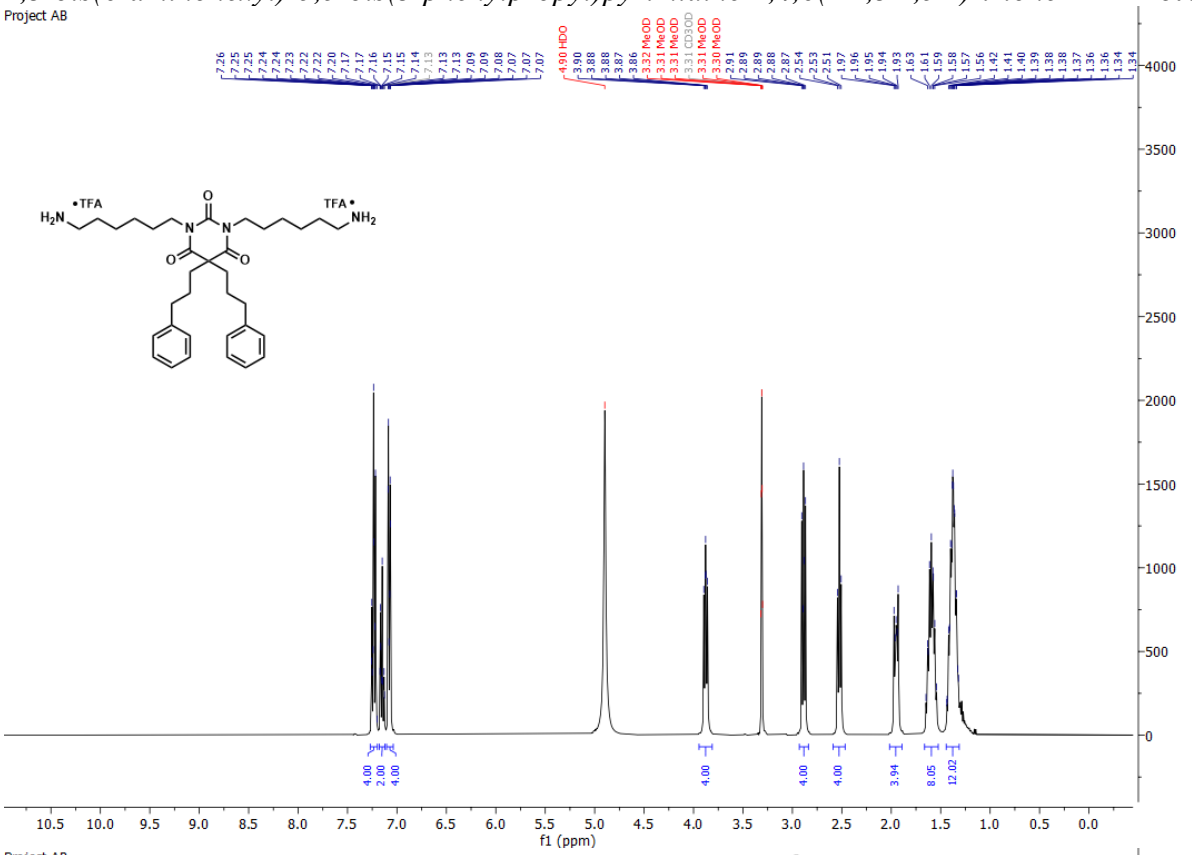

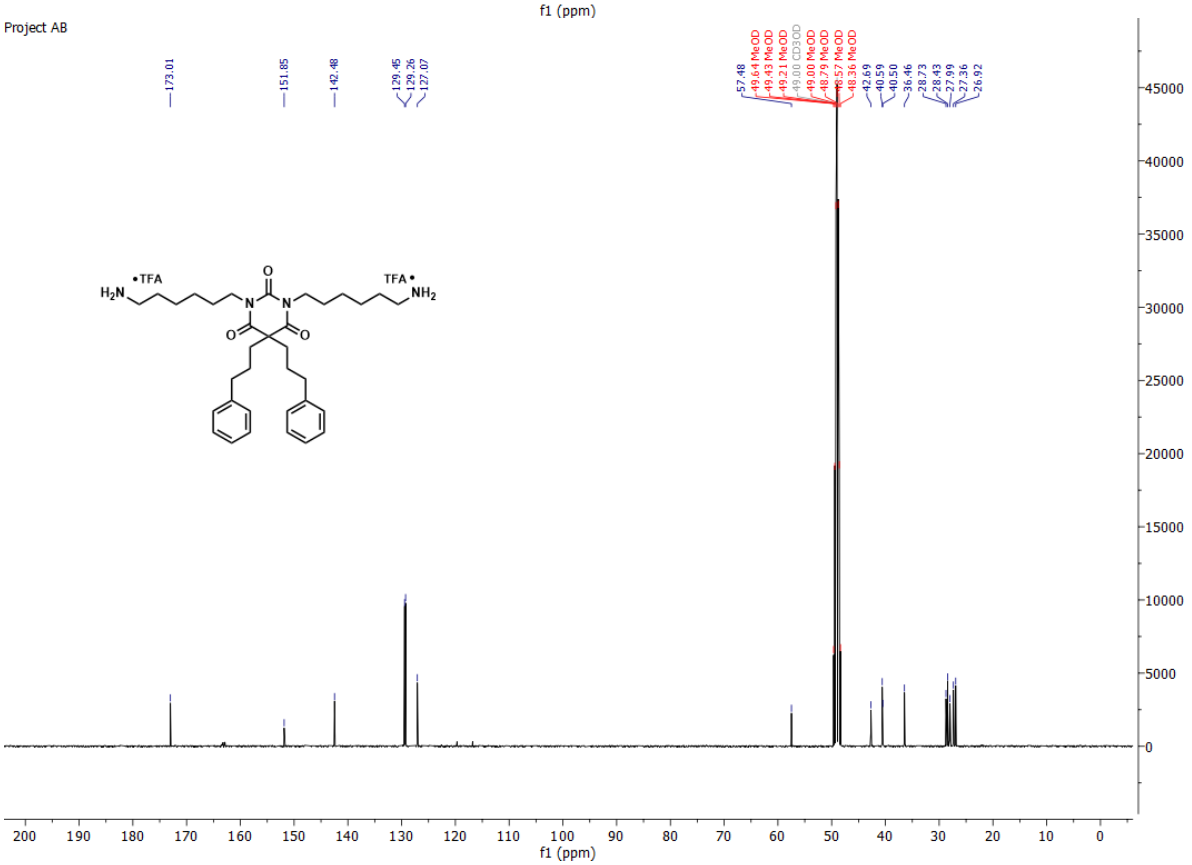

1,3-bis(4-(methylamino)butyl)-5,5-bis(3-phenylpropyl)pyrimidine-2,4,6(1H,3H,5H)-trione **MPM-4:1**.

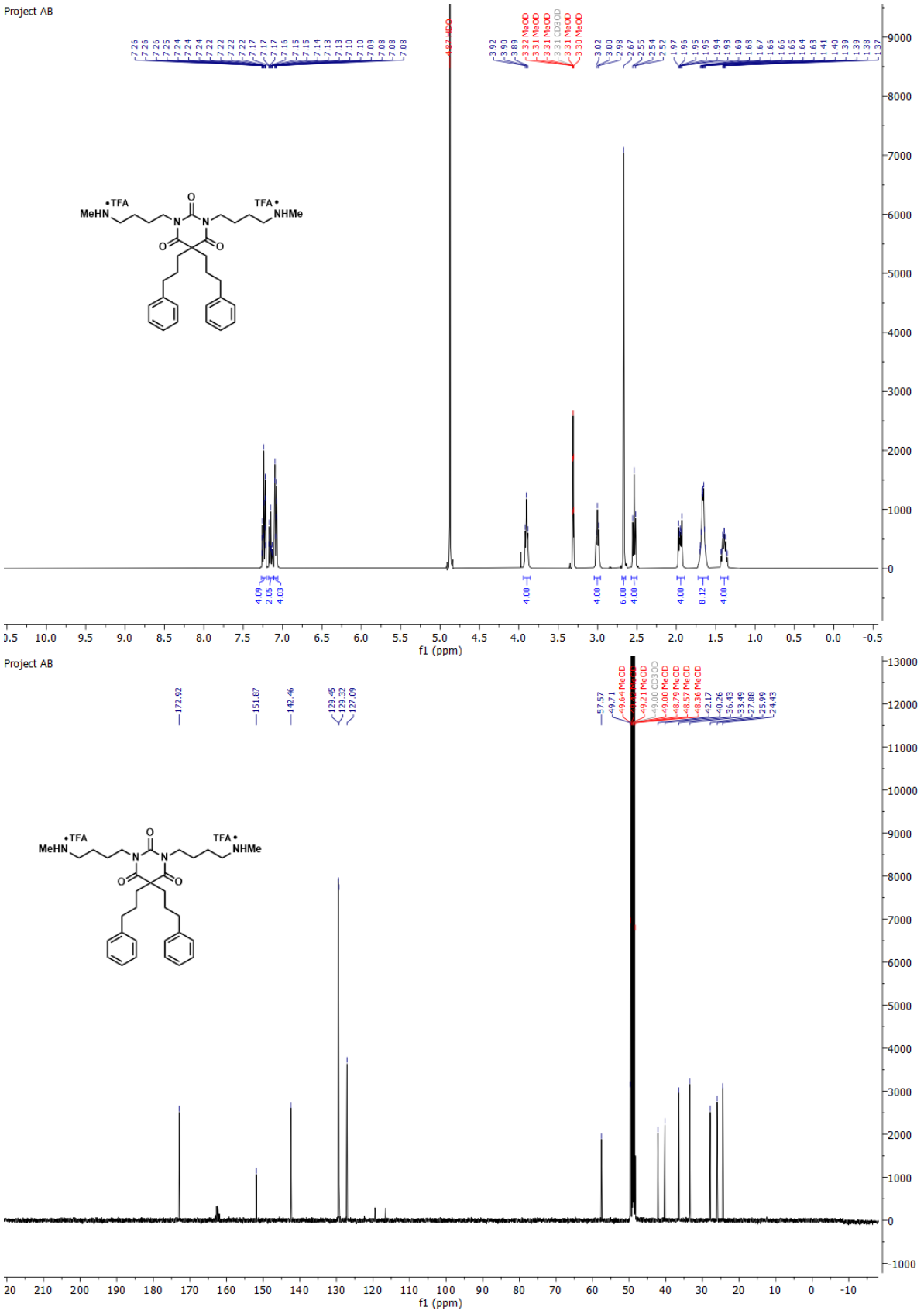

1,3-bis(4-(dimethylamino)butyl)-5,5-bis(3-phenylpropyl)pyrimidine-2,4,6(1H,3H,5H)-trione **MPM-4:2**.

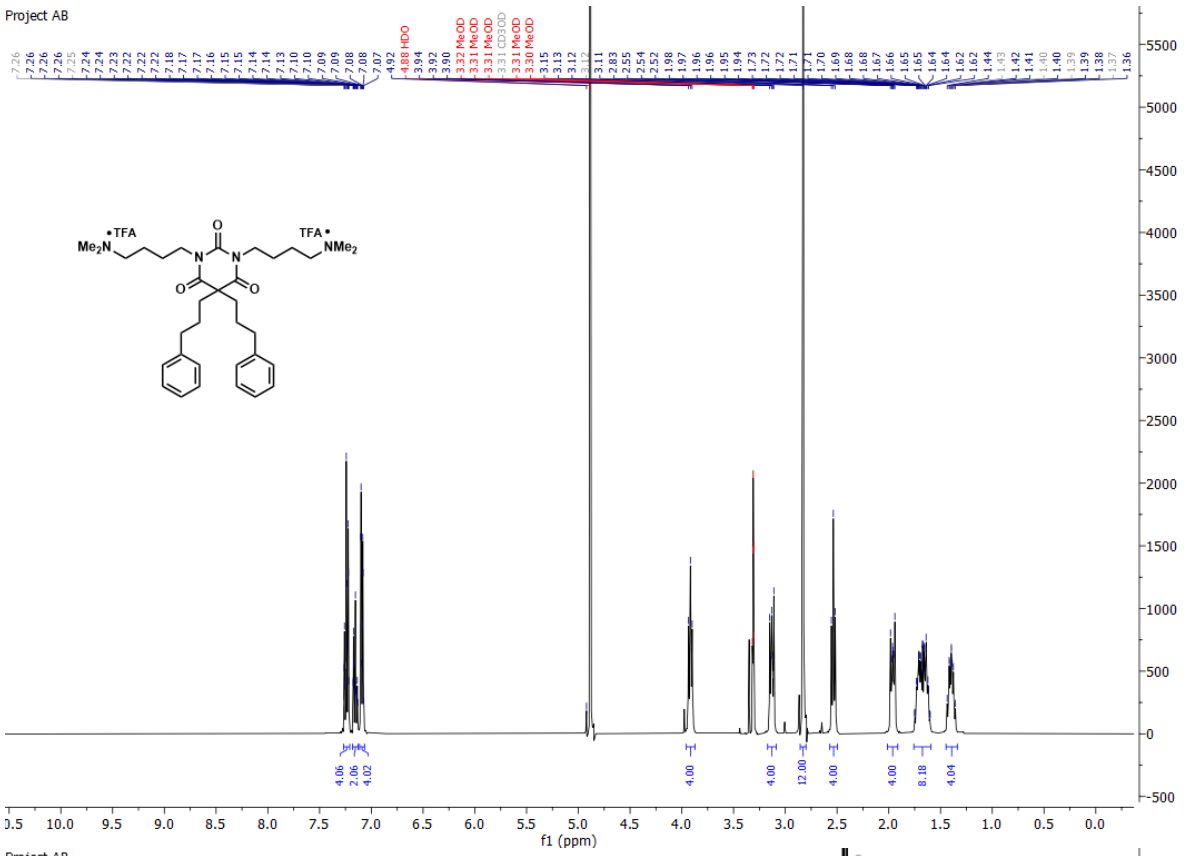
Project AB
•TFA
Me2N
TFA•
NMe2
f1 (ppm)

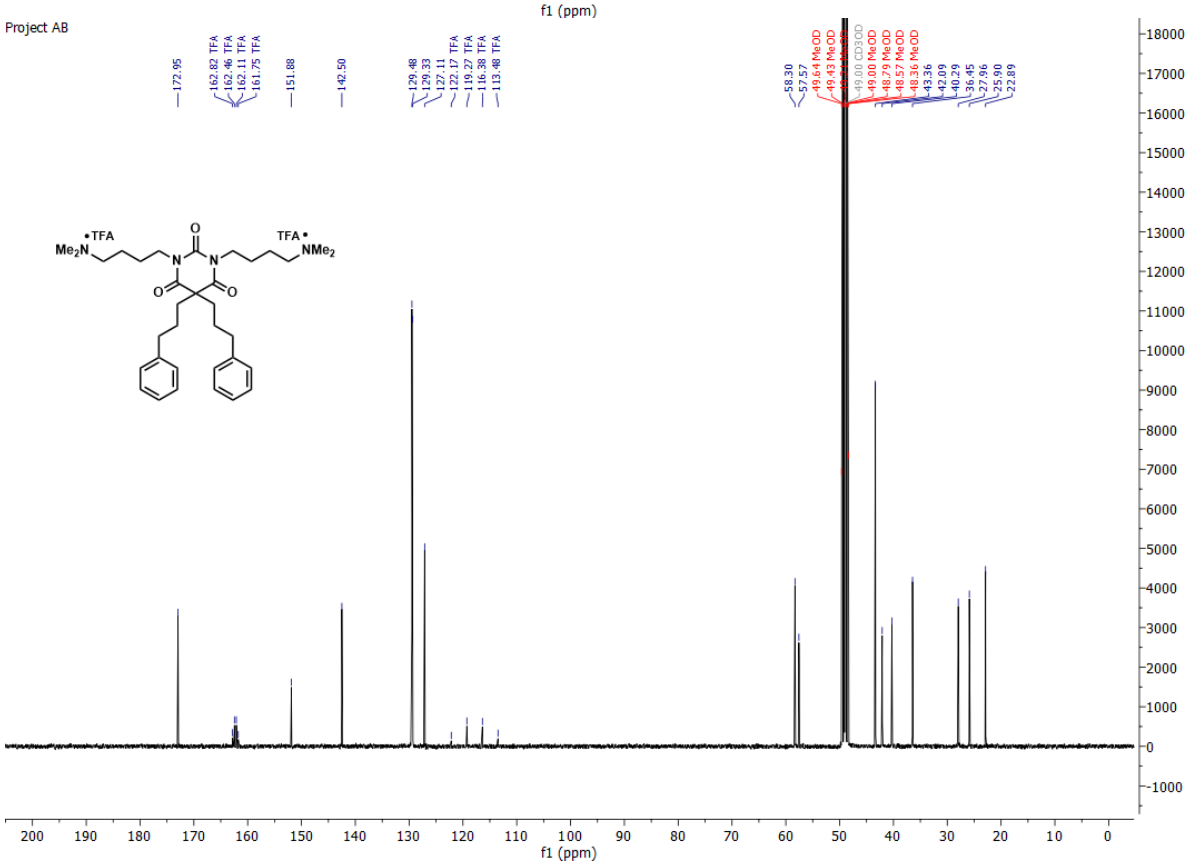
Project AB
•TFA
Me2N
TFA•
NMe2
f1 (ppm)

4,4'-(2,4,6-trioxo-5,5-bis(3-phenylpropyl)dihydropyrimi-dine-1,3(2H,4H)-diyl)bis(N,N,N-trimethylbutan-1-aminium) **MPM-4:3**.

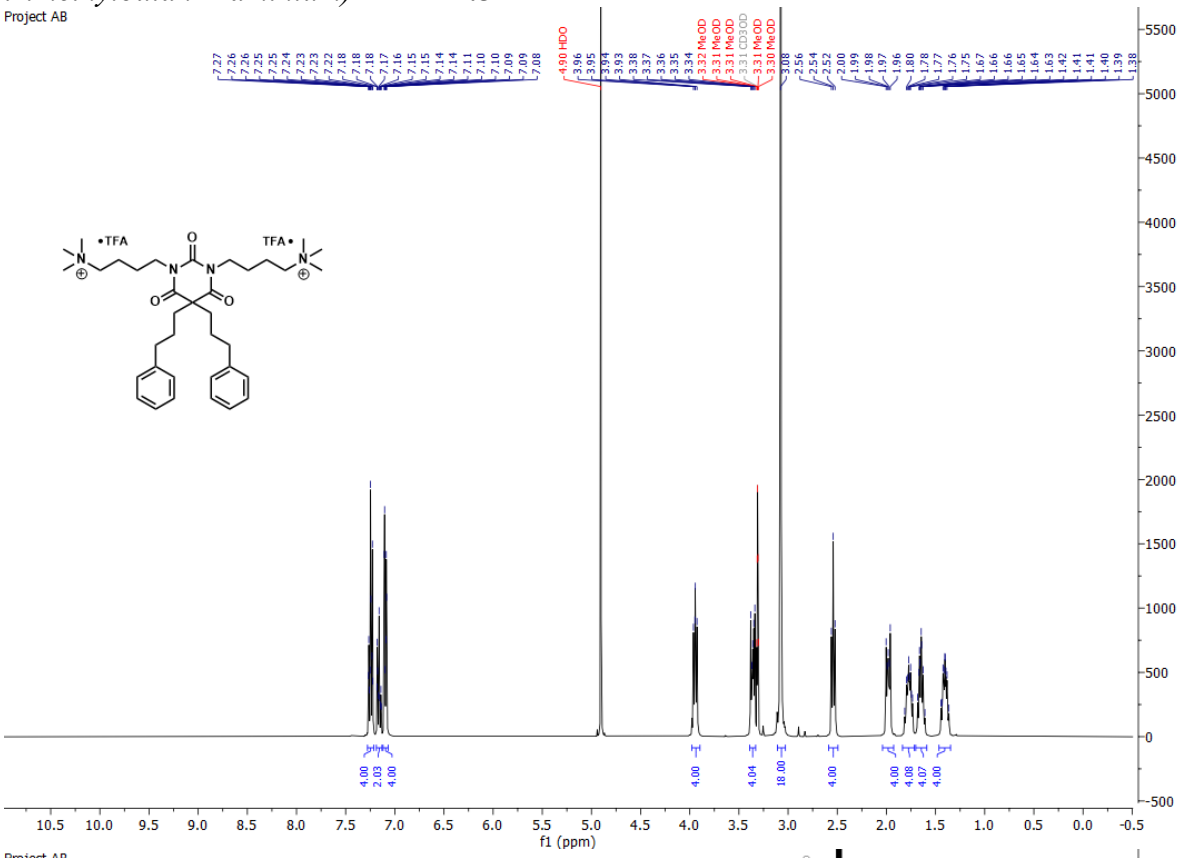

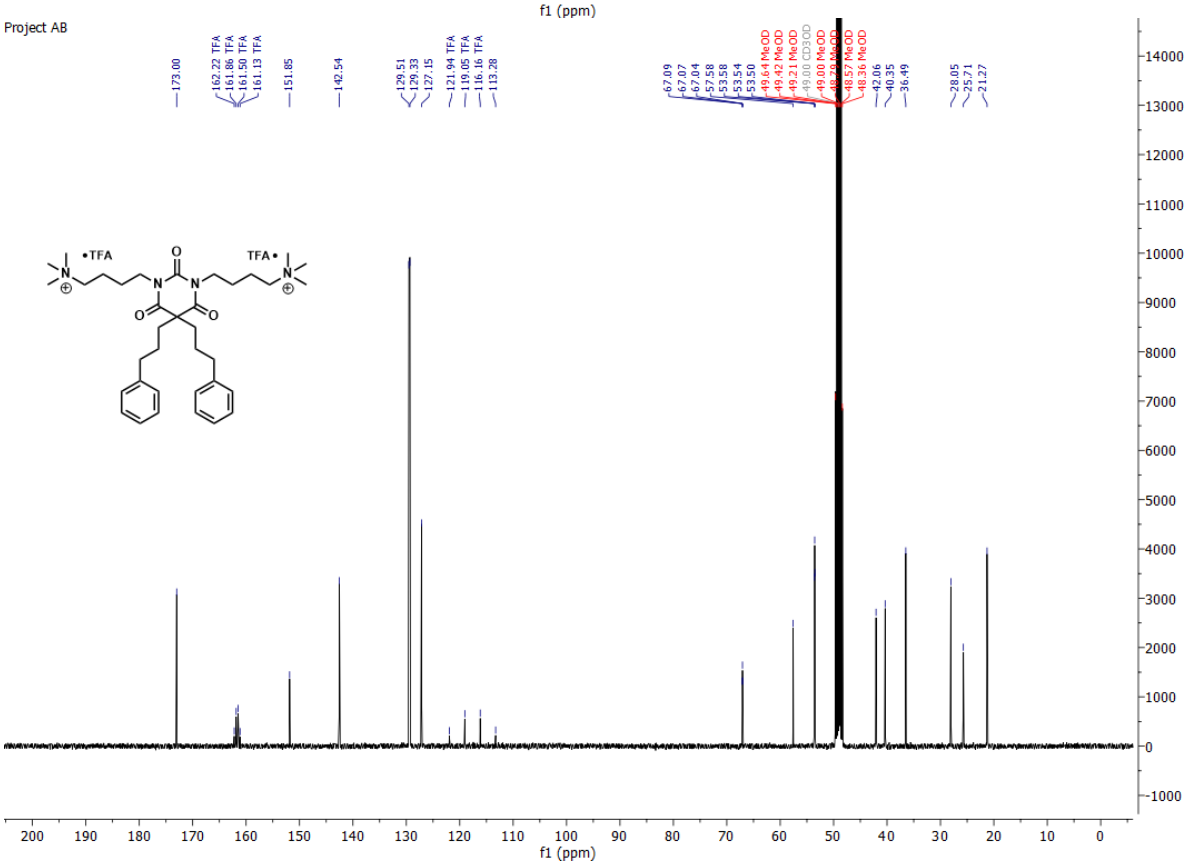

1,3-bis(3-(dimethylamino)propyl)-5,5-bis(3-phenylpropyl)-pyrimidine-2,4,6(1H,3H,5H)-trione **MPM-3:2**.

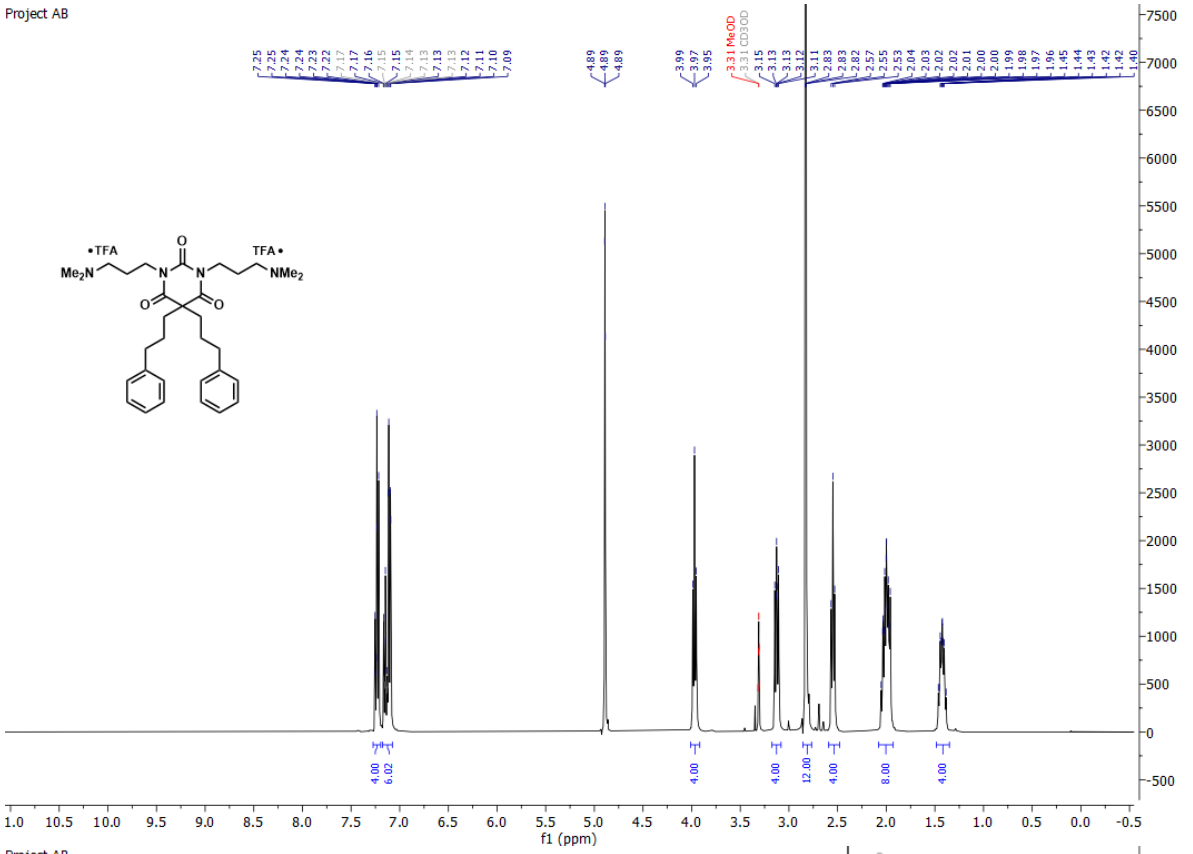

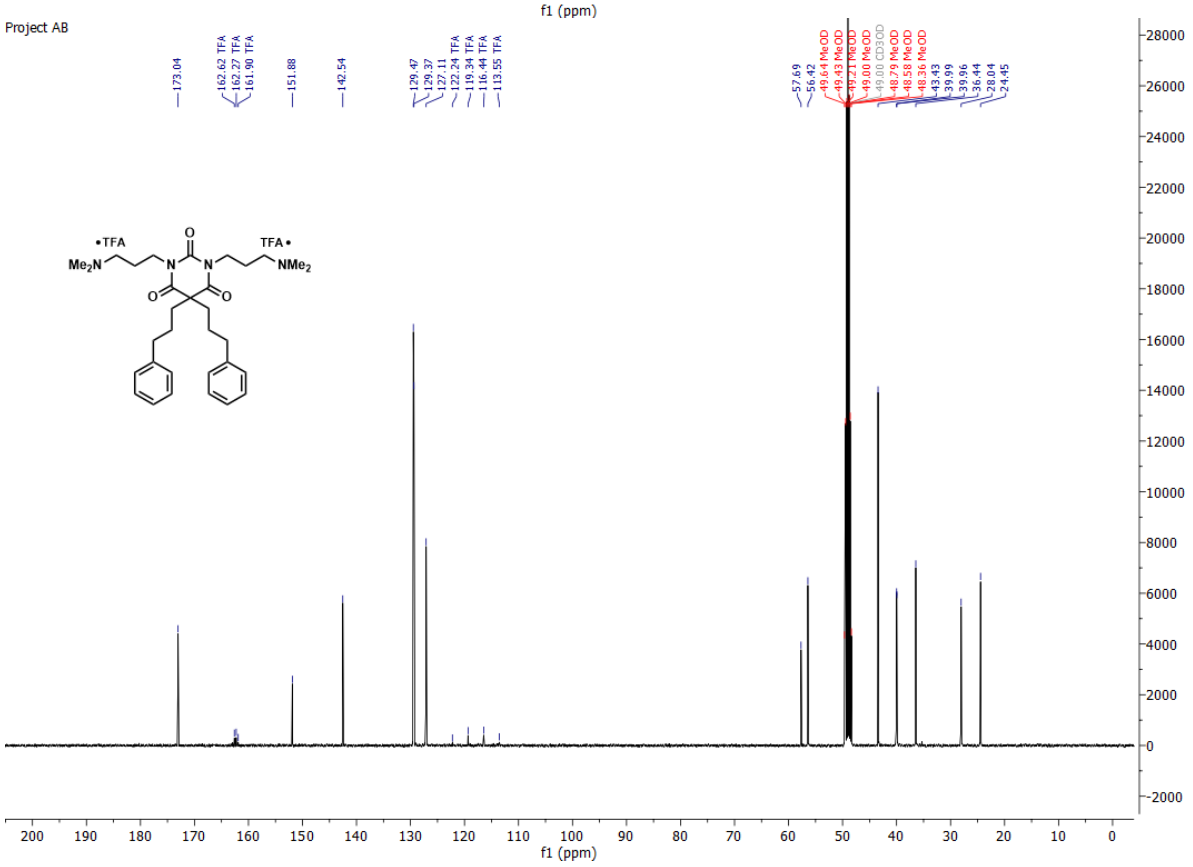

1,3-bis(2-(dimethylamino)ethyl)-5,5-bis(3-phenylpropyl)pyrimidine-2,4,6(1H,3H,5H)-trione **MPM-2:2**.

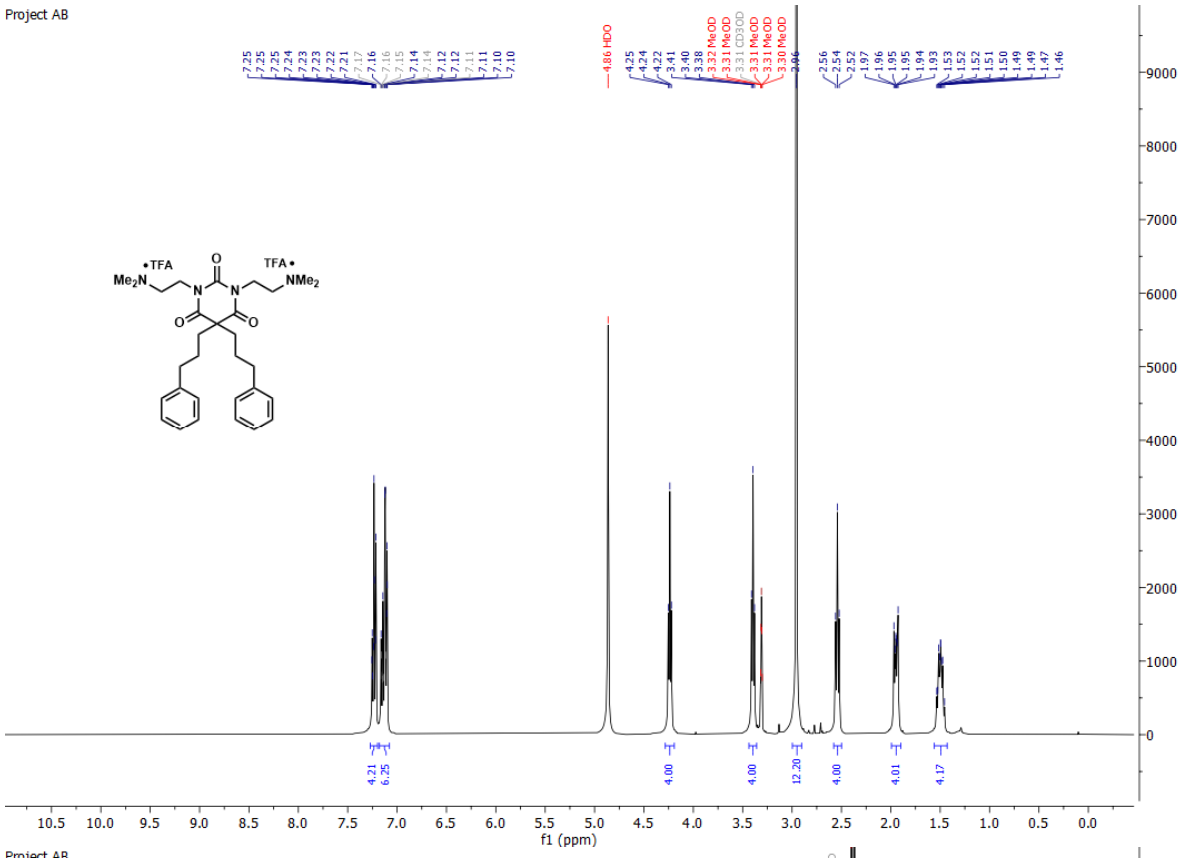

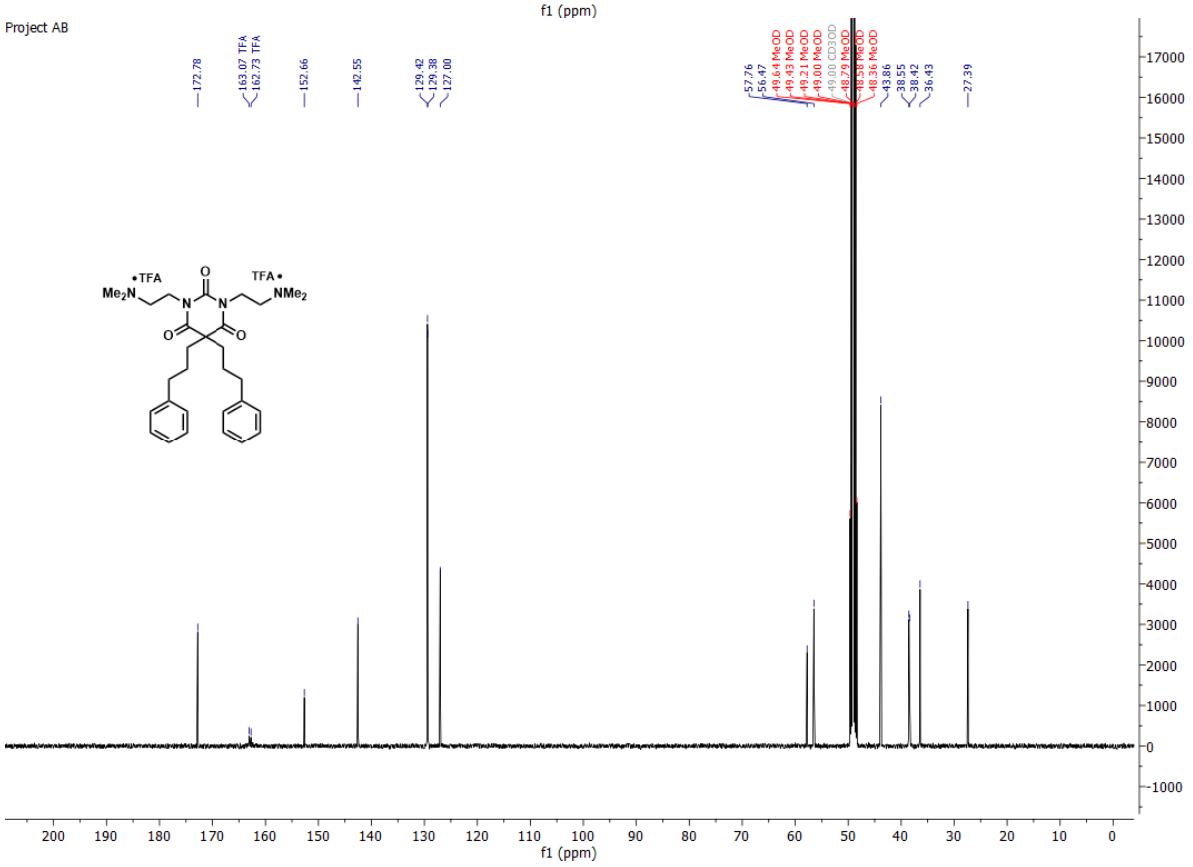

3 SFC traces

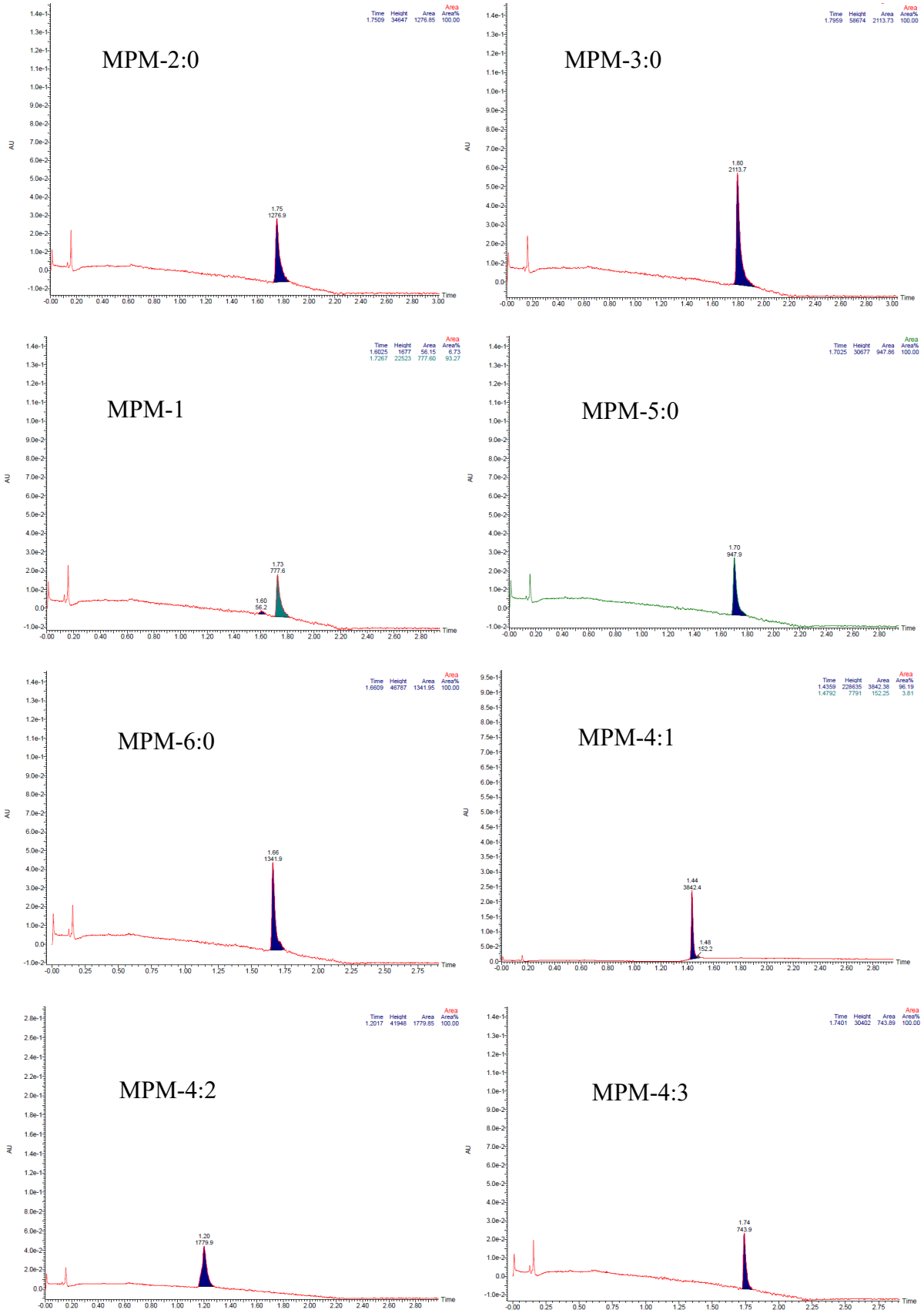

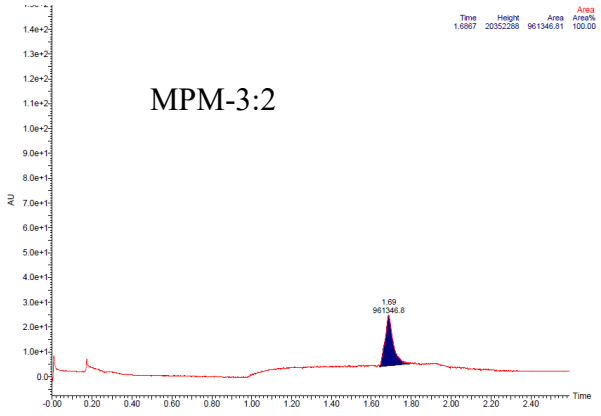

4 References

(1) von Hofsten, S.; Paulsen, M. H.; Magnussen, S. N.; Ausbacher, D.; Kranz, M.; Bayer, A.; Strøm, M. B.; Berge, G. The marine natural product mimic MPM-1 is cytolytic and induces DAMP release from human cancer cell lines. *Sci. Rep.* **2022**, *12* (1), 1-15.

Paper III

Intratumoral Injection with the Marine Natural Product Mimic MPM-1 Causes Complete Remission of B16F1 Melanoma

Susannah von Hofsten[1], Manuel K. Langer[2], Dominik Ausbacher[3], Morten B. Strøm[3], Synnøve Norvoll Magnussen[1] and Gerd Berge[1]

[1]Department of Medical Biology, Faculty of Health Sciences, UiT – The Arctic University of Norway, Tromsø, Norway

[2]Department of Chemistry, Faculty of Science and Technology, UiT – The Arctic University of Norway, Tromsø, Norway

[3]Department of Pharmacy, Faculty of Health Sciences, UiT – The Arctic University of Norway, Tromsø, Norway

Keywords: Immunogenic cell death, in vivo, melanoma, calreticulin, histology

Abstract

MPM-1 is a synthetic compound designed with inspiration from a class of natural products called *eusynstyelamides*, which have been isolated from arctic marine animals in the past. A previous study demonstrated that MPM-1 could induce hallmarks of immunogenic cell death in vitro in the oral squamous cell carcinoma cell line HSC-3. Intratumoral treatment with compounds that induce immunogenic cell death in cancer cells can cause the stimulation of an adaptive anti-tumor immune response which culminates in the activation of tumor-specific cytotoxic T cells. In the current study, the ability of MPM-1 to induce immunogenic cell death in vivo in a B16F1 melanoma mouse model was investigated. In vitro studies demonstrated that MPM-1 stimulated cell surface exposure of the "eat-me"-signal calreticulin in B16F1 cells as well as early plasma membrane rupture. Intratumoral injection of MPM-1 in subcutaneous B16F1 tumors caused complete remission in all treated animals. However, upon rechallenge with the same cells, tumors developed in 8/10 previously cured mice. This indicated that treatment with MPM-1 had not stimulated a sufficiently strong immune response to generate long-term immunological memory. However, blood sample analysis revealed that the number of neutrophils and lymphocytes increased after treatment. Histological analysis demonstrated that the tissue around treated tumors was characterized by acute inflammation, as well as a significant increase in $CD4^+$ cells on day 9/10 after treatment.

Introduction

Intratumoral immunotherapy with cytolytic compounds is a promising novel treatment mode for solid tumors (1). Cytolytic compounds that have the ability to induce immunogenic cell death cause exposure and release of damage associated molecular patterns (DAMPs) as well as the release of tumor antigens from the dying cells (2). This has recruiting and activating effects on immune cells, which in turn may lead to the activation of a natural anti-tumor immune response where tumor specific $CD8^+$ T cells are activated (3).

The marine natural product mimic MPM-1 is a synthetic compound which is intended as a potential anticancer agent for the local treatment of solid tumors. We have previously shown that MPM-1 is cytolytic and induces several of the hallmarks of immunogenic cell death in vitro in a study mainly focused on the human oral squamous cell carcinoma cell line HSC-3 (4). This suggests that intratumoral injections with MPM-1 could have the ability to induce an anti-tumor immune response in vivo.

The design of MPM-1 was inspired by the *eusynstyelamides*, which are natural products that have previously been isolated from arctic bryozoans (5). MPM-1 contains a barbiturate scaffold which is connected to two cationic groups and two bulky lipophilic groups, giving it an amphipathic structure overall (6). This makes it similar to the *eusynstyelamides* as well as to other known inducers of immunogenic cell death, such as the small peptide derivative LTX-401 and the peptide LTX-315 (7). MPM-1 contains the same lipophilic groups as LTX-401, a compound which has been shown to elicit strong anticancer activity and immunogenic effects in vivo in a rat model (8).

Although the in vitro results with MPM-1 indicate that is has the ability to induce immunogenic cell death, the general consensus is that it is only possible to verify a compound's ability to induce immunogenic cell death through in vivo studies (3). Several different models for the detection of immunogenic cell death in vivo have been developed. In the past, we have successfully used a model based on the intratumoral injection of compound into subcutaneously established B16F1 melanoma tumors in syngeneic C57BL/6 mice (9). In the current study, we employ this model to study the immunogenic effects of MPM-1.

Results

MPM-1 causes plasma membrane rupture and cell surface exposure of calreticulin

Our previous study showed that MPM-1 had activity against B16F1 cells (4). However, to verify that the mode of death induced by MPM-1 in B16F1 cells was of a similar nature as that in HSC-3 cells, flow cytometric analysis was used. A standard apoptosis assay where B16F1 cells were stained with fluorescently labeled Annexin V, which binds to phosphatidylserine (PS) in the plasma membrane, and propidium iodide (PI), which only stains cells with a compromised cell membrane, was performed. Cells in early apoptosis have intact plasma membranes but expose PS in the outer layer of the plasma membrane. Such cells therefore stain positive for Annexin V, but negative for PI. No such cells were detected among the MPM-1 treated B16F1 cells (Figure 1AB). Instead, MPM-1 caused the appearance of Annexin V–/PI+ and Annexin V+/PI+ cells, thus indicating that MPM-1 causes early membrane rupture in B16F1 cells and a more necrosis like death.

Cell surface exposure of calreticulin, a DAMP that functions as an “eat me”-signal during immunogenic cell death, was also studied via flow cytometry on MPM-1 treated B16F1 cells. The results showed that MPM-1 could induce a significant increase in cell surface calreticulin in alive B16F1 cells (Figure 2CD). The most significant increase was seen in cells treated for four hours with 20 µM MPM-1. However, 10 µM MPM-1 also induced a significant increase in cell surface calreticulin both after 4 and 24 hours. The cells that been treated with 20 µM MPM-1 for 24 hours all had completely ruptured plasma membranes, indicating that they were completely dead. Taken together, these results indicate that the mode of death induced by MPM-1 in B16F1 cells is similar to what has previously been demonstrated in HSC-3 cells (4).

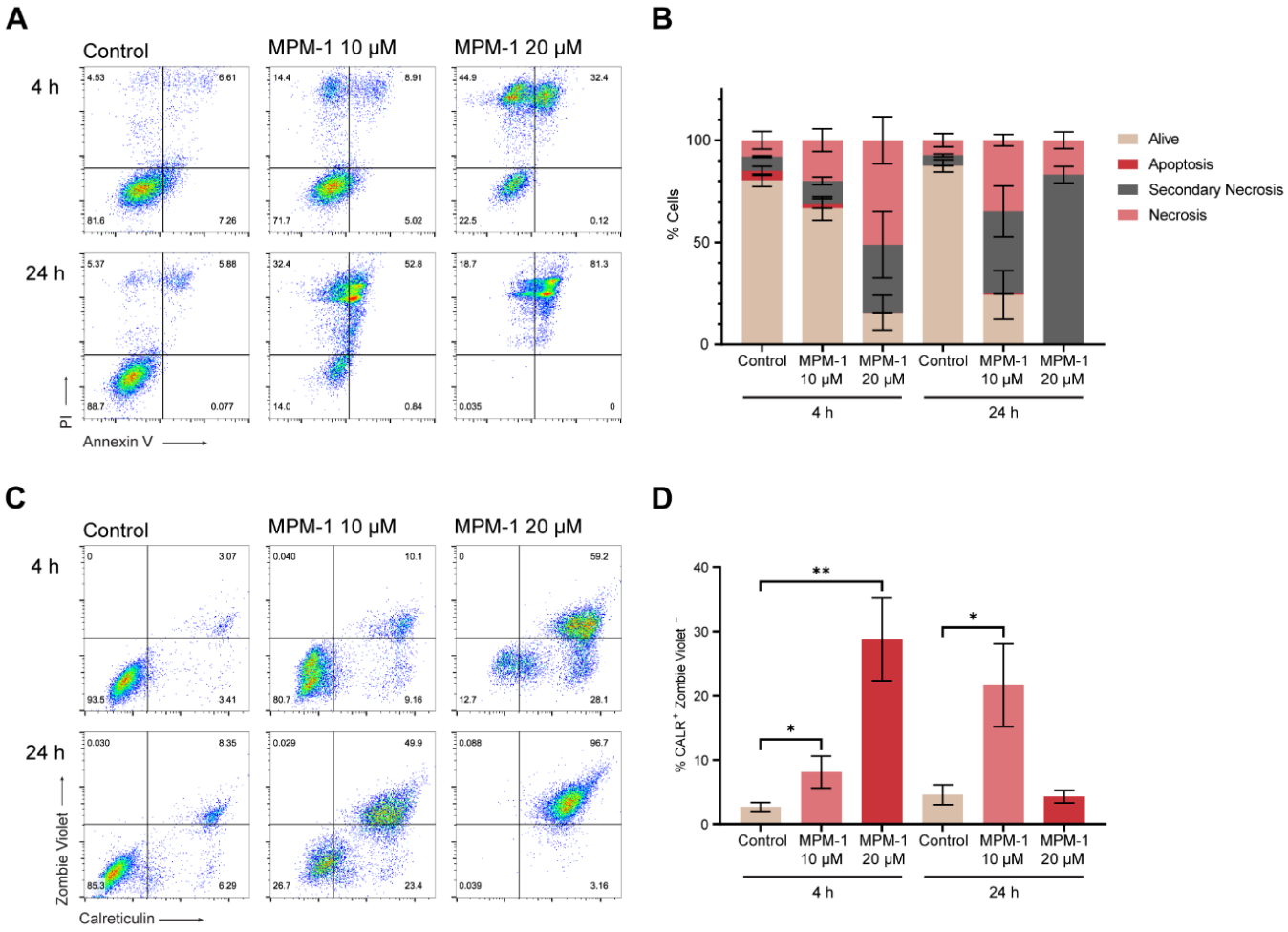

Figure 1 The mode of death induced by MPM-1 was analyzed by flow cytometry in B16F1 cells treated with 10 or 20 µM MPM-1 for 4 or 24 hours (**A**). The percentage of alive (AV–/PI–), apoptotic (AV+/PI–), necrotic (AV–/PI+) and secondary necrotic (AV+/PI+) cells was determined and the mean results from three independent experiments is shown in (**B**). Cell surface exposure of calreticulin by B16F1 cells treated with 10 or 20 µM MPM-1 for 4 or 24 hours was assessed by flow cytometry (**C**). The percentage of alive (Zombie Violet$^-$) cells expressing cell surface calreticulin was determined in three independent experiments (**D**). Significant differences between treated and untreated groups were determined by unpaired t-test.

MPM-1 induced complete remission of established B16F1 tumors but no long-term immunological protection

To assess the ability of MPM-1 to induce immunogenic cell death in vivo, we established subcutaneous B16F1 tumors on the flank of syngeneic C57BL/6 mice and subjected them to intratumoral injections with MPM-1. First, we employed a rechallenge model, where the aim was to determine whether intratumoral treatment with MPM-1 could cause both tumor remission and stimulation of an anti-tumor immune response that would provide long-term protection from B16F1 cancer cells. This was done by rechallenging mice that had become tumor free upon treatment with MPM-1 with a new injection of B16F1 cells (Figure 2A).

The results revealed that intratumoral treatment of B16F1 tumors with 0.5 mg MPM-1 for two consecutive days caused complete remission of established tumors in all treated mice (Figure 2BC). In all control mice treated with PBS, the tumors kept growing and eventually caused such a heavy tumor burden that the mice had to be sacrificed.

Mice that had been treated with MPM-1 and remained tumor free for at least four weeks were then subjected to a rechallenge with B16F1 cells. Age-matched naïve mice which had not been subjected to any previous tumor challenge were simultaneously inoculated with B16F1 cells for comparative reasons. The results revealed that there was some tendency towards immunological protection from B16F1 cells in mice previously cured by MPM-1. Two of the mice previously healed by MPM-1 remained completely tumor free after the rechallenge, while all naïve mice developed tumors (Figure 2DE). However, this result is not statistically significant (Fisher's exact test: $p=0.263$). There was also a tendency towards faster tumor growth in the naïve mice as compared to the MPM-1 treated mice. This was especially noticeable on day 14 post rechallenge, but again, the difference was not statistically significant (Figure 2F).

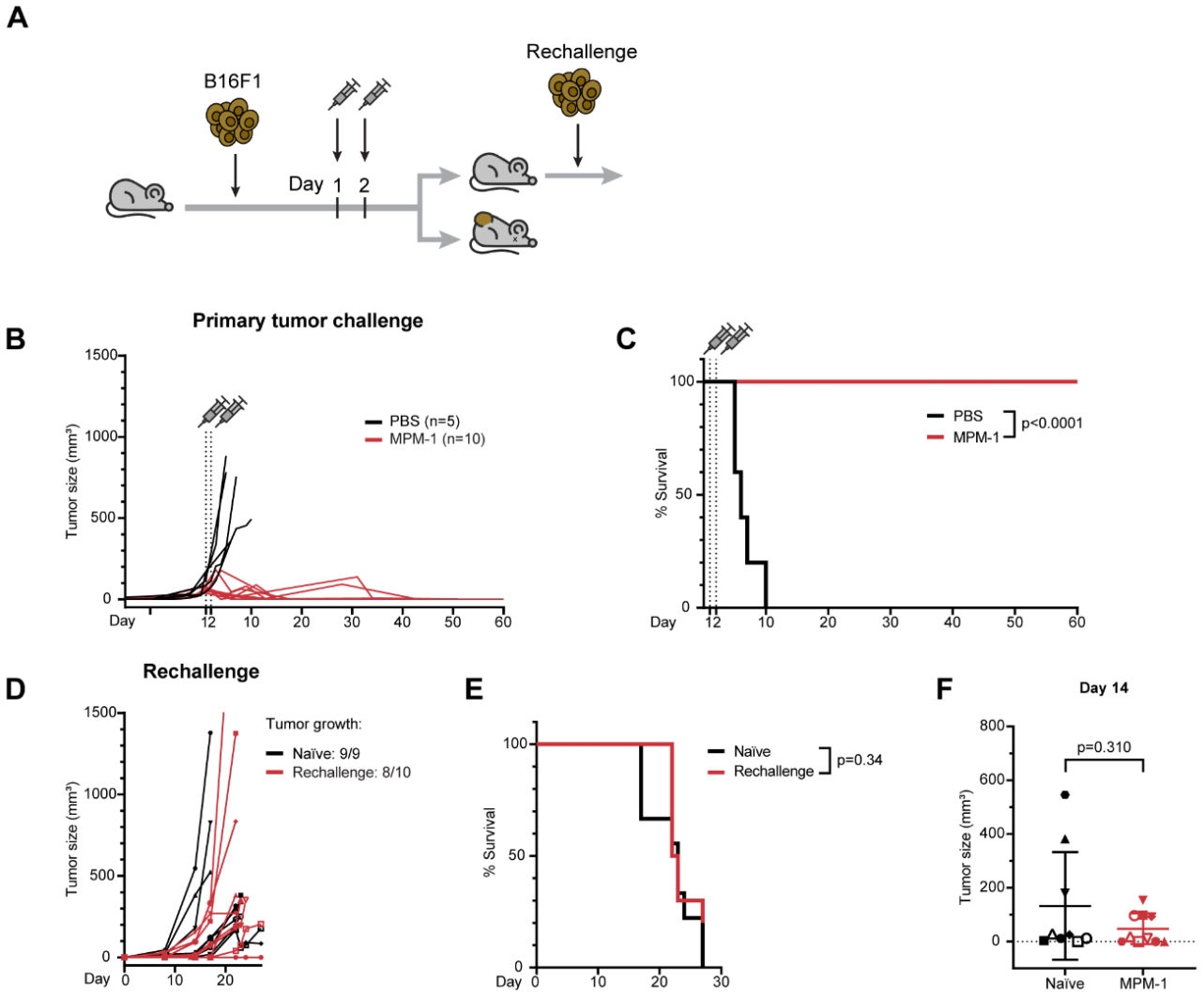

Figure 2 Schematic overview of the rechallenge study (**A**). B16F1 tumors were established subcutaneously on the flank of C57BL/6 mice. When the tumors reached 4-5 mm in diameter, they were treated with intratumoral injections of MPM-1 (0.5 mg, n=10) or PBS (vehicle control, n=5) for two days in a row. Tumor growth was regularly monitored by caliper measurement (**B**). All PBS treated mice had to be sacrificed due to heavy tumor burden, while all MPM-1 treated mice became tumor free and survived the treatment (**C**). Tumor free mice were subjected to a rechallenge with B16F1 cells. Age-matched control mice with no prior tumor challenges (naïve, n=9) were simultaneously also inoculated with B16F1 cells. Tumor growth was monitored by caliper measurement (**D**). Two of the mice previously treated with MPM-1 remained tumor free after the rechallenge, while tumors developed in all naïve mice (**E**). The mean tumor size for MPM-1 treated and naïve mice is shown for day 14 post rechallenge (**F**). Statistical significance was calculated with the Mann-Whitney *U* test. For the survival plots, statistical significance was calculated with the Mantel-Cox test.

Progression of immune response over time

To study the effects of intratumoral treatment with MPM-1 over time and at greater detail, we performed an additional in vivo study where mice were sacrificed at three different timepoints after treatment with MPM-1 (Figure 3A). Blood samples from the saphenous vein were acquired throughout the study, and upon sacrifice the tumors were retained for histological analyses. Control mice treated with PBS were sacrificed at two different time points. Tumor growth was monitored regularly by caliper measurements (Figure 3B). All the PBS treated mice had to be sacrificed by day 7 due to heavy tumor burden. Two MPM-1 treated mice also had to be sacrificed before the planned time point due to tumor growth. These mice were sacrificed without acquiring a saphenous vein blood sample first or preserving the tumor. They are therefore not included in the following analyses.

The composition of different types of leukocytes present in the saphenous vein blood samples was analyzed by use of a hematology analyzer. The results revealed that the number of neutrophils increased after treatment with MPM-1 (Figure 3C). On day 9/10, the number of neutrophils was significantly higher than in untreated and PBS treated mice. For lymphocytes, the numbers also increased after MPM-1 treatment and reached the highest levels on day 15 (Figure 3D).

Tumor sections were stained with hematoxylin and eosin (H&E), as well as for the presence of $CD4^+$ and $CD8^+$ cells. Both the $CD4^+$ and $CD8^+$ cells were primarily located in the stroma surrounding the tumors. Only a small number of these cells seemed to have infiltrated into the tumors. For this reason, as well as because the tumor cells are intrinsically brown due to their melanin content, making them difficult to distinguish from cells that have been stained, CD4 and CD8 staining was scored only in the stroma. A hotspot scoring approach was taken where three hotspots demonstrating a high degree of positive staining were selected from each slide and the percentage area showing positive staining was determined by automatic analysis in each hotspot. In general, there were more $CD4^+$ cells as compared to $CD8^+$ cells. The staining of CD4 demonstrated that the MPM-1 treated tumors from day 9/10 contained the highest number of $CD4^+$ cells (Figure 3E). There were no significant differences in the number of $CD8^+$ cells across the different groups (Figure 3F). There seemed to be a tendency towards a time-dependent increase in the MPM-1 treated tumors. Nevertheless, the PBS treated tumors contained similar numbers of $CD8^+$ cells.

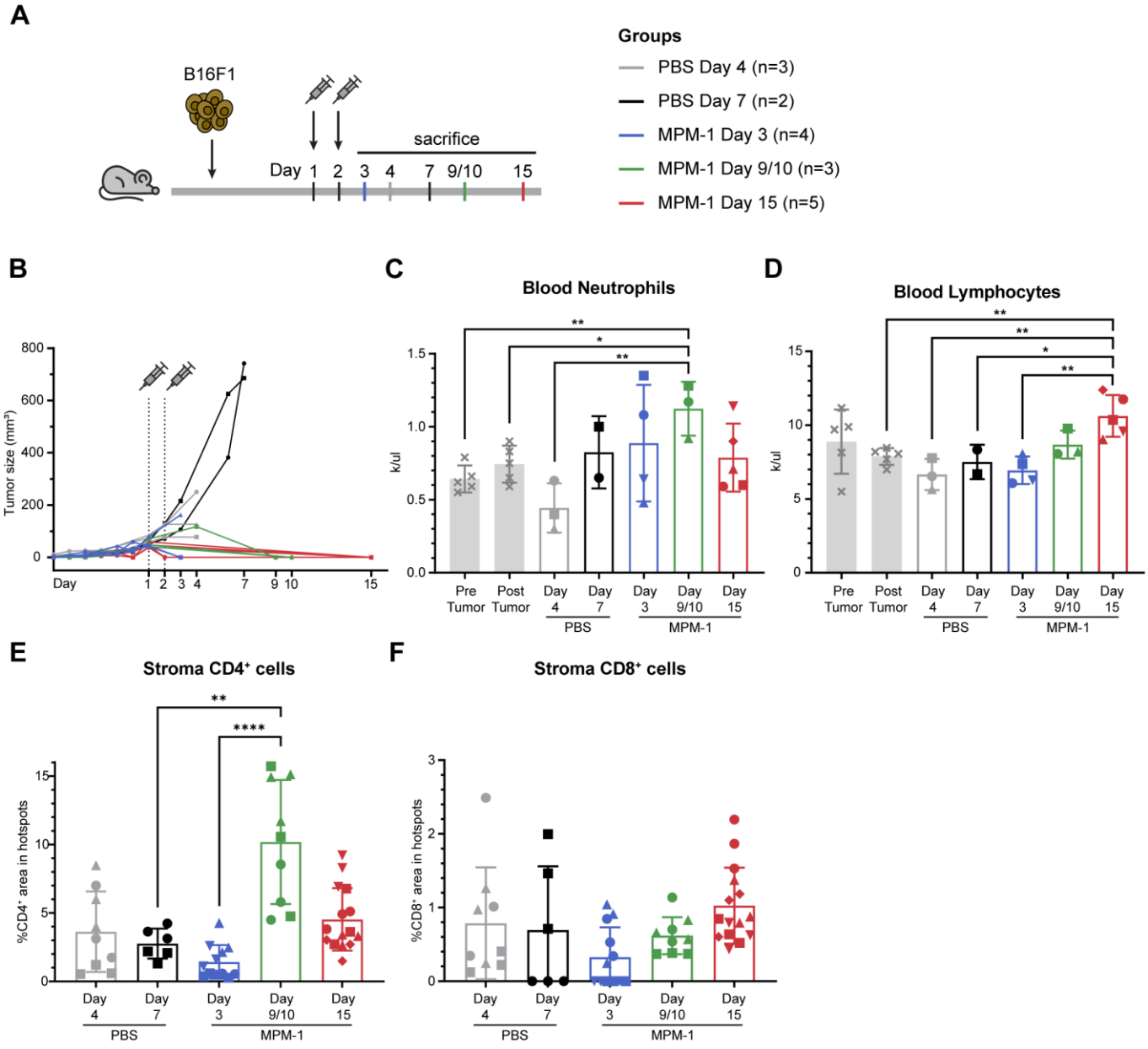

Figure 3 Schematic overview of the time course study (**A**). B16F1 tumors were established subcutaneously on the flank of C57BL/6 mice. When the tumors reached 4-5 mm in diameter, they were treated with intratumoral injections of MPM-1 (0.5 mg) or PBS (vehicle control) for two consecutive days (Day 1 and 2). PBS treated mice were sacrificed on day 4 (n=3) and day 7 (n=2) while MPM-1 treated mice were sacrificed on day 3 (n=4), day 9/10 (n=3) and day 15 (n=5). Tumor growth was regularly monitored by caliper measurement (**B**). Blood samples from the saphenous vein were acquired pre tumor inoculation, post tumor inoculation, and on the day of sacrifice for all mice. Samples acquired pre and post tumor inoculation from five arbitrary mice, as well as all blood samples from the day of sacrifice were analyzed for the number of neutrophils (**C**) and lymphocytes (**D**) they contained with a hematology analyzer. Statistically significant differences were calculated with the unpaired t test. Tumor sections from sacrificed mice were stained and scored for the presence of $CD4^+$ (**E**) and $CD8^+$ (**F**) cells in three hotspots per section. Statistically significant differences were calculated with the unpaired t test.

Representative images of the stained tumor sections are shown in Figure 4. H&E staining demonstrated that PBS treated tumors contained large areas of necrosis and bleeding (Figure 4LO). However, the majority of the tumor cells appeared viable, and the rate of tumor growth indicated that they were actively proliferating. In MPM-1 treated tumors from day 3, large areas of bleeding and acute inflammation, characterized by the presence of many cells with multi-lobulated nuclei, could be seen around the tumor (Figure 4G). The tumors contained both necrotic and viable cells (Figure 4F). In the stroma, some $CD4^+$ cells could be seen, but there were few or no $CD8^+$ cells (Figure 4PU). On day 9/10, the inflammatory response seemed to be less acute, but still ongoing (Figure 4H). At this time point, the morphology of the tumor cells was similar to that in the tumors from day 3. In the stroma, there was a substantial increase in the number of $CD4^+$ cells and somewhat more $CD8^+$ cells (Figure 4QV). MPM-1 treated tumors from day 15 were visibly smaller and completely eradicated in one sample. The tumor area contained few cells that looked viable, and the tissue appeared to be damaged (Figure 4N). The stroma of these tumors contained fewer inflammatory cells. Instead, large numbers of fibroblasts could be seen, demonstrating that a wound healing process had been initiated (Figure 4J). In general, the $CD4^+$ and $CD8^+$ cells associated with the MPM-1 treated tumors were located throughout large areas of the stroma. However, in the PBS treated tumors, these cells seemed to primarily be located close to the tumor border.

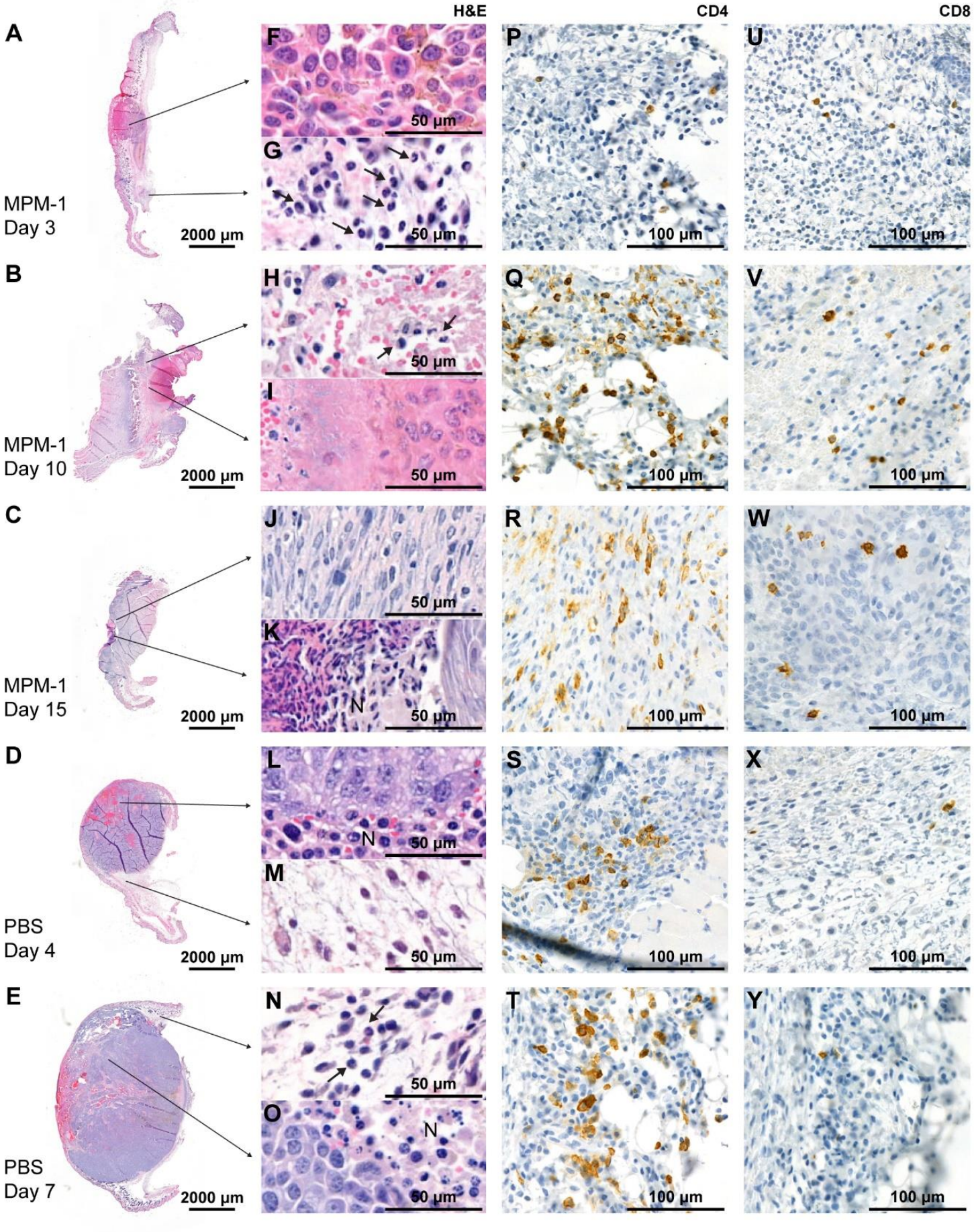

Figure 4 Tumor sections from MPM-1 and PBS treated tumors. Whole tumors and surrounding stroma stained with H&E are shown in (**A-E**) along with zoomed in representative areas from tumor (**F, I, K, L, O**) and stroma (**G, H, J, M, N**). Arrows point to multi-lobulated neutrophils and N marks areas of necrosis. Representative hotspot areas for CD4 (**P-T**) and CD8 (**U-Y**) staining in the stroma.

Discussion

MPM-1 is a natural product mimic which shares several features with known inducers of immunogenic cell death, such as LTX-401 (8). Previous in vitro studies have suggested that MPM-1 is also able to induce immunogenic cell death (4). In the current study we have shown that intratumoral injections with MPM-1 can induce complete remission of established B16F1 tumors in C57BL/6 mice. However, only a statistically insignificant fraction of cured mice was protected from tumor growth when rechallenged with the same B16F1 cells. This result suggests that MPM-1 did not stimulate a sufficiently strong anti-tumor immune response to provide long-term immunological protection from B16F1 cells. This could indicate that MPM-1 is not an effective inducer of immunogenic cell death.

The mode of death induced by MPM-1 in B16F1 cells in vitro suggests that in vivo treatment with MPM-1 should have some activating effects on the immune system. The rapid rupture of the plasma membrane upon treatment of B16F1 cells with MPM-1, as demonstrated by positive PI staining, indicates that these cells can passively release inflammatory DAMPs such as HMGB1 and ATP to the extracellular environment (10, 11). This was previously demonstrated in HSC-3 cells (4). In addition, MPM-1 induced cell surface expression of the "eat-me" signal calreticulin on B16F1 cells. Cell surface calreticulin can stimulate cells of the innate immune system to phagocytose the dying tumor cells and cross-present tumor antigens to cells of the adaptive immune system. Release of HMGB1 and ATP, and cell surface exposure of calreticulin are all hallmarks of immunogenic cell death (2).

It has been demonstrated previously that even though in vitro assays suggest that a compound is an effective inducer of immunogenic cell death, subsequent studies in vivo can demonstrate the opposite, highlighting the importance of in vivo experimentation when studying potential inducers of immunogenic cell death (3). The chemotherapeutic drug gemcitabine was shown to induce DAMP release in cancer cells in vitro but was not able to stimulate a protective anti-tumor immune response in vivo (12). The same study found that the reason for this was that while gemcitabine induced DAMP release, it simultaneously induced release of the so-called "inhibitory DAMP" prostaglandin E_2, which negatively affected the activation and maturation of dendritic cells. There is a possibility that MPM-1 also induces release of prostaglandin E_2 or other inhibitory DAMPs.

Other reasons why MPM-1 failed to establish long-term immunological protection from B16F1 tumors in the current study may be related to the design of the study. As previously mentioned, we and others have successfully employed the same model for the study of immunogenic cell

death before (9, 13). Thus, the chosen mouse strain and cell line is not expected to have negatively influenced the result. However, it should be noted that in previous studies using this model, tumors have been established on the abdomen rather than on the flank as in the current study. As the abdomen has increased vascularization as compared to the flank, this could mean that a higher number of immune cells reach tumors established on the abdomen. However, several other common models for the study of immunogenic cell death are also based on the establishment of flank tumors (3). Moreover, a sufficiently strong activation of anti-tumor immune responses should be able to protect against future tumors in any location.

Another factor relating to study design which may have influenced the results of the current study is the treatment dose and regimen. The selected dose of 0.5 mg MPM-1 per intratumoral injection was based on previous studies with similar compounds as well as on the results from a pilot study where three different doses of MPM-1 were tested (unpublished results). The pilot study suggested that doses higher than 0.5 mg MPM-1 caused too much necrosis in the tissue surrounding the tumor to be considered safe. The fact that the two consecutive injections of 0.5 mg did efficiently eradicate established tumors indicates that this dose was not too low. Instead, there is a possibility that the dose was too high to stimulate the desired immune response. It could be that the tumor cells were simply killed by the treatment in a manner comparable to surgical resection. While the histological analyses demonstrated acute inflammation around MPM-1 treated tumors, this may not have led to sufficient activation of the adaptive immune system, which is required for the formation of immunological memory.

Previous studies on immunogenic cell death using the B16F1 mouse model and intratumoral injection of compound have seen substantial CD3 staining, which marks both $CD4^+$ and $CD8^+$ cells, in the tumors after treatment (9, 13). In a similar study of LTX-401 in hepatocellular carcinoma, $CD3^+$ and $CD8^+$ cells were found inside the tumor as well as around the tumor border (8). Compared to the results demonstrated in these studies, the degree of CD4 and CD8 staining seen in the current study was low. This correlates with the insufficient vaccination effect of MPM-1 treatment.

Nevertheless, the increased number of blood lymphocytes seen in MPM-1 treated mice on day 15 does suggest some activation of the adaptive immune system. So does the immunohistochemistry staining of CD4, which demonstrated that the number of stromal $CD4^+$ cells on day 9/10 was high. $CD4^+$ T cells can produce IFNγ and TNFα, which can help to stimulate the activation of anti-tumor $CD8^+$ T cells. Still, the number of $CD8^+$ T cells in the tumor stroma was generally low in all treated groups. This indicates that MPM-1 had not caused

the expected activation and infiltration of tumor specific cytotoxic $CD8^+$ T cells which is the goal of treatments that induce immunogenic cell death (3).

It cannot be concluded from the results presented in the current study whether the increase in stromal $CD4^+$ cells or the increased number of blood lymphocytes after MPM-1 treatment are due to a specific response against the B16F1 cells or if they are connected to other circumstances. For instance, it is known that factors like age and stress affect the composition of leukocytes in mouse blood (14). However, the number of lymphocytes generally decreases both with increased age and stress, suggesting that the increase seen in the current study was not a consequence of these matters. The neutrophil count is known to increase with age, as well as with inflammation (14). As the histological analyses revealed that the area around MPM-1 treated tumors contained large numbers of neutrophils, characterized by their multi-lobulated nuclei, the increased number of blood neutrophils was likely due to inflammation in the tumor area.

Based on the results from the current study, it is not possible to conclude that MPM-1 is an effective inducer of immunogenic cell death. The fact that tumors were established in 8/10 mice previously cured by MPM-1 suggests that it had not activated a sufficiently strong adaptive immune response to create immunological memory. The low number of $CD8^+$ T cells detected by immunohistochemistry staining supports this notion. However, the tissue surrounding MPM-1 treated tumors was characterized by inflammation and some increase in CD4 staining, indicating that treatment with MPM-1 could cause activation of some part of the immune system. As previously discussed, the poor vaccination effect could be due to the treatment regimen and dose selected for the current study. Nevertheless, the fact that the primary B16F1 tumors were completely eradicated in all mice upon intratumoral injections with MPM-1 in the rechallenge study suggests that MPM-1 does have some therapeutic effect.

Materials and Methods

Cell Culture

B16F1 cells (RRID: CVCL_0158), were obtained from the American Type Culture Collection (ATCC, Manassas, VA, USA). Cells were kept at 37ºC with 5% CO_2 and cultured in high glucose Dulbecco's Modified Eagle's Medium (DMEM, Sigma-Aldrich) supplemented with 10% fetal bovine serum (FBS).

Flow cytometry

For both the apoptosis assay and the detection of cell surface calreticulin, B16F1 cells were seeded, 300 000 cells/well in 6-well plates and left to adhere overnight. Then, the media was removed and replaced by 2 ml complete media containing 10 or 20 µM MPM-1. The cells were stimulated for 4 or 24 hours before the cell supernatants were collected, the cells were trypsinized and then spun down with the supernatants.

For the apoptosis assay, a commercial kit was used (#88-8005-74, Thermo Fisher Scientific). The cells were washed once in PBS and once in binding buffer before being incubated with FITC labeled Annexin V diluted 1:25 in 1x binding buffer for 30 minutes. Next, the cells were washed in binding buffer before being incubated with PI diluted 1:100 in binding buffer for at least 5 minutes before analysis.

For detection of cell surface calreticulin, the cells were washed in PBS before being incubated with the viability dye Zombie Violet (#423114, BioLegend, San Diego, CA, USA) diluted 1:500 in PBS for 20 minutes. Next, the cells were incubated with an anti-calreticulin antibody (#ab2907, Abcam) diluted 1:100 in FACS buffer (2%BSA in PBS) for 30 minutes. The cells were then fixed in 4% formaldehyde for 15 minutes and washed twice in FACS buffer before being incubated with the Alexa Fluor 488 conjugated goat anti-rabbit secondary antibody (#A11034, Thermo Fisher Scientific) diluted 1:250 in FACS buffer for 30 minutes. The cells were then washed once in FACS buffer before analysis.

Flow cytometry was performed on the LSR Fortessa (BD Biosciences, Franklin Lakes, NJ, USA) and analysis was done in FlowJo™ v.10 (https://www.flowjo.com/).

Animals

Female 6-week old C57BL/6 wild-type mice (strain: C57BL/6NRj) were obtained from Janvier Labs (Route de Genest, France). All animals were housed in the same room, with a 12h/12h day-night cycle. They were kept in cages especially designed for mice, with a maximum of five mice in each cage, and they were allowed ad libitum access to high quality food and water.

Each cage contained environmental enrichments such as nest material, chewing sticks and housing. Animals were weighed and monitored at least three times per week. All experimental procedures were approved by the Norwegian Food Safety Authority (Mattilsynet, FOTS ID: 26320), and conducted in accordance with local and European Ethical Committee guidelines.

Tumor inoculation and treatment

B16F1 cells were harvested, washed and resuspended to $1x10^6$ cells/mL in serum free RPMI-1640. 50 µl of cell suspension (50 000 cells) was inoculated subcutaneously on the right flank. When tumors reached 4-5 mm in diameter, they were treated with an intratumoral injection of MPM-1 (0.5 mg in 50 µl PBS) or PBS only (50 µl) for two consecutive days. Mice were monitored and tumor volumes were measured by use of an electronic caliper at least twice per week. For the rechallenge study, mice were kept alive as long as they remained healthy. If tumors reached >10 mm in diameter or the mice showed signs of discomfort or pain, they were sacrificed. For the study of the effect of MPM-1 over time, MPM-1 treated mice were sacrificed on day 3 (n=4), day 9 (n=1), day 10 (n=2) or day 15 (n=5) of the study. Mice sacrificed on day 9 and 10 were considered part of the same experimental group. PBS-treated mice were sacrificed on day 4 (n=3) or day 7 (n=2). In this study, blood samples from the saphenous vein were obtained before tumor inoculation, after tumor inoculation but before commencement of treatment, as well as on the day of sacrifice. Approximately 100 µl was collected in heparin tubes each time. The samples were analyzed on a ProCyte DX hematology analyzer (IDEXX, Westbrook, ME, USA). The remaining blood was centrifuged at 4300 g for 10 minutes and plasma was transferred to a separate tube. Plasma from mice belonging to the same experimental groups was pooled and the samples were kept at -70 °C until use. Upon sacrifice, tumors were collected and fixed in 4% formaldehyde before being dehydrated and paraffin embedded. 4 µm thick sections were prepared for analysis.

H&E staining

Tumor section slides were deparaffinized in xylene and rehydrated in graded ethanol baths. Next, they were stained with hematoxylin for 30 seconds, washed in water and treated with Scott's solution for 15 seconds. Then, the slides were washed in water, treated with 96% ethanol for 10-30 seconds and incubated with eosin for 30 seconds. The slides were washed in water and treated with 96% ethanol for 10-30 seconds. Lastly, the slides were dehydrated in ethanol and xylene before a coverslip was mounted on top.

Immunohistochemistry

Tumor section slides were deparaffinized in xylene and rehydrated in graded ethanol baths. Antigen retrieval was performed by boiling the slides in Tris-EDTA pH 9. The slides were then incubated in 0.3 % H_20_2 for 10 minutes to block endogenous peroxidase activity and then washed in PBS three times. Next, the slides were blocked in 5 % goat serum in PBS for 20 minutes at RT. For staining of CD4 the slides were incubated for 1 hour at RT with the primary antibody (#183685, Abcam, Cambridge UK) diluted 1:1000 in blocking solution. For staining of CD8, the slides were incubated overnight at 4°C with the primary antibody (#217344, Abcam) diluted 1:2000 in blocking solution. The slides were then washed three times in PBS before being incubated with rabbit HRP EnVision+ (Agilent Dako, Santa Clara, CA, USA) for 30 minutes. The slides were washed three times in PBS before being incubated with DAB+ chromogen (Agilent Dako) for 10 minutes. They were then washed three times in water before being counterstained with hematoxylin for 30 seconds and Scott's solution for 15 seconds. The slides were then dehydrated in ethanol and xylene, and a coverslip was mounted on top.

Analysis of immunohistochemistry staining

Stained slides were scanned on a Panoramic 250 digital scanner (3DHISTECH, Budapest, Hungary) and studied in CaseViewer 2.4. (https://www.3dhistech.com/solutions/caseviewer/). To determine the degree of CD4 and CD8 positive staining in the tumor stroma, three hotspots demonstrating a high degree of positive staining were manually selected from each slide. The hotspots were squares of 0.1 mm^2 located within 2 mm from the tumor border. The percentage of CD4 or CD8 positive staining in each hotspot was determined by analyzing the hotspot images in ImageJ (https://imagej.net/ij/download.html), using the threshold function on the red channel to determine the area of positive staining.

Funding

This study received funding from the AKM fund from UiT – The Arctic University of Norway.

References

1. Vitale I, Yamazaki T, Wennerberg E, Sveinbjornsson B, Rekdal O, Demaria S, et al. Targeting cancer heterogeneity with immune responses driven by oncolytic peptides. Trends Cancer. 2021;7(6):557-72.
2. Galluzzi L, Buque A, Kepp O, Zitvogel L, Kroemer G. Immunogenic cell death in cancer and infectious disease. Nat Rev Immunol. 2017;17(2):97-111.
3. Galluzzi L, Vitale I, Warren S, Adjemian S, Agostinis P, Martinez AB, et al. Consensus guidelines for the definition, detection and interpretation of immunogenic cell death. J Immunother Cancer. 2020;8(1).
4. von Hofsten S, Paulsen MH, Magnussen SN, Ausbacher D, Kranz M, Bayer A, et al. The marine natural product mimic MPM-1 is cytolytic and induces DAMP release from human cancer cell lines. Scientific Reports. 2022;12(1):15586.
5. Tadesse M, Tabudravu JN, Jaspars M, Strom MB, Hansen E, Andersen JH, et al. The antibacterial ent-eusynstyelamide B and eusynstyelamides D, E, and F from the Arctic bryozoan Tegella cf. spitzbergensis. J Nat Prod. 2011;74(4):837-41.
6. Strøm MB, Bayer A, Engqvist SOM, Paulsen MH, Ausbacher D. 2018. Barbituric acid derivatives comprising cationic and lipophilic groups. WO/2018/178198. PCT/EP2018/058011.
7. Zhou H, Sauvat A, Gomes-da-Silva LC, Durand S, Forveille S, Iribarren K, et al. The oncolytic compound LTX-401 targets the Golgi apparatus. Cell Death Differ. 2016;23(12):2031-41.
8. Mauseth B, Camilio KA, Shi J, Hammarstrom CL, Rekdal O, Sveinbjornsson B, et al. The novel oncolytic compound LTX-401 induces antitumor immune responses in experimental hepatocellular carcinoma. Mol Ther Oncolytics. 2019;14:139-48.
9. Camilio KA, Berge G, Ravuri CS, Rekdal O, Sveinbjørnsson B. Complete regression and systemic protective immune responses obtained in B16 melanomas after treatment with LTX-315. Cancer Immunol Immunother. 2014;63(6):601-13.
10. Scaffidi P, Misteli T, Bianchi ME. Release of chromatin protein HMGB1 by necrotic cells triggers inflammation. Nature. 2002;418(6894):191-5.
11. Iyer SS, Pulskens WP, Sadler JJ, Butter LM, Teske GJ, Ulland TK, et al. Necrotic cells trigger a sterile inflammatory response through the Nlrp3 inflammasome. Proceedings of the National Academy of Sciences of the United States of America. 2009;106(48):20388-93.
12. Hayashi K, Nikolos F, Lee YC, Jain A, Tsouko E, Gao H, et al. Tipping the immunostimulatory and inhibitory DAMP balance to harness immunogenic cell death. Nature Communications. 2020;11(1):6299.
13. Eike LM, Mauseth B, Camilio KA, Rekdal Ø, Sveinbjørnsson B. The Cytolytic Amphipathic β(2,2)-Amino Acid LTX-401 Induces DAMP Release in Melanoma Cells and Causes Complete Regression of B16 Melanoma. PloS one. 2016;11(2):e0148980.
14. O'Connell KE, Mikkola AM, Stepanek AM, Vernet A, Hall CD, Sun CC, et al. Practical murine hematopathology: a comparative review and implications for research. Comp Med. 2015;65(2):96-113.